AD-A052 759 BOEING VERTOL CO PHILADELPHIA PA F/G 1/3
FINITE ELEMENT ANALYSIS FOR COMPLEX STRUCTURES (HELICOPTER TRAN--ETC(U)
JAN 78 R W HOWELLS, J J SCIARRA DAAJ02-75-C-0053
UNCLASSIFIED D210-11232-1 USAAMRDL-TR-77-32 NL

1 OF 3
AD
A052759

USAAMRDL-TR-77-32

(12)

SC

FINITE ELEMENT ANALYSIS FOR COMPLEX STRUCTURES (HELICOPTER TRANSMISSION HOUSING STRUCTURAL MODELING)

R. W. Howells, J. J. Sciarra
Boeing Vertol Company
(A Division of The Boeing Company)
Boeing Center, P. O. Box 16858 – Location
Philadelphia, Pa. 19142

January 1978

Final Report for Period July 1975 - May 1977

Approved for public release;
distribution unlimited.

Prepared for

APPLIED TECHNOLOGY LABORATORY
U. S. ARMY RESEARCH AND TECHNOLOGY LABORATORIES (AVRADCOM)
Fort Eustis, Va. 23604

APPLIED TECHNOLOGY LABORATORY POSITION STATEMENT

This work was conducted to develop and demonstrate a comprehensive, finite element analytical technique with the capability for analyzing and improving designs of helicopter transmission housings made of metal and/or composite materials. Because the components in a transmission system operate in a complex dynamic environment wherein all components interact and influence each other, a comprehensive analysis method was necessary to analyze the housing as a unique component of the system.

This report is considered to provide a reasonable insight for improving transmission design by improving the design and performance of its housing. The analysis methods and their results are being used with other transmission R&D programs at the Applied Technology Laboratory.

Gim Shek Ng of the Technology Applications Division served as project engineer for this effort.

UNCLASSIFIED

SECURITY CLASSIFICATION OF THIS PAGE (When Data Entered)

19 REPORT DOCUMENTATION PAGE		READ INSTRUCTIONS BEFORE COMPLETING FORM
1. REPORT NUMBER 18 USAAMRDL TR-77-32	2. GOVT ACCESSION NO.	3. RECIPIENT'S CATALOG NUMBER
4. TITLE (and Subtitle) 6 FINITE ELEMENT ANALYSIS FOR COMPLEX STRUCTURES (HELICOPTER TRANSMISSION HOUSING STRUCTURAL MODELING).		5. TYPE OF REPORT & PERIOD COVERED 9 Final Report. Jul[redacted]75 — May [redacted]77
		6. PERFORMING ORG. REPORT NUMBER 14 D210-11232-1
7. AUTHOR(s) ~~Advanced Power Train Technology Group~~ 10 R. W. Howells, J. J. Sciarra		8. CONTRACT OR GRANT NUMBER(s) 15 DAAJ02-75-C-0053 new
9. PERFORMING ORGANIZATION NAME AND ADDRESS Boeing Vertol Company (A Division of The Boeing Company) Boeing Center, P.O. Box 16858 Philadelphia, Pennsylvania 19142		10. PROGRAM ELEMENT, PROJECT, TASK AREA & WORK UNIT NUMBERS 62209A 16 1F262209AH76 00 ~~EK~~ 17 00
11. CONTROLLING OFFICE NAME AND ADDRESS Applied Technology Laboratory U.S. Army Research and Technology Laboratories (AVRADCOM) Fort Eustis, VA 23604		12. REPORT DATE 11 Jan[redacted]78
		13. NUMBER OF PAGES 213 12 216p.
14. MONITORING AGENCY NAME & ADDRESS(if different from Controlling Office)		15. SECURITY CLASS. (of this report) UNCLASSIFIED
		15a. DECLASSIFICATION/DOWNGRADING SCHEDULE

16. DISTRIBUTION STATEMENT (of this Report)

Approved for public release; distribution unlimited.

17. DISTRIBUTION STATEMENT (of the abstract entered in Block 20, if different from Report)

18. SUPPLEMENTARY NOTES

19. KEY WORDS (Continue on reverse side if necessary and identify by block number)

Transmissions
Structural Analysis
Loads
Analytical Technique

20. ABSTRACT (Continue on reverse side if necessary and identify by block number)

The objective of the Finite Element Analysis for Complex Structures program was to develop and demonstrate a comprehensive, finite element analytical technique with the capability and flexibility for analyzing helicopter transmission housings made of metal and/or composite materials. The work encompassed the study of thermal distortion and stress, stress and deflection due to static and dynamic loads, load path definition, dynamic response (over) over

DD FORM 1 JAN 73 1473 EDITION OF 1 NOV 65 IS OBSOLETE

UNCLASSIFIED

SECURITY CLASSIFICATION OF THIS PAGE (When Data Entered)

403 682 JOB

20. Abstract (Continued)

and the control of structural energy distribution. The results were used to optimize strength and weight, and to assess operational housing life, failsafety/safe life, and reliability. Some emphasis was placed on heat transfer analyses. Additional objectives were to integrate this housing analysis method with existing methods to form a comprehensive transmission analysis, and to validate these design tools so that they might be applied to future transmission configurations.

This program and the resulting technology represent a major step toward the long-range objective of a highly reliable, minimum weight, advanced technology transmission system. Prerequisite to the achievement of this goal is the extension of technology to meet the new analytical design techniques required. Significant research has been devoted to improving individual transmission components such as gears, bearings, and lube systems. However, a transmission is a complex dynamic system wherein all components interact and influence each other; hence a comprehensive, unified analysis is necessary to optimize the components as a system for the unique operating environment characteristic of a specified transmission.

A finite element model and analytical methods were applied to analyze a CH-47C helicopter's forward rotor transmission and also to define design modifications for structural optimization. All work conducted is compatible with the nationally available NASTRAN finite element computing program, Levels 15.5 and 16.0, so that structural load paths, stresses, natural frequencies, mode shapes, and thermal effects can be determined from a multi-purpose standardized source. Operating stresses and distortion of the housing have been experimentally measured and correlated with values predicted by NASTRAN in order to validate the model.

<u>PREFACE</u>

This report covers the work accomplished during the 23-month period from July 1975 through May 1977.

The work outlined herein has been performed under U.S. Army Contract DAAJ02-75-C-0053 and under the technical cognizance of Mr. Gim Shek Ng, Applied Technology Laboratory, U.S. Army Research and Technology Laboratories (AVRADCOM), Fort Eustis, Virginia.

This program was conducted at the Boeing Vertol Company under the technical direction of Mr. A. J. Lemanski (Program Manager), Chief of the Advanced Power Train Technology Department. Principal Investigators for the program were Mr. John J. Sciarra (Project Engineer) and Mr. Robert W. Howells.

TABLE OF CONTENTS

LIST OF ILLUSTRATIONS

Figure | Page

Figure		Page

Figure		Page

LIST OF TABLES

INTRODUCTION

The design of a helicopter drive system presents a difficult challenge. The continually escalating requirement for improved power-to-weight ratio capability is further complicated by the additional demands for extended service life, improved reliability/maintainability, better survivability/vulnerability and reduced vibration/noise levels. Faced with such an array of design constraints, the helicopter drive system design team must consistently push technology beyond the state of the art.

In addition to these technological advancements, a major goal for helicopter improvement is to reduce operating cost. Since 30 percent of the total helicopter direct maintenance cost is associated with the drive system, drive system cost is a significant part of the total operating cost (Figure 1). Service life duration of the major transmission components is a prime contributor to the operating cost. The most effective way to reduce the drive system cost is to extend the average service life of major transmission components (gears, bearings, splines, retention hardware, interface connections and joints, and lubrication system components). Increased life will reduce spares procurement, maintenance requirements, depot facilities, and labor.

Considerable research has been devoted to investigating and improving individual transmission components such as gears, bearings, and lubrication systems. Conversely, helicopter transmission housings had not previously received the attention necessary to define fully and optimize their functional requirements, and a gap in transmission technology existed in this area. Complex structures such as rotor transmission housings used in current helicopters are not generally designed for stiffness characteristics, however they have high strength margins for safe life and seldom exhibit gross structural failures. However, since the housing provides structural support to the internal components, its physical characteristics significantly affect overall transmission performance and life in terms of internal bearing capacity, gear capacity, fretting, misalignments, and load maldistributions. Therefore, the full benefits of advancements achieved in component technology cannot be realized in practice until the housing has been optimized.

A major constraint in meeting cost improvement goals is the deflections of the present housings under operating load conditions. Housing deflections under load have been identified as a cause of accelerated wear and surface deterioration of gears, bearings, splines, retention hardware, and interface connections and joints. In addition, these deflections result in excessive gear misalignment which greatly increases the dynamic force (excitation) at the gear meshes, resulting in vibration and noise generation. Reduction in the magnitude of these housing deflections by structural optimization and/or advanced materials offers great promise for both prolonging the life of the transmission components and substantially reducing the vibration and noise level without a system weight penalty.

To continue to improve transmission analysis capability, a detailed understanding of the structural and thermal aspects of the transmission housing must be developed and integrated with the existing component analyses. This effort for further research in the stress and dynamic characteristics of a helicopter transmission housing uses the finite element technique. The effects of thermal growth, structural deformation and operational housing life can be accurately studied. Along with structural design, fabrication and/or modification, and testing, this program also attempts to analyze the housing for fail-safe/safe-life design.

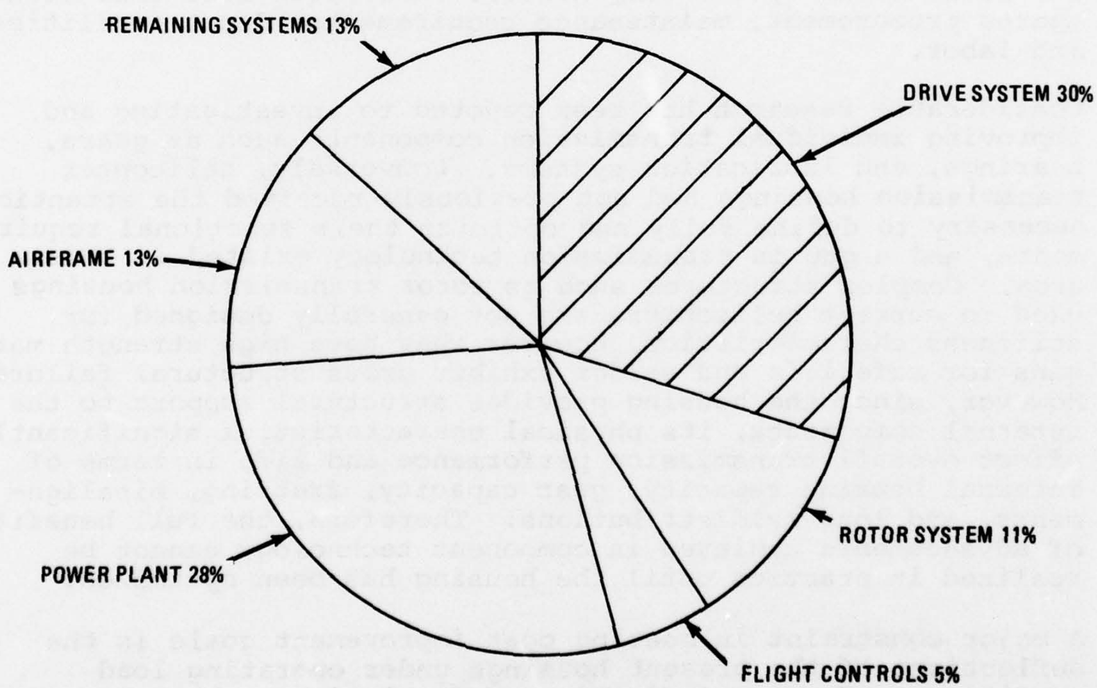

Figure 1. Breakdown of Direct Maintenance Costs

BACKGROUND

To provide an understanding of the configuration, functional requirements, and design criteria for a helicopter transmission, a brief description is included here. A typical contemporary helicopter main transmission housing is composed of three major parts with essentially separate functions: the upper cover, the ring gear, and the case. An example of this configuration, the CH-47C forward rotor transmission is shown in Figure 2. The upper cover supports the rotor shaft and provides lugs for mounting the transmission to the airframe. Hence, the rotor system loads are transmitted through the upper cover into the airframe. The case contains and supports the main bevel gears and may also include a tail rotor or sync shaft drive, lube pump, or accessory drives. The transmission may also have a separate sump for containment of the lubricant, as does the CH-47C, or it may use an integrally closed lower portion of the case for this purpose. The stationary ring gear, which connects the upper cover and case, contains the planetary gear system. The entire housing also performs the functions of sealing in the lubricant, providing passages for lubricant delivery, protecting critical transmission components, and dissipating heat by conduction and radiation. Figure 3 shows the transmission case in detail, since much of the work herein is concentrated on analysis of the case.

The upper-cover design criteria, in order of importance, include ultimate, fatigue, and crash load conditions. The gear case design criteria include stiffness for gear mounting and fatigue loads in certain areas. The ring gear must provide adequate strength to react the planetary gear loads and to support the case and must provide sufficient stiffness to maintain planet/ring gear tooth alignment. The requirement for oil containment exists for all of the housing parts.

Because of the complex geometry and the many functions that the typical housing must perform, transmission housings have traditionally defied analysis. Due to the lack of analytical methods for predicting and optimizing its many functional load paths, transmission housings have evolved as generally thick-walled cast or forged structures made of aluminum or magnesium. With the increasing power, size and weight of helicopter transmissions, the resulting over-design produces undetermined, but probably substantial, weight penalties. Figure 4, which presents a weight breakdown for a typical helicopter transmission, shows that the housing weight is 24% of the total transmission weight. It is recognized that minimum wall thickness in nonstructural areas is limited by the casting process. Nevertheless improvements in weight can be realized in the thicker structural support regions.

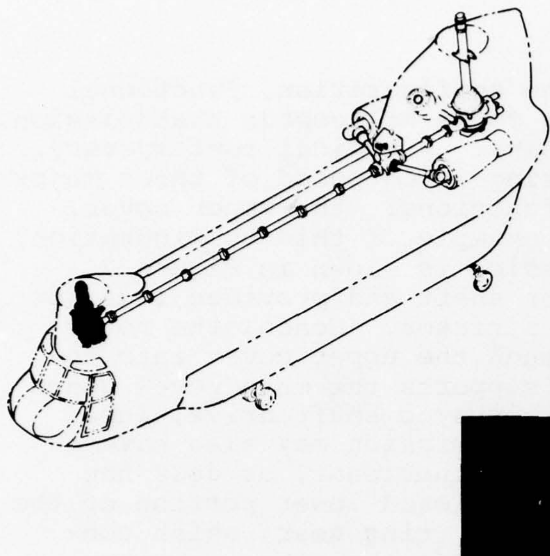

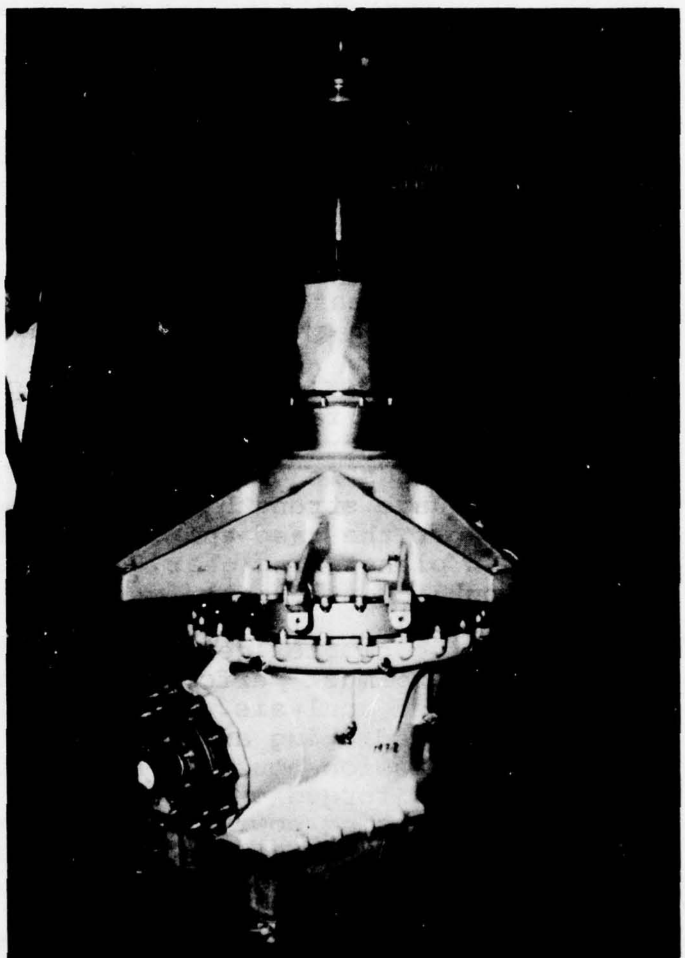

Figure 2. CH-47C Forward Rotor Transmission

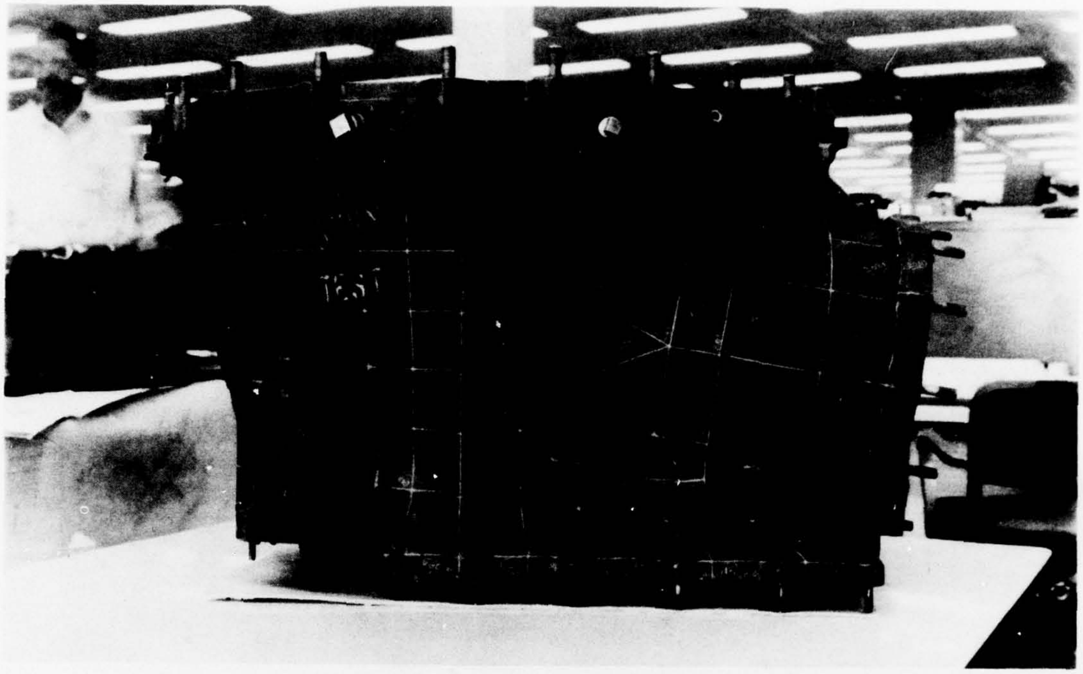

Figure 3. CH-47C Forward Rotor Transmission Case – a. Left Side View

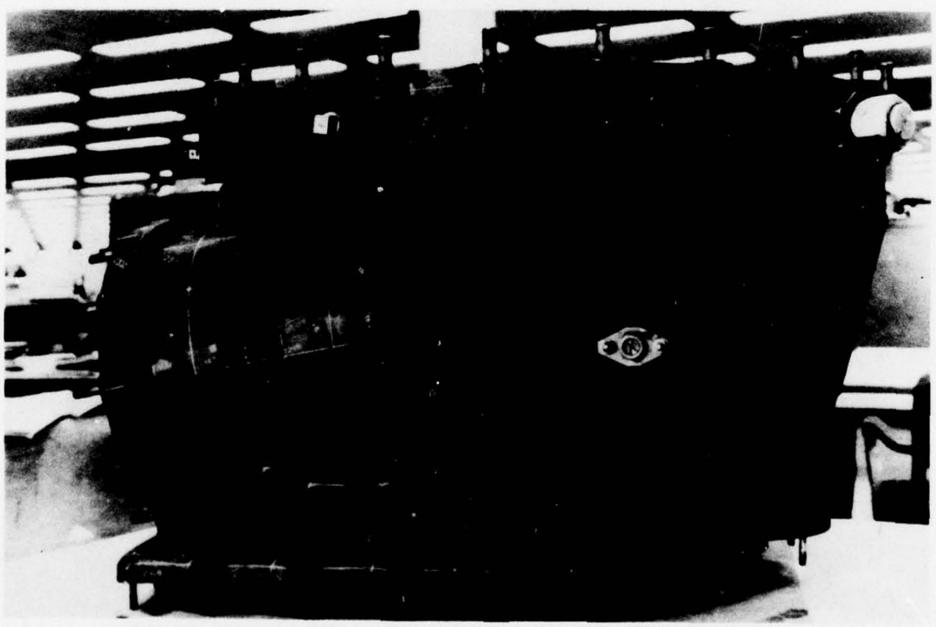

Figure 3. Continued – b. Right Side View

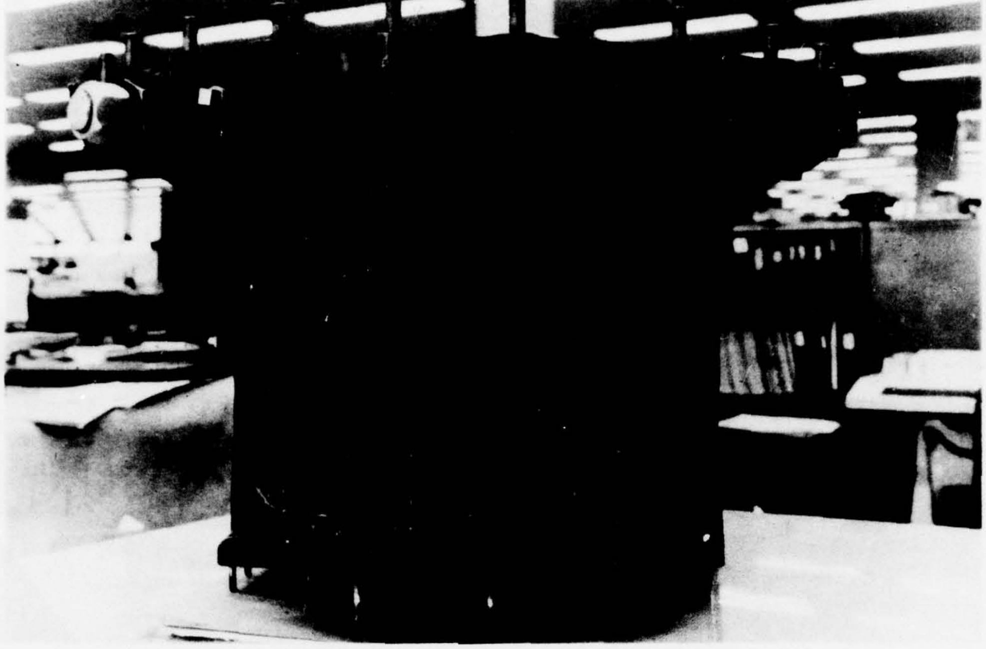

Figure 3. Continued – c. Front View

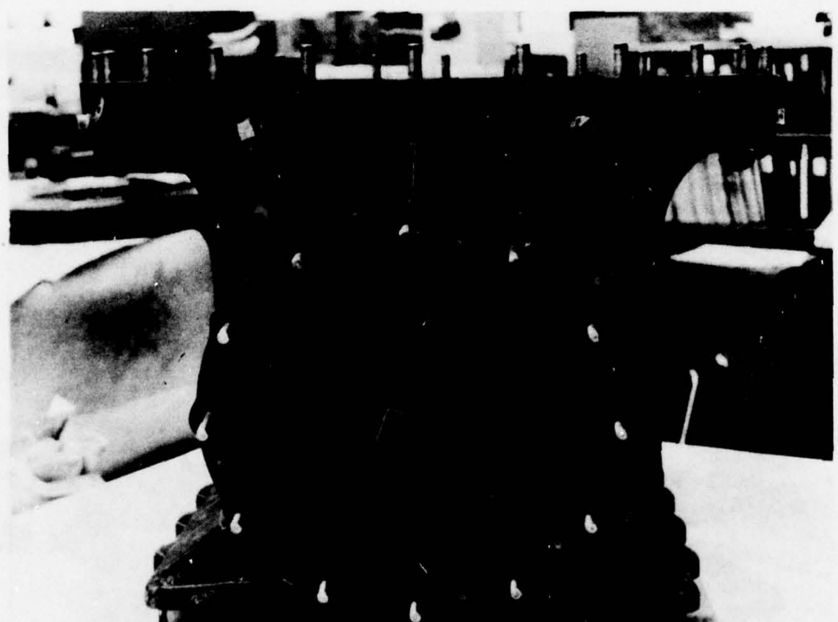

Figure 3. Continued – d. Aft View

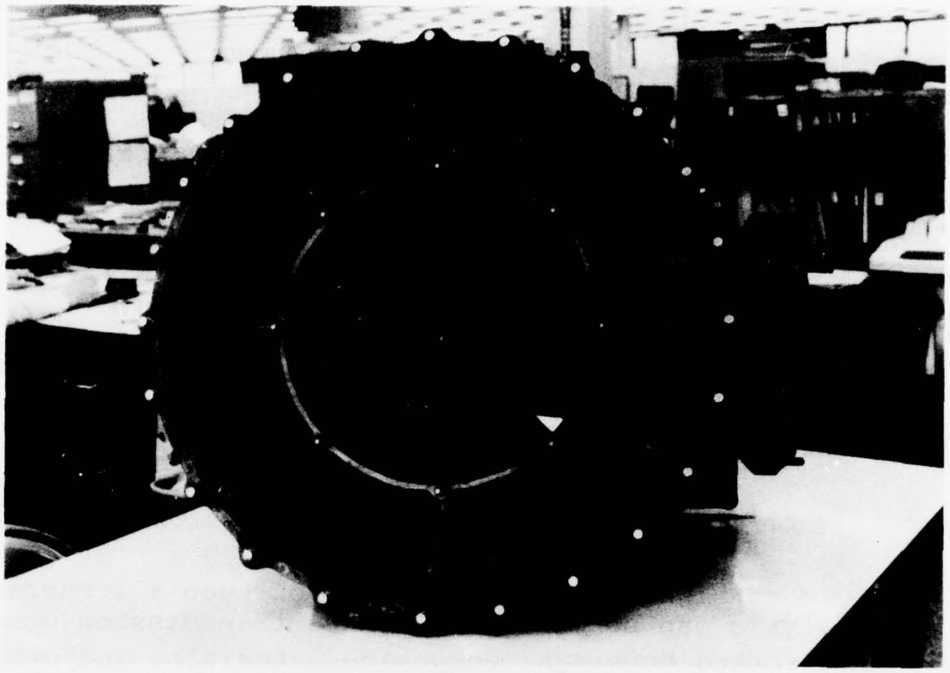

Figure 3. Continued – e. Top View

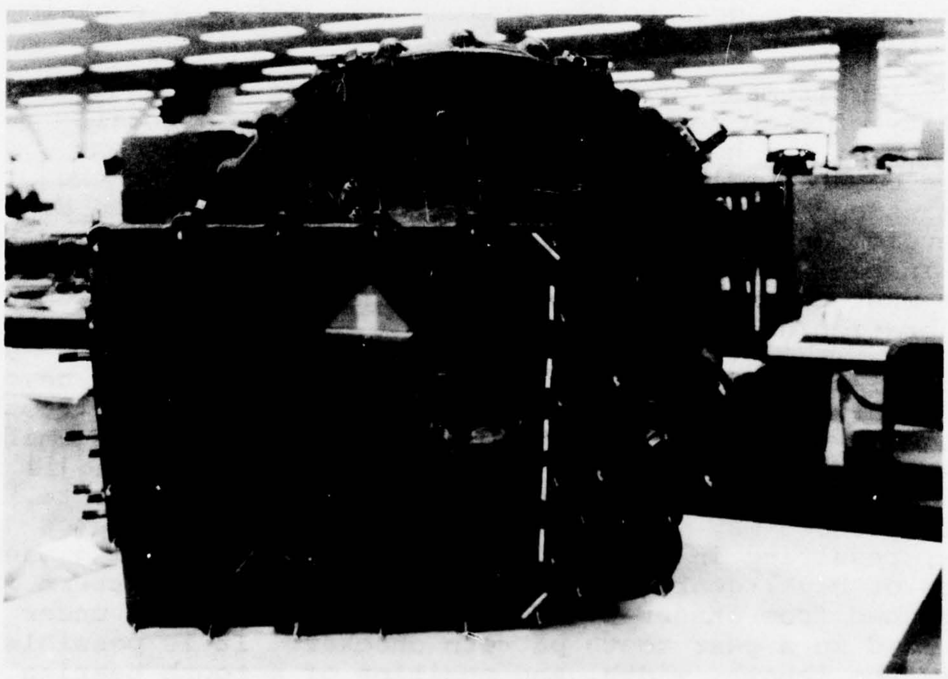

Figure 3. Continued – f. Bottom View

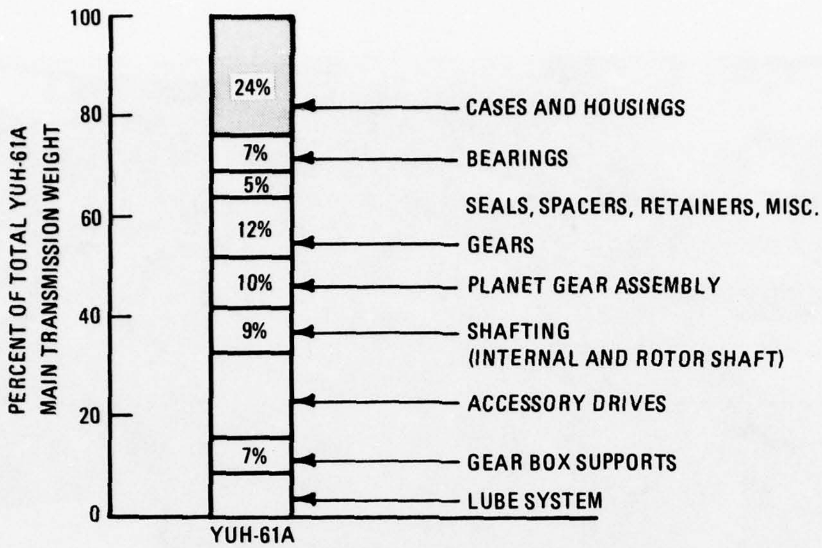

Figure 4. Example of Main Transmission Weight Breakdown

Considerably more significant application of such a structural load path analysis can be made to advanced transmission concepts employing fabricated housings, composite materials, and other advanced concepts, which will permit greater design flexibility. For example, major load paths could be selectively reinforced while the thickness of non-load carrying regions of the housing wall could be reduced to the minimum necessary for containment of the lubricant.

A basic requirement of a helicopter transmission is dimensional stability of each gear-mesh, which implies dimensional stability of the housing and bearing mounting locations. Because of the influence of the housing stiffness on the transmission internal components, it must be optimized during the development of an advanced technology transmission system. Also, initial knowledge of the dynamic stability of the system must be obtained to avoid resonances and the accompanying vibration/noise.

Analytical evaluation of the load-carrying capacity of bevel gears involves assumptions regarding the nature of the tooth bearing for the specific gear mountings under load. A uniform stress distribution across the tooth and rigid mounting is typically assumed. Unless these assumptions are accurate, actual stresses may vary considerably from the calculated values, resulting in a possible life reduction. During manufacture of bevel gears, the desired tooth contact pattern is established from observation of the pattern obtained under light load in a gear tooth pattern checker. It is possible to vary the length, width, and position of a tooth bearing by selection of grinding wheel diameters and grinding machine settings. This procedure is known as developing the tooth bearing contact pattern.

With gear mountings that are rigid, the behavior of the tooth bearing under load is usually more predictable, and thereby can be developed using previous experience. However, in the case of aircraft applications, the mounting designs are markedly different in that rigidity is sacrificed in favor of weight reduction. Therefore, it is seldom possible to accurately predict, during the design stage, the size and position of the tooth contact pattern required at no load in order to obtain the desired bearing pattern in the final gear mountings. A study of the mounting design and operating conditions together with a judgement based on experience must be utilized to establish the initial tooth bearing. From this point, the development of the final tooth bearing is accomplished by actual trial of the gears in their final mountings.

Predicted improvements in the load capacity for gears and bearings may be offset in practice by poor load distribution resulting from misalignment caused by the deflection of mounting surfaces within the housing (Figure 5). The detrimental effects of misalignment on gear teeth is documented by the AGMA (Reference 1). Gear tooth bending and surface contact stresses are proportional to load distribution factors (K_m, C_m). These factors evaluate the effects of nonuniform load distribution.

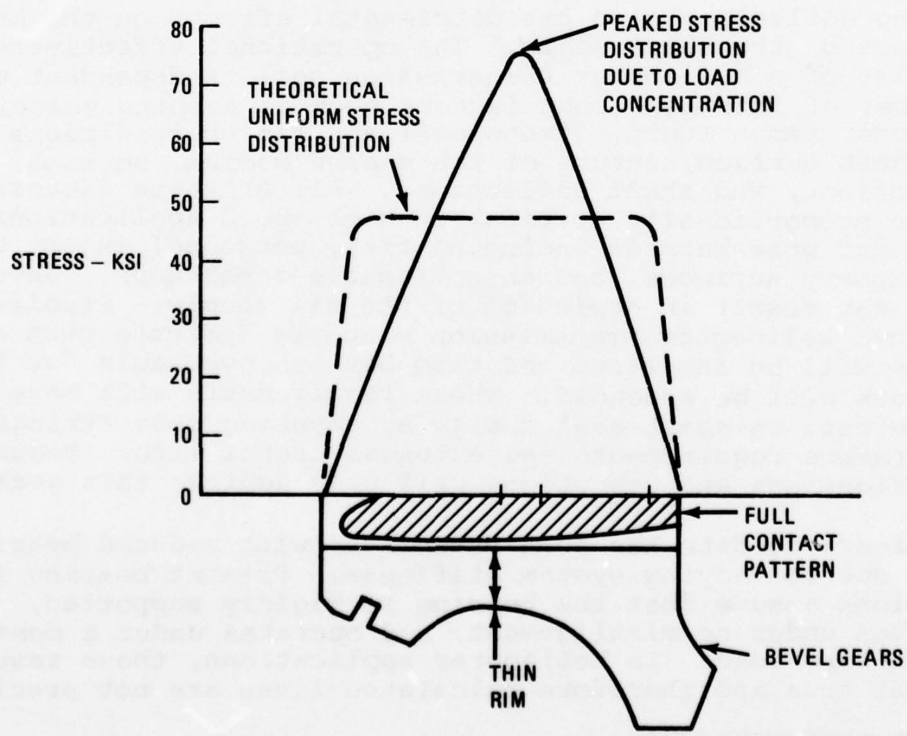

Figure 5. Measured and Theoretical Stresses in Thin Rimmed Bevel Gears

---

1. American Gear Manufacturers Association Standard 210.02.

They are dependent upon several factors including gear mesh misalignment due to housing distortion caused by loads and thermal variations (Figures 6 and 7). The effect of different rates of misalignment is shown in Figure 8. F_m represents the face width having 100-percent contact for a given tangential load and misalignment error. Uneven load distribution caused by significant shaft misalignment will result in tooth pitting and scuffing failures. Gear mesh misalignment is also important from the aspect of vibration/ noise generation (Figure 9, Reference 2).

Shifting of the gear tooth contact pattern may also be caused by differential thermal growth. When two bevel gears are properly mounted, and given that the gears have been properly manufactured and the bearing/gear positioning shim stack "heights" are properly assembled, the cone centers are coincident (at room temperature). Since the gears and bearings are made of steel and the housing and bearing cartridges are made of magnesium, differential thermal expansion (thermal coefficient of mag approximately twice that of steel) would cause the relative positions of the bevel pinion and gear to change. The cone centers would not be coincident at operating temperature and the tooth pattern and stress distribution across the tooth would change.

Housing deflection also has detrimental effects on the performance of the shaft seals. The operational effectiveness and life of a helicopter transmission seal is dependent upon a number of interdependent factors such as rubbing velocity, pressure, temperature, dimensional and finish conditions of the shaft surface, nature of the sealed medium, housing deflections, and shaft deflections. All of these factors become proportionally critical in high speed applications. "Leakers" pose hazards including fire, personnel injury due to slippery surfaces, and objectionable appearance. Severe seal leaks can result in depletion of the oil supply. Studies of advanced helicopter transmission concepts indicate that shaft speeds will be increased and time between overhauls for transmissions will be extended. These requirements will have a direct effect on shaft seal design by imposing more stringent performance requirements and extended useful life. Reduction of deflections and vibrations will help achieve this goal.

Experience to date has been associated with reduced bearing lives due to varying system stiffness. Present bearing life equations assume that the bearing is rigidly supported, operates under no misalignment, and operates under a constant and uniform load. In helicopter applications, these assumptions are not true and therefore calculated lives are not precise.

---

2. George C., GEAR NOISE SOURCES AND CONTROLS, Detroit Diesel Allison, Division of General Motors Corporation.

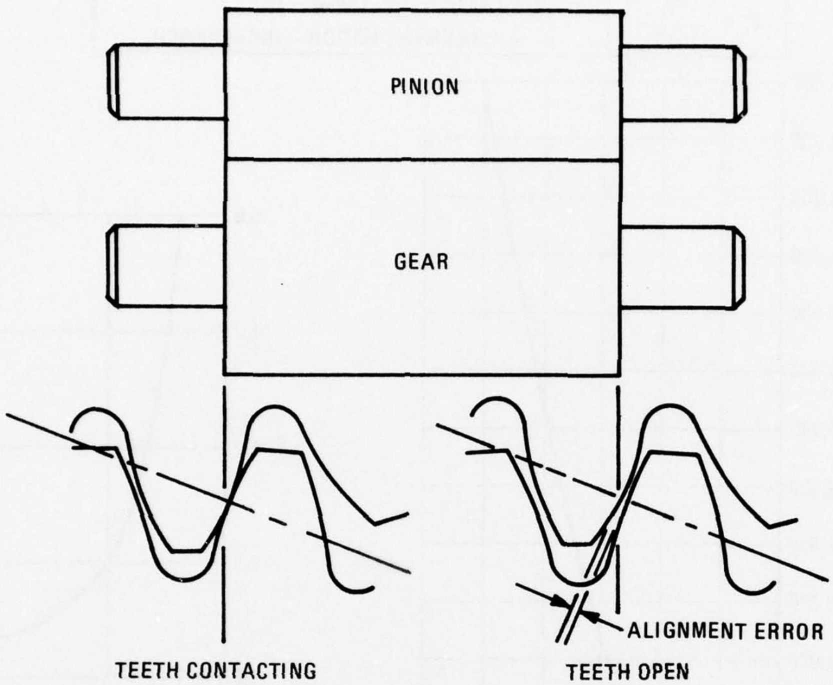

(REFERENCE 1)

Figure 6. Example of a Pinion and Gear Misalignment Under No Load

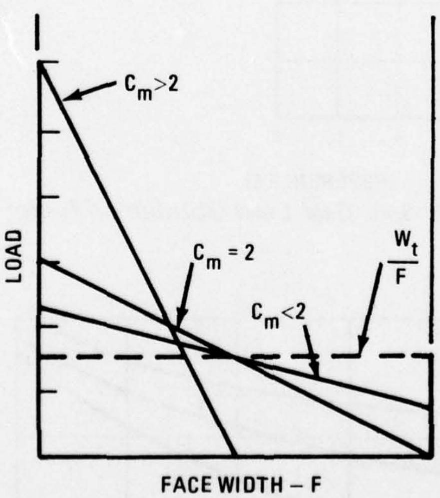

(REFERENCE 1)

Figure 7. Load Distribution Across Face Width for Various Contact Conditions

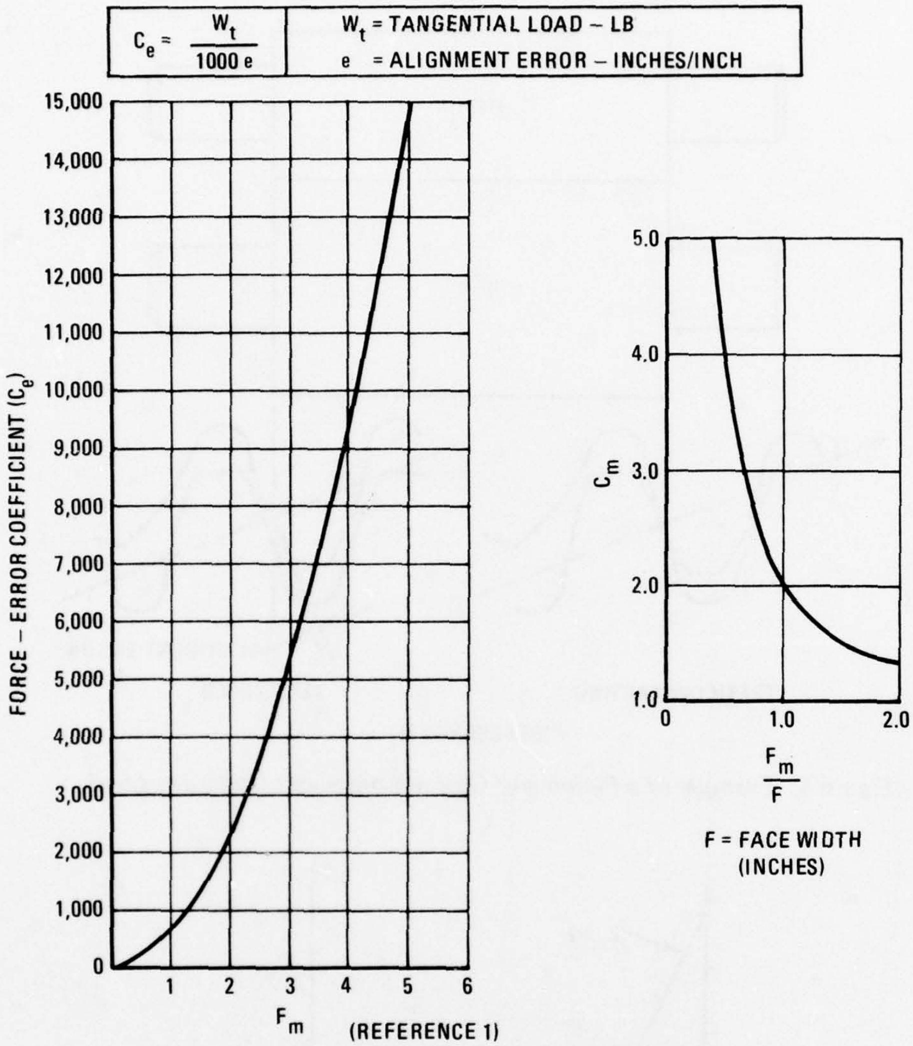

Figure 8. Spur Gear Load Distribution Factor — c_m

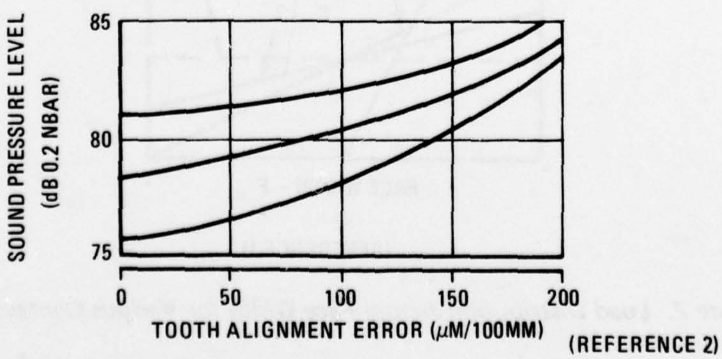

Figure 9. Influence of Tooth Alignment Error on Gear Noise

Early bearing failures have resulted from shaft misalignment (edge loading) and nonuniform housing support (local hard spots). Present methods of bearing analysis, which include complex computer programs, have very limited capabilities of evaluating the effect of structural shapes and flexibility on bearing life. An example of this type of problem has been experienced during the testing of a large swashplate bearing (Reference 3). This bearing was sized by the best available computer programs and modified in an attempt to account for structure deflection. After 239 hours of testing, two bearings failed due to distress caused by the ball riding over the edge of the inner and outer races. Investigation of the failure revealed that relatively large structure deflection (0.016 inch ring separation) resulted in high local loading and excessive race depth requirements. The severe effect of misalignment on bearing life is further shown in Figure 10.

In order to reduce this type of failure, special consideration must be given to the uniform, rigid support of critical components. Reduced shaft and housing deflection will result in better performance and life of gears, bearings, and seals. Therefore, analytical methods must be developed which will permit evaluation of important design parameters, allow trade-studies, and provide guidance to designers. The specific topics being investigated under this program and the areas of anticipated benefit are summarized in Table 1.

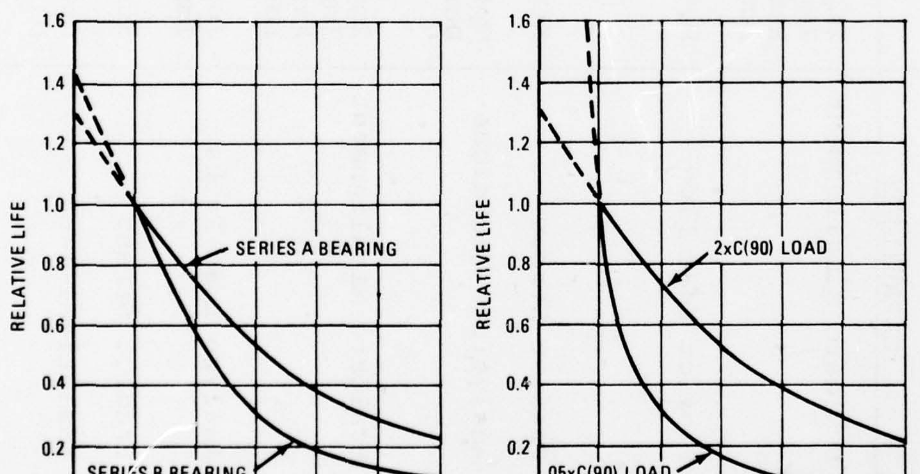

Figure 10. Effect of Misalignment on Service Life (REFERENCE 4)

3. Lenski, J. W., HLH SWASHPLATE FAILURE ANALYSES, Boeing Vertol Inter-Office Memorandum 8-7462-1-40, dated 10 July 1974.

4. Leibensperger, R. L., WHEN SELECTING A BEARING LOOK BEYOND CATALOG RATINGS, Machine Design, April 1975, Pages 142-147

TABLE 1. AREAS OF INVESTIGATION

	CAPABILITY	POTENTIAL IMPROVEMENTS	PARAMETER AFFECTED
Thermal Analysis	Evaluate Misalignment	Improved Load Capacity Improved Load Distribution Reduced Vibration/Noise Longer Life of Components	Weight Reliability Reliability Reliability
	Predict Heat Flow	Develop Oil-Off Operating - Capability - Develop Higher-Temperature Integral Cooling System	Survivability Vulnerability
	Predict Stress	Structural Efficiency	Weight
	Analytical Technique	Optimize New Transmission During Initial Design	Weight, R/M, V/S and Producibility
Stress Analysis	Evaluate Misalignment	Improved Load Capacity Improved Load Distribution Reduced Vibration/Noise Longer Life of Components	Weight Reliability Reliability Reliability
	Analyze Load Paths	Improved Load Capacity Improved Fail-Safety	Weight Survivability
	Predict Stress	Structural Efficiency	Weight
	Analytical Technique	Optimize New Transmission During Initial Design	Weight, R/M, V/S and Producibility

ANALYTICAL/COMPUTER METHODOLOGY

For the work conducted under this contract, the finite element technique using the NASTRAN computer program was selected for structurally analyzing the housing stresses, dynamic response, deflections, and thermal effects, as well as strength, weight, and fail-safe/safe life.

The development of this approach results in an advanced tool for analyzing a transmission housing through the use of finite element techniques. Since NASTRAN is used, the results indicate the feasibility of using NASTRAN as a versatile transmissions design tool, specifically in the areas of:

1. Thermal distortions, cooling requirements.
2. Stress Analysis
   A. Maneuver Loads
   B. Crashworthiness simulation using inertia relief capability of NASTRAN (Rigid Format 2).
3. Dynamic analysis due to n per rev hub excitations.
4. Weight reduction through optimization schemes such as strain energy distribution or fully stressed design analysis.
5. Design of conceptual transmissions.
6. Reduction of bearing misalignment by developing a stiffer case and evaluating geometry and slope changes. Reduction of load maldistribution across gear teeth and improved gear life by similar means.
7. Consideration of fail-safe/safe life, survivability and vulnerability by, for example, simulating a crack in the model.
8. Assess radar cross-section by evaluating scale plots of the transmission drawn at any specified orientation.
9. Effects of nonlinear behavior of bearings.

The contractor has utilized pre- and post-processor computer programs compatible with NASTRAN to improve its utility. Examples of such programs are SAIL II (an input data generator) and S-83 (strain energy analysis).

The automatic generation of grid point coordinates, element connectivity, etc., is essential for complex models. Boeing has developed a sophisticated finite element input capability for use with NASTRAN entitled SAIL II (Structural Analysis Input Language). This preprocessor allows the user to take advantage of any pattern that occurs in the data by making available straight-forward techniques for describing algorithms to generate blocks of data. Grid points and element connections may be generated. This program, although proprietary to the contractor, has been utilized, and is available for purchase by industry. An alternative for nodal generation and/or connectivity would be user generated WATFOR computer programs which would punch-out the NASTRAN input bulk data cards. Although the contractor has used SAIL II and feels that this program is more versatile, other users of NASTRAN can conduct the same work by alternate methods. The Boeing Vertol SAIL II computer program will be compatible for use with NASTRAN Level 16.

For ease of identification a complex model is typically subdivided into several regions and the grid points in each region are labeled with a specific, but arbitrary, series of numbers. Although these grid point numbers act only as labels, they effect the bandwidth of the stiffness and mass matrices. In order to minimize the matrix bandwidth for most efficient running of NASTRAN, the BANDIT computer program (Reference 5) can be used to automatically renumber and assign internal sequence numbers to the grid points. The output from BANDIT is a set of SEQGP cards that are then included in the NASTRAN bulk data deck, and which relate the original external grid numbers to the internal numbers. numbers.

After reviewing many of the structural optimization methods in existence (see Appendix A), strain energy and stress-ratio resizing techniques were employed. For applications such as helicopters where weight is critical, it is more appropriate to evaluate the strain density (strain energy/volume) distribution within a structure which provides guidance for structural optimization. A strain density analysis for dynamics applications has been

---

5. Everstine, G., BANDIT - A COMPUTER PROGRAM TO RENUMBER NASTRAN GRID POINTS FOR REDUCED BANDWIDTH, Naval Ship Research and Development Center Technical Note AML-6-70, February 1970.

developed by Boeing Vertol under ARO Contract DAHC04-71-C-0048 (Reference 6). Expanding upon this work, a post-processor program (S-83) compatible with NASTRAN has been developed for analysis of the strain density distribution throughout a structure for dynamics application and is based on the concept that for a given load condition, a uniform strain density under distortion yields a maximum stiffness/minimum weight structure. This program uses stress data output by NASTRAN, calculates the strain density of each element, and tabulates these from highest to lowest. By employing the ALTER feature of NASTRAN, a checkpoint tape containing the stresses for each element is generated. The post-processor program uses the data stored on the checkpoint tape to calculate the strain density of NASTRAN plate elements and tabulates the elements in descending order of strain densities. The structural elements with the highest strain density are the best candidates for effective optimization since a minimal weight change will yield a maximum benefit. By locally altering the housing wall to change the mass and stiffness in these areas of high strain density, the structure can be optimized. This strain density distribution concept can also be utilized statically to identify structural load paths and to evaluate the efficiency of the housing structural design (stiffness/weight). The S-83 strain density computer program can be used for both static and dynamic analyses (including thermal effects). Under modal distortion for a given natural frequency, a uniform strain density yields a maximum lowest eigenvalue/minimum weight structure. The computer model, pre- and post-processor programs, and all computer data and format are compatible with NASTRAN (commercial or Schwendler version). The capabilities of NASTRAN for automated plotting and analysis of composite materials are also utilized.

In order to be able to realistically determine thermal distortions/stresses for a new or conceptual transmission case, it is necessary to calculate the output of the heat sources which are the gear meshes and bearings. Since this capability does not exist in NASTRAN, the results of the existing Boeing Vertol computer program, which have been extensively used and thoroughly validated for the analysis of bearings (S04) and gears (R20 bevel, R23 spur and helical), were applied to calculate power dissipation and the resultant heat generation. Using these results as the driving potential for the thermal analysis, NASTRAN was then run for a steady-state heat

6. Sciarra, J., USE OF THE FINITE ELEMENT DAMPED FORCED RESPONSE STRAIN ENERGY DISTRIBUTION FOR VIBRATION REDUCTION, U.S. Army Research Office - Durham, Final Report Contract DAH-C04-71-C-0048, July 1964.

solution (heat balance) using the housing model. Cooling was provided by modeling the oil flow and incorporating it into the solution. Nodal temperatures were punched out automatically on cards in a format compatible with NASTRAN input. A thermal distortion/stress analysis followed using the same basic model. This was accomplished using Rigid Format 1 (Static Analysis) of NASTRAN.

The use of computer programs that are proprietary to Boeing Vertol presents no gap in the final product to be delivered under this contract. The bevel gear program (R20) is based on Gleason commercially available dimension sheet methods, and the spur/helical gear program (R23) is based on standard AGMA information. The rolling element bearing analysis program (S04) was purchased by Boeing Vertol from Mr. A. B. Jones, bearing consultant, and is also commercially available to other users. Furthermore, most industrial and commercial potential users of the finite element structural analysis method have their own gear/bearing analyses.

The present NASTRAN transmission model uses elements with a solid homogeneous cross-section which allow for both membrane and bending stiffness. The material properties are isotropic. These conditions represent the solid cast structure of current helicopter transmissions. However, the following options exist within NASTRAN to allow analysis of structures made of composite materials:

- A solid homogeneous cross-section element with anisotropic material properties.
- Sandwich plate elements that can reference different materials for membrane, bending, and transverse shear properties, each of which may have either isotropic or anisotropic material properties.
- A general element whose properties are defined directly by the user in terms of influence coefficient or stiffness matrices.

The particular element chosen is dependent upon the type of composite material to be represented. The NASTRAN model may also be modified to analyze fabricated truss type structures.

The flowchart presented in Figure 11 summarizes the overall transmission housing analysis. The previously existing work and the items developed herein have been identified, and it is shown how the work herein contributes to the overall design goals.

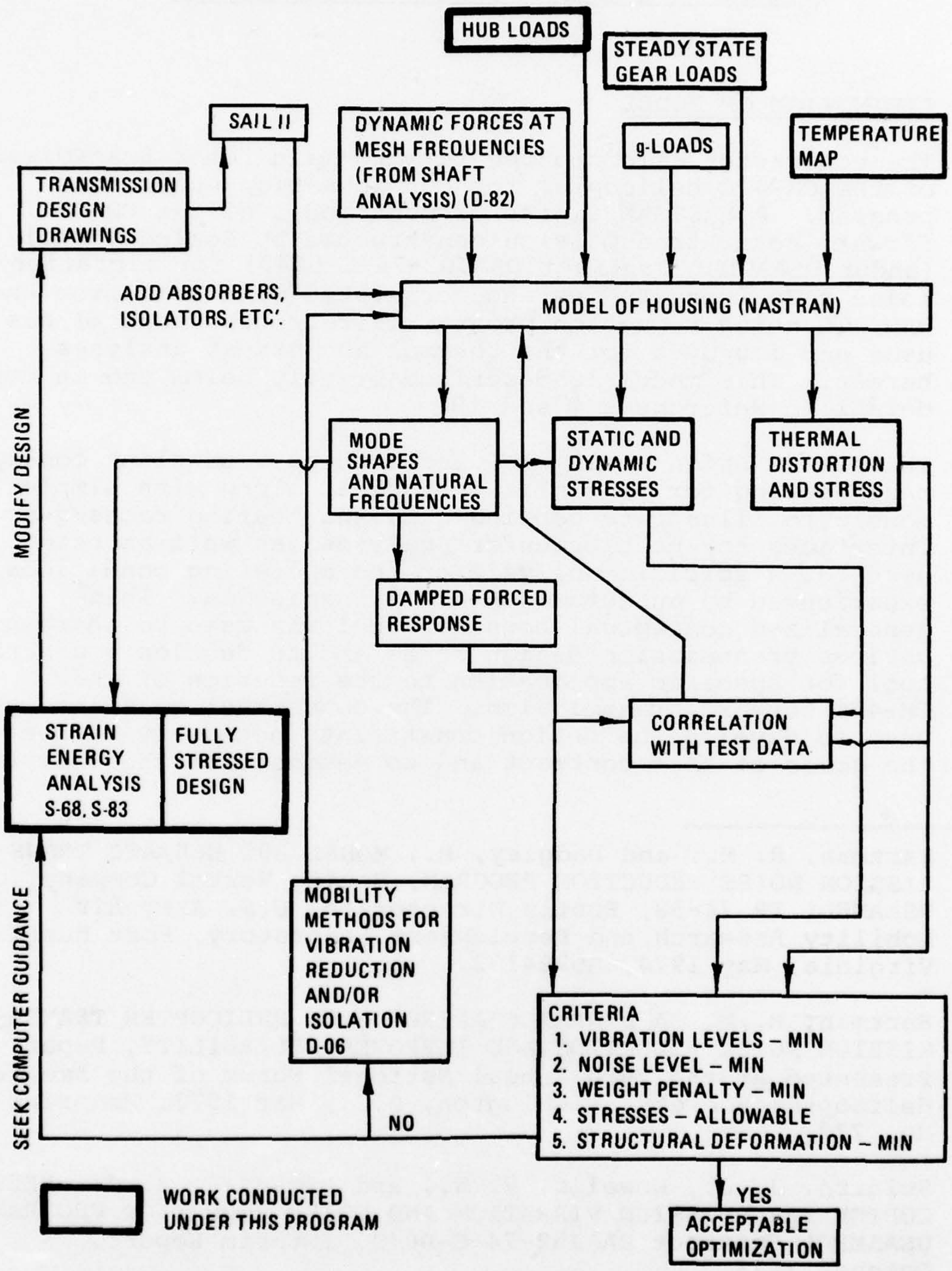

Figure 11. Flow Diagram of Transmission Housing Analysis

DESIGN ANALYSIS OF TRANSMISSION HOUSING

I. DEFINITION OF MODEL

The contractor selected the forward main rotor transmission of the CH-47C helicopter for consideration under this program. A NASTRAN finite element model of the CH-47 forward rotor transmission constructed by Boeing Vertol (under USAAMRDL Contract DAAJ02-74-C-0040) for vibration/noise reduction studies and correlated with data from the HLH/ATC noise reduction program (References 7 and 8) was used and improved for the thermal and stress analyses herein. This model is described briefly below and in more detail in References 9 and 10.

The transmission model was used both as a baseline conceptual housing for generalized studies, along with simpler models to illustrate cooling fins and bearing races/gear interfaces for heat transfer analyses, as well as being used for a specific analysis of the operating conditions experienced by an actual CH-47C transmission. This generalized conceptual housing model was used to address various transmission design areas and to develop a general tool for specific application to the redesign of the CH-47C forward transmission. The conceptual baseline was used to develop the design constraints necessary to meet the goals of this contract and to demonstrate the analytical

---

7. Hartman, R. M., and Badgley, R., MODEL 301 HLH/ATC TRANSMISSION NOISE REDUCTION PROGRAM, Boeing Vertol Company, USAAMRDL TR 74-58, Eustis Directorate, U.S. Army Air Mobility Research and Development Laboratory, Fort Eustis, Virginia, May 1974, AD784132.

8. Hartman, R. M., A DYNAMICS APPROACH TO HELICOPTER TRANSMISSION NOISE REDUCTION AND IMPROVED RELIABILITY, Paper Presented at the 29th Annual National Forum of the American Helicopter Society, Washington, D.C., May 1973, Preprint No. 772.

9. Sciarra, J. J., Howells, R. W., and Lemanski, A. J., HELICOPTER TRANSMISSION VIBRATION AND NOISE REDUCTION PROGRAM, USAAMRDL Contract DAAJ02-74-C-0040, Interim Report, October 1975.

10. Howells, R. W., and Sciarra, J. J., FINITE ELEMENT ANALYSIS USING NASTRAN APPLIED TO TRANSMISSION VIBRATION/NOISE REDUCTION, NASA TMX-3278, September 1975.

technique developed through design of a housing to meet the design constraints selected. Several areas of potential improvement needing further consideration have been identified:

- Housing Material - Desirable Properties
  - Inherently high stiffness and strength.
  - Good high temperature strength to provide gear and shaft support even when running under emergency lube conditions and under operating temperatures of 350°F.
  - Use material forms like composites or rolled sheet which lend themselves to very thin sections in areas where oil containment is the main requirement.
  - The housing material strength/elongation properties should accept the hydraulic ram effect that cracks castings after ballistic impact.
  - Should not support combustion as magnesium does.
  - Inherent cooling capabilities.
- Housing Construction and Geometry
  - Minimize interfaces, doubled thicknesses, and bolted joints.
  - Simplify the rotor load path and minimize bending as far as possible.
  - Locate gears as rigidly as possible by reacting their loads through a direct, short and rigid load path. Locate bearings to minimize bending loads on the support structure.
  - Insure rigid support locations at housing/rotating component interfaces.

The above design features and the increasing performance demands placed upon helicopter transmissions have led to interest in the possible use of advanced composite materials for transmission housings. Although composites have been applied with much success for many aircraft parts, their use for transmission housings is new. Many design areas must be addressed: load path definition for orientation of non-isotropic material properties; fabrication, tooling and machining methods; thermal properties, etc.

A USAAMRDL/BHC program (Reference 11) was previously conducted to evaluate carbon/epoxy as a possible transmission housing material. Machining of the carbon/epoxy material was found to be difficult, and grinding had to be used almost exclusively to finish the composite housing. Also, the thermal conductivity and structural integrity of the carbon/epoxy housing was found to be poor. Stiffness was slightly improved as evidenced by gear development testing. The lack of success of this particular program should not deter the pursuit of composites as a housing material. Conversely, the problems encountered during the program indicate the need for accurate analysis and careful design as well as the development of acceptable fabrication procedures.

For example, structural failures occurred at bonded joints in tension. Such a design does not utilize the properties of composites properly and must be avoided. Another example is the concern over the low thermal conductivity of nonmetal composites. Graphite/polyimide has a lower thermal conductivity than magnesium by a factor of about 25 to 1, thus heat dissipation from the housing will be less than that of a magnesium equivalent and areas of higher temperature will be more localized. Since convection cooling through a magnesium case accounts only for an estimated 15% of the total heat rejection, the estimated weight penalty for the cooling system resultant is not prohibitive.

The second probable effect of the thermal conductivity difference is in the areas immediately adjacent to the bearings. Bearing heat will not be carried away as fast as it is with a magnesium housing. The coefficient of thermal expansion of molded polyimide with chopped graphite reinforcement is 6×10^{6} inch/inch°F, which is very close to steel (6.5×10^{6}). The effect on the bearing should be beneficial under conditions of both normal operation and lube interruption. That is, the temperature of the outer race should remain closer to the inner race under all conditions and thus eliminate the temperature gradient across the bearing, which is responsible for bearing seizure under abnormal conditions. Also, the housing will not expand away from the outer race when the thermal growth coefficients are matched. This will also tend to maintain a constant internal clearance and stabilized operating conditions in both normal and abnormal lubrication situations. The conclusion is that molded chopped graphite

---

11. Battles, Roy A., DYNAMIC TESTING OF A COMPOSITE MATERIAL HELICOPTER TRANSMISSION HOUSING, Bell Helicopter Company, USAAMRDL TR 75-47, Eustis Directorate, U.S. Army Air Mobility Research and Development Laboratory, Fort Eustis, Virginia, September 1975, AD A015521.

composite bearing supports, with thermal coefficients matched to bearing materials, will improve the ability to operate at design conditions as well as at abnormal lube conditions.

The finite element analysis considered herein is an essential tool necessary to handle the composite material properties most efficiently. Such analyses in combination with advanced materials promise to yield helicopter transmissions with substantially improved performance and lower life-cycle cost.

By utilizing the existing model of the CH-47C forward rotor transmission, the contractor has been able to:

- Cost-effectively conduct the thermal/stress analysis presented herein.
- Concentrate effort on the application of the model to derive useful information rather than on model building.
- Directly apply results of other related contracts.

Further reasons for selecting this model include:

- Model validation has provided confidence in its accuracy.
- Use of a widely accepted and throughly validated computer program (NASTRAN).
- Extensive computer-generated plotting capability used to debug the model.
- Cross-checking of the model, design drawings, and hardware.
- Good correlation of the model and hardware weights (Table 2).
- Test data is available from previous Boeing Vertol programs for model validation and correlation.
  - Housing displacements from HLH/ATC noise reduction program (Reference 7).
  - Housing temperatures from thermal mapping program (Reference 12).
- Hardware is available for further testing and modification.

---

12. Tocci, R. C., Lemanski, A. J., and Ayoub, N. J., TRANSMISSION THERMAL MAPPING, Boeing Vertol Company, USAAMRDL TR 73-24, U.S. Army Air Mobility Research and Development Laboratory, Fort Eustis, Virginia, May 1973, AD 767875.

TABLE 2. SUMMARY OF CH-47 FORWARD TRANSMISSION HOUSING NASTRAN MODEL.

MODEL PARAMETERS

	NUMBER GRID POINTS	NUMBER ELEMENTS	NUMBER DEGREES OF FREEDOM				BANDWIDTH			CPU TIME (HOURS)*
			TOTAL	SINGLE-POINT CONSTRAINT	OMIT	RETAINED	FULL	REDUCED	ACTIVE COLUMNS	
Upper Cover	160	202	960	184	614	162	34	162	0	.20
Ring Gear	216	192	1296	216	828	252	-	252	0	.1
Case	477	540	2862	529	2024	309	61	309	0	.6
TOTAL	853	934			For Dynamic Analysis Only					

*RIGID FORMAT 1 ON IBM 370

COMPARISON OF CALCULATED AND ACTUAL WEIGHTS*

	MODEL	HARDWARE	DIFFERENCE
Sump	3.7 kg (8.2 lb)	5.5 kg (12.2 lb)	**
Case	25.1 kg (55.4 lb)	24.6 kg (54.2 lb)	+ 2.2%
Ring Gear	34.9 kg (77.0 lb)	34.9 kg (77.0 lb)	0% (Lumped Masses for Teeth)
Upper Cover	62.8 kg (138.5 lb)	64.1 kg (141.4 lb)	- 2.0%

*(Case weight based on AZ91C cast magnesium alloy, density .065 lb/in^3; upper cover weight based on 2014-T6 forged aluminum, density .101 lb/in^3, both per MIL-HDBK-5B 1 September 71.)

**Model excludes internal passageways.

The Boeing Vertol CH-47 forward rotor transmission housing is composed of three major sections: upper cover, ring gear, and case (including sump). The upper cover provides lugs for mounting the transmission to the airframe and transmits the rotor system loads. The case contains and supports the main bevel gears. The ring gear, which connects the upper cover and case, contains the planetary gear system. This natural division of the housing was adhered to for ease of modeling (Figure 12).

The geometric grid points for the model were defined from design drawings and by cross-checking on an actual housing. CQUAD2 (Quadrilateral) and CTRIA2 (Triangular) homogeneous plate (membrane and bending) elements were used to connect the grid points and to build the NASTRAN structural model. A Boeing Vertol preprocessor program (SAIL II - Structural Analyses Input Language) for the automatic generation of grid point coordinates and structural element connections was used. This preprocessor allows the user to take advantage of any pattern which occurs in the data by providing straightforward techniques for describing algorithms to generate blocks of data. The extensive computer generated plotting capability of NASTRAN was used to debug the structural model.

For ease of identification the housing was subdivided into several regions, and the grid points in each region were labeled with a specific, but arbitrary, series of numbers. Although these grid point numbers act only as labels, they effect the bandwidth of the stiffness and mass matrices. In order to minimize the matrix bandwidth for most efficient running of NASTRAN, the BANDIT computer program (Reference 5) was used to automatically renumber and assign internal sequence numbers to the grid points. The output from BANDIT is a set of SEQGP cards that are included in the NASTRAN bulk data deck and which relate the original external grid numbers to the internal numbers.

The model includes grid points representative of the structure where the shafts are supported by their bearings. These grid points are used to apply the dynamic and static loads to the housing. Each geometric grid point has six possible degrees of freedom (three translational and three rotational). To conveniently evaluate the motion normal to the housing surface, numerous local coordinate systems were defined and oriented such that the displacements and accelerations calculated at each grid point could be referred to as a coordinate system having an axis normal to the housing surface. One degree of freedom, rotation about the normal to the surface, was constrained since the stiffness for this component is undefined for NASTRAN plate elements. The other two rotational degrees of freedom were omitted. All translational degrees of freedom were retained to accurately represent the motion of the actual housing. The model parameters are summarized in Table 2.

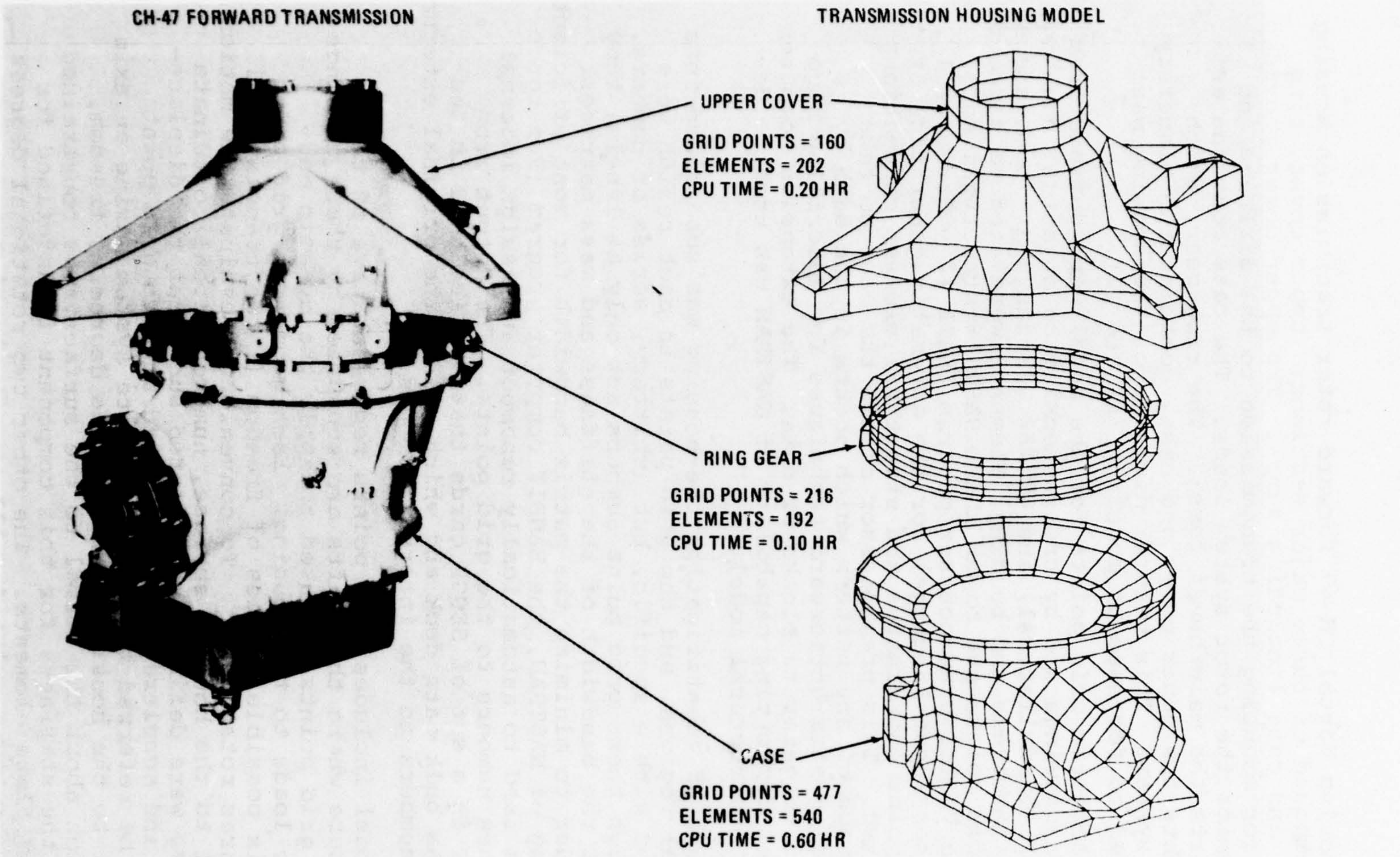

(DEVELOPED UNDER USAAMRDL DAAJ02-74-C-0040)

Figure 12. Boeing Vertol CH-47 Helicopter Forward Rotor Transmission Housing and NASTRAN Model

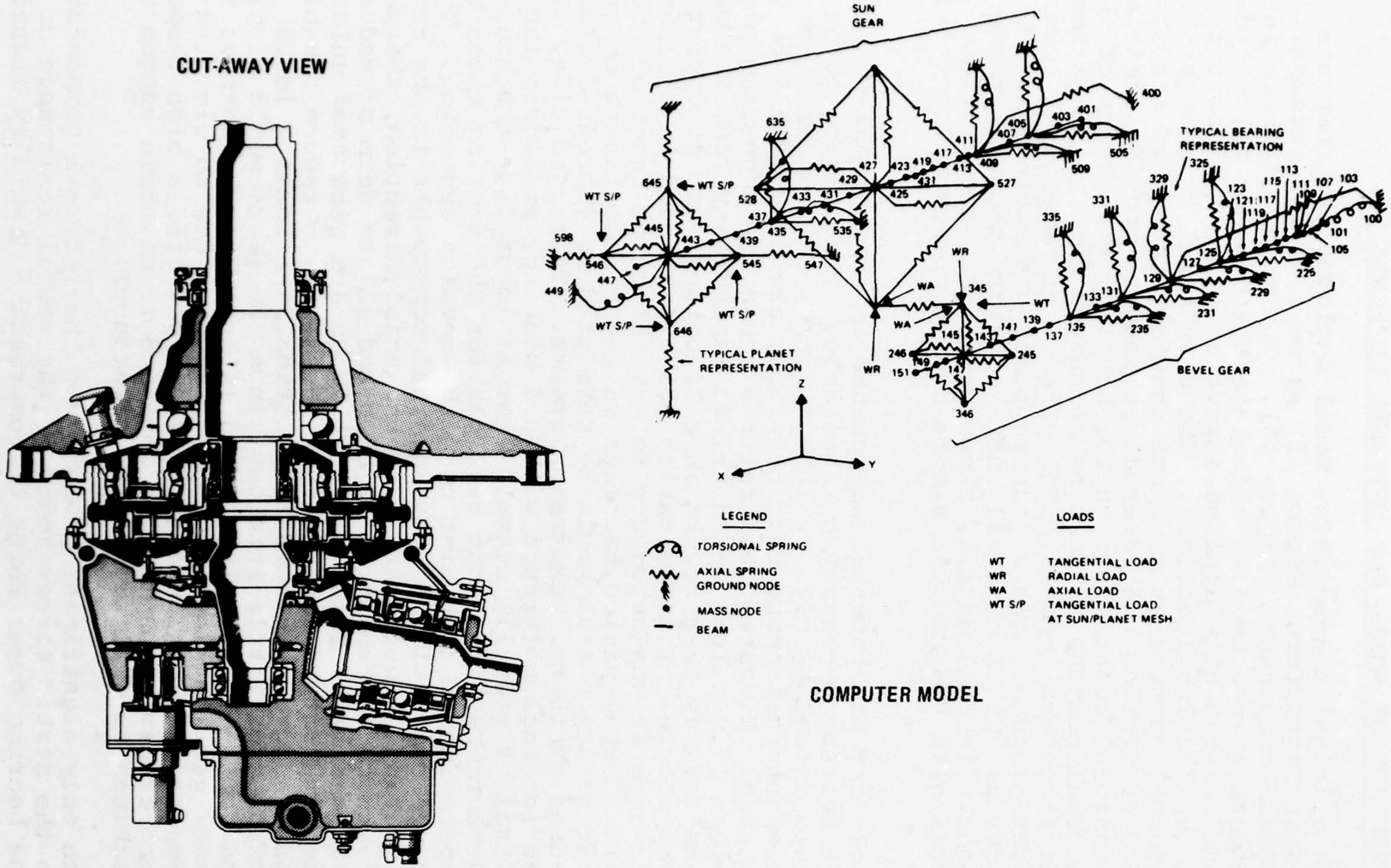

Figure 13. CH-47C Forward Transmission Internal Components

II. EXTENSION OF MODEL FOR INTERNAL COMPONENTS

The original transmission model included the complete housing structure (Figure 12) as well as the internal dynamic components (Figure 13). The model of these internal components was used to calculate the dynamic forces that were subsequently applied analytically to the housing model at the bearing locations. The structural aspects of the internal components were not considered. Since for static load conditions the internal components provide additional structural constraints on the housing, the effect of these internal components must be accounted for in the thermal and structural models. The effects of bevel, sun lower and upper planetary gears, and supporting structure were considered. It is generally not necessary to model these components in full detail, since only their gross effect on the housing is desired. A simple beam representation is adequate.

Including the internal components in the thermal model was neither necessary or desirable. The bearing outer races (steel $\alpha_s = 7.5 \times 10^{-6}$ in/in/°F), which are the case/internal component interface, are press fit into the housing. Elevated temperatures cause the magnesium case ($\alpha_m = 15.0 \times 10^{-6}$ in/in/°F) to expand away from the outer race and may even result in a "floating" fit at operating temperature. This situation was experienced in Reference 12, where it was necessary to key the outer races of the spiral bevel pinion bearings in their case liners to prevent rotation that would be permitted by increased clearances caused by thermal expansion/growth. This condition, plus the internal tolerance within a bearing, precludes the transmittal of radially outward thermal loads into the housing. Furthermore, it is not possible for the bearing races to impose radial restraint upon the housing expansion. Thus, no representation of the internal components in the radial direction is necessary. In the axial direction, thermal growth of the shafting is absorbed in the form of reduced gear backlash, Thus, no axial loads are generated unless the temperature exceeds that necessary to reduce the backlash to zero. In such a situation, the housing loads would be of little interest since the gears would distress and fail. Figures 14, 15 and 16 indicate the changes in bevel gear backlash and root clearance due to elevated temperatures. Allowing for these effects, a high temperature transmission must be designed to maintain adequate backlash as well as bearing clearances.

The only significant property of the internal components in the static stress model is the radial resistance of the bearing outer races to compressive (radially inward) forces acting on the housing.

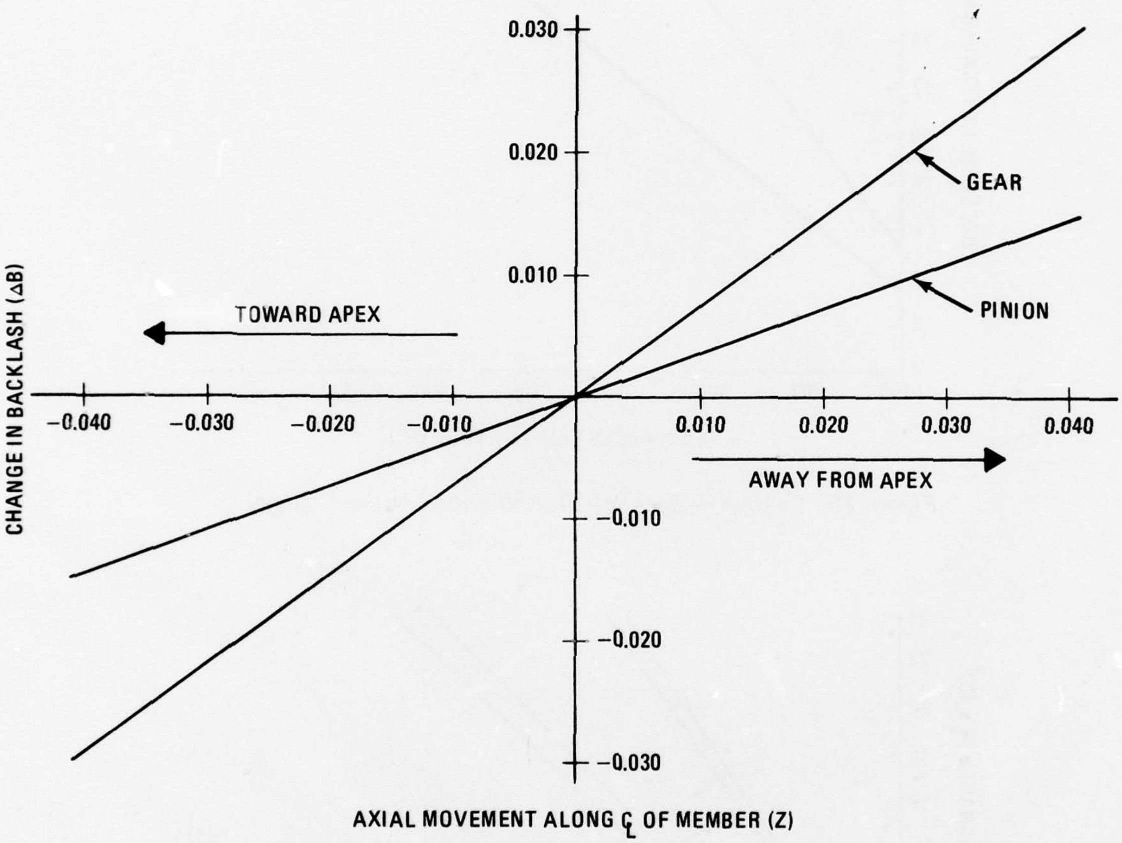

Figure 14. Change in Backlash Due to Axial Movement

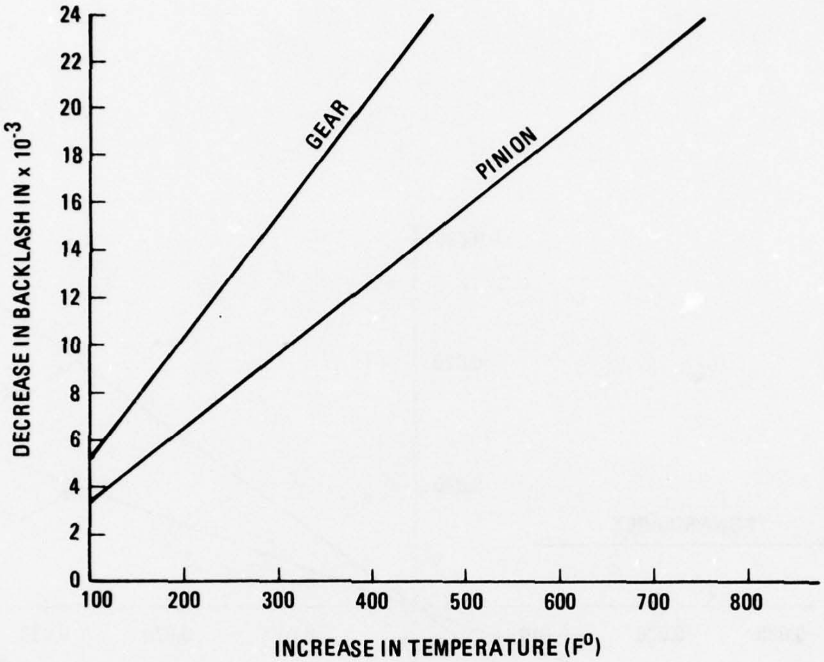

Figure 15. Change in Backlash Due to Temperature Change

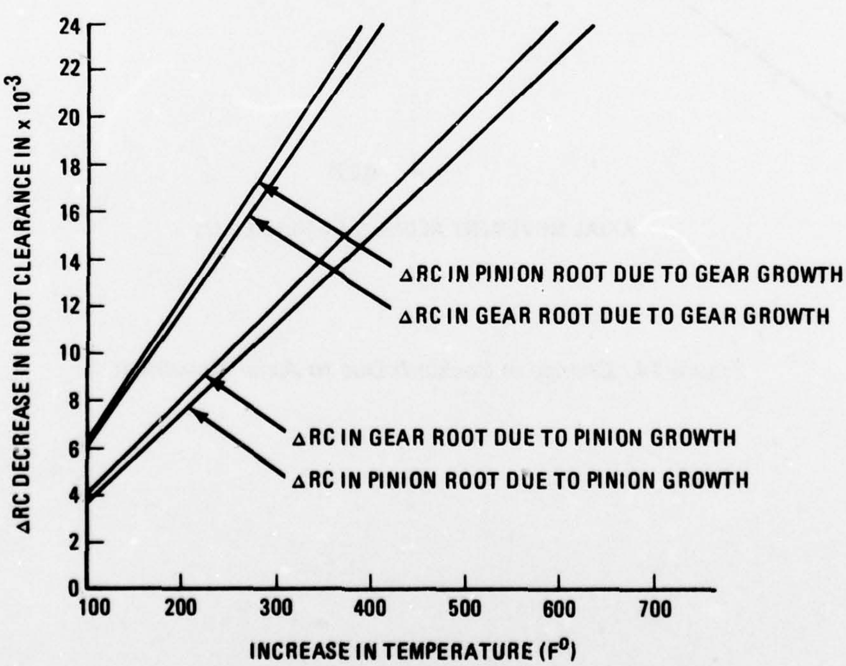

Figure 16. Change in Root Clearance Due to Temperature Change

bearing races offer no resistance to radially outward forces on the housing. A problem arises here due to the nature of the beam element. No capability exists in NASTRAN for a beam which will act in compression only. Thus, a beam model of a bearing race will also act to impose unwanted restraint on the housing directed radially inward. This could be circumvented by first analyzing the housing model without including the beams representing the races and thereby defining those housing/bearing interfaces with radially inward deflections. A beam model could then be inserted at these points to resist the radially inward forces and the analysis could be rerun. Figure 17 indicates the bearing/housing interfaces.

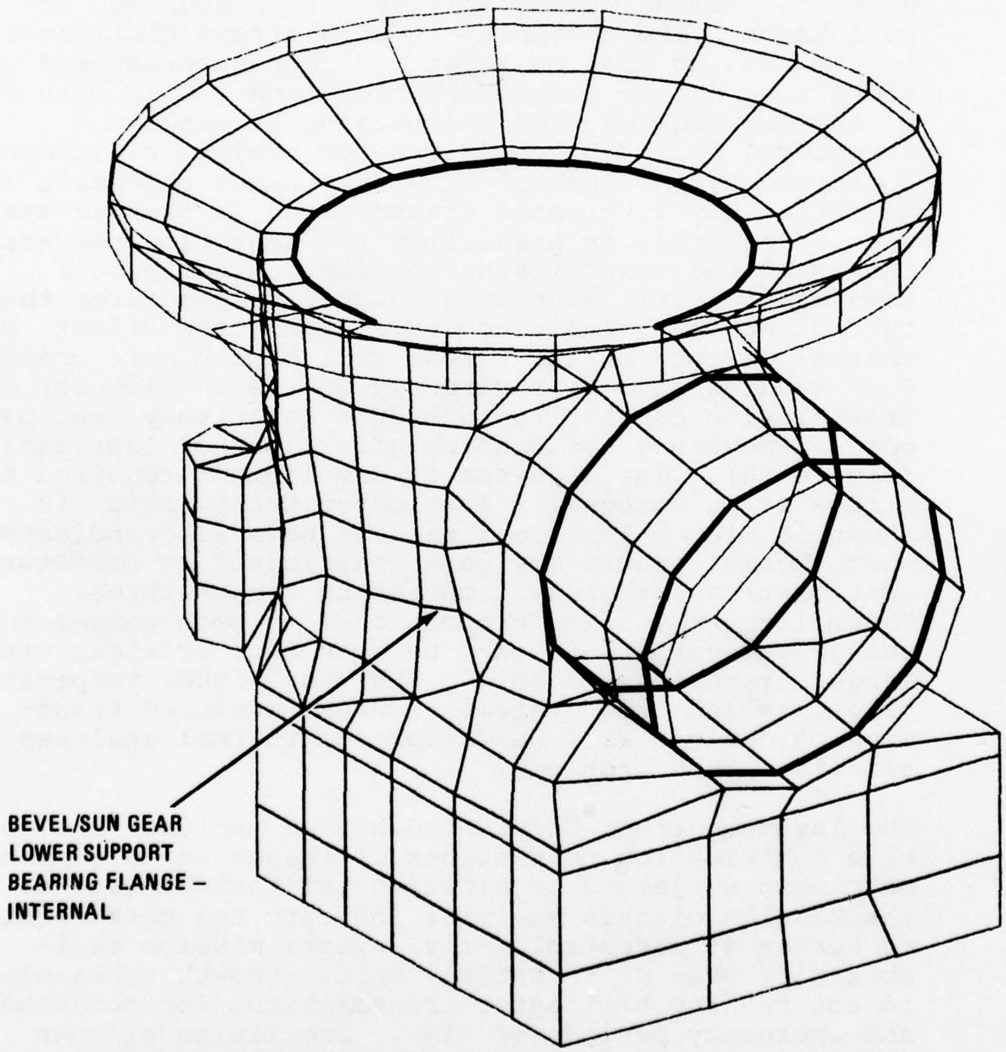

Figure 17. Shaded Lines Indicate Bearing Outer Race/Housing Interfaces

III. THERMAL DISTORTION AND THERMAL STRESS ANALYSIS

1. General

A complete thermal analysis must consider thermally induced deflections and stress as well as heat transfer characteristics. The capability for predicting the thermal distortion of a transmission housing under operating conditions is important from the aspects of load capacity improvement and avoidance of premature component distress. The sensitivities of bevel gear load capacity to tooth pattern and of bearing performance to mounting tolerances, both of which are affected by the dimensional stability of the housing, are well known. The thermally induced stress distribution in the housing must be known and then superimposed upon the stress due to static/dynamic loads. Only with such a detailed knowledge of the housing stress can a structural design be optimized for maximum efficiency. Furthermore, in line with the long range objective of an integrally lubricated transmission, a thermal analysis is required for predicting the heat flow characteristics of the transmission housing. Since such a transmission will operate at higher temperatures than current conventionally cooled systems, the effects of thermal distortion and stress will become more critical. Such studies also bear directly on the development of transmission capability to endure relatively long periods of emergency hot running after loss of lubricant (Figure 18). The sequence of development required to arrive at an integrally lubricated transmission is shown in Figure 19. Test results have also indicated that thermal growth may be a contributor to premature gear distress at present operating temperatures. Thermal growth, being proportional to both temperature change and component size, becomes more critical with larger transmissions (e.g., HLH) and higher temperatures (e.g., sealed-lube systems). Thus, advanced transmission designs will need improved thermal analyses to alleviate such problems.

The investigations documented herein indicate the relative contribution to distress of transmission components when subjected to differential thermal growth. The results of this analysis indicate the work required to arrive at acceptable drive system mission reliabilities when differential thermal growth takes place in hot running helicopter transmissions for continuous and emergency periods of time. The finite element transmission housing model discussed in a previous section is ideally suited for application to a thermal analysis. Figure 20 describes the thermal model of the housing.

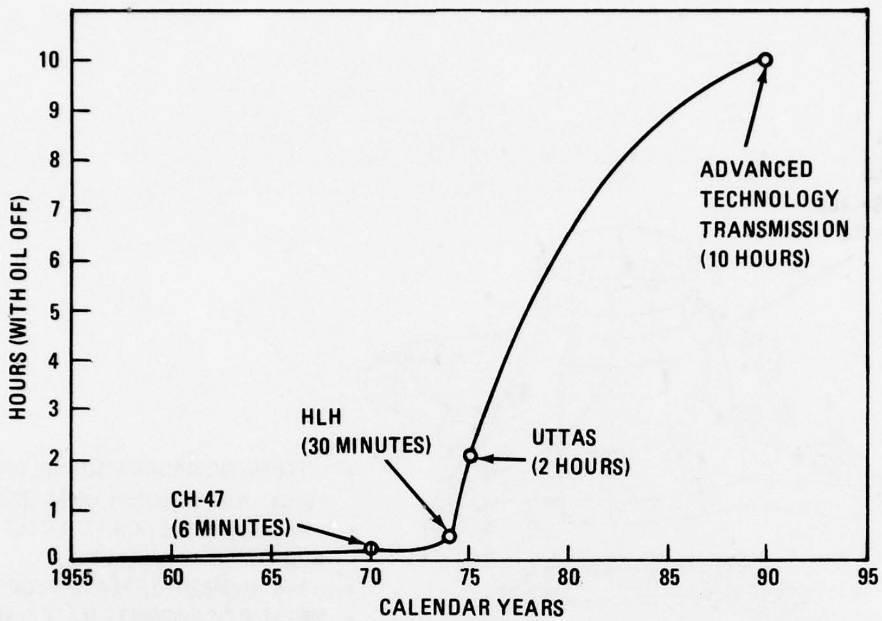

Figure 18. Emergency Oil-Off Capability Goals

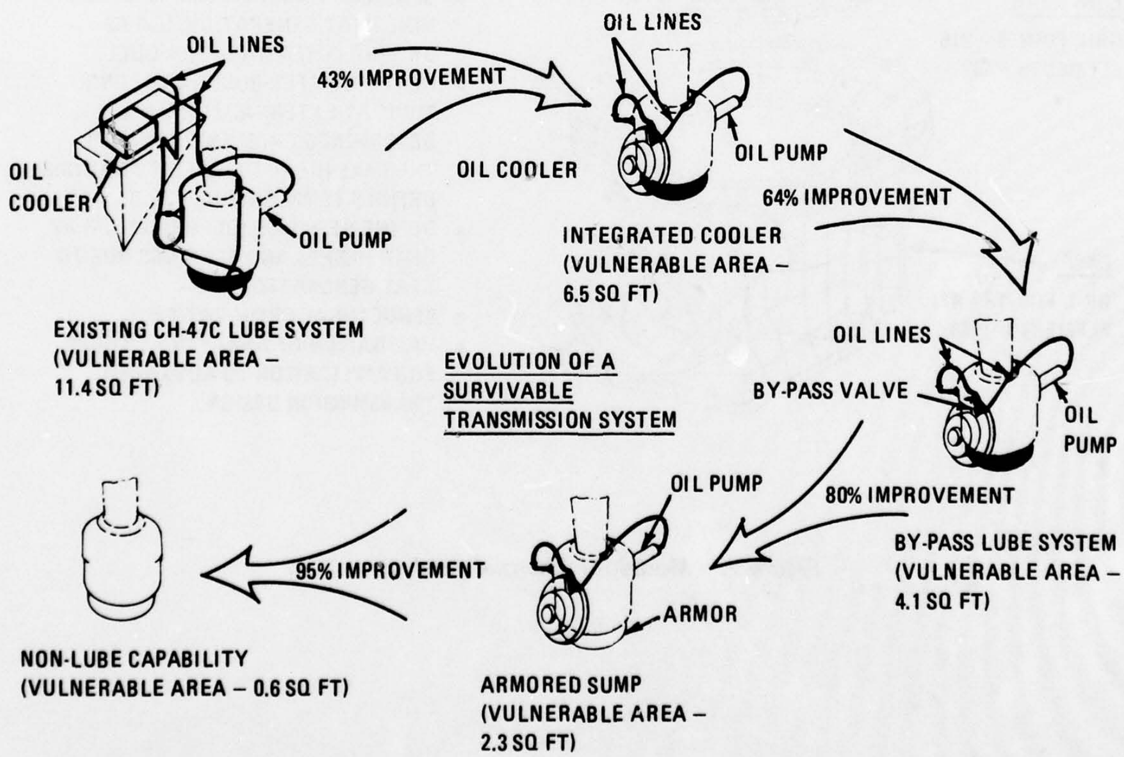

Figure 19. Sequence of Development Required to Arrive at a Factory Sealed Advanced Technology Transmission

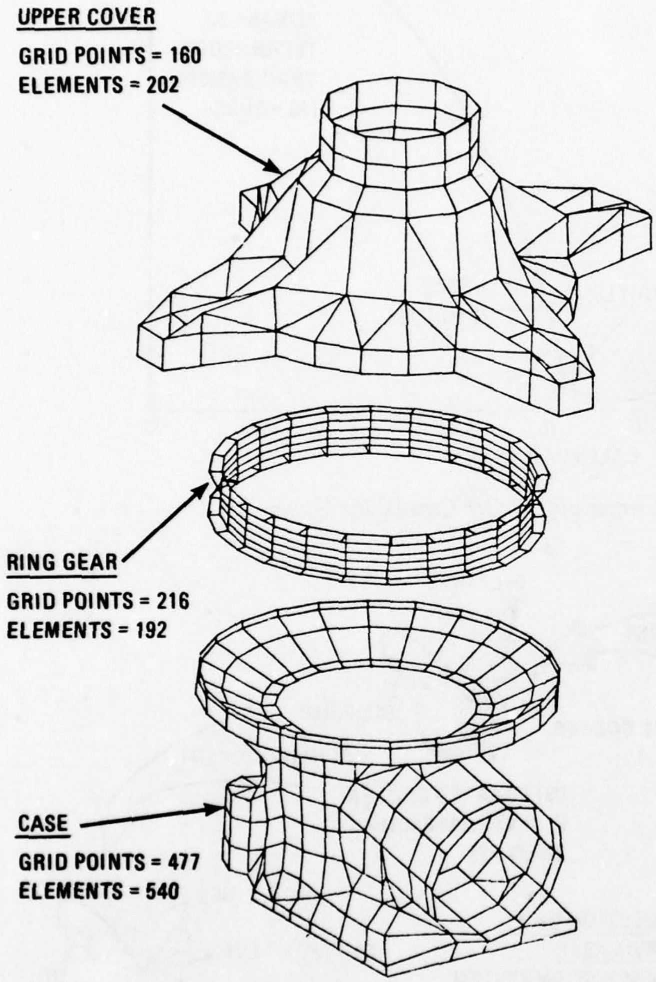

- AUTOMATIC GENERATION OF GRID POINTS AND ELEMENT CONNECTIONS.
- USE SAME GRIDS FOR STRUCTURAL AND THERMAL ANALYSIS.
- HOUSING MADE OF PLATE ELEMENTS
- METAL OR COMPOSITE MATERIAL.
- THERMAL DISTORTION AND THERMAL STRESS.
- GEAR/BEARING ANALYSIS TO DETERMINE HEAT GENERATION, USE AS DRIVING POTENTIAL FOR MODEL.
- HEAT TRANSFER BOUNDARY CONDITIONS AT EXTERNAL SURFACES DETERMINED FROM ENVIRONMENT.
- THERMAL (HEAT TRANSFER) ANALYSIS DEFINES TEMPERATURE FIELD.
- DEFINE RESPONSE (DEFORMATION) AT GEAR MESHES AND BEARINGS DUE TO HEAT GENERATED.
- STRUCTURAL OPTIMIZATION.
- VALIDATION OF ANALYTICAL TOOLS FOR APPLICATION TO ADVANCED TRANSMISSION DESIGN.

Figure 20. Model for Thermal Analysis

Steady-state heat transfer analyses may be accomplished with the existing finite element model of the CH-47C forward transmission housing using the NASTRAN program. The NASTRAN heat flow capability analysis is compatible with the structural analysis capability. Using the same model (grid points, coordinate system, elements, constraints and sequencing) as used for a structural analysis, the steady-state temperatures at each grid point may be calculated and provided directly in punched form for later use in a thermal stress/deformation analysis (static structural analysis). This NASTRAN housing model may also be modified to handle a thermal analysis of fabricated housings and/or composite materials such as metal-matrix, which will be particularly valuable for application to advanced transmission development.

Input to the model for a thermal analysis requires knowledge of the thermal boundary conditions at specified locations on the housing. The driving potential for a thermal analysis is the power dissipation by bearings and gears at operating conditions. This originated from other Boeing Vertol computer programs. The temperature distribution obtained from the steady-state temperature analysis can then be input to NASTRAN to provide a thermal stress (static) analysis. Thermal stresses and distortions result. The thermal distortions obtained are of particular use in determining the adequacy of clearances for a longer life transmission. The thermal analysis is outlined in Figure 21.

A sample NASTRAN thermal stress analysis presented below shows good correlation and indicates the feasibility of using NASTRAN for thermal analyses. The model, a rectangular plate, is given a temperature gradient which causes internal loads and elastic deflections. The temperature load is constant in the y direction and symmetric about the y-axis. Since membrane elements are used to model the structure, it is necessary to remove all rotational degrees of freedom and translational degrees of freedom normal to the plate. The symmetric boundary conditions were modeled by constraining the displacements normal to the planes of symmetry. Figure 22 shows a comparison of stresses predicted by NASTRAN and the experimentally measured stresses.

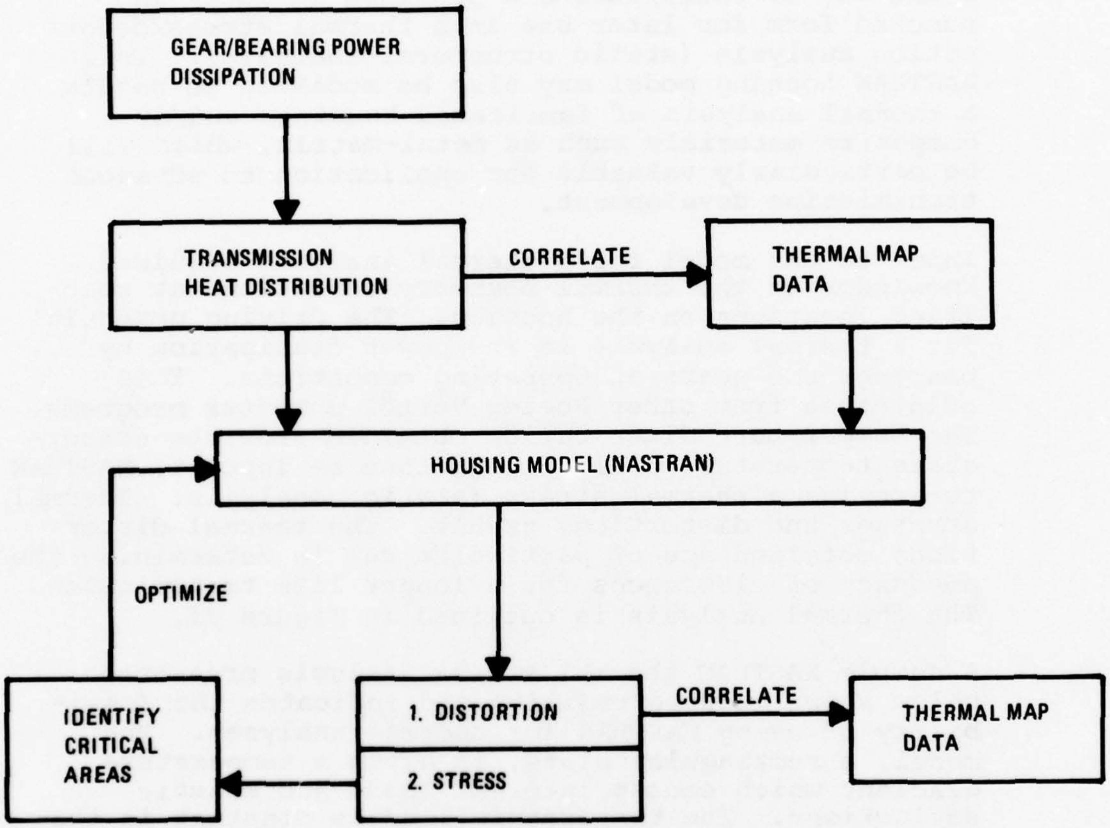

Figure 21. Flow Diagram of NASTRAN Thermal Analysis

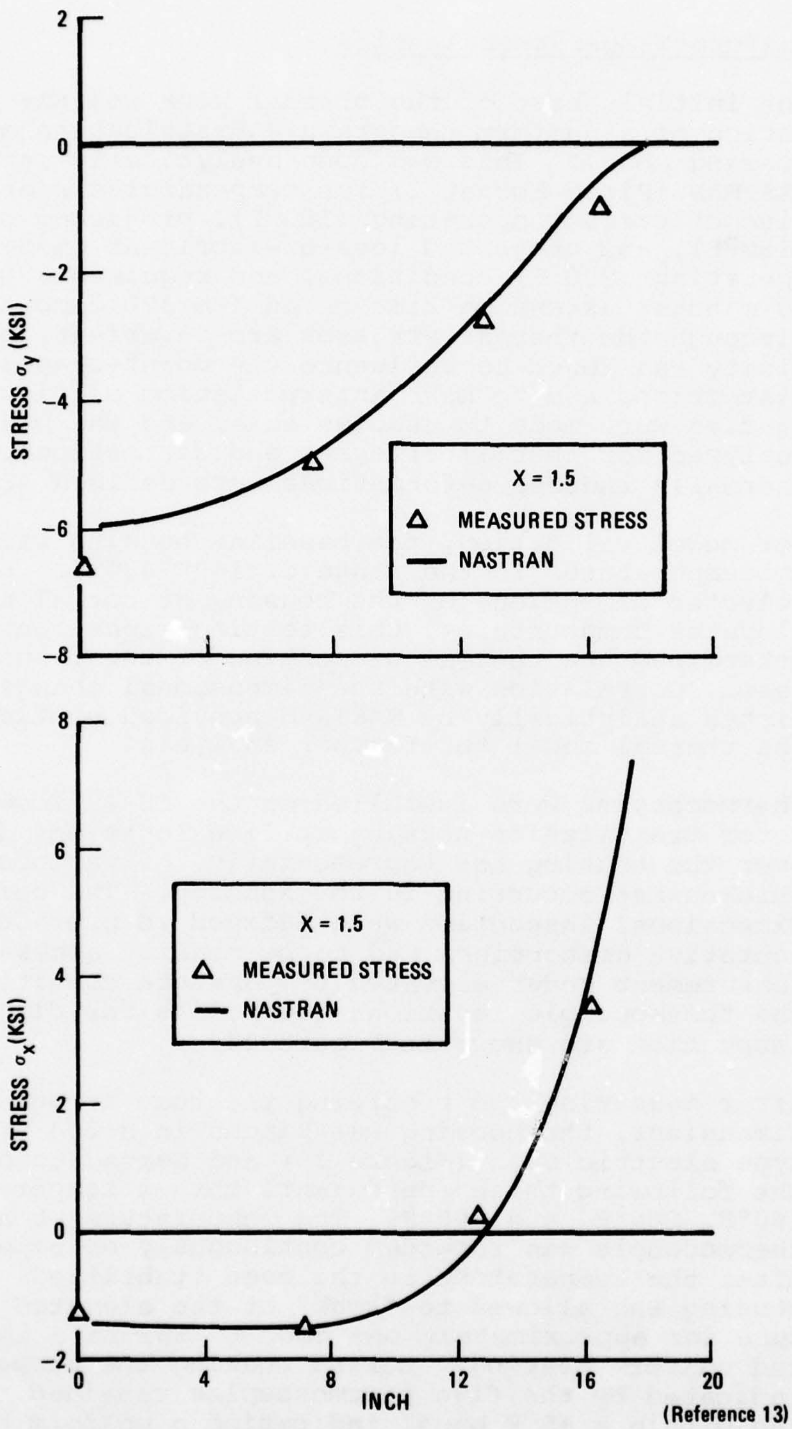

Figure 22. Comparison of NASTRAN and Experimental Stresses for Free Rectangular Plate With Thermal Loading

13. NASTRAN User's Manual Level 15, June 1972

2. Uniform Temperature Testing

The initial phase of the thermal work was the application of a uniform temperature distribution over the housing model. This was done analytically using NASTRAN (Rigid Format 1) for temperatures representative of current operating (160°F), projected operating (350°F), and projected loss-of-lubricant emergency operating (700°F) conditions, and required a total of 40 minutes execution time on an IBM 370 computer. Although the thermal stresses are invariant, boundary fixity was found to influence the point-by-point distortions and to make interpretation difficult. Studies were made to resolve this, and the housing was analyzed for thermal stresses and distortions. The thermally induced deformations were defined (Figure 23).

For model validation, the baseline housing was heated to temperatures in the range of 160°-400°F. By measuring selected dimensions of the housing at normal and elevated temperatures, this testing experimentally determined the thermal distortion of the transmission case. Correlation with the dimensional changes predicted analytically by NASTRAN provided confidence in the thermal model for further analysis.

Thermocouples were installed on the CH-47 forward rotor transmission housing at five locations dispersed over the housing and representative of various wall thicknesses occurring in the housing. The points for dimensional inspection were defined to provide representative distortions and to be readily accessible for measurement under elevated temperature conditions. The thermocouple locations and points for dimensional inspection are shown in Figure 24.

After measuring and recording the room temperature dimensions, the housing was placed in a 204 kW walk-in type electric oven (Figure 25) and heated to each of the following three approximate target temperatures: 160°F, 280°F, and 400°F. The temperature at each thermocouple was recorded continuously on paper tape. After the temperature in the oven stabilized, the housing was allowed to "soak" at the elevated temperature for approximately one hour to insure a thorough and uniform heating. During soaking the temperatures indicated by the five thermocouples remained constant and within a ±5°F band, indicating a uniform heating of the housing.

After soaking, the specified housing dimensions were measured. The housing remained in the oven during measurement in order to minimize heat loss, but the

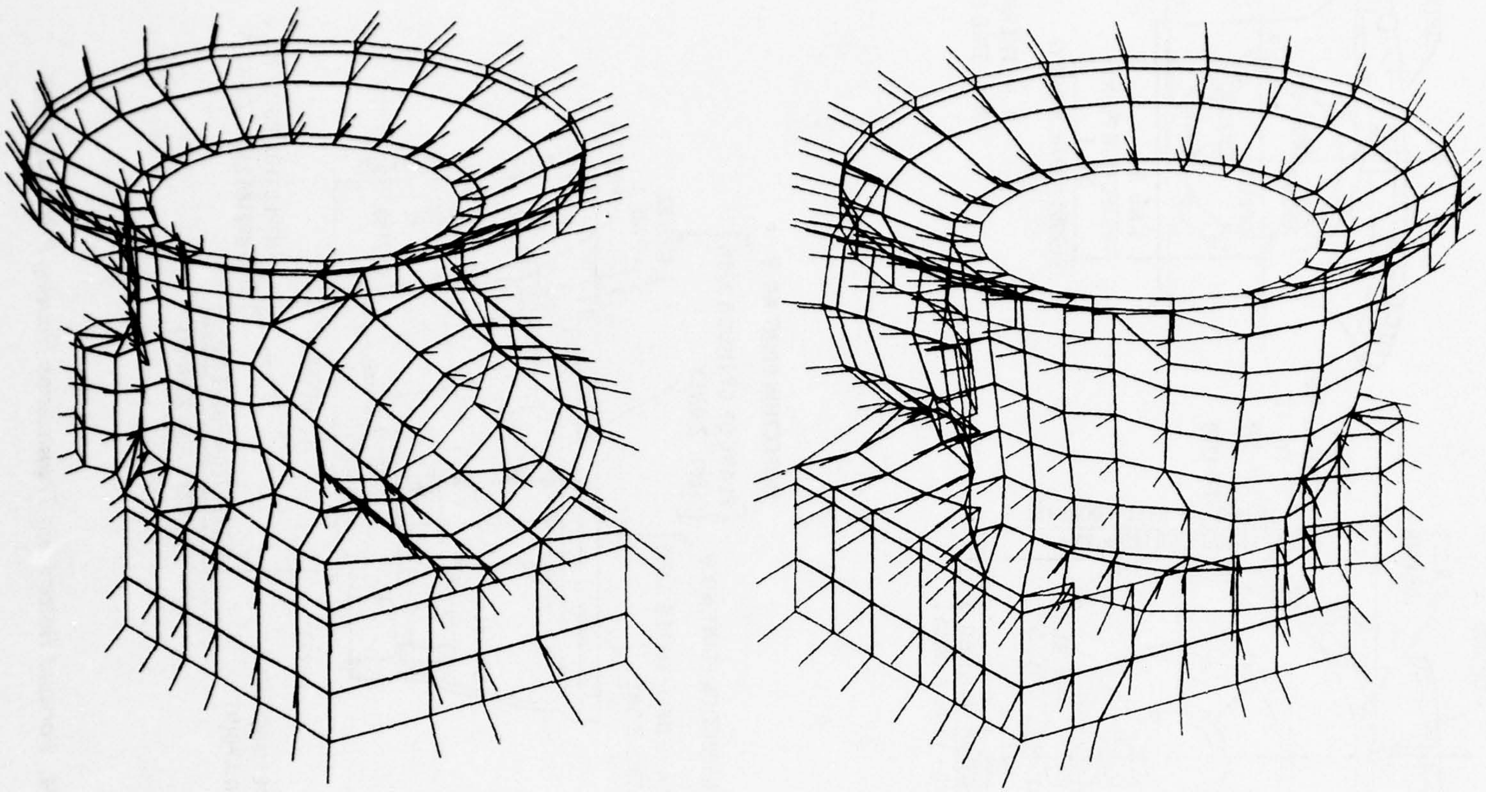

	SUBCASE	TEMPERATURE	MAXIMUM DEFORMATION
NOTE: VECTORS	1	160°F (71°C)	0.02414542 (0.0612CM)
INDICATE DIS-	2	350°F (177°C)	0.07244312 (0.1839CM)
	3	700°F (371°C)	0.16140204 (0.4100CM)

Figure 23. CH-47 Forward Transmission Case Uniform Temperature Analaysis, Static Deformation Due to Elevated Temperatures

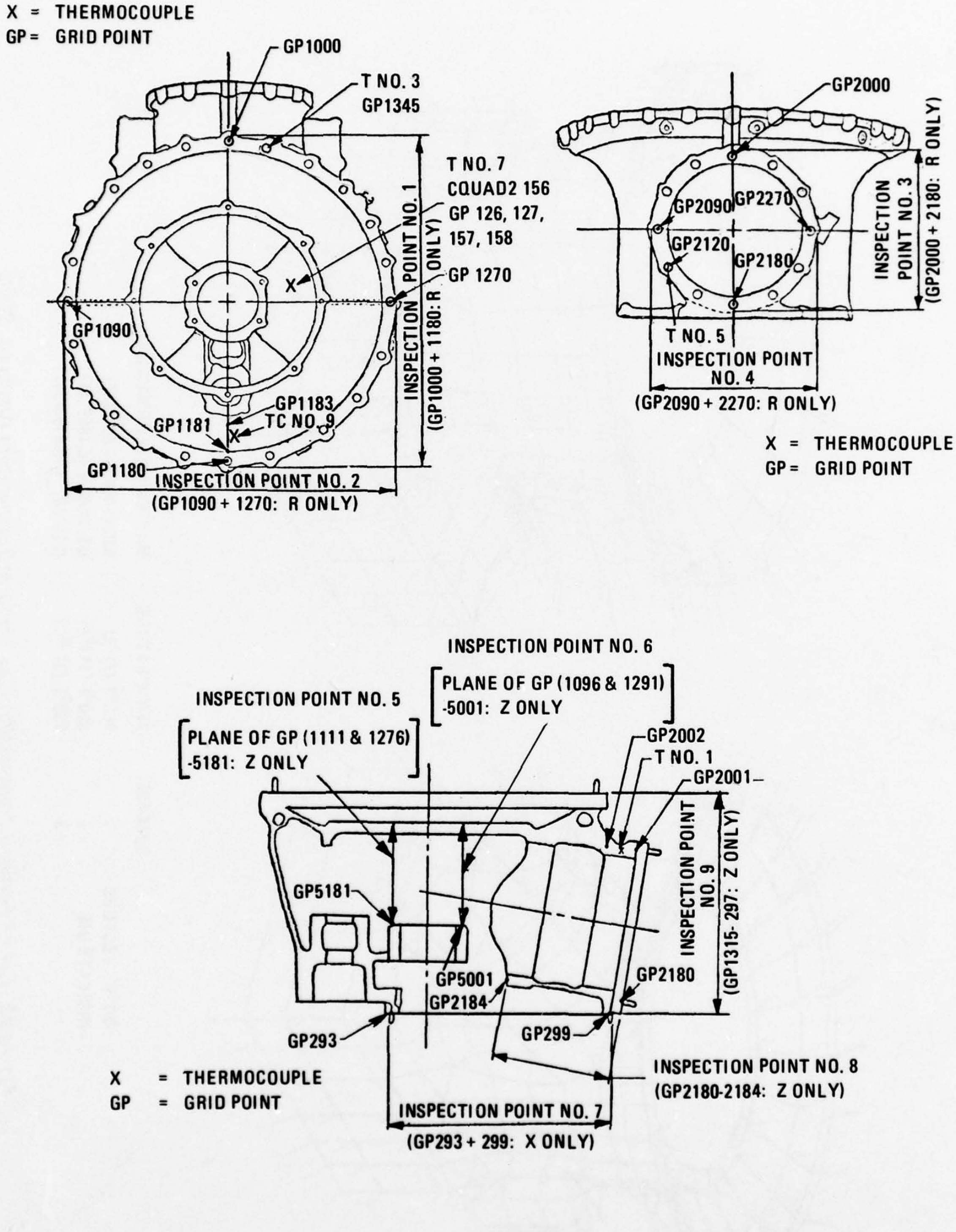

Figure 24. Forward Rotor Main Transmission Housing P/N 114D1089

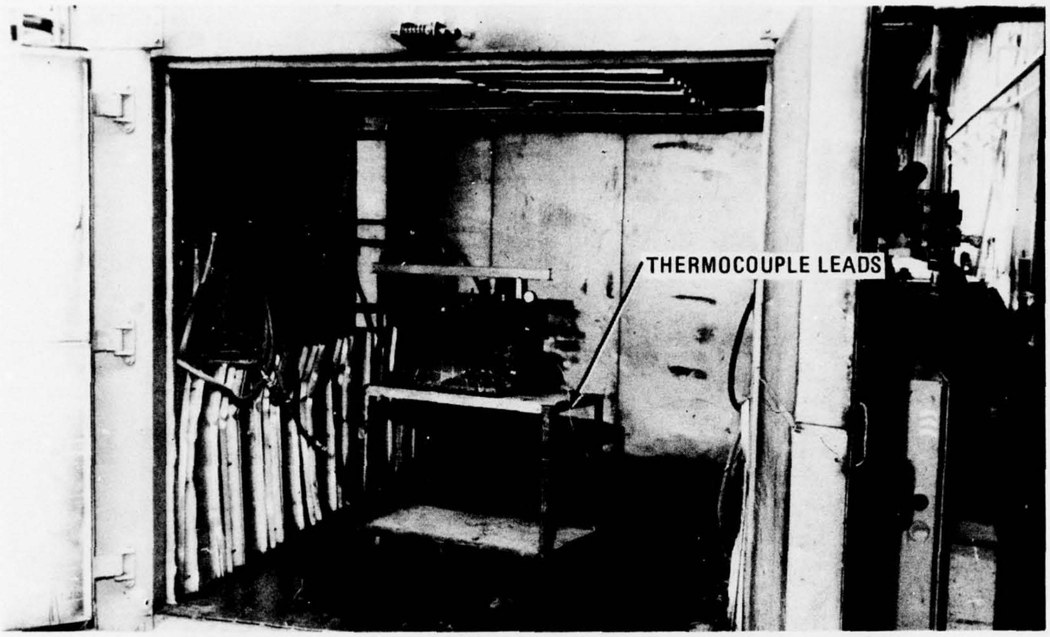

Figure 25. CH-47C Forward Rotor Transmission Housing in Dispatch Oven

oven doors were partially open and the oven was turned off. During the measurement, the housing temperature was continuously recorded on paper tape and the tape was annotated to show the temperature at the time each dimensional check was made (Figure 26). Typically, about four dimensions could be measured at the 160°F range and about two dimensions at the 400°F range before the housing temperature decreased substantially. The experimental setup is shown in Figures 27 through 30.

The instruments used for the measurements are shown in Figure 31. Table 3 summarizes the equipment used in the testing and indicates the reliability of the dimensions taken. When evaluating the reliability of the dimensional data taken at elevated temperatures, consideration must be given to the facts that some growth of the inspection gages occurred when taken into the oven and also the inspector had to work in an uncomfortably hot environment.

The experimental data obtained is plotted in Figure 32 as the change in linear dimensions versus temperature. Also shown in the figure are the theoretical changes in the dimensions as predicted both by the NASTRAN thermal analysis and by a simple linear thermal expansion calculation. The agreement of the data and analytical methods confirms the validity of the model, which can thus be used with confidence to predict deformations of the housing.

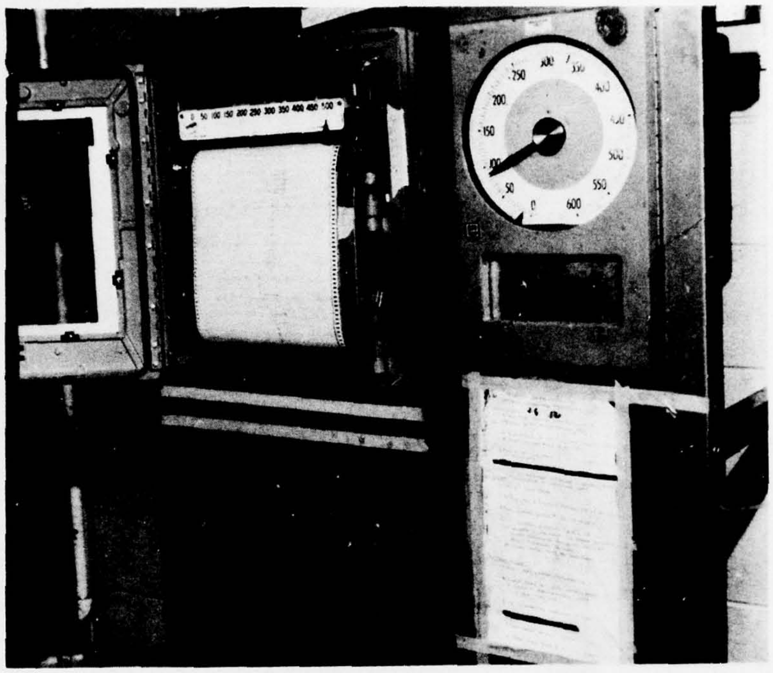

Figure 26. Control and Data Monitoring Panel for Dispatch Oven

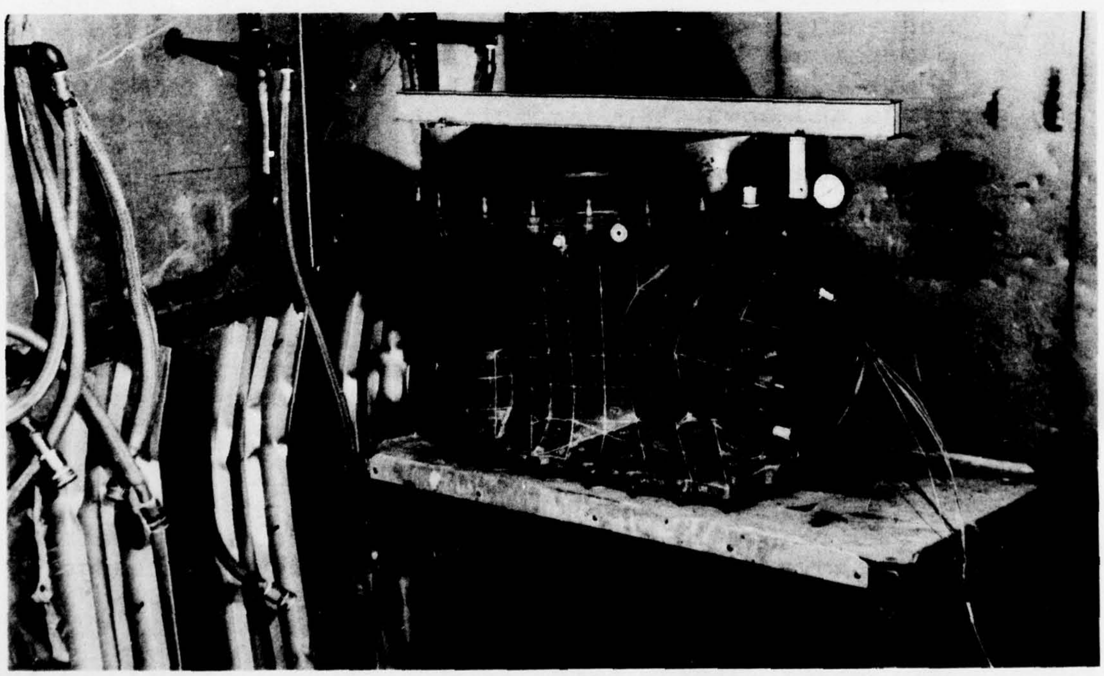

Figure 27. Measurement Procedure — Bar-Type Dial Indicator Gage

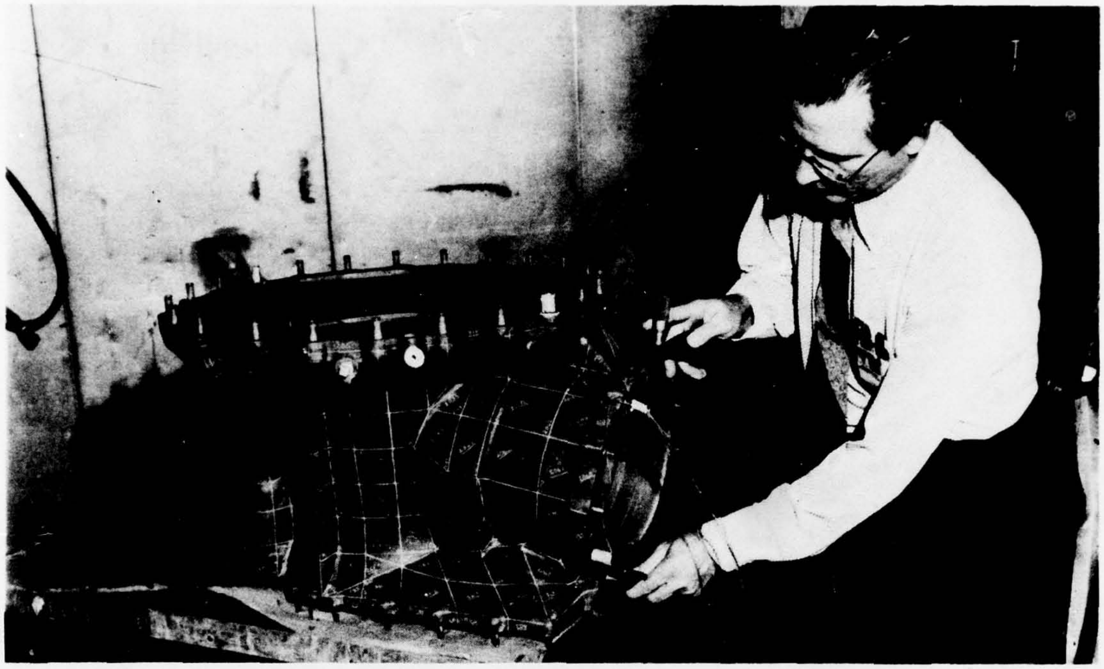

Figure 28. Measurement Procedure – Outside Micrometer

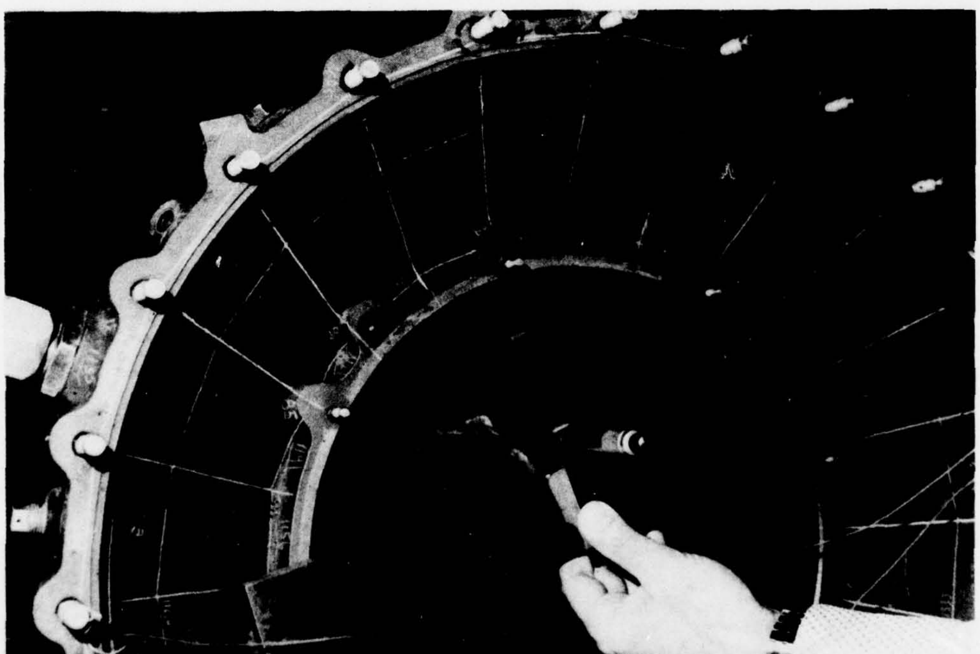

Figure 29. Measurement Procedure – Depth Gage

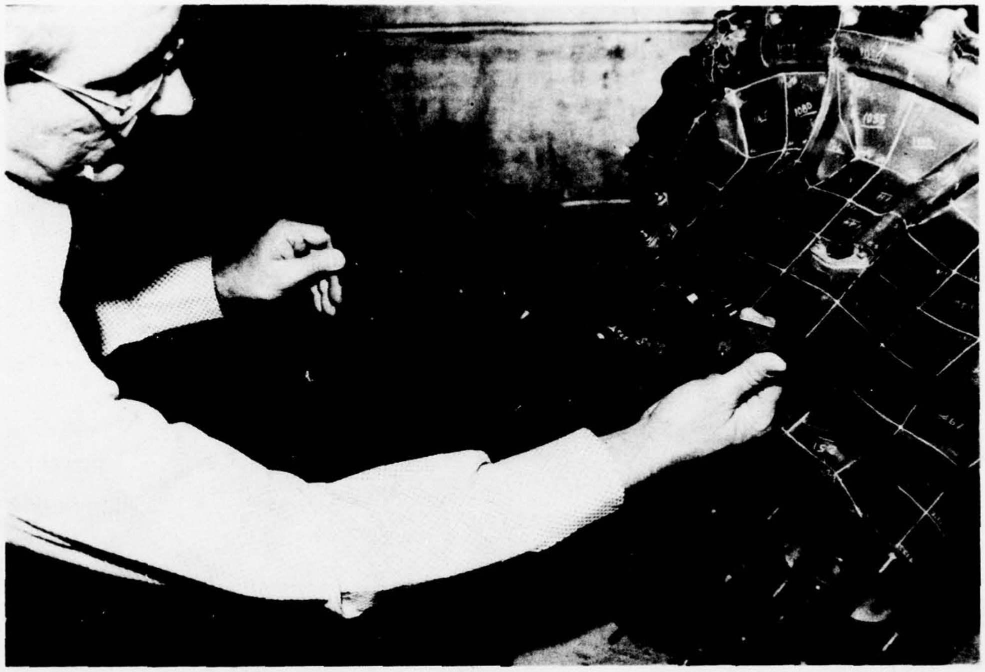

Figure 30. Measurement Procedure — Vernier Caliper

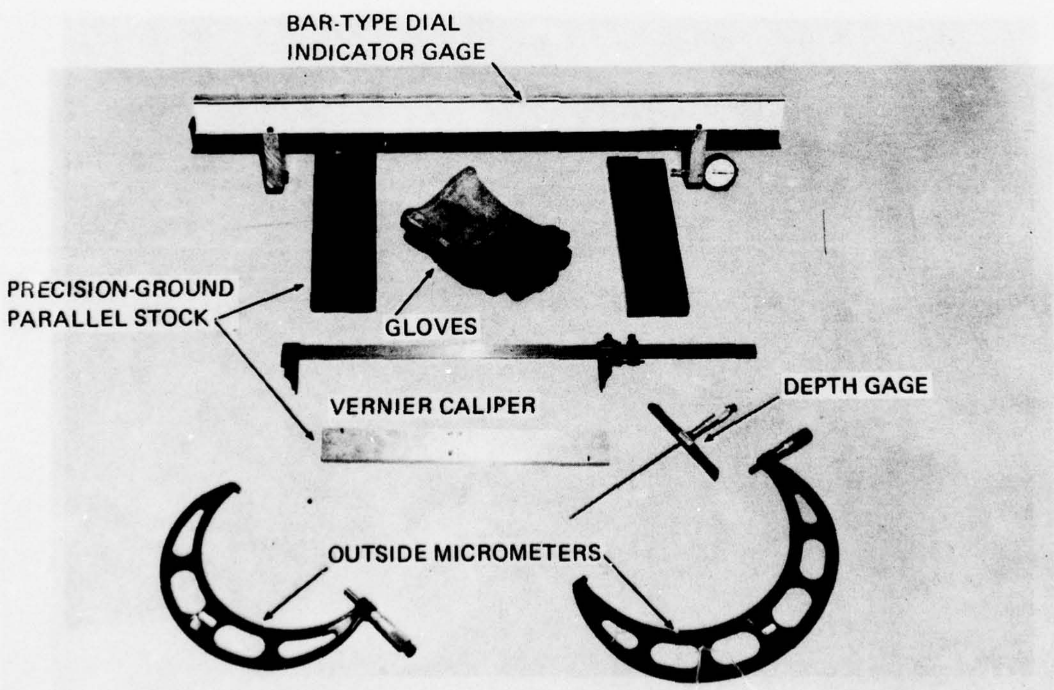

Figure 31. Measuring Instruments

TABLE 3. EQUIPMENT USED TO PERFORM UNIFORM TEMPERATURE TESTING

INSPECTION POINT	MEASURING INSTRUMENT	RELIABILITY RATING*	REMARKS
1 & 2	Bar type dial indicator snap gage	8-9	Gives a very reliable dimension.
3 & 4	11- to 12-inch outside micrometer	7-8	Gives a reliable dimension.
5 & 6	8- to 9-inch depth gage	6-7	Gives a reliable dimension, but an unmachined surface was checked.
7	0- to 24-inch Vernier caliper	6-7	Gives a reliable dimension.
8	8- to 9-inch outside micrometer	5-6	Gives a reliable dimension, but an unmachined surface was checked
9	0-to 24-inch Vernier caliper	2-3	Gives a reliable dimension, but the geometry of the surfaces checked made proper orientation of the caliper difficult.

*Estimated reliability level for inspection points using a 1 to 10 rating scale, 10 being the most reliable.

Oven - Despatch Oven Company, Minneapolis, Minnesota

Style	S-300	Type	Electric (Walk In)
Volts	P-400 G-110	Phase	3 1
K.W.	204	Amps	H-268 M-14.85
Temp (Max)	550°F		
Serial No.	71826		

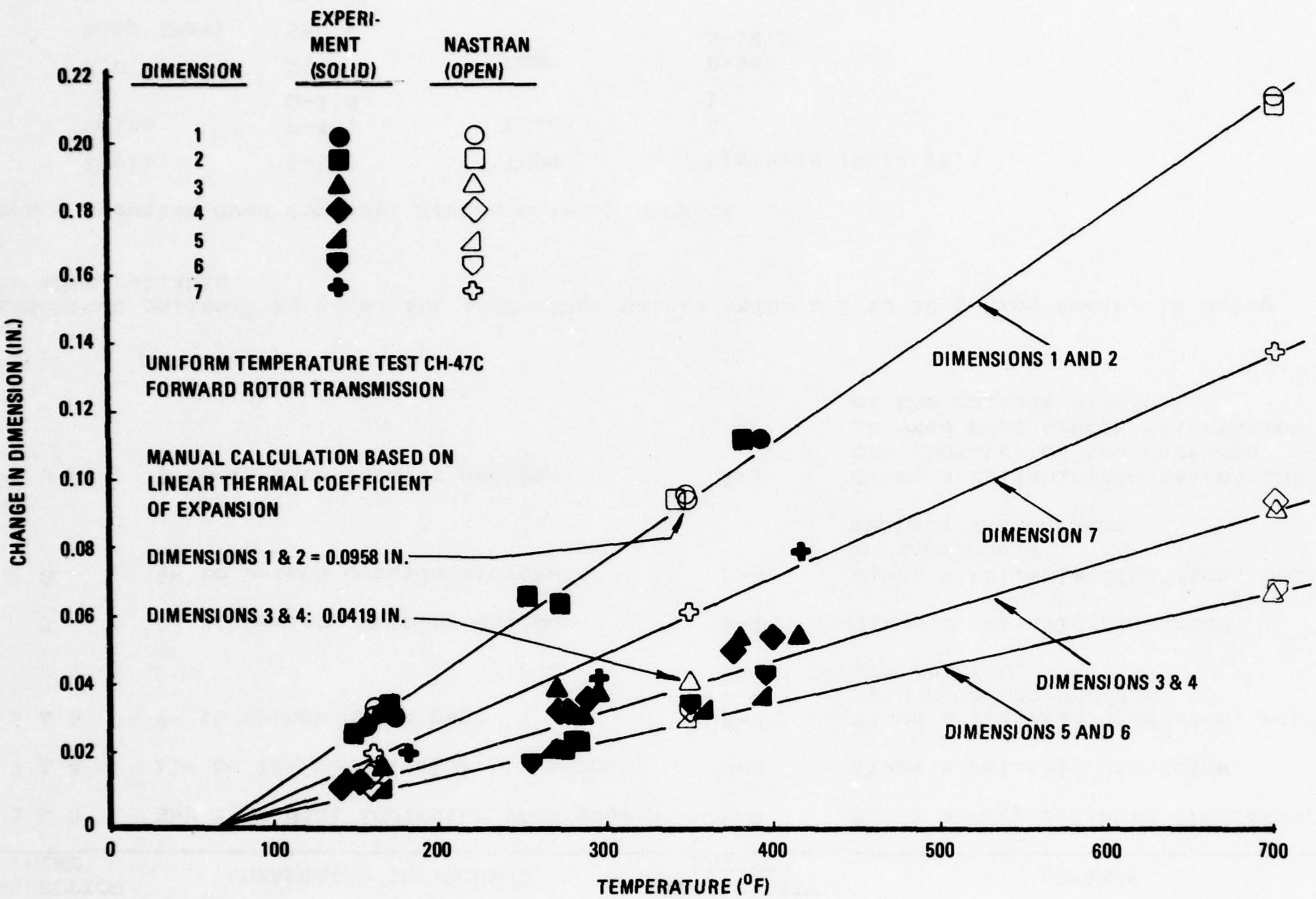

Figure 32. Transmission Housing Dimensional Changes as a Function of Temperature

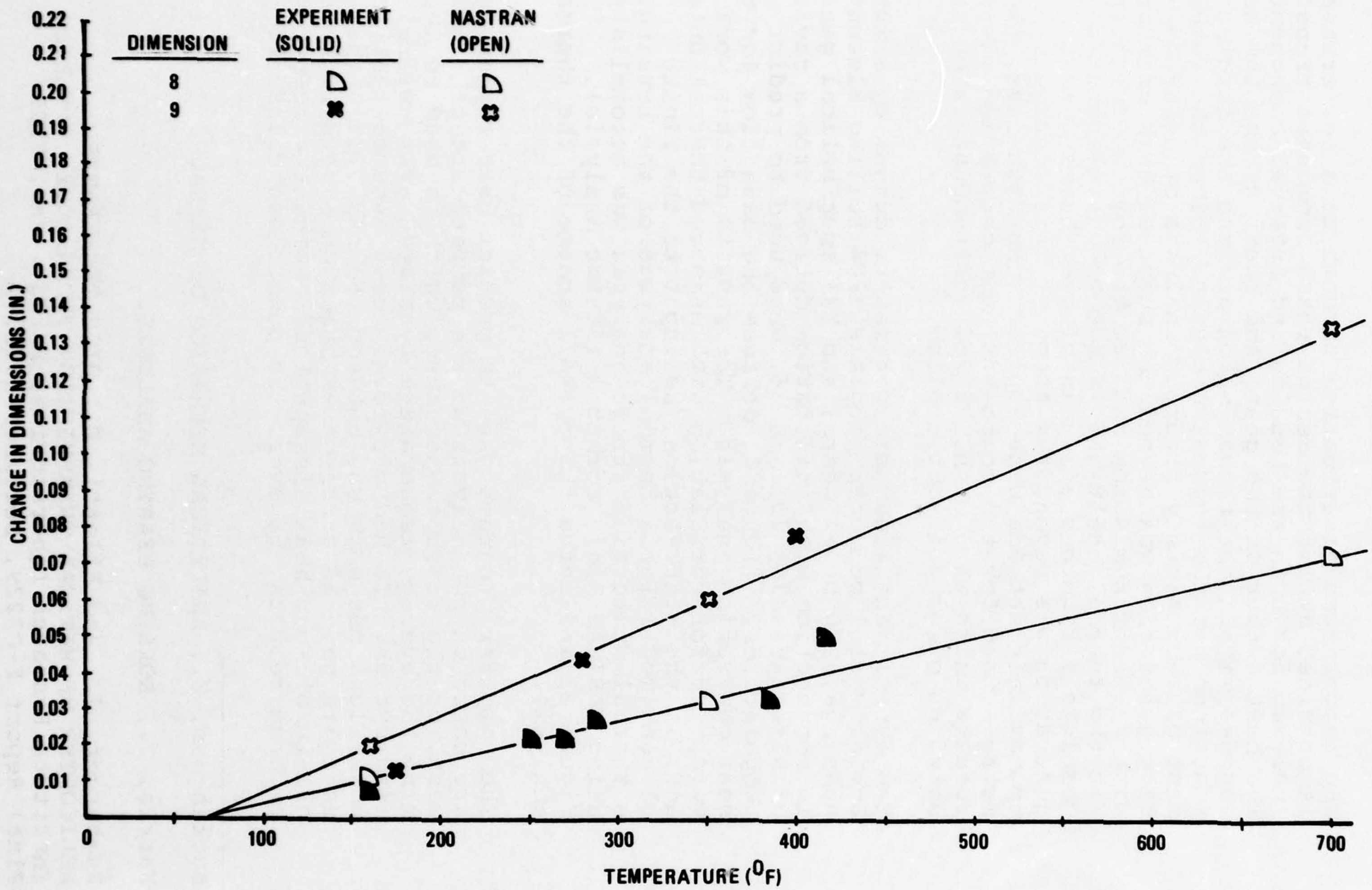

Figure 32. Continued

3. Gear/Bearing Thermal Simulation

The temperature distribution throughout a new transmission is obtained during the design phase from heat transfer analyses for both the housing and internal components. The heat output of the gears and bearings are the heat sources within the transmission and are the forcing functions for the thermal analysis. Since the development of a completely rigorous analysis of gear/bearing heat generation was beyond the scope of this contract, within the transmission and are the forcing functions for the thermal analysis. Since the development of a completely rigorous analysis of gear/bearing heat generation was beyond the scope of this contract, approximate methods were applied. Nevertheless, the methods used for the component heat generation yielded results which were within 6% of independent calculations based on oil-in/oil-out cooling.

The dynamic and kinematic parameters output by existing Boeing Vertol computer programs (S04 rolling element bearings, R20 bevel gears, and R23 spur/helical gears), in conjunction with information derived from a review of References 14, 15, and 16, were used to predict temperatures. Figure 33 defines the data flow for the heat generation analysis. The results of this work were used for correlation with measured thermal data and, in the next section, as input to the finite element model for a thermal analysis of the housing. A thermal distortion/stress analysis was accomplished using NASTRAN Rigid Format 1 (Static Analysis). Figure 21 indicates the overall scheme of the thermal analysis.

The computer programs used to predict gear temperatures are based on an analysis of the temperature at a gear mesh, or the flash temperature, which is used to determine the average temperature generated over several mesh cycles. It had previously been assumed that the power loss per mesh was between .5% and .75%. The .5% estimate gave an error of 9% based on a comparison of oil-in/oil-out heat dissipation. Using the computer program results, however, the power loss calculated for

---

14. Buckingham, E., ANALYTICAL MECHANICS OF GEARS.

15. Harris, T., ROLLING BEARING ANALYSES.

16. Rumbarger, J., and Filetti, E., HIGH TEMPERATURE HELICOPTER MECHANICAL TRANSMISSION TECHNOLOGY, Franklin Institute Research Laboratories, Phila., Pa., FIRL Final Report F-C3229, December 1971.

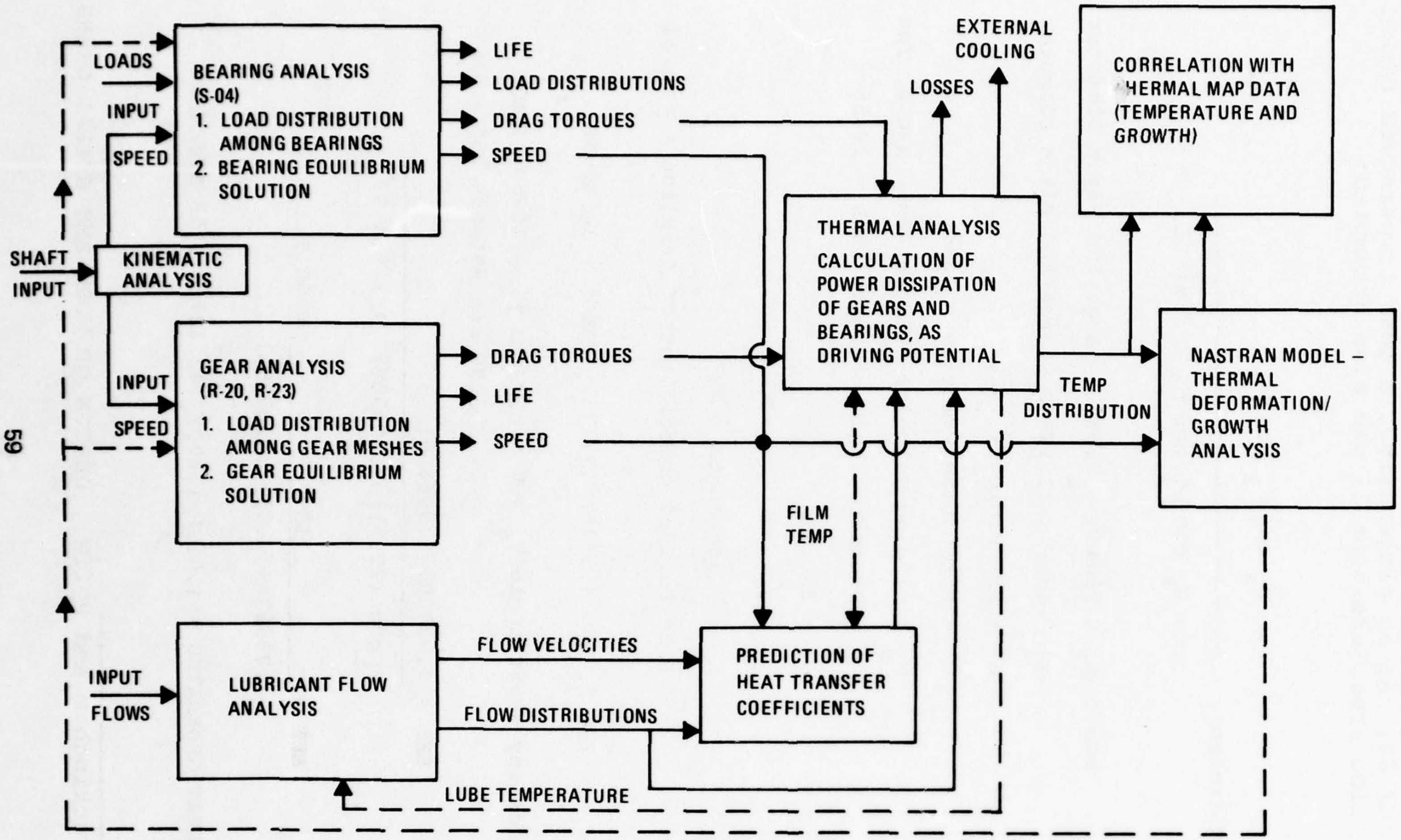

Figure 33. Flow of Heat Generation Analysis

the bevel mesh was .2% for a better system correlation of 6%. As an alternative, a gear temperature formulation from Reference 17 was also attempted:

$$\text{Efficiency} = \frac{\cos \phi_n \cos \psi_1 \cos \psi_2}{\cos \phi_n \cos \psi_1 \cos \psi_2 + f \sin \Sigma}$$

where R_1 = Pinion = 7.55/2 Large End Pitch Diameter

R_2 = Gear = 13.278/2 Large End Pitch Diameter

n = RPM Pinion = 7460

V = Pitch Line Velocity = fpm

V_S = Sliding Velocity Between Basic Racks, fpm

θ_n = Pressure angle of basic rack = 22.5°

ψ_1 = 25°

ψ_2 = 25°

Σ = Shaft angle = 99°

f = Assumed coefficient of friction f = 0.01

$V = .5236\ R_1\ n = (.5236)\ (3.775)\ (7460) = 14745.36$

For any shaft angle $V_S = V \sin\Sigma / \cos \psi_2 = 16069.$ fpm

$= 14{,}745.36 \sin 99° / \cos 25°$

$$\text{EFF} = \frac{(.92388)\ (.906308)^2}{\left[\cos (22.5)\right]\ (.906308)^2 + f \sin 99^{\circ}}$$

$$\text{EFF} = \frac{.75887}{.75887 + (.01)\ (.987688)} = 98.7\%$$

HEAT GENERATED = (.013) (3600) (42.42) = 1758 BTU/MIN

---

17. Buckingham and Ryffel, DESIGN OF WORM AND SPIRAL GEARS.

A computer program in the "BASIC"language with sample results (BTU/MIN) for various assumed coefficients of friction is also included(Figures 34 and 35). Reference 18 was also utilized.

```
10    INPUT P1, P2, P3, P4
20    A=COS(P1)*COS(P2)*COS(P3)
30    FOR I=1 TO 50
40    E=0.01*I
50    E=E*SIN(P4)
60    E=E+A
70    E=A/E
80    PRINT P1;P2;P3;P4;E
90    E=1-E
100   B=E*3600*42.42
110   F=0.01*I
120   PRINT "COEFF OF FRICTION="F;"BTU/MIN="B
130   NEXT I
140   END
AVERAGE POWER LOSS =    0.769HP =    32.590BTU/MIN
```

Figure 34. "Basic" Computer Program for Heat Generated by Spiral Bevel Gears (Hewlett Packard Minicomputer)

```
722.5,25.,25.,99.
 22.5      25     25     99        0.988488388
COEFF OF FRICTION = 0.01    BTU/MIN= 1757.961316
 22.5      25     25     99        0.977238794
COEFF OF FRICTION= 0.02     BTU/MIN= 3475.909312
 22.5      25     25     99        0.966242373
COEFF OF FRICTION= 0.03     BTU/MIN= 5155.194742
 22.5      25     25     99        0.955490674
COEFF OF FRICTION= 0.04     BTU/MIN= 6797.10824
 22.5      25     25     99        0.944975617
COEFF OF FRICTION= 0.05     BTU/MIN= 8402.88363
 22.5      25     25     99        0.934689474
COEFF OF FRICTION= 0.06     BTU/MIN= 9973.701007
 22.5      25     25     99        0.924624852
COEFF OF FRICTION= 0.07     BTU/MIN= 11510.689.64
 22.5      25     25     99        0.914774669
COEFF OF FRICTION= 0.08     BTU/MIN= 13014.93069
 22.5      25     25     99        0.905132146
COEFF OF FRICTION= 0.09     BTU/MIN= 14487.4597
 22.5      25     25     99        0.895690784
COEFF OF FRICTION= 0.1  BTU/MIN= 15929.26905
```

Figure 35. Sample Computer Output for Various Assumed Coefficients of Friction

---

18. Faires, V., DESIGN OF MACHINE ELEMENTS, The MacMillan Company, New York, 4th Edition, 1965.

The output from computer program S04 has been applied to predict the temperatures of rolling element bearings. Some work has been done in this area by Rumbarger and Filetti (Reference 16). Since the heat generated by the bearings is comprised of two parts, the shearing of the interface oil film and by the friction of the rolling elements, two separate calculations must be combined (Figure 36). Also, the heat generation is a function of load, sliding velocity, and coefficient of friction. Sample procedures for calculating the heat generated by both angular contact ball bearings and roller bearings are outlined in Appendix B.

Lubrication characteristics of the CH-47C forward transmission have been determined. Table 4 indicates the oil flow for forced convective cooling of the internal components, and Figure 37 indicates the orifice locations numbered according to Table 4. The stabilized thermal power at the bearings and gears act as heat sources for a NASTRAN analysis including conductivity, natural and forced convection, and radiation (Stefan-Boltzmann Law) (Figures 38 and 39). Resulting overall temperatures can then be used in a NASTRAN static analysis in order to determine thermal distortions and stresses.

Thermal power has been determined for all gear meshes (Figure 40). Samples of the computer output for the CH-47C forward transmission are shown in Figure 41 (bevel gear program R20) and Figure 42 (spur and helical gear program R23).

A tabulation of the heat generated by the CH-47C forward transmission internal components is provided in Table 5.

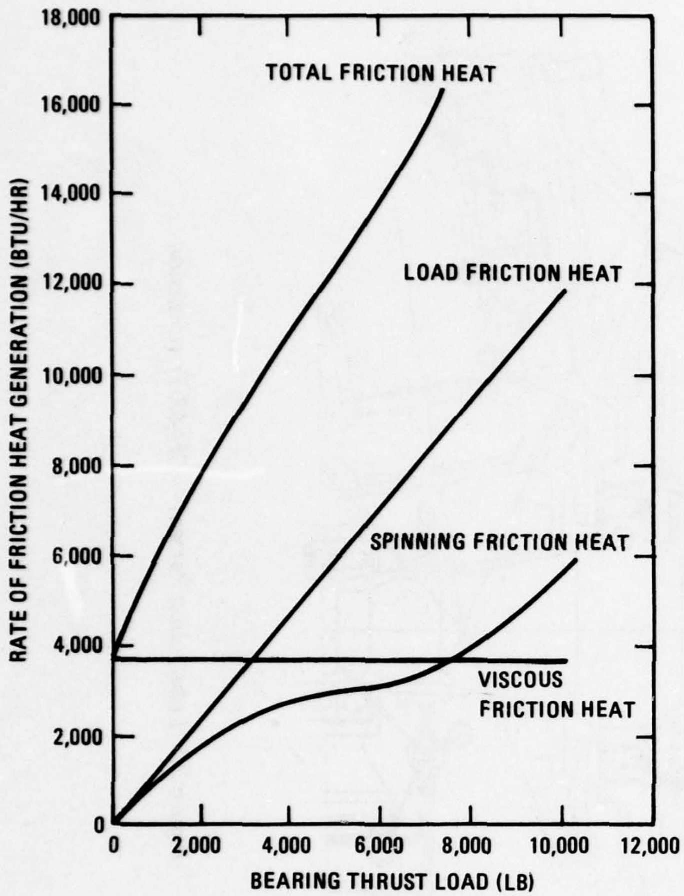

Figure 36. Friction Heat Generation Versus Load; 218 Angular-Contact Ball Bearing 10,000 RPM, 5 Centistokes Oil, Jet Lubrication

TABLE 4. LUBRICATION PER GEAR/BEARING YIELDING CONVECTIVE COOLING CH-47 FWD TRANSMISSION.

TARGET NO.	PART LUB'D	DIAMETER, INCHES ORFICE SIZE	FLOW GPM @ 60 PSI	NO. OF HOLES	SPLASH ZONE TARGET DIAMETER INCHES
1	Ball Brg	0.040	0.27	1	0.12
2	Roller Brg	0.040	0.27	1	0.15
3	Spher Brg	0.051	0.44	1	0.11
4	Spher Brg	0.078	6.25	6	0.20
5	Planet Brg	0.051	2.64	6	0.15
6	Planet Brg	0.051	1.32	3	0.13
7	Roller Brg	0.040	0.27	1	0.22
8	SB Gear	0.161	4.42	1	0.38
9	Spur Gear	0.040	0.54	2	0.21
10	Ball Brg	0.050	1.76	4	0.15
11	Sun Gear	0.051	1.76	4	0.20
12	Planet Gear	0.051	2.64	6	0.20
13	Roller Brg	0.061	0.61	1	0.16
14	Ball Brg	0.040	0.27	1	0.17
15	Ball Brg	0.040	0.27	1	0.16
16	Roller Brg	0.040	0.27	1	0.16
17	Ball Brg	0.040	0.27	1	0.18
18	Ball Brg	0.040	0.27	1	0.19
19	Spur Gear	0.040	0.27	1	0.12
		d	Q		

PUMP CAPACITY 24 GPM
ACTUAL PUMP PRESSURE 56.1 PSI

$$Q\ (GPM) = 22\ d^2 \sqrt{\Delta PRESSURE}$$

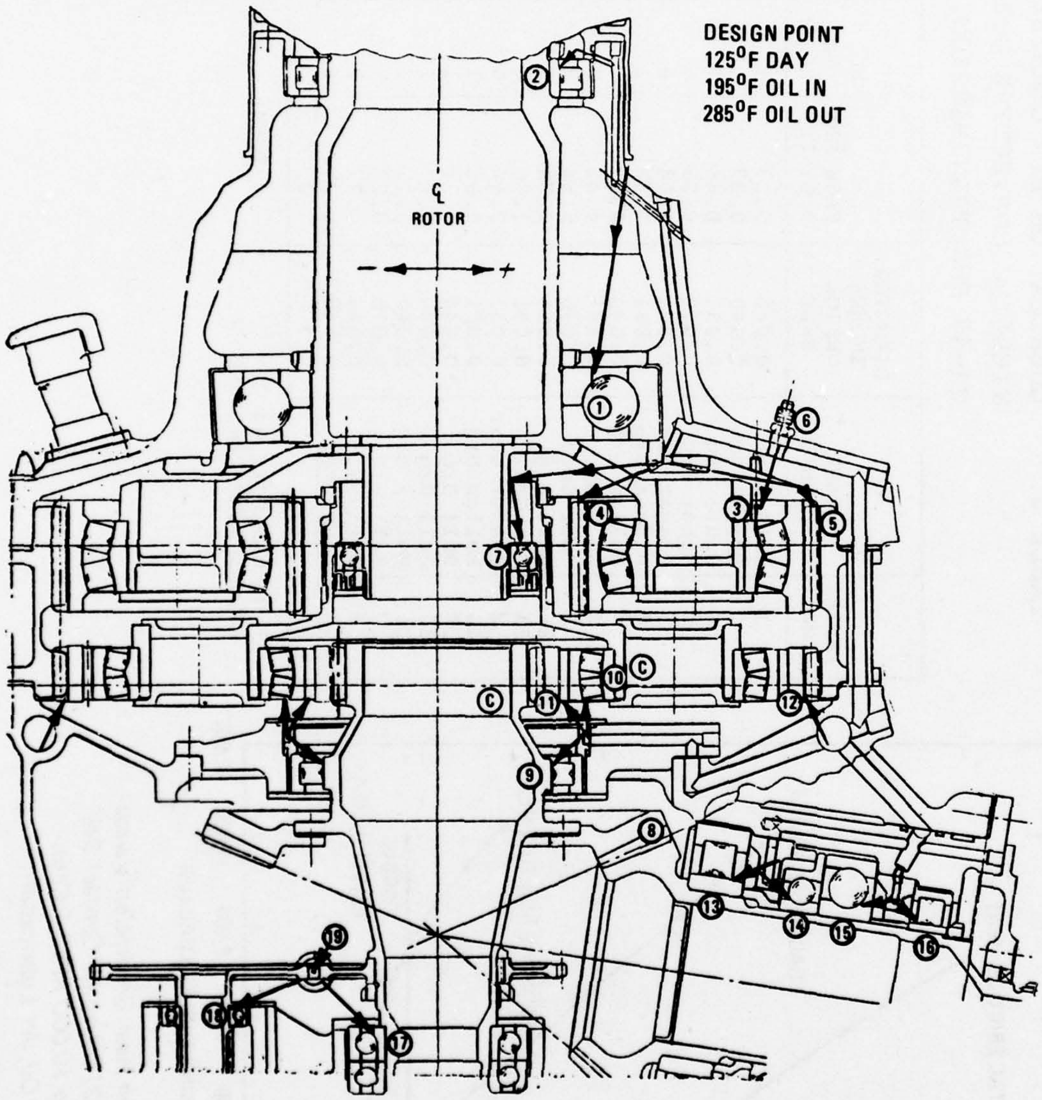

Figure 37. Lubrication Pattern – CH-47 Transmission

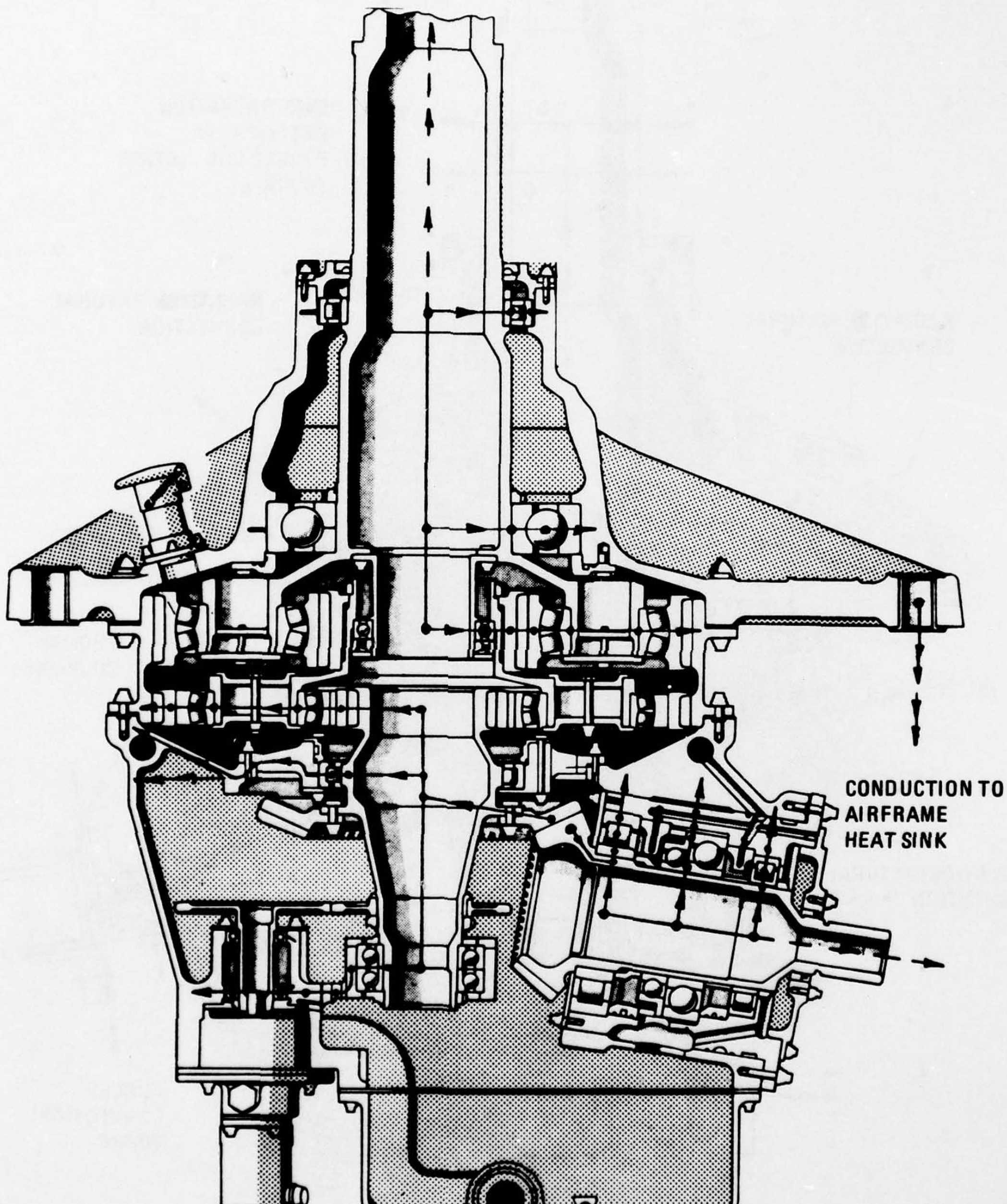

Figure 38. Illustration of Internal Conductive Heat Paths of Specimen Transmission

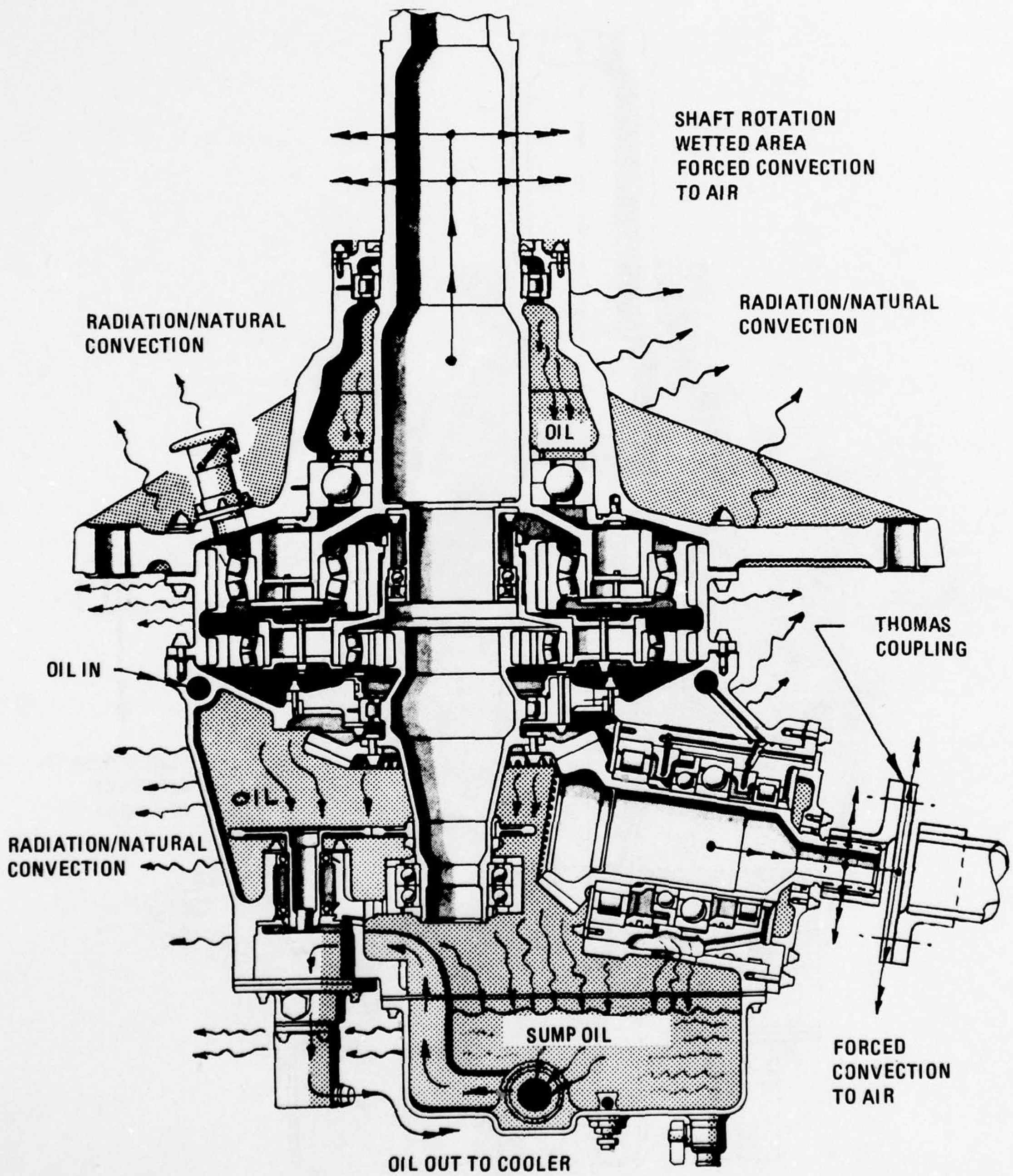

Figure 39. Illustration of Radiation/Natural Convection and Forced Convection (Oil) Heat Paths of Specimen Transmission

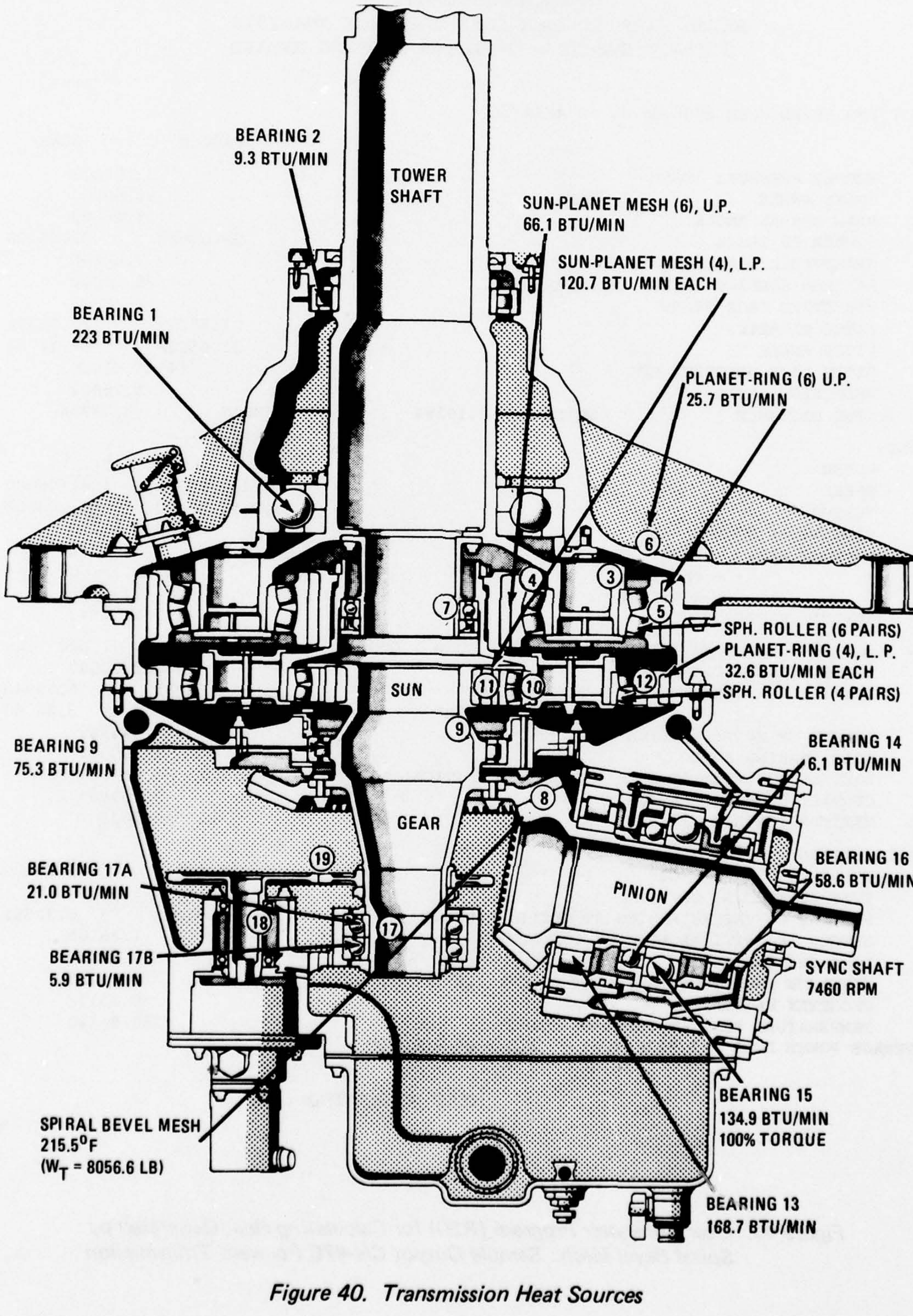

Figure 40. Transmission Heat Sources

RAYMOND J. DRAGO
BEVEL GEAR SURFACE LOAD CAPACITY ANALYSIS
CONTACT STRESS - G-FACTOR SCORING HAZARD

CH-47C FWD BEVEL MESH RUN FOR J. S. 4/14/76

	PINION	GEAR
NORMAL PRESSURE ANGLE	22.50000	
SHAFT ANGLE	99.00000	
MEAN SPIRAL ANGLE	25.00000	
NUMBER OF TEETH	29.00000	51.00000
TRANSVERSE DIAMETRAL PITCH OUTER	3.84100	
MAXIMUM SURFACE FINISH (MICROINCHES)	20.00000	
EFFECTIVE FACE WIDTH	2.18800	
PITCH DIAMETER	7.55012	13.27779
PITCH ANGLE	31.65230	67.34764
PITCH LINE VELOCITY FPM	14745.01000	
REDUCTION RATIO	1.75862	
CONE DISTANCE OUTER = 7.19384	MEAN = 6.09984	
STRESS:		
POWER	3600.000	
SPEED	7460.00000	4241.96000
TORQUE	30414.20000	53487.03000
TANGENTIAL TOOTH LOAD	8056.61700	
CONTACT RATIO - FACE	1.50491	
- PROFILE	1.25868	
- MODIFIED	1.96189	
INERTIA FACTOR	1.01942	
KO = 1,000 KV = 1,000 KM = 1,100 KS = 0,714 CS = 1,000 CF =	1.000	
ELASTIC COEFFICIENT	2800.00000	
PROFILE CURVATURE RADIUS - PITCH POINT	1.69785	6.59948
- CRITICAL POINT	1.87387	6.42346
LENGTH OF CRITICAL LINE OF CONTACT	1.544348	
LOAD SHARING RATIO	1.000000	
DISTANCE BETWEEN TOOTH MIDPOINT AND CRITICAL POINT	-0.017148	
CONTACT GEOMETRY FACTOR	0.094451	
MAXIMUM CONTACT STRESS	211021.3000	
SCORING HAZARD:		
THERMAL CONSTANT, C1	41.00000	41.00000
THERMAL FACTOR, CG	1.00000	
PROFILE CURVATURE RADIUS AT CRITICAL POINT	1.97082	6.32651
LENGTH OF CRITICAL LINE OF CONTACT	1.46105	
LOAD SHARING RATIO	0.70570	
DISTANCE FROM TOOTH MIDPOINT TO CRITICAL POINT	0.18285	
GEOMETRY FACTOR, G	0.00178	
TEMPERATURE RISE AT CRITICAL POINT	215.50340	

AVERAGE POWER LOSS = 7,3178 H.P. = 310,6389 BTU/MIN

HEAT GENERATED

Figure 41. Gear Computer Program (R20) for Calculating Heat Generated by Spiral Bevel Mesh. Sample Output CH-47C Forward Transmission

TAN. LOAD LBS.	SCORNG FACTOR	FRICT. COEFF.	TEMP. RISE F DEG	FINAL TEMP. F DEG	FILM THCK. MICRO	INSTANTANEOUS POWER LOSS HP	BTU/MIN
0.	0.0026	0.0600	0.00	200.00	0.000	0.00	0.00
4773.	0.0009	0.0600	18.64	218.64	12.245	1.23	52.24
4773.	0.0000	0.0600	0.00	200.00	13.624	0.00	0.00
4773.	0.0008	0.0600	16.91	216.91	15.053	1.29	54.74
682.	0.0020	0.0600	9.15	209.15	22.210	0.47	20.05
0.	0.0026	0.0600	0.00	200.00	0.000	0.00	0.00
682.	0.0023	0.0600	10.61	210.61	13.603	0.39	16.52
1364.	0.0020	0.0600	15.59	215.59	12.821	0.69	29.46
2046.	0.0017	0.0600	18.17	218.17	12.536	0.92	38.80
2728.	0.0014	0.0600	19.00	219.00	12.438	1.05	44.50
3410.	0.0012	0.0600	18.41	218.41	12.436	1.10	46.50
4773.	0.0009	0.0600	18.63	218.63	12.246	1.23	52.22
4773.	0.0007	0.0600	13.74	213.74	12.589	0.93	39.25
4773.	0.0005	0.0600	8.99	208.99	12.935	0.62	26.17
4773.	0.0002	0.0600	4.38	204.38	13.282	0.31	12.99
4773.	0.0000	0.0600	0.10	200.10	13.632	0.01	0.31
4773.	0.0002	0.0600	4.47	204.47	13.984	0.32	13.73
4773.	0.0004	0.0600	8.72	208.72	14.338	0.64	27.26
4773.	0.0006	0.0600	12.86	212.86	14.694	0.97	40.93
4773.	0.0008	0.0600	16.91	216.91	15.053	1.29	54.72
4092.	0.0010	0.0600	18.58	218.58	15.725	1.39	58.85
3410.	0.0012	0.0600	19.21	219.21	16.481	1.39	59.08
2728.	0.0014	0.0600	18.73	218.73	17.358	1.31	55.38
2046.	0.0016	0.0600	17.06	217.06	18.428	1.12	47.68
1364.	0.0018	0.0600	14.00	214.00	19.859	0.85	35.92
682.	0.0020	0.0600	9.15	209.15	22.210	0.47	20.05

Figure 42. Typical Computer Output for Calculating Thermal Power Generated by Gear Teeth

TABLE 5. HEAT GENERATED BY COMPONENTS

MESHES (GEARS, FIGURE 40)			IDENTIFICATION
6	66.1	396.6	UP Sun-Planet
4	120.7	482.8	LP Sun-Planet
6	25.7	154.2	UP Planet-Ring
4	32.6	130.4	LP Planet-Ring
1		1145	Spiral Bevel
		2309.05 BTU/MIN	

BEARINGS (FIGURE 40)	FRICTION	VISCOUS	TOTAL	TYPE
Pinion No. 16	34.8	23.8	58.6	Roller
Pinion No. 15	109.5	25.6	134.9	Ball
Pinion No. 13	128.0	40.7	168.7	Roller
Lower Sun No. 17A	15.2	5.8	21.0	Upper Ball
Lower Sun No. 17B	.14	5.8	5.9	Lower Ball
Lower Sun No. 9	55.6	19.7	75.3	Roller
LP No. 10	411.6	18.0	429.6	Roller
UP No. 4	409.8	5.0	414.8	Roller
Rotor No. 1	21.2	1.1	22.3	Ball
Rotor No. 2	8.7	.6	9.3	Roller
	1194.5	146.1	1340.4 BTU/MIN	

TOTAL $= 3649.4 \frac{\text{BTU}}{\text{MIN}} = 86.03$ HP

TOTAL HP $= 3600.$, % Lost $= 2.39$

EFFICIENCY $= 97.6\%$

TOTAL HEAT GENERATED $= 4262.6 \cdot 60 \frac{\text{SEC}}{\text{MIN}} = 218964. \frac{\text{BTU}}{\text{HR}}$

The heat generated by all the bearings as well as other pertinent data is shown in Figure 43. In order to obtain a comparative relationship, an assessment of the heat capacity of the transmission oil was made. The following oil-in/oil-out temperatures shown in Table 6 were obtained by experiment (Reference 12).

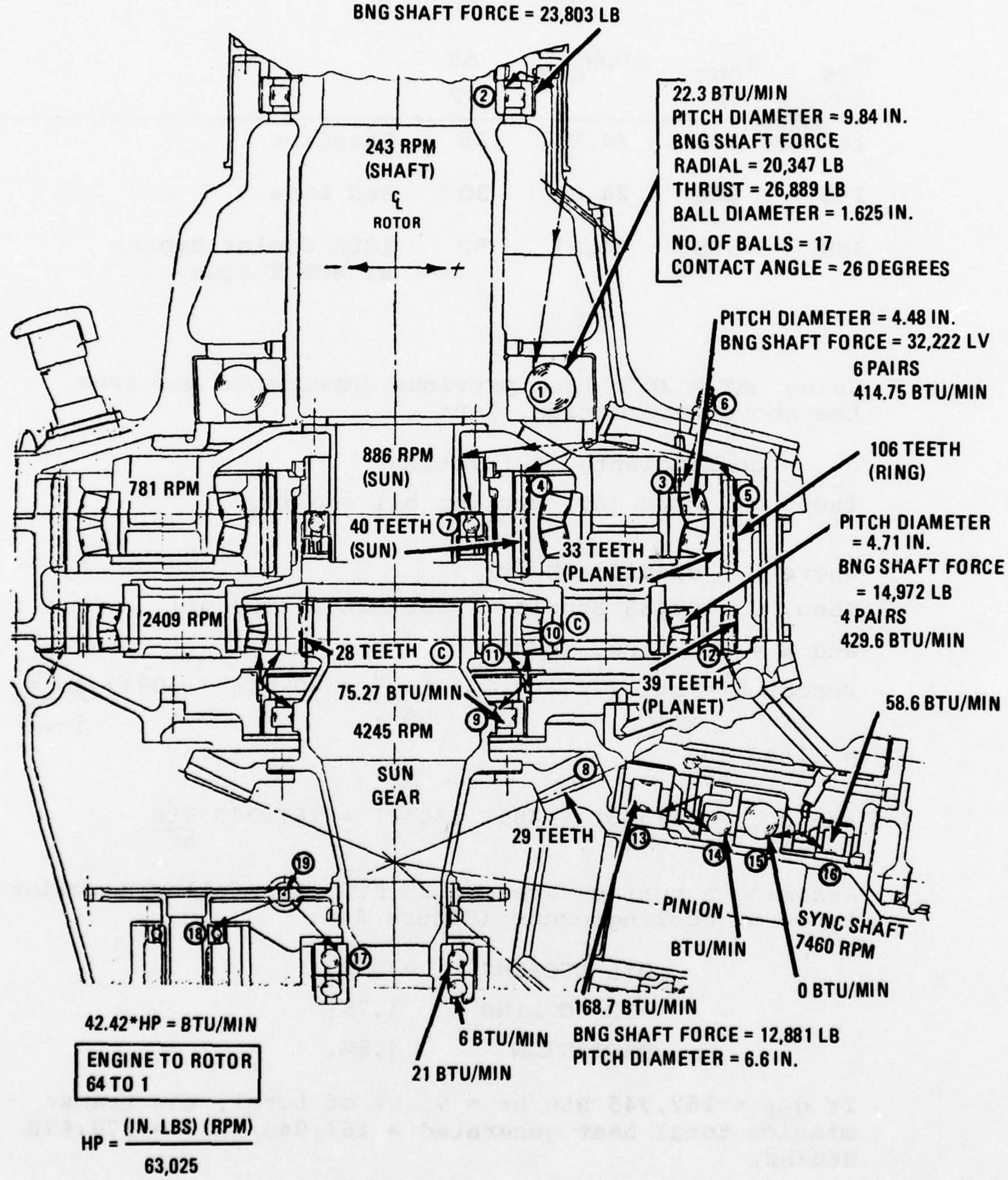

Figure 43. Bearing Heat Generation CH-47 Forward Transmission 100% Torque, 3600 HP

TABLE 6. OIL-IN/OIL-OUT TEMPERATURES

T_{IN} °F	T_{OUT} °F	$FLOW_{GPM}$	ΔT °F	
160	185	24.81	25	Baseline
256	286	24.81	30	Red Line
348	398	24.81	50	100% Cooler Bypass at 40% Torque

Using $\Delta T = 30^{\circ}F$ from previous experience and from the above information, let:

q_{cf} = coefficients of friction

Then, $q_{cf} = WC\ (\Delta T)\ \frac{Btu}{hr}$ for oil cooling,

Where C = specific heat

Then, C = 0.485 Btu/lb °F for MIL-L-7808 oil

and W = oil flow, lb/hr

Hence, $W = \frac{gal}{min}\ (24.)\ *\ 231\ \frac{in.^3}{gal.}\ *\ 60\ min\ *\ .0347\ \frac{lb}{in.^3} =$

$= 11543\ \frac{lb}{hr}$

and $q_{cf} = (11543)\ (.485)\ (30°F) = 167{,}945\ \frac{Btu}{hr}$

Assuming a surface area of 29 FT^2, the following major types of cooling occur (Figure 44):

OIL COOLING	93.5%,
AIR COOLING	1.7%,
RADIATION	4.8%.

If q_{cf} = 167,945 Btu/hr = 93.5% of total, the transmission total heat generated = 167,945/.935 = 179,620 Btu/hr.

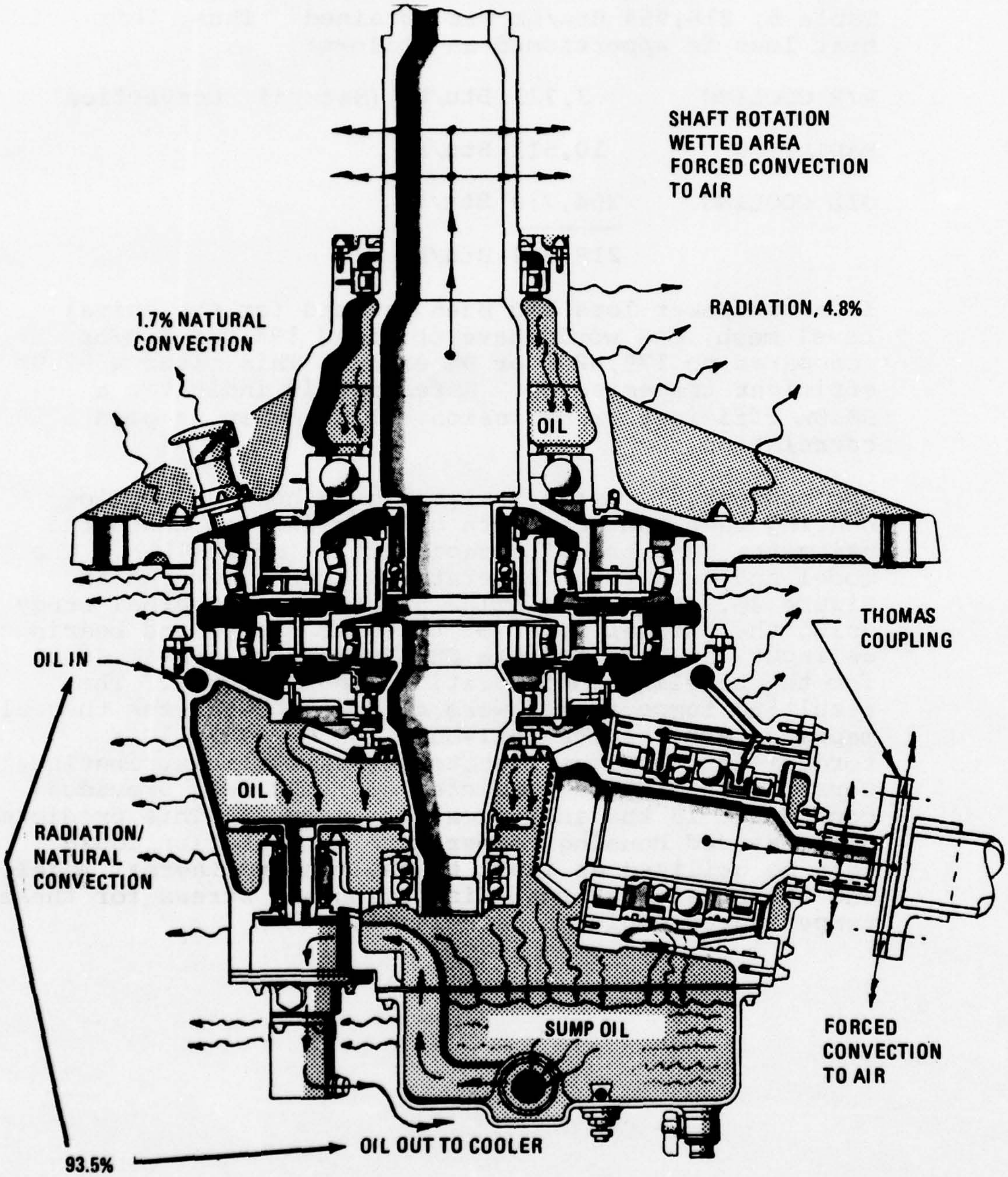

Figure 44. Illustration of Radiation/Natural Convection and Forced Convection (Oil) Heat Paths of Specimen Transmission

From the calculation of heat generated shown in Table 5, 218,964 Btu/hr was obtained. Thus, this heat loss is apportioned as follows:

AIR COOLING	3,723	Btu/hr (Natural Convection)
RADIATION	10,511	Btu/hr
OIL COOLING	204,730	Btu/hr
	218,964	Btu/hr

If a .5% power loss had been assumed for the spiral bevel mesh, one would have obtained 196,044 Btu/hr (compared to 179,620) or 9% error. This gives a 97.9% efficient transmission. Reference 12 indicates a 98.6% efficient transmission. This again is good correlation.

The conceptual design analysis of a heat generating bearing race and gear with oil cooling was conducted using the heat transfer capabilities of NASTRAN. The model and resulting temperatures are summarized in Figure 45. Using a similar procedure, a thermal study using the thermal power of the gear meshes and bearings as input was made for the CH-47C forward transmission for the baseline configuration (100% torque). The resulting temperatures were correlated with the thermal mapping test results (oil-out, 180°F $\pm$ 10%, 100% torque) for the steady state temperature distribution. Correlation of this predicted and test data provided confidence in the analytical techniques. This predicted and measured housing temperature distribution could then be utilized as input to the housing thermal model, and the housing thermal distortion and stress for these temperatures could be calculated.

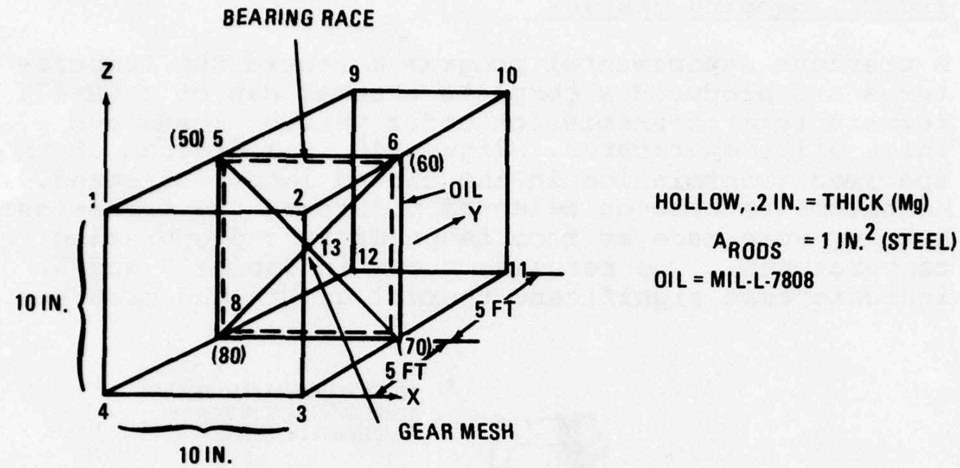

$$K_{MG} = 88.5 \ \frac{BTU}{HR/FT/^{0}F} \ \frac{1 \ HR}{60 \ MIN} \ \frac{1 \ FT}{12 \ IN.} = .123 \ \frac{BTU}{MIN/IN./^{0}F}$$

$$K_{STEEL} = 26.4/60*12) = .0367 \ \frac{BTU}{MIN/IN./^{0}F}$$

MODEL AND THERMAL CONDUCTIVITIES

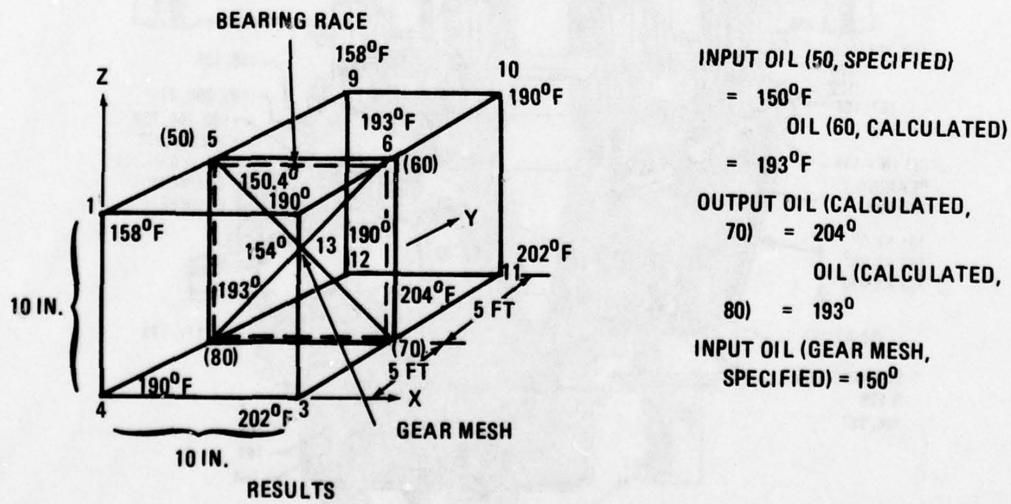

RESULTS

Figure 45. Conceptual Drawing and Sample Calculations

4. Thermal Mapping Studies

A previous experimental program measured the temperatures and produced a complete thermal map of a CH-47C forward rotor transmission under various loads and inlet oil temperatures. Figure 46 is a diagram of the specimen transmission in the closed loop test stand. Measurements between selected points on the transmission housing were made at room temperature and operating temperatures. The results, shown in Tables 7 and 8, indicate that significant thermal growth had occurred.

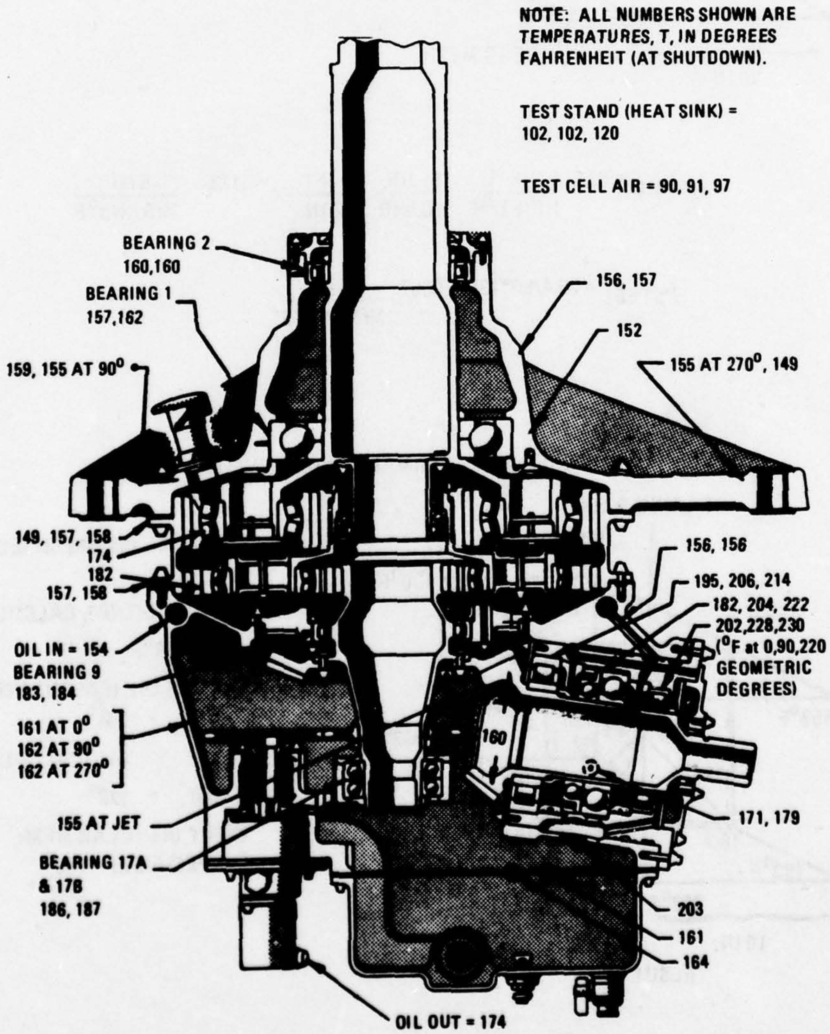

Figure 46. Typical Thermal Map of CH-47 Forward Transmission (Reference 12)

TABLE 7. MEASUREMENTS OF THERMAL GROWTHS (CASE ELEMENTS)

DIMENSIONS OR DIAMETERS*	LOCATIONS*
D1 (Dia.)	Around Planetary Stages
D2 (Dia.)	
D3 (Dia.)	
D4 (Dia.)	
D5 (Dia.)	Rotor Shaft Radial Bearing Housing
D6 (Dia.)	Pump Housing
D7 (Dia.)	Sync Shaft
D8 (Dia.)	
D9 (Dia.)	Sync Shaft Coupling
X1 (Dim.)	Point thru Rib at Cone ℄ S/B and ℄ Shaft at D7 Diameter
X2 (Dim.)	Diagonal: ℄ S/B Cone and Sump Flange at Bearing C
X3 (Dim.)	Between B and C Bearings on ℄ Shaft and Cone ℄ S/B
Z1 (Dim.)	S/B Cone Center and Plane 2
Z2, 1 (Dim.)	Outer Points
Z2, 2 (Dim.)	Inner Points
Z3 (Dim.)	Between Planes 4 and 5

TABLE 8. DIMENSIONAL GROWTH PARAMETER EVALUATION

DIMENSION IDENTITY	l_c (inches) at T_c Cool		l_h (inches) at T_h Hot		ΔT $T=T_h-T_c$ (°F)	$\frac{\Delta l}{l_c}/\Delta T$ x 10^6	COEFFICIENT OF EXPANSION k x 10^6
	l_c	T_c(°F)	l_h	T_h			
D1 (Mag.)	24.860	73	24.900	190	117	13.8	15.1
D2 (Steel)	24.826	73	24.842	190	117	5.5	6.53
D3			NOT MEASURED				
D4 See Note	24.877	73	24.940	190	117	21.6	13.1
D5 (Alum. Aly.)	10.500	73	10.516	215	142	10.7	13.1
D6 (Alum.)	5.579	73	5.595	215	142	20.2	13.1
D7 (Mag.)	12.501	73	12.533	230	157	16.3	15.1
D8 (Mag.)	12.444	73	12.470	230	157	13.3	15.1
D9 (Steel)	2.643	73	2.645	180	107	7.07	6.53
X1 (Mag.)	15.520	73	15.558	260	187	13.1	15.1
X2 (Mag.)	10.638	73	10.718	250	177	.	15.1
X3 (Mag.)	9.690	73	9.710	250	177	15.2	15.1
Z1 (Mag.)	7.864	73	7.899	240	167	26.6	15.1
Z2, 1 (Steel)	4.275	73	4.261	220	147	22.3	6.53
Z2, 2 (Steel)	3.243	73	3.237	220	147	12.6	6.53
Z3 (Alum.)	15.634	73	15.682	210	137	22.4	13.1

<u>NOTE</u> - Measured on adjacent aluminum.

To further investigate the effects of temperature upon a transmission housing, the thermal distortions and stresses were calculated using the NASTRAN model and thermal map data from Reference [12] for the following conditions:

OIL-OUT	TORQUE (%)
$185^{o}F \pm 10\%$	100
$286^{o}F \pm 10\%$	100
$400^{o}F \pm 10\%$	100

The temperature within each oil-out condition was independent of torque. The NASTRAN static analysis (Rigid Format 1) was used to calculate the thermal distortions and stresses, and dimensional stability of critical housing points and misalignment effects were evaluated.

The computer-generated plot in Figure 47 shows the regions of the housing where it interfaces with the bearings. The vectors plotted indicate the displacements at each grid point due to the applied temperature distribution for the $185^{o}F$ oil-out condition. By evaluating the distortion of the bearing interface at each end of the respective supporting shafts individually and then evaluating the relative distortion between the shaft ends, the thermally induced misalignment of the pinion shaft and the bevel/sun gear shaft was calculated. By comparing the relative misalignment between the pinion and gear shafts, the overall effect of temperature upon the gear mesh alignment may be assessed.

A NASTRAN post-processor program uses the grid point displacement and geometry data to calculate the induced misalignments. A sample output for the $185^{o}F$ case is provided as Appendix C. This program indicated that the induced slopes of the pinion and bevel/sun shafts are .0003 in./in. and .0004 in./in., respectively (Figure 48). Also, the displacements at the pinion and bevel gear pitch diameters are .005 and .008 inch, respectively.

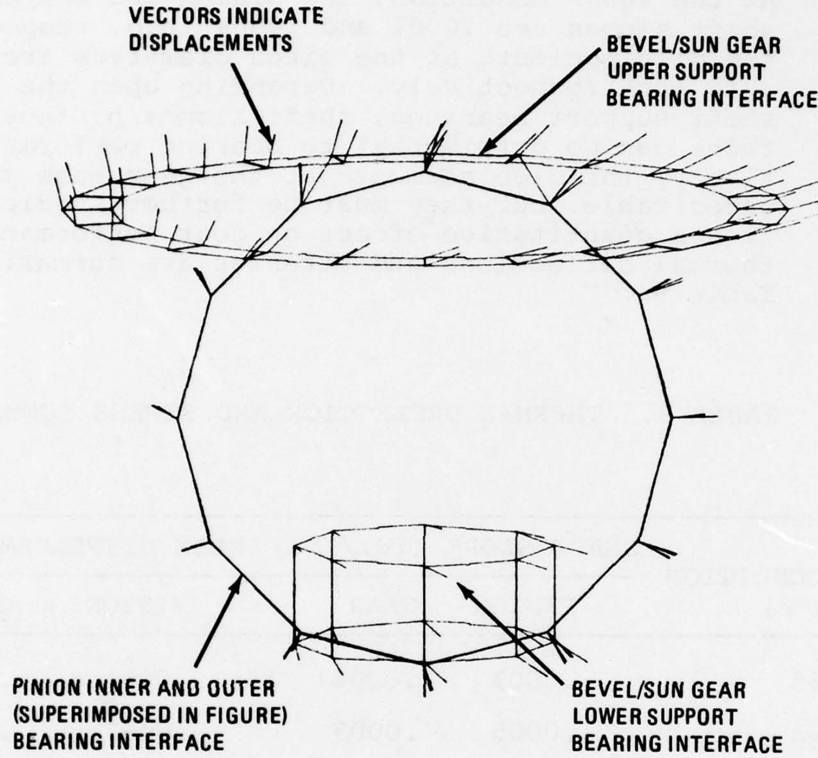

Figure 47. Induced Displacements at Housing/Bearing Interface Due to Temperature — 185°F (85°C) Oil Out

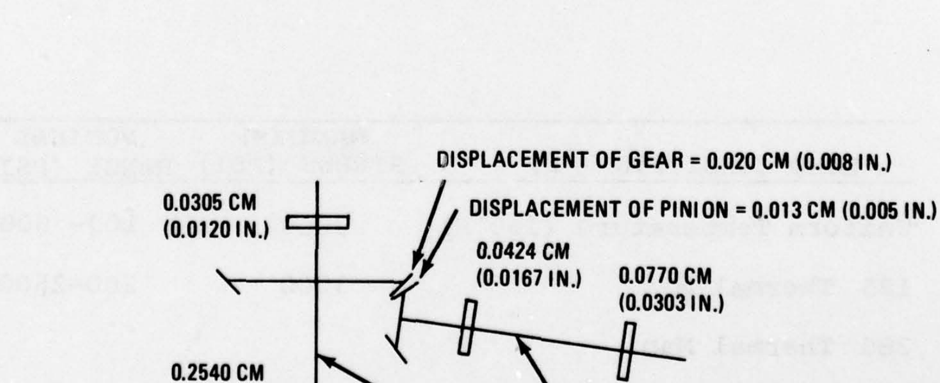

Figure 48. Displacement of Internal Components Due to Imposed Temperature Distribution (Thermal Map Data 185°F (85°C))

At the 400°F condition, the pinion and sun/bevel gear shaft slopes are .0007 and .0009 inch, respectively; the displacements at the pitch diameters are .013 and .015 inch respectively. Depending upon the type of shaft support bearings, shaft slopes of these magnitudes can be detrimental to bearing performance. Similarly, the displacements at the gear mesh point are undesirable, but they must be further studied to establish a quantitative effect on gear performance. The thermal deflections and stresses are summarized in Table 9.

TABLE 9. THERMAL DEFLECTION AND STRESS SUMMARY

LOAD CONDITION (°F)	SHAFT SLOPE (IN./IN.)		MESH DISPLACEMENT (IN.)	
	PINION	GEAR	PINION	GEAR
185	.0003	.0004	.0051	.0080
286	.0005	.0007	.0087	.0111
400	.0007	.0009	.0130	.0150

LOAD CONDITION (°F)	MAXIMUM STRESS (PSI)	NOMINAL RANGE (PSI)
Uniform Temperature (160°F)	2000	100- 600
185 Thermal Map	3200	200-2500
286 Thermal Map		
400 Thermal Map		

5. Thermal Studies

For the thermal analysis the following heat rejection means were identified:

- Conduction (to a heat sink; e.g., airframe)
- Radiation
- Convection
  - Natural (free)
  - Forced (oil)
- Changes of State

Reference 12 indicated that the amount of heat rejection by conduction, radiation, and natural convection was small in comparison to the forced convection due to lubricant cooling. Little data is available regarding heat absorption due to change of state. In one test, smoke-off (change of state) was recorded at $240^{\circ}F$ with aggravated smoke-off (vaporization) at $300^{\circ}F$. The following equations were useful as a basis for the thermal studies:

- Radiation: The Stefan-Boltzmann Law:

$$q_r = A\varepsilon\sigma\,(T_1^{\,4} - T_2^{\,4}) = A\varepsilon\sigma\,\left((t_1 + 460)^4 - (t_2 + 460)^4\right)$$

where, q_r = heat rejection rate, Btu/hr

A = black gray body (specimen transmission) surface area, ft = 29 ft^2

T_1 = black-gray body surface temperature (equal to oil-out temperature), °R

T_2 = temperature of surroundings (test cell wall temperature - ambient air temperature), 560°

ε = emissivity/absorptivity constant; optimistically assumed at 0.9

σ = Stefan-Boltzmann constant assumed at 0.173 x 10^{-8}

which becomes

$$q_r = 4.5153 \times 10^{-8} \left((t_1 + 460)^4 - (t_2 + 460)^4 \right)$$

- Convection:

<u>Natural Convection</u>

$$q_{cn} = h\,A\,(t_1 - t_2)$$

where q_{cn} = heat rejection, Btu/hr

A = specimen transmission surface area = 29 ft^2

h = $0.22\,(t_1 - t_2)^{1/3}$

D = specimen transmission average diameter = 2 ft

t_1 = specimen transmission surface temperature °F or °R

t_2 = ambient air temperature, same degree unit

which becomes

$$q_{cn} = 6.38\,(t_1 - t_2)^{4/3}$$

<u>Forced Convention (Oil)</u>

$$q_{cf} = WC\,(t_1 - t_3)$$

where W = oil flow, 8775 lb/hr

C = 0.485 Btu/lb/°F

t_1 = specimen transmission oil-out temperature, °F

t_3 = specimen transmission oil-in temperature, °F

Based on test results $(t_1 - t_2) = \Delta t = 30°F$, and q_{cf} = 8775 x 0.485 x 30 = 127,676 Btu/hr heat rejected by oil for 100 percent CH-47C transmission power.

The same test indicated an efficiency for the CH-47 forward rotor transmission of 98.6 percent. At 100 percent CH-47C forward transmission power (3600 SHP), the heat rejection rate is 128,000 Btu/hr (2134 Btu/min). For 75 percent and 50 percent powers, the heat rejection rates are 96,000 Btu/hr (1600 Btu/min) and 64,000 Btu/hr (1067 Btu/min) respectively. The family of curves in Figure 49 indicates the three specimen power levels and heat rejection rate versus average case temperature. When the oil cooler is fully by-passed and heat rejection is accomplished by natural convection and radiation alone, the case temperatures theoretically would reach those points indicated by the intersection of the curves with the zero percent ordinate. However, an analysis of the aft transmission test does not bear this out. With the evidence of smoke-off beginning at 240°F and terminal temperature at 320°F, it appears that other means of heat rejection are operating. Otherwise, the case temperature would reach approximately 430°F. The straight line intersection, both the lowest curve and 240°F and the zero percent ordinate at 330°F, represents a cutoff of case temperature rise to match test experience.

After conducting the initial model development and validation, studies were performed to evaluate a closed transmission system with no external cooler. Such factors as air flow and use of cooling fins were considered. The housing model was modified to include cooling fins of various configuration and total area. Fin cooling assuming an oil-out temperature of 200°F was investigated.

Assuming the conservative .75% power loss figure for the spiral bevel mesh, a study of forced convection (air) to eliminate the oil-cooling lines (204,730 Btu/hr) was conducted. For the conceptual study, assume that a transmission housing is represented by a 2-foot-diameter by 3-foot-high cylinder. The Nusselt number for the flow perpendicular to the longitudinal axis, from Reference 19, is

$$Nu_d = .43 + C\,(Re_d)^m$$

where Re_d, the Reynold's number, $= \dfrac{u_m d}{\nu}$ and

u_m = mean air velocity (ft/sec)

d = cylinder diameter (ft)

ν = kinematic viscosity of air (ft^2/sec)

---

19. Eckert and Drake, HEAT AND MASS TRANSFER, McGraw-Hill, 1959.

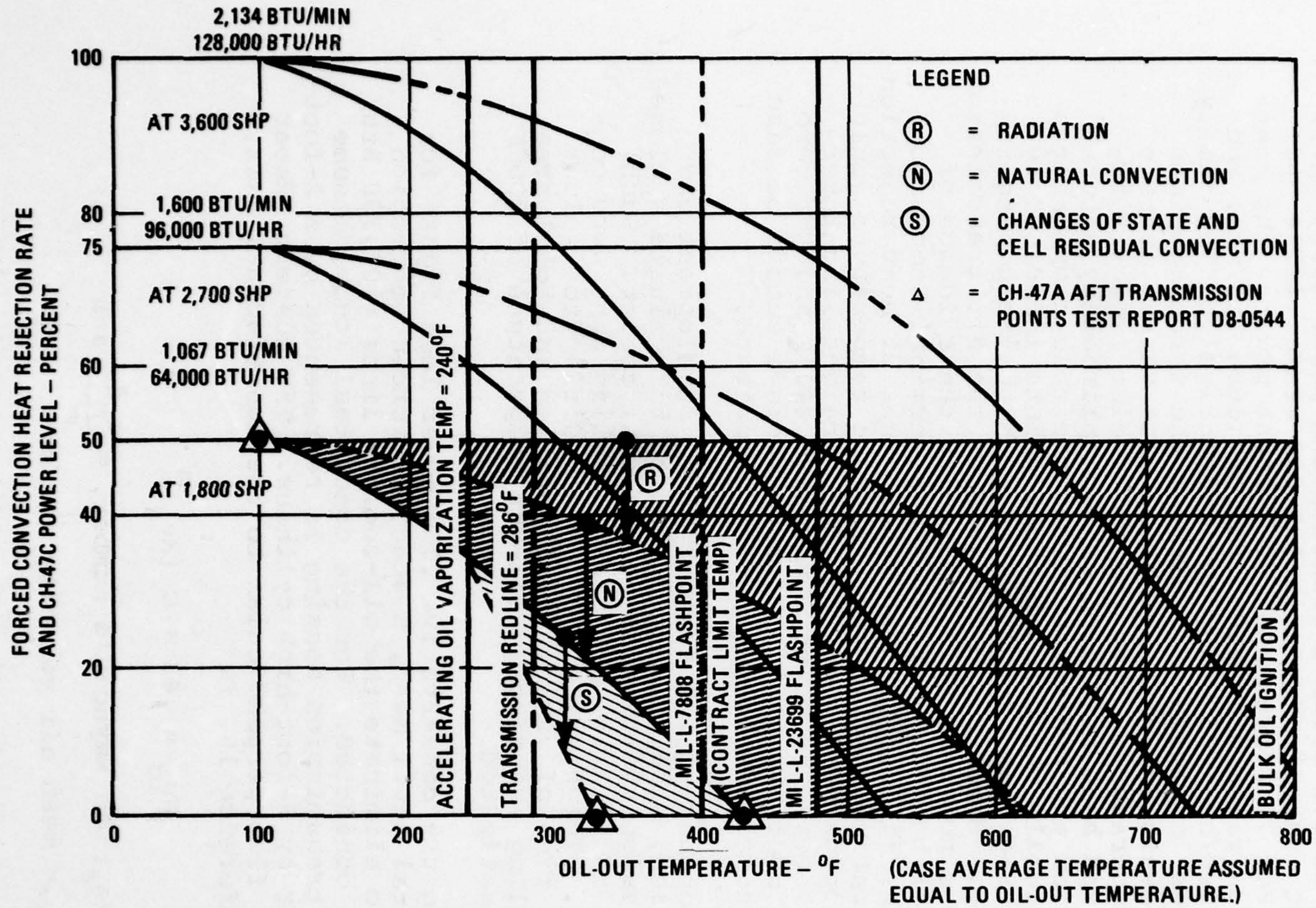

Figure 49. Theoretical Temperature Projection for Given Heat Rejection Rates and Power Levels (Based on CH-47 Forward Transmission Efficiency of 98.6 Percent) (Reference 12)

In order to determine u_m for an unfinned transmission, assume the ambient temperature to be 100°F.

$$\vartheta = 18.1 \times 10^{-5}\ FT^2/SEC,$$

$$K = .01565\ BTU/HR\ FT\ {}^{o}F\ \text{(Thermal Conductivity)},$$

$$\left.\begin{array}{l} C = .0239 \\ m = .805 \end{array}\right\} \text{(From Reference 19)}$$

The Nusselt number may also be expressed as

$$Nu_d = \frac{hd}{K} = \frac{2h}{.01565}$$

where h = film heat transfer coefficient (Btu/hr ft^2 °F).

$$\text{Then}\quad h = \frac{.01565}{2} Nu_d = \frac{.01565}{2} [.43 + C(Re_d)^m]$$

$$h = \frac{(.01565)}{2}\left[.43 + .0239 \left\{\frac{2\ u_m}{18.1 \times 10^{-5}}\right\}^{.805}\right]$$

$$h = .0034 + .3363\ (u_m)^{.805}$$

Assuming conservatively that the effective area of the cylinder is the frontal area (Figure 50), then,

$$Q = h\ A_{eff}\ \Delta T = h\ (9.42)\ (200^oF - 100^oF)\ \text{Btu/hr}$$

Here the cylinder surface temperature is assumed to be 200°F, and the ambient temperature = 100°F.

This gives

$$h = \frac{204748}{942} = 217.4$$

Hence,

$$u_m = 3101.0\ \text{ft/sec} \approx 2114\ \text{mph}$$

The Reynold's number in Figure 51 is low (1260). Here the Reynold's number is 7,144,750; at high Reynold's numbers, the film heat transfer increases on the back of the cylinder. In fact, at Re = 50,000, h is the same on the front and back.

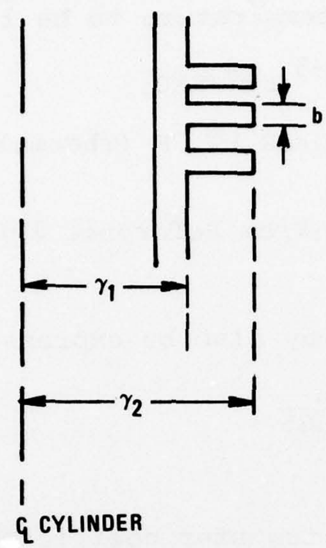

Figure 50. Effective Area of a Finned Cylindrical Surface

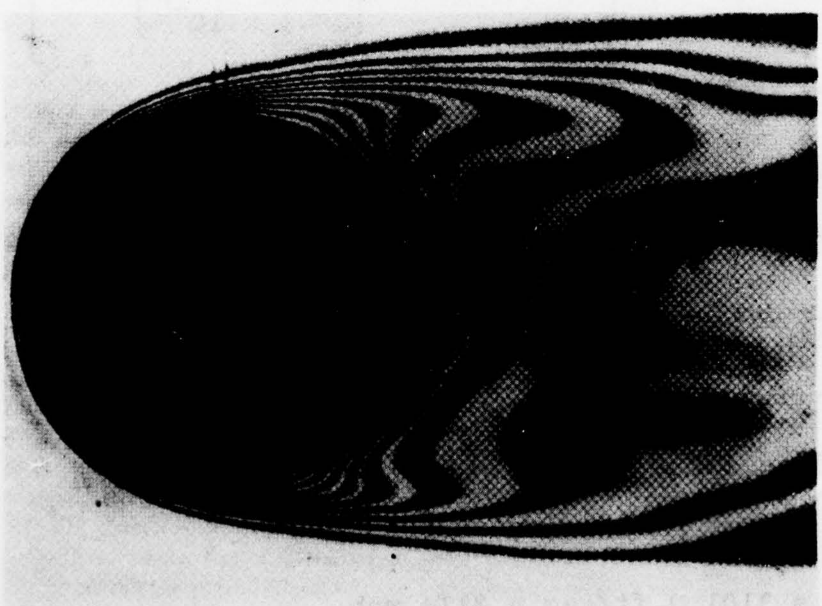

Figure 51. Isotherms Around a Cylinder Cooled by a Fluid Flowing Normal to its Axis, as Revealed by an Interference Photograph. Re = 1,260

Repeating the calculations gives

$$u_m = 1308.7 \text{ ft/sec} = 892.2 \text{ mph}$$

If the shape of the transmission is considered (Table 10), then

$$u_m = \log^{-1}\left[\frac{4.142 - \log C}{m} - 4.04\right] \text{ ft/sec}$$

yields:

CONFIGURATION	u_m (ft/sec)
1	4273
2	13058
3	6314
4	1328

TABLE 10. COEFFICIENTS FOR CALCULATION OF HEAT TRANSFER FROM CYLINDERS WITH DIFFERENT CROSS SECTIONS TO AN AIR FLOW NORMAL TO THEIR AXES (Reference 19)

Cross section	Re_d	C	m	Configuration
→ □	5,000–100,000	0.0921	0.675	1
→ ◇	5,000–100,000	0.222	0.588	2
→ ⬡	5,000–100,000	0.138	0.638	3
→ ⬡	5,000– 19,500	0.144	0.638	
→ ⬡	19,500–100,000	0.0347	0.782	4

Such air velocities are not only impossible, but they would cause a heat increase by converting internal skin friction into heat. As a second resort, fins may be added. In fact, they can be combined with a forced air flow.

A conceptual design is made for the previous cylinder to find the number of fins 2 inches long and 1 inch thick that would be required in a forced air flow of 50 ft/sec (34 mph).

$$Q_1 \text{ (with fins)} = 2\pi\gamma_1 b K \sqrt{\beta}\,(\Delta T)\, Z =$$

Heat Loss Per Fin, BTU/HR

where:

$$Z = \frac{I_1(\gamma_2\sqrt{\beta})\,K_1(\gamma_1\sqrt{\beta}) - K_1(\gamma_2\sqrt{\beta})\,I_1(\gamma_1\sqrt{\beta})}{I_1(\gamma_2\sqrt{\beta})\,K_o(\gamma_1\sqrt{\beta}) + K_1(\gamma_2\sqrt{\beta})\,I_o(\gamma_1\sqrt{\beta})},$$

$$\beta = \frac{2h}{Kb},$$

K_{mg} = 100 Btu/hr ft °F (Conductivity of Magnesium)

γ_1 = 12 in.

γ_2 = 14 in.

b = 1 in. (see Figure 50)

Let

$T_{AMBIENT} = 100^oF$,

$T_{SURFACE} = 200^oF$, and

V = 50 ft/sec (Forced Convection),

I_1, I_o, K_1 and K_o are Bessel functions.

Now,

$$Re_d = \frac{(50)\ (2)}{.000181} = 552{,}486$$

$$Nu_d = .43 + .0239\ (552486)^{.805} = \frac{2h}{.01565}$$

$$= 1002.66 = \frac{2h}{.01565}$$

$$h \quad = 7.845 \text{ Btu/hr ft}^2\ °F$$

Using the previous method of calculation, the forced convective cooling of the cylinder with no fins is:

Q_o = (7.846) (18.84) (100) = 14781.9 BTU/HR

With the addition of one fin,

$$\beta = \frac{(2)\ (7.846)\ (12)}{(100)\ (1")} = 1.883,\ \sqrt{\beta} = 1.3722,$$

$$\gamma_1\sqrt{\beta} = \frac{12}{12}\ (1.3722) = 1.3722,\quad \gamma_2\sqrt{\beta} = 1.6009$$

Q_1 = (2π) (1') (1/12) (100) (1.3722) (100) Z =

7184.8 Z per fin. Now

I_1 (1.6009) = 1.086	K_1 (1.3722) = .3368
I_1 (1.3722) = .862	K_1 (1.6009) = .2406
I_o (1.3722) = 1.531	K_o (1.3722) = .2541

$$Z = \frac{(1.086)(.3368) - (.2406)(.862)}{(1.086)(.2541) + (.2406)(1.531)} = \frac{.1584}{.6443} = 2458$$

Hence, Q_1 = 1766 Btu/hr per fin

In order to eliminate the oil cooling of 204,748 Btu/hr, it would require 116 fins. For a 3-foot high, 1-inch-thick fin, this is impossible. Hence, the air velocity of 50 ft/sec (34 mph) must be increased. On the other hand, the thickness of the fins could be decreased.

If

$$V = 100 \text{ ft/sec}$$

$$Re_d = \frac{(100)\ (2)}{.000181} = 1{,}104{,}974$$

$$Nu_d = .43 + .0239\ (1{,}104{,}972)^{.805} = 1751.5 = \frac{2h}{.01565}$$

$$h = 13.7$$

$$Q_o = 25810.8 \text{ for no fins}$$

$$\beta = \frac{(2)\ (13.7)\ (12)}{(100)\ (1)} = 3.288\ ,\ \sqrt{\beta} = 1.81$$

$$\gamma_1\sqrt{\beta} = 1.81\ ,\ \gamma_2\sqrt{\beta} = 2.117$$

Hence $Q_1 = (2\pi)\ (1')\ (1/12)\ (100)\ (1.81)\ (100)\ Z = 9477.1$

$I_1\ (2.117) = 1.78$	$K_1\ (1.81) = .180$
$I_1\ (1.81) = 1.33$	$K_1\ (2.117) = .121$
$I_o\ (1.81) = 2.00$	$K_o\ (1.81) = .144$

$$Z = \frac{(1.78)\ (.180) - (.180)\ (1.33)}{(1.78)\ (.144) + (.121)\ (2.00)} = \frac{.1595}{.4983} = .320$$

$Q_1 = 3033$ Btu/hr per fin. This gives 68 fins (b = 1 ft) which is again impossible.

If V = 25 ft/sec = 17 mph,

$Q_1 = 1008$ Btu/hr, 203 fins, 1 in. thick, which is clearly impractical.

In summary:

V (ft/sec)	FIN COOLING (Btu/hr)	NUMBER OF FINS	HEIGHT (ft)
25	1008	203	16.9
50	1766	116	9.7
100	3033	68	5.7

Now, let b = .5 in. (fin thickness) and let V = 50 ft/sec.

$$Re_d = \frac{(50)\ (2)}{.000181} = 552{,}486 \text{ as before}$$

Hence,

$$h = 7.846$$

$$\beta = \frac{(2)\ (7.846)\ (12)}{(100)\ (.5)} = 3.766, \quad \sqrt{\beta} = 1.94\ ,$$

$$\gamma_1 \beta^{1/2} = 1.94\ , \quad \gamma_2 \beta^{1/2} = 2.263$$

Hence, $Q_1 = (2\pi)\ (1)\ (\frac{.5}{12})\ (100)\ (1.94)\ (100)\ Z = 5078.9\ Z$

$I_1\ (2.263) = 2.035$	$K_1\ (1.940) = .1527$
$I_1\ (1.940) = 1.5086$	$K_1\ (2.263) = .1003$
$I_o\ (1.940) = 2.1926$	$K_o\ (1.94) = .1235$

$$Z = \frac{(2.035)\ (.1527) - (.1003)\ (1.5086)}{(2.035)\ (.1235) + (.1003)\ (2.1926)} = \frac{.1594}{.4712} = .3383$$

$$Q_1 = (.3383)\ (5078.9) = 1718 \text{ Btu/hr}$$

This gives 119 fins, which is again impractical. Some results from a computer program to predict fin cooling with forced air flow across a cylinder (Appendix D) are summarized in Table 11.

TABLE 11. RESULTS OF FIN COOLING STUDY

V (ft/sec)	LENGTH (in.)	THICKNESS (in.)	COOLING (Btu/hr)	NUMBER OF FINS	HEIGHT OF FINS (ft)
50.	2.	.1	1505	136	1.1
50.	2.	.2	1629	126	2.1
50.	2.	.3	1676	122	3.05*
50.	2.	.5	1716		Impractical*
50.	2.	1.0	1747		Impractical*
20.	2.	.1	782	262	2.2
20.	2.	.2	815	251	Impractical*
20.	2.	.3			
20.	2.	.5			
20.	2.	1.0			

*The accumulative height of the fins must be less than the height of the cylinder (3 feet).

Figure 52 shows the feasibility of using thin fins with forced air convection to replace external oil cooling (V = 50 FT/SEC). A fan delivering a nominal 20 ft/sec with 262 2-inch fins, .1 inch thick, is in the realm of possibility also. It is noteworthy that fin cooling is insensitive to fin thickness above about 0.6 inch.

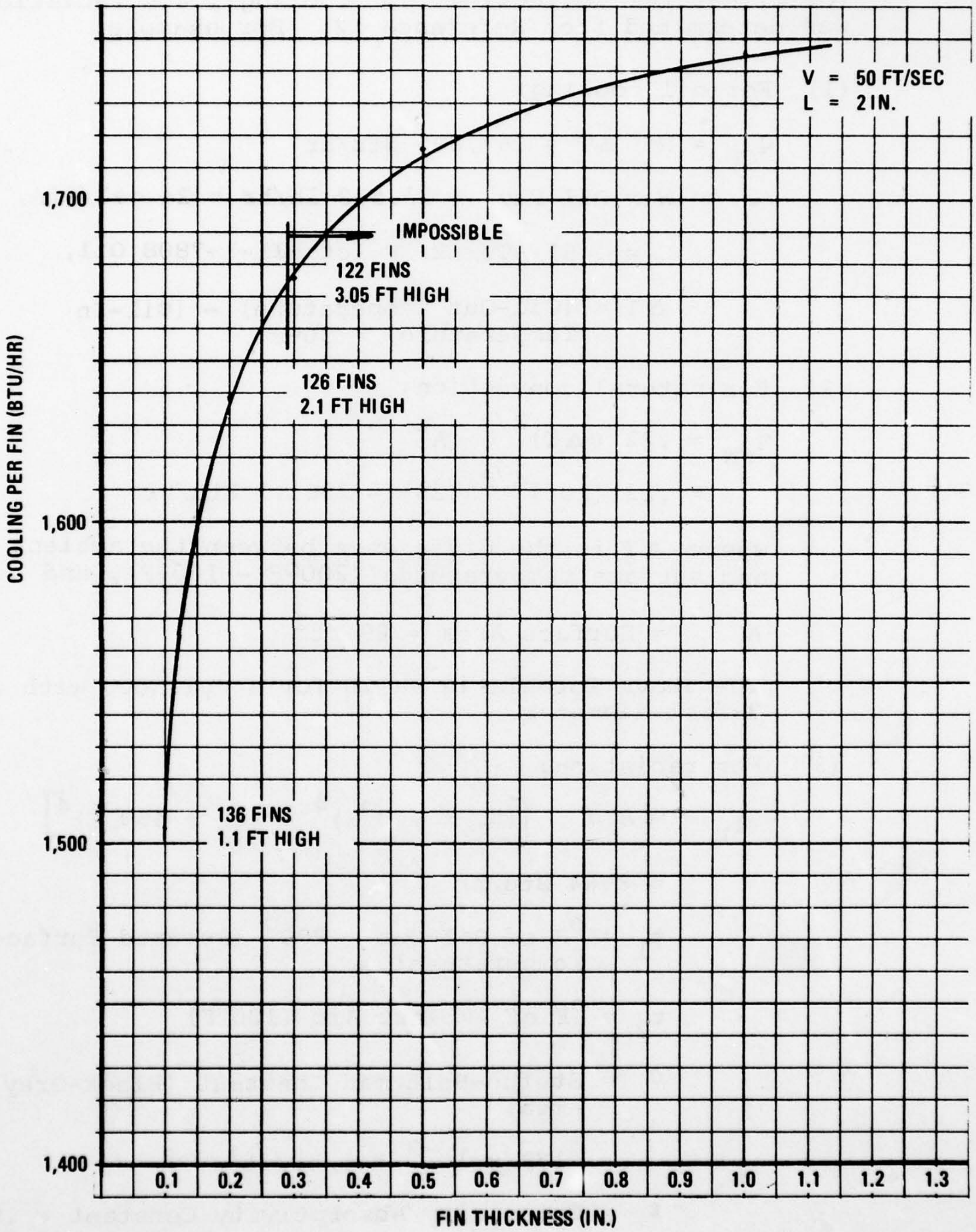

Figure 52. Fin Cooling Requirement to Eliminate Oil Cooling

AD-A052 759 BOEING VERTOL CO PHILADELPHIA PA F/G 1/3

FINITE ELEMENT ANALYSIS FOR COMPLEX STRUCTURES (HELICOPTER TRAN--ETC(U)

JAN 78 R W HOWELLS, J J SCIARRA DAAJ02-75-C-0053

UNCLASSIFIED D210-11232-1 USAAMRDL-TR-77-32 NL

2 OF 3

AD A052759

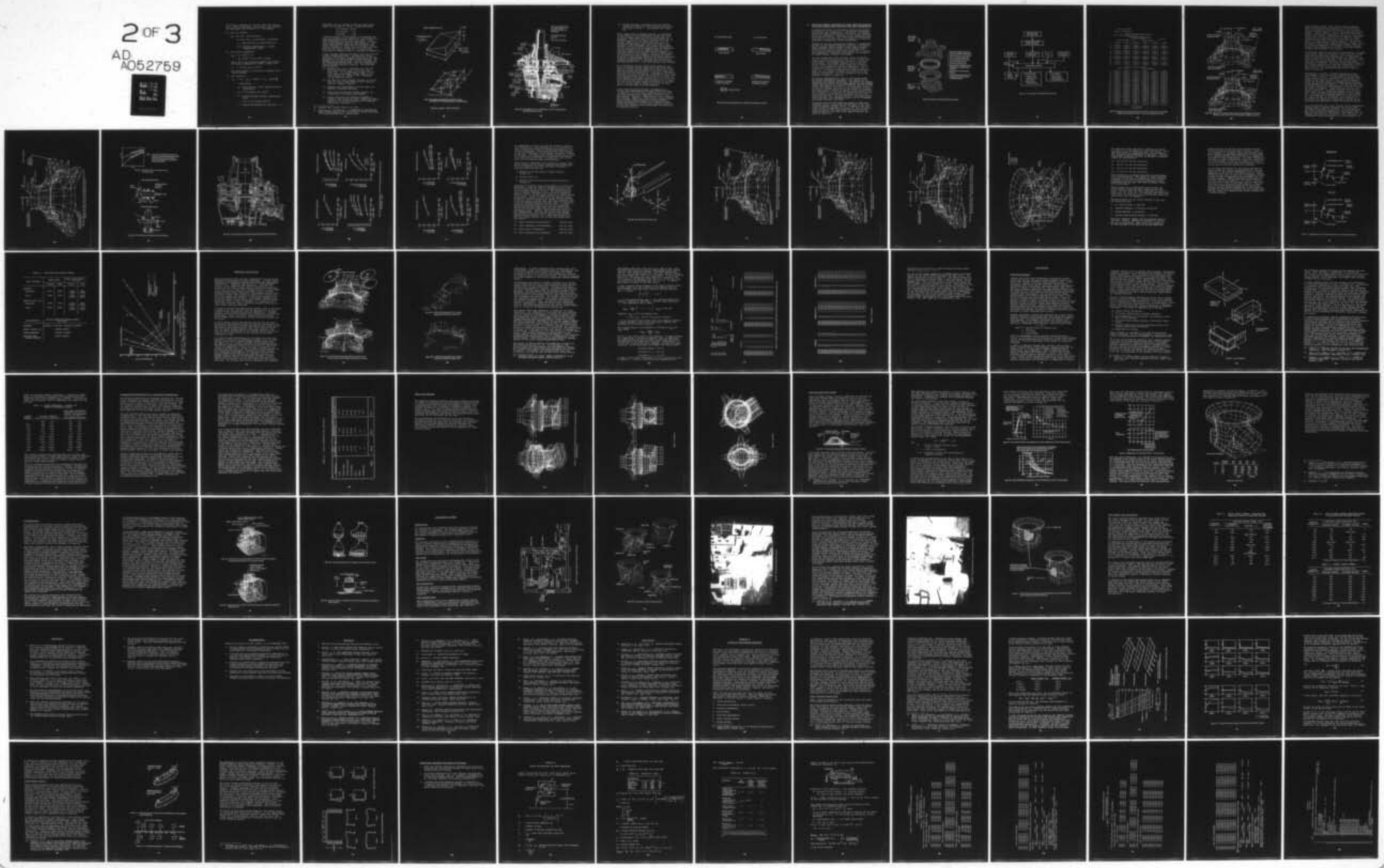

The relative importance of forced convection cooling (oil), natural convection (air cooling), and radiation was determined from Reference 12. For example,

(1) For oil cooling:

$$q_{CF} = WC \ \Delta T = 167{,}800 \text{ Btu/hr}$$

W = Oil Flow = 11,532 lb/hr = 24 gal/min,

C = .485 BTU/LB/$^{\circ}$F for MIL-L-7808 Oil,

ΔT = (Oil-Out Temperature) - (Oil-In Temperature) = 30°F

(2) For natural convection:

$$q_{CN} = .22 \ (\Delta T)^{4/3} \ (A)$$

$$= .22 \ (100)^{4/3} \ (29) = 2961.3 \text{ Btu/hr}$$

where ΔT is the difference between the ambient and surface temperatures (200°F - 100°F), and

A = Surface Area = 29 ft^2

The above formula is valid for a cylinder with a 2-foot diameter.

(3) For radiation:

$$q_r = A\varepsilon\sigma \left[(t_1 + 460^{\circ}\text{F})^4 - (t_2 + 460^{\circ}\text{F})^4\right]$$

$$= 8564 \text{ Btu/hr}$$

t_1 = $^{\circ}$F of Oil-Out = 200° (Assumed Surface Temperature)

t_2 = $^{\circ}$F of Ambient Air (100°F)

σ = Stefan-Boltzman Constant (Black-Grey Area)

= .173 x 10^{-8} Btu/hr/ft^2/$^{\circ}$R^4

ε = Emissivity/Absorptivity Constant = .9

Therefore, the oil cooling is the most significant means of heat removal; and on a percentage basis:

Oil Cooling = 93.5%

Air Cooling = 1.7%

Radiation = 4.8%

A thermal analysis of the cooling fin conceptual design was completed using NASTRAN for three conditions: Temperature specified at root, heat input at root, and a combination of these two conditions. The theoretical and computer solutions were obtained. The model consisted of a metal fin of triangular cross-section attached to a plane surface to help carry off heat for the latter (Figure 53). Further detail including the computer output is provided in Appendix D.

A heat transfer analysis was made of the entire CH-47C forward transmission case. Included were forced convective oil cooling, thermal conductivity and heat generated by the input pinion/sun gear bearings. The NASTRAN run was made in order to print and punch out the temperature distribution. This was followed by a thermal stress/distortion analysis. The following was determined:

(1) NASTRAN Level 15.5.1 (Reference 20) will not work when starting from a structural check-point tape. It is necessary to punch out the input data using "ECHØ = PUNCH, SØRT" in the case control, and "ALTER 4,138", "ENDALTER", in the executive control.

(2) The cost of a heat transfer analysis is only 8% that of a full stress analysis and is only 2% that of a dynamic analysis.

(3) Computer core requirements are half those of a statics or dynamics solution.

(4) Correlation (Figure 54) yielded somewhat low values where oil cooling was applied.

(5) Forced convective oil cooling in NASTRAN is limited. For a given oil flow, downstream temperatures of the oil are the same as the upstream temperatures (Reference 21).

---

20. NASTRAN User's Manual Level 15.5, 1976

21. Thornton, E., and Wieting, A., COMPARISON OF NASTRAN AND MITAS THERMAL ANALYSIS OF A CONVECTIVELY COOLED STRUCTURE, 1975 Fourth NASTRAN User's Experiences.

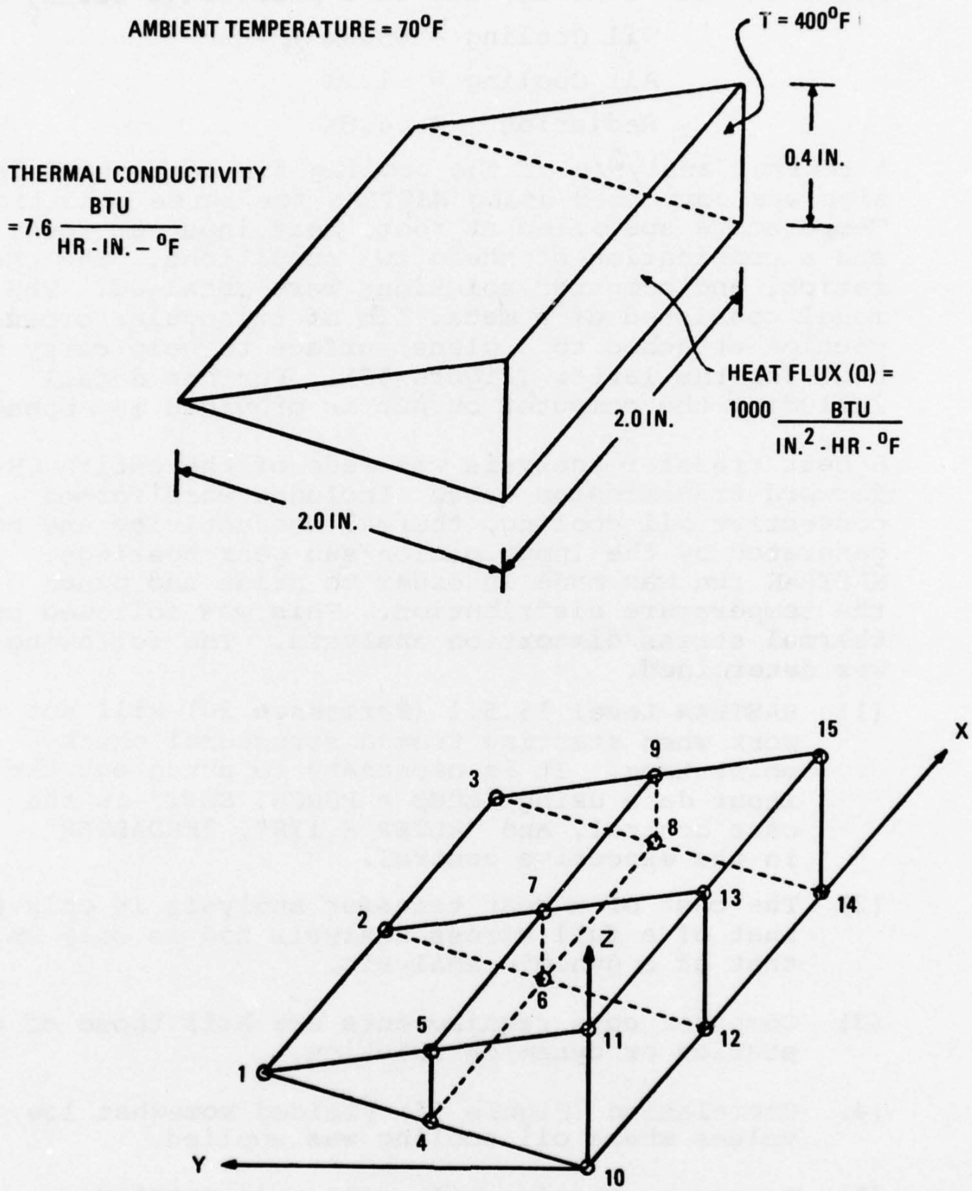

NOTE: THE COOLING FIN IS ASSUMED TO BE INFINITELY LONG.
FOR SYMMETRY, THE Y-Z SURFACES ARE LEFT UNCONSTRAINED.

Figure 53. Example — Heat Flow Problem

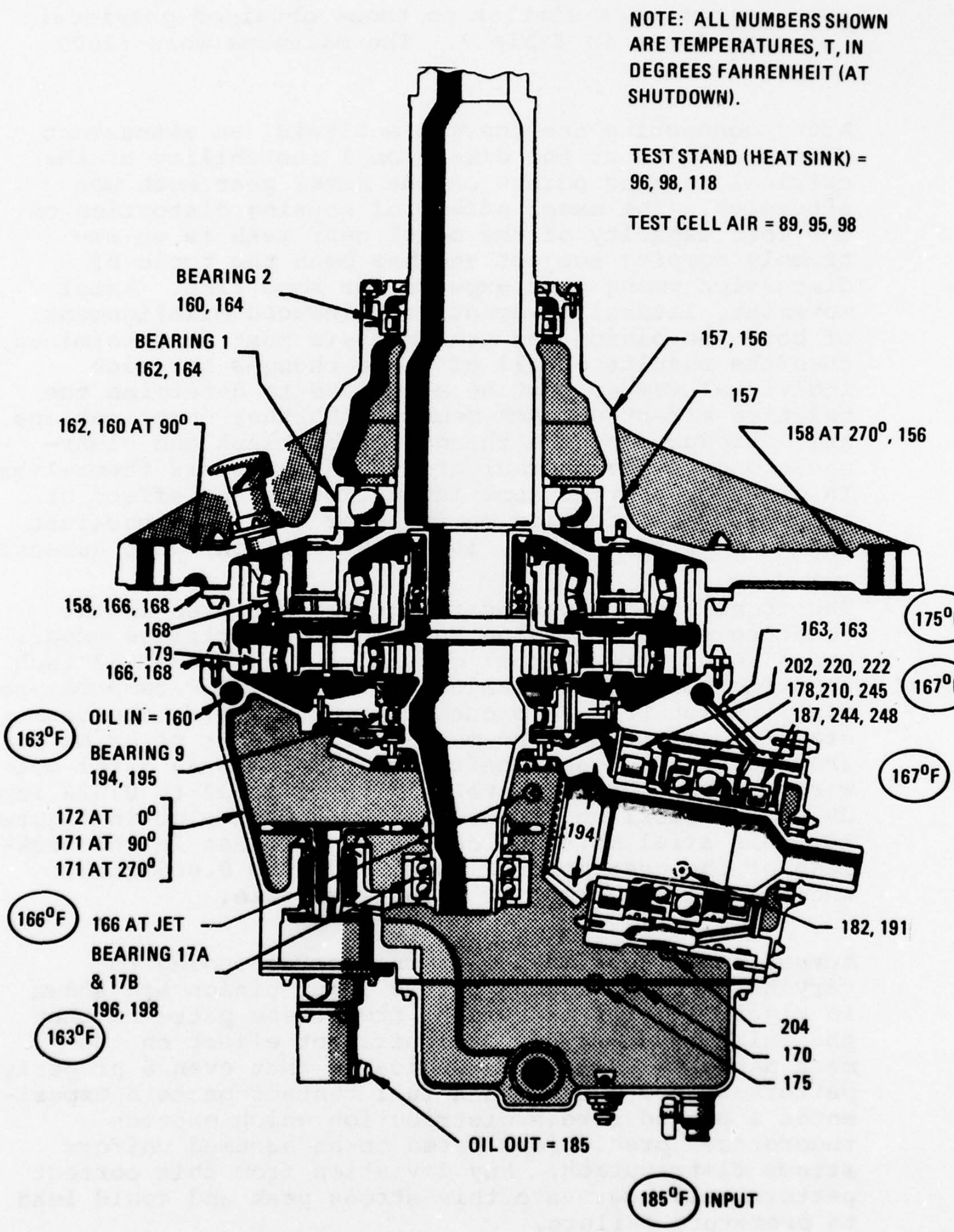

Figure 54. Thermal Map of Test 1 at 100 Percent Torque. Correlation with NASTRAN Results (Circled)

(6) Thermal stresses calculated using the punched output were similar to those obtained previously and shown in Table 9. The maximums were ± 2000 psi.

After conducting the thermal analysis, an assessment of the effects of the dimensional instability of the critical housing points on the bevel gear mesh was attempted. The exact effect of housing distortion on the load capacity of the bevel gear mesh is an extremely complex subject and has been the topic of discussion among gear experts for some time. Axial movement, lateral movement, and induced misalignment, of both the pinion and gear members must be determined, then the results of all of these changes for each individual member must be evaluated to determine the relative effect on each member. Further complications are introduced by the changes in backlash and clearances due to the thermal growth of the gears themselves. In order to provide some indication of the effect of temperature distortion on the gear mesh, the backlash and mesh pattern (i.e., load distribution) were assessed.

The transmission housing flange which serves as the mounting surface for the input pinion cartridge experienced an outward thermal growth of 0.029 to 0.032 inch when the housing was subjected to the 185°F temperature distribution from Reference 12. Considering the bearing stack-up, mounting, and method of transfer of axial load from housing to gear shaft, the result is an axial outward movement of the bevel pinion of 0.019 to 0.022 inch. Using the backlash versus axial movement plot in Figure 14, this axial movement causes an increase in the backlash of the gear mesh of about 0.007 to 0.008 inch, which is on the order of a 100% increase.

Actual bevel gear mesh patterns corresponding to varying axial positions of the input pinion are shown in Figure 55. It is evident from these patterns that the axial movement has a significant effect on the mesh pattern. Figure 5 indicates that even a properly patterned gear mesh with a full contact pattern experiences a peaked stress distribution which exceeds theoretical predictions based on an assumed uniform stress distribution. Any deviation from this correct pattern will aggravate this stress peak and could lead to premature failure.

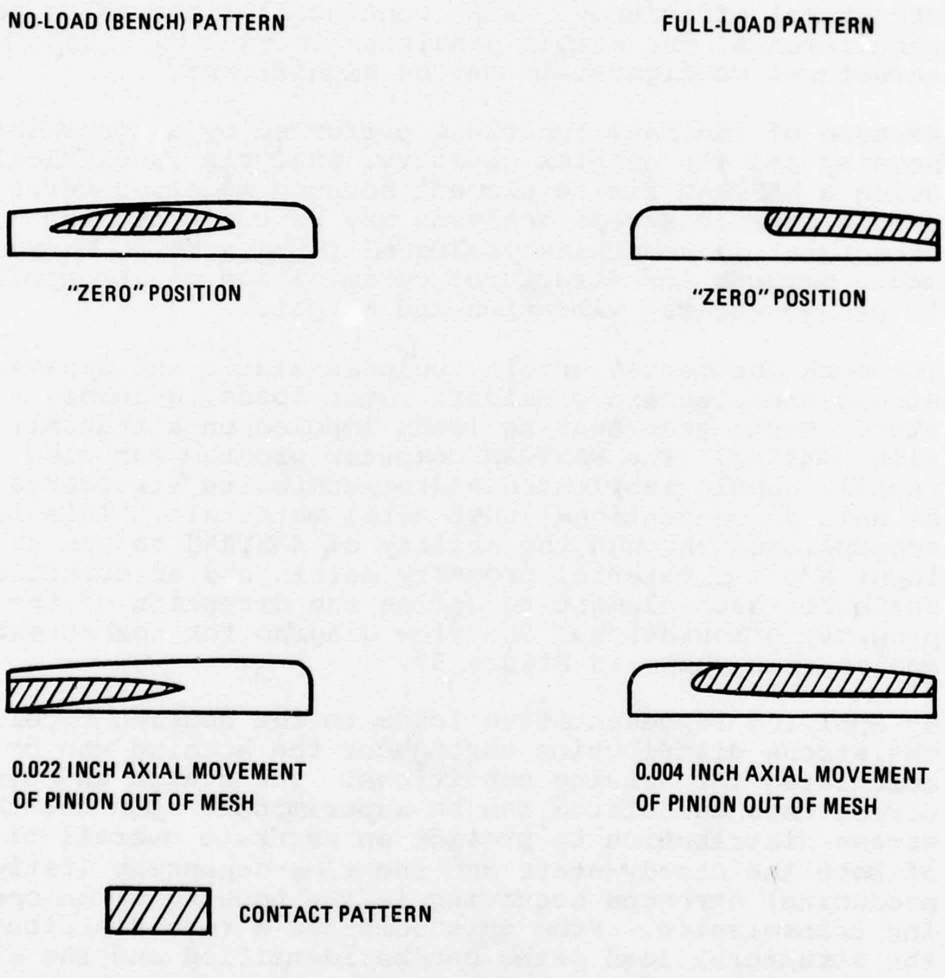

Figure 55. Bevel Gear Mesh Patterns at Different Axial Positions of Pinion

IV. STATIC AND DYNAMIC TRANSMISSION STRESS ANALYSIS INCLUDING IN-FLIGHT DYNAMIC ROTOR LOADS AND LOAD PATH DETERMINATION

An analytical method for accurately defining the stress distribution and load paths in a helicopter transmission housing has been investigated. Previously, the designer had little guidance for selection of the design with best structural efficiency. With continually increasing power requirements, the weight penalties imposed by nonoptimum structural configuration may be significant.

Because of the many functions performed by a transmission housing and its complex geometry, analysis is difficult. Using a NASTRAN finite element housing model, however, a static/dynamic stress analysis may be conducted and structural deformations predicted (Figure 56). Furthermore, methods for structural optimization can be applied to reduce stress, vibration and weight.

The work documented herein includes static and dynamic stress analyses and considers rotor loads, g-loads, and steady-state gear/bearing loads imposed on a transmission housing. The NASTRAN computer program can also readily handle fabricated and/or composite structures as well as conventional cast metal materials. This is accomplished through the ability of NASTRAN to use as input a 6 x 6 material property matrix and an orienting angle for each element to define the direction of the property orientation. The flow diagram for the stress analysis is shown in Figure 57.

By applying representative loads to the housing model, the stress distribution throughout the housing can be calculated for varying conditions. The static and dynamic stress thus calculated can be superimposed upon the thermal stress distribution to provide an accurate overall picture of both the steady-state and the time-dependent (fatigue producing) stresses occurring in the housing of an operating transmission. From this combined stress distribution, the structural load paths can be identified and the structural portions of the housing segregated from the nonstructural portions. By utilization of structural optimization methods, wall thickness changes can be recommended and weight reduction evaluated.

Vibratory 3-per-rev hub loads and steady 1g loads were calculated using a proprietary Boeing Vertol rotor loads analysis computer program (L-02). A sample of the computer output is summarized in Figure 58. The calculated 3-per-rev dynamic hub loads which were applied to the housing model via the rotor shaft support bearings are shown in Figure 59.

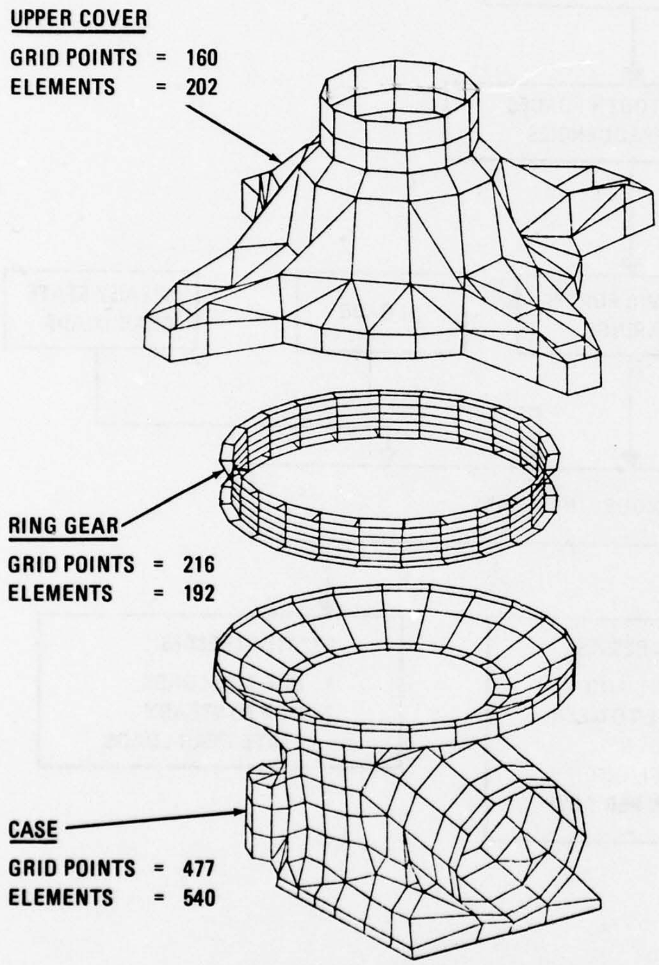

- AUTOMATIC GENERATION OF GRID POINTS AND ELEMENT CONNECTIONS.
- HOUSING MADE OF PLATE ELEMENTS.
- METAL OR COMPOSITE MATERIAL.
- STATIC STRESS AND DISTORTIONS.
- LOAD PATH IDENTIFICATION.
- STRUCTURAL OPTIMIZATION.
- REDUCE STRESS CONCENTRATIONS BY CHANGING WALL THICKNESS AND GEOMETRY.
- SURVIVABILITY AND FAILSAFETY STUDIES.
- VALIDATION OF ANALYTICAL TOOLS FOR APPLICATION TO ADVANCED TRANSMISSION DESIGN.

Figure 56. Model for Dynamic/Static Stress Analyses

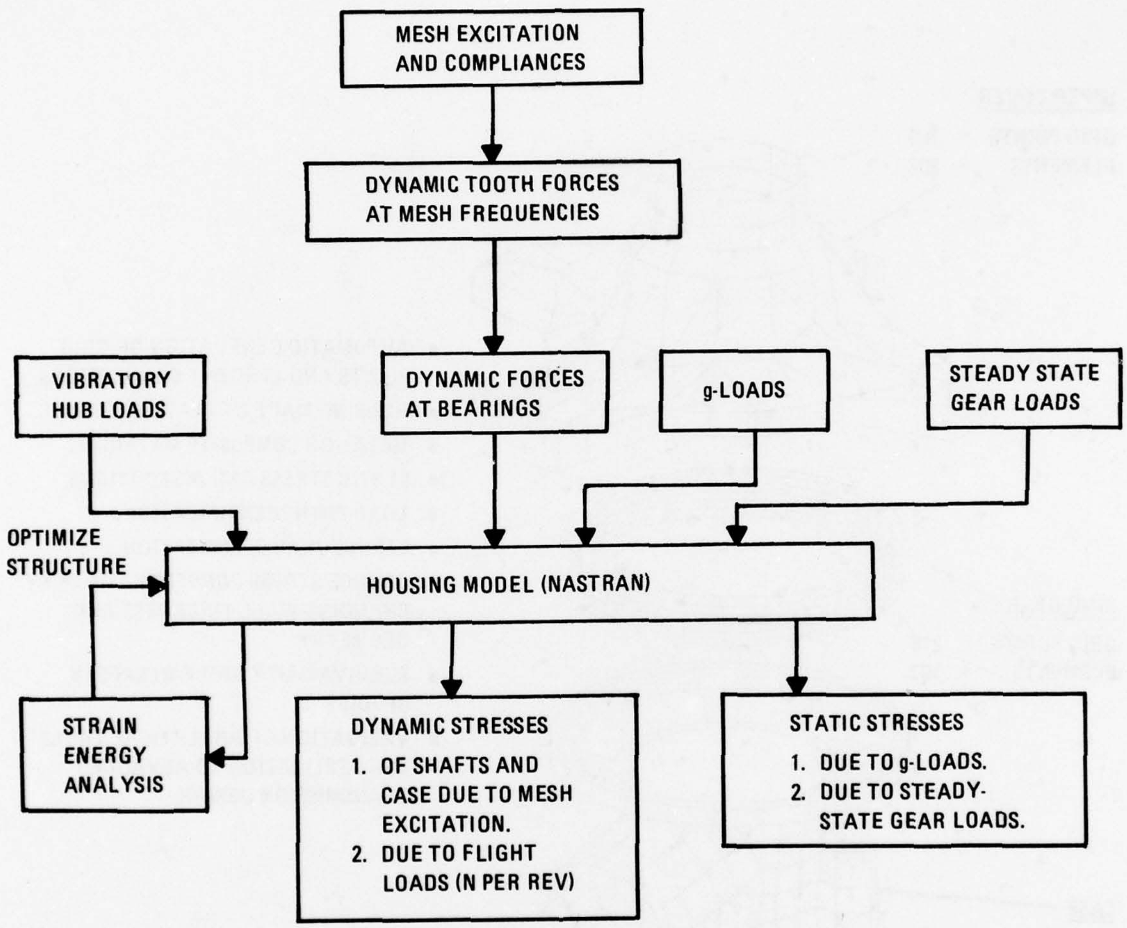

Figure 57. Flow Diagram of NASTRAN Stress Analysis

3/Rev Sine Component

3/Rev Cosine Component

ADVANCED ROTOR AEROELASTICITY PROGRAM LO2

CH47C 150KTS FWD RTR 72-123-01

LOWER ROTOR HUB FORCES AND MOMENTS

HARMONIC COMPONENT OF

1-g Loads

	FIXED HUB FORCES			FIXED HUB MOMENTS		
	FX	FY	FZ	MX	MY	MZ
0	2.5641D 02	2.9696D 02	2.5038D 04	-1.3761D 04	8.4337D 04	-7.1915D 05
3C	-1.1319D 03	4.5407D 01	-8.7918D 02	-1.8189D 02	-1.0776D 04	-9.6423D 03
3S	-3.7297D 02	-9.4752D 02	-3.4093D 03	-1.2021D 04	-1.7310D 04	1.5865D 03
3R	1.1918D 03	9.4861D 02	3.5209D 03	2.1803D 04	2.0390D 04	9.7719D 03
6C	-6.8316D 01	3.1825D 02	3.7131D 02	5.7416D 03	1.0213D 03	-3.0808D 02
6S	-3.3351D 02	-2.7621D 02	8.0052D 02	9.8234D 03	2.5336D 03	7.1321D 03
6R	3.4044D 02	4.2140D 02	8.8244D 02	1.1378D 04	2.7318D 03	7.1387D 03
9C	-1.3672D 02	-1.6253D 02	2.8826D 02	5.9121D 03	-3.0823D 03	2.2133D 03
9S	6.0188D 01	-1.8969D 02	3.8605D 02	6.3592D 03	3.5924D 03	1.4223D 03
9R	1.4938D 02	2.4980D 02	4.8180D 02	8.6829D 03	4.7335D 03	2.6309D 03
12C	2.5247D 01	-1.6117D 01	3.5492D 02	1.1906D 03	1.4538D 03	-3.2988D 03
12S	1.6117D 01	2.5247D 01	1.3993D 02	-1.5995D 03	9.0104D 02	1.3221D 04
12R	2.9952D 01	2.9952D 01	3.8151D 02	1.9940D 03	1.7104D 03	1.3626D 04

AZIMUTHAL VARIATION OF VIBRATORY

	FIXED HUB FORCES			FIXED HUB MOMENTS		
	FX	FY	FZ	MX	MY	MZ
0	-1.3117D 03	1.8501D 02	1.3531D 02	-5.3450D 03	1.0168D 04	-1.1036D 04
15	-1.2836D 03	-9.1719D 02	-2.5177D 03	-1.2413D 04	1.1793D 03	4.1752D 03
30	-3.3959D 02	-1.0922D 03	-3.8118D 03	-2.2932D 04	-2.0469D 04	-2.8265D 03
45	7.9081D 02	-6.5883D 02	-2.4677D 03	2.0246D 03	-2.3486D 04	6.6773D 03
60	1.2256D 03	4.1925D 02	1.3172D 03	1.9209D 04	-5.2181D 03	3.8221D 03
75	5.6612D 02	3.9700D 02	3.4089D 03	2.9679D 04	9.8031D 02	1.6687D 04
90	5.2672D 02	4.2347D 02	3.7790D 03	1.3829D 04	2.1334D 04	-3.1549D 03
105	-1.7428D 02	1.2435D 03	1.5684D 02	-2.4053D 04	1.5511D 04	-1.4344D 04
120	-1.3117D 03	1.8501D 02	1.3531D 02	-5.3450D 03	1.0168D 04	-1.1036D 04
135	-1.2836D 03	-9.1719D 02	-2.5177D 03	-1.2413D 04	1.1793D 03	4.1752D 03
150	-3.3959D 02	-1.0922D 03	-3.8118D 03	-2.2932D 04	-2.0469D 04	-2.8265D 03
165	7.9081D 02	-6.5883D 02	-2.4677D 03	2.0246D 03	-2.3486D 04	6.6774D 03
180	1.2256D 03	4.1925D 02	1.3172D 03	1.9209D 04	-5.2181D 03	3.8221D 03
195	5.6612D 02	3.9700D 02	3.4089D 03	2.9679D 04	9.8031D 02	1.6687D 04
210	5.2672D 02	4.2347D 02	3.7790D 03	1.3829D 04	2.1334D 04	-3.1549D 03
225	-1.7428D 02	1.2435D 03	1.5684D 02	-2.4053D 04	1.5511D 04	-1.4344D 04
240	-1.3117D 03	1.8501D 02	1.3531D 02	-5.3450D 03	1.0168D 04	-1.1036D 04
255	-1.2836D 03	-9.1719D 02	-2.5177D 03	-1.2413D 04	1.1793D 03	4.1752D 03
270	-3.3959D 02	-1.0922D 03	-3.8118D 03	-2.2932D 04	-2.0469D 04	-2.8265D 03
285	7.9081D 02	-6.5883D 02	-2.4677D 03	2.0246D 03	-2.3486D 04	6.6774D 03
300	1.2256D 03	4.1925D 02	1.3172D 03	1.9209D 04	-5.2181D 03	3.8221D 03
315	5.6612D 02	3.9700D 02	3.4089D 03	2.9679D 04	9,8031D 02	1.6687D 04
330	5.2672D 02	4.2347D 02	3.7790D 03	1.3829D 04	2.1334D 04	-3.1549D 03
345	-1.7428D 02	1.2435D 03	1.5684D 02	-2.4053D 04	1.5511D 04	-1.4344D 04
AVE	1.2686D 03	1.1678D 03	3.7954D 03	2.6866D 04	2.2410D 04	1.5515D 04

ROTOR HORSEPOWER

2.7956D 03

Figure 58. Sample Rotor Loads Program Output (CH-47C Forward Rotor at 243 RPM, 50,000 LB Gross Weight, 150 KTS – 3-Per-Rev and Steady (1g) Loads.

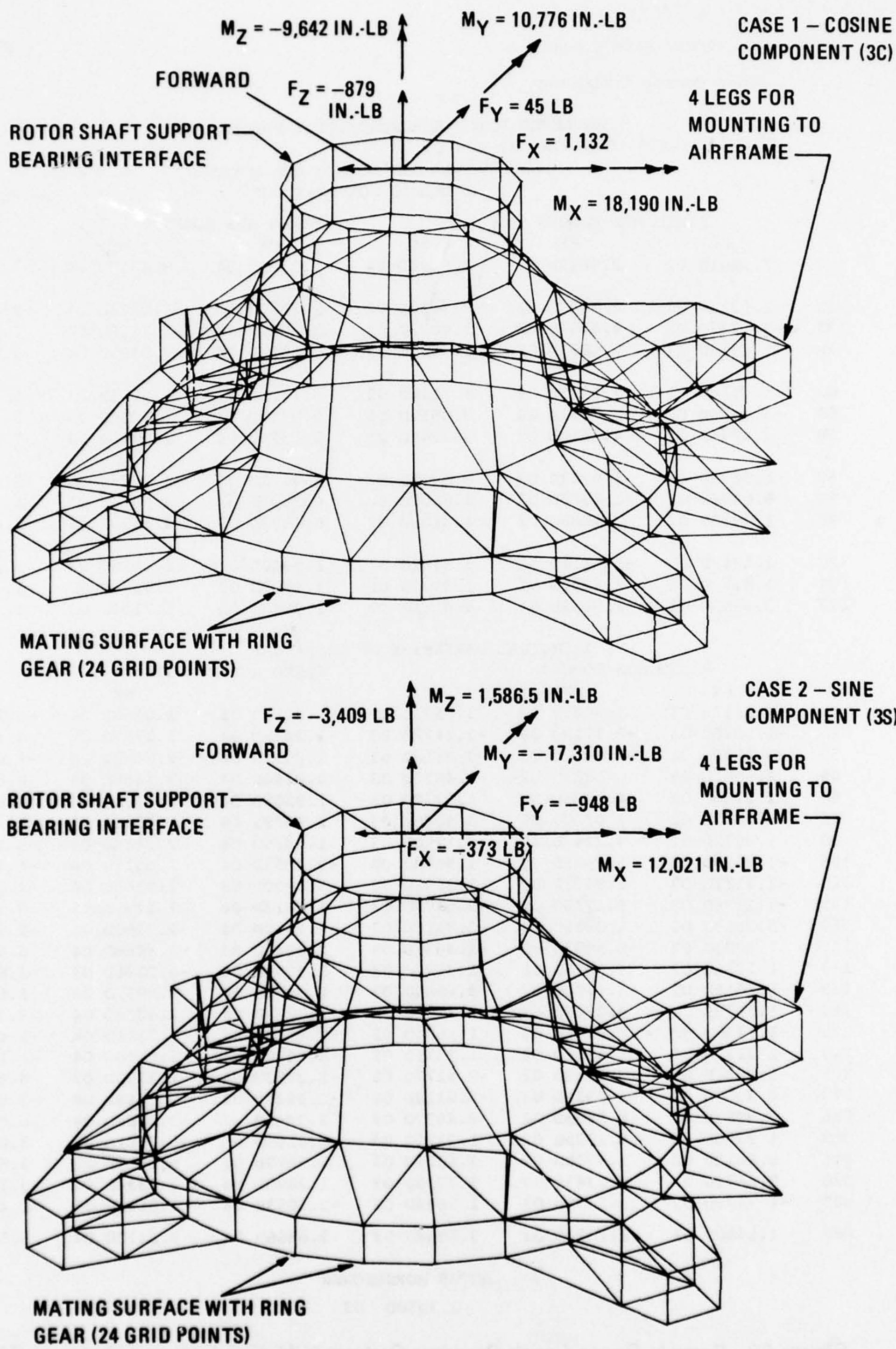

Figure 59. Application of Dynamic Rotor Loads to Housing Model (3-Per-Rev Hub Vibratory Loads, CH-47C Forward Transmission, 50,000 LB, 150 KT).

Another Boeing Vertol finite element computer program (D82) determines shaft deformations due to mesh excitation and translates these deformations into vibratory internal bearing loads for use in the structural analysis program. These vibratory internal loads have been thoroughly investigated in Reference 9 and will not be pursued further here, but the results will be applied. Natural frequencies and mode shapes for the housing have been calculated and stored on magnetic tape and are used for both of the above dynamic stress analyses. Applying the vibratory 3-per-rev hub loads and the dynamic loads due to the internal components, the NASTRAN vibratory response analysis (Rigid Format 11) was used to calculate dynamic response and stresses of the housing.

Steady-state loads of two types were considered: 1g steady level flight loads and transient g-loads for three flight maneuvers including the ultimate. All of these loads, which include both forces and moments, are applied to the housing model via the bearings. The three maneuver conditions are calculated similarly to the inertia relief capability of NASTRAN. The static stress distribution for the housing using each of these load conditions is calculated using NASTRAN static analysis (Rigid Format 1). Application of the calculated steady 1g hub loads is shown in Figure 60.

Furthermore, the effect of bearing nonlinearity was investigated. Since the bearings deflect nonlinearly under load (Figure 61), the load paths generated under a static loading would be different if the bearings were assumed to be linear elastic. This could be analyzed using the nonlinear feature of NASTRAN called piecewise linear analysis (Rigid Format 6). The bearings retaining the CH-47C forward transmission pinion and sun gear have nonlinear stiffnesses. The bearings (13 to 16, 9 and 17) are shown in Figure 62. Other nonlinear bearings are shown in Figure 63. These are bearings 1 and 2 for the rotor shaft, the upper planetary spherical roller bearings 4 and the lower planetary spherical roller bearing 10. The stiffness of the bearings is a function of rotor torque and may be calculated. This variation in stiffness as a function of percentage of torque for the pinion-sun gear bearings is shown in Figures 64 and 65.

Since the bearings are a small portion of the transmission housing model, a separate computer run could be made assuming the bearings to be linear. The load paths for the linear case can be compared to the nonlinear load paths to ascertain the differences. The costs of the two computer runs would be considered in the evaluation. It is probable that the nonlinearity of the bearings is of

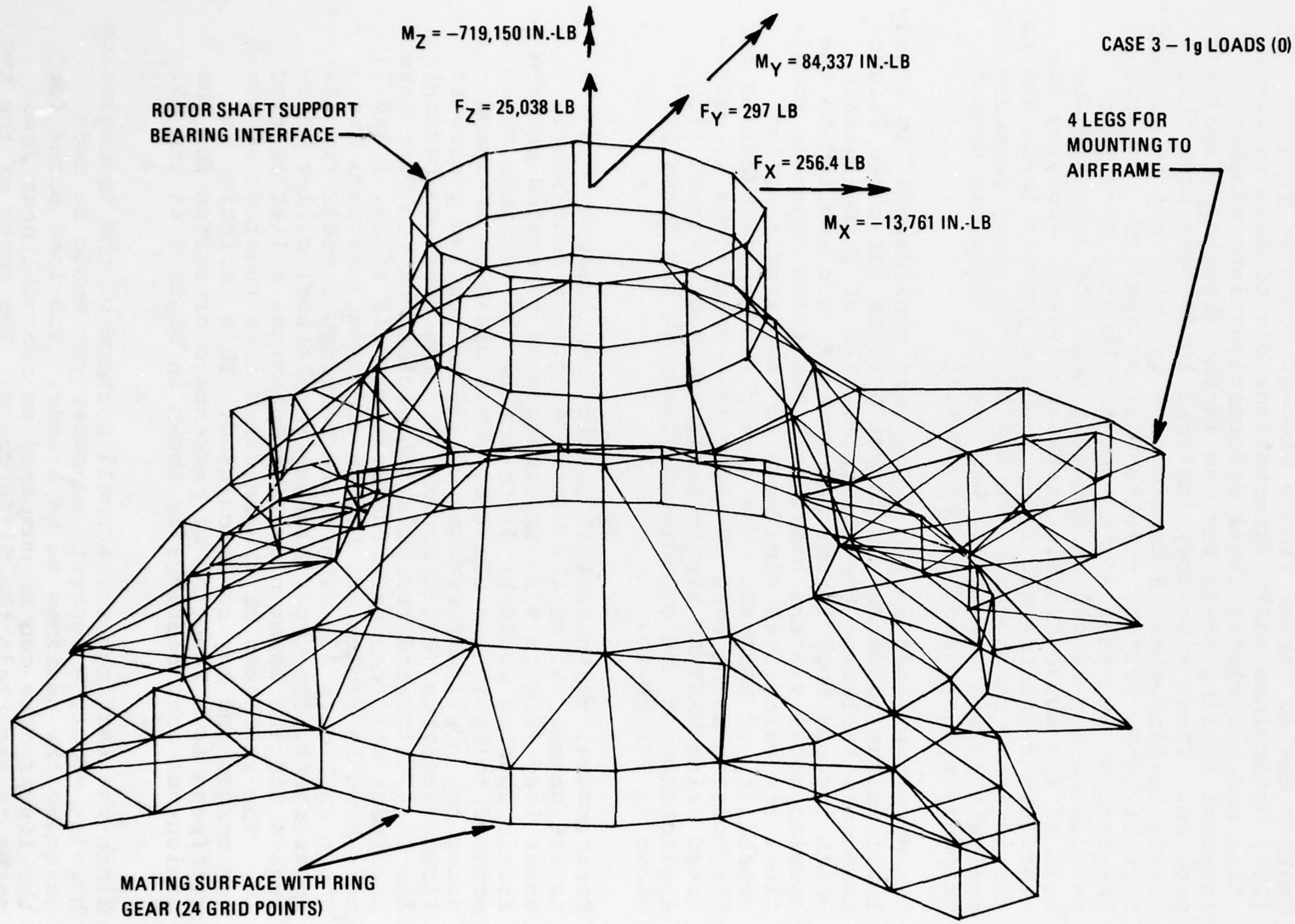

Figure 60. Application of Static Loads to Housing Model (Static Hub Loads, lg Level Flight CH-47C Forward Transmission, 50,000 LB, 150 KTS).

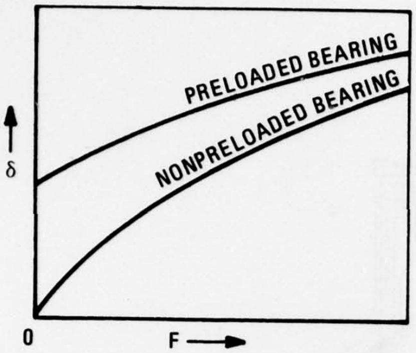

NOTE: AS THE LOAD INCREASES, THE RATE OF THE INCREASE OF DEFLECTION DECREASES, THEREFORE PRELOADING (TOP LINE) TENDS TO REDUCE THE BEARING DEFLECTION UNDER ADDITIONAL LOADING.

Figure 61. Deflection Versus Load Characteristics for Ball Bearings

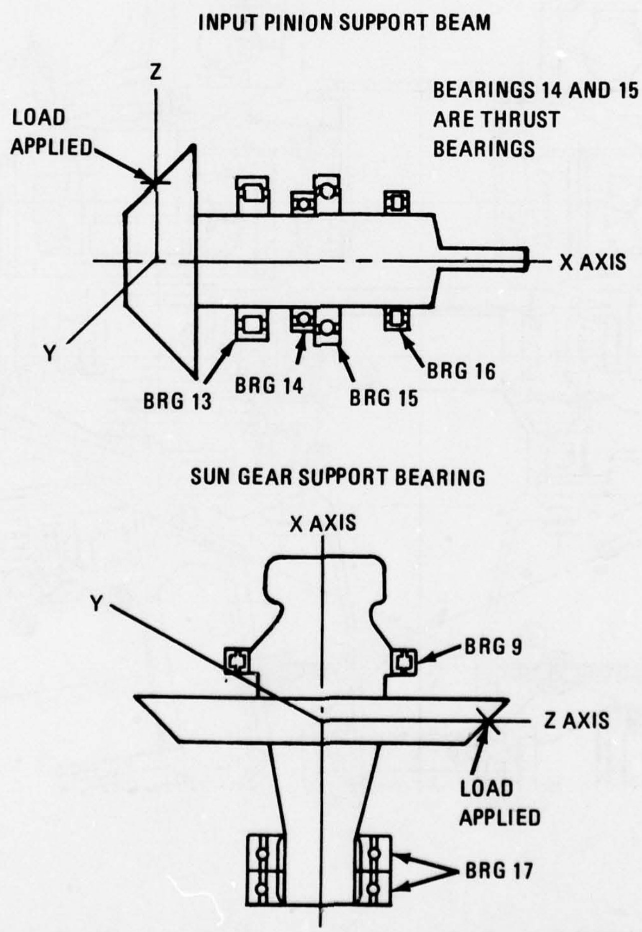

Figure 62. CH-47C Forward Transmission Support Bearings

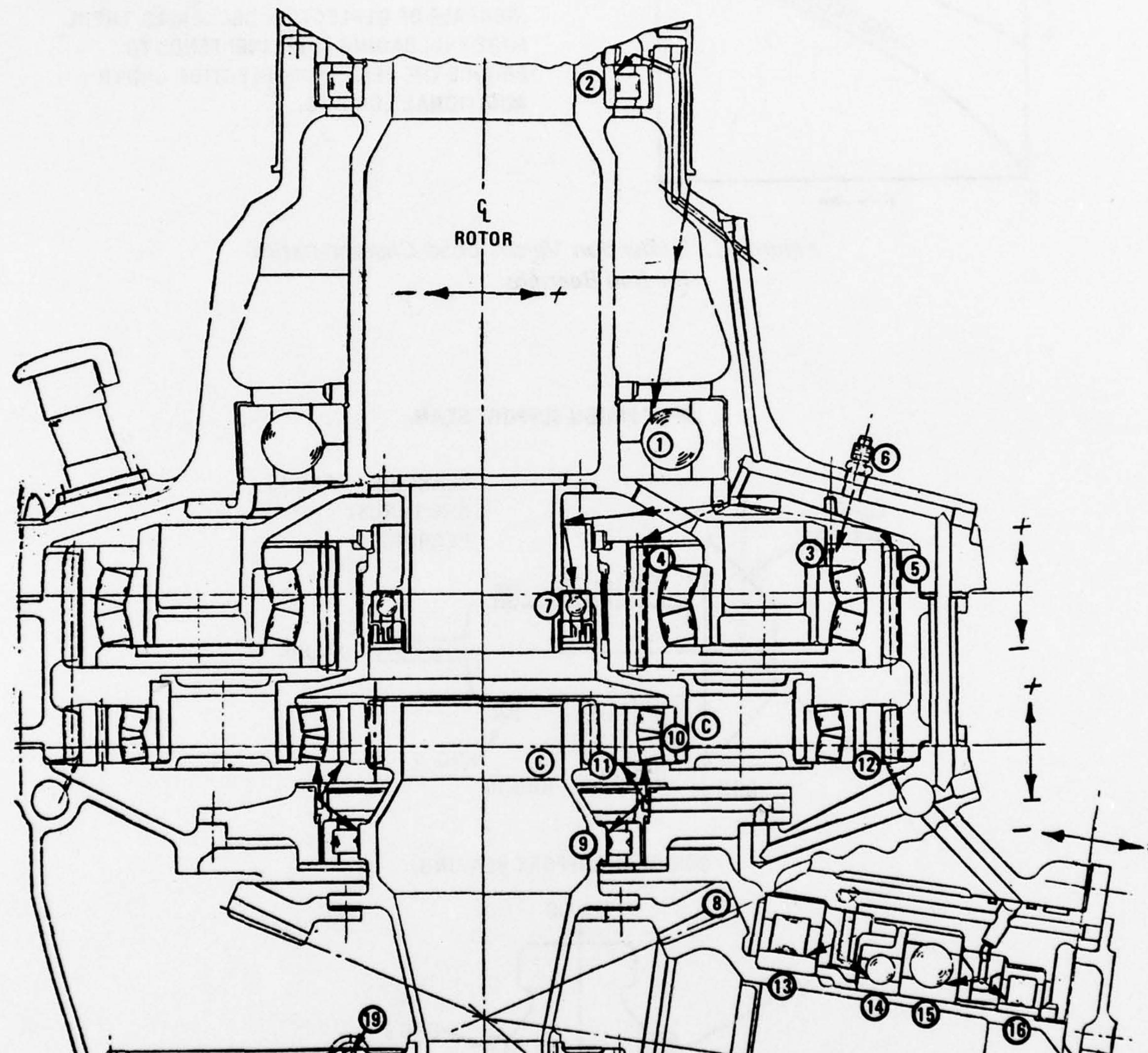

Figure 63. CH-47C Forward Transmission Bearing System (Nonlinear Stiffness).

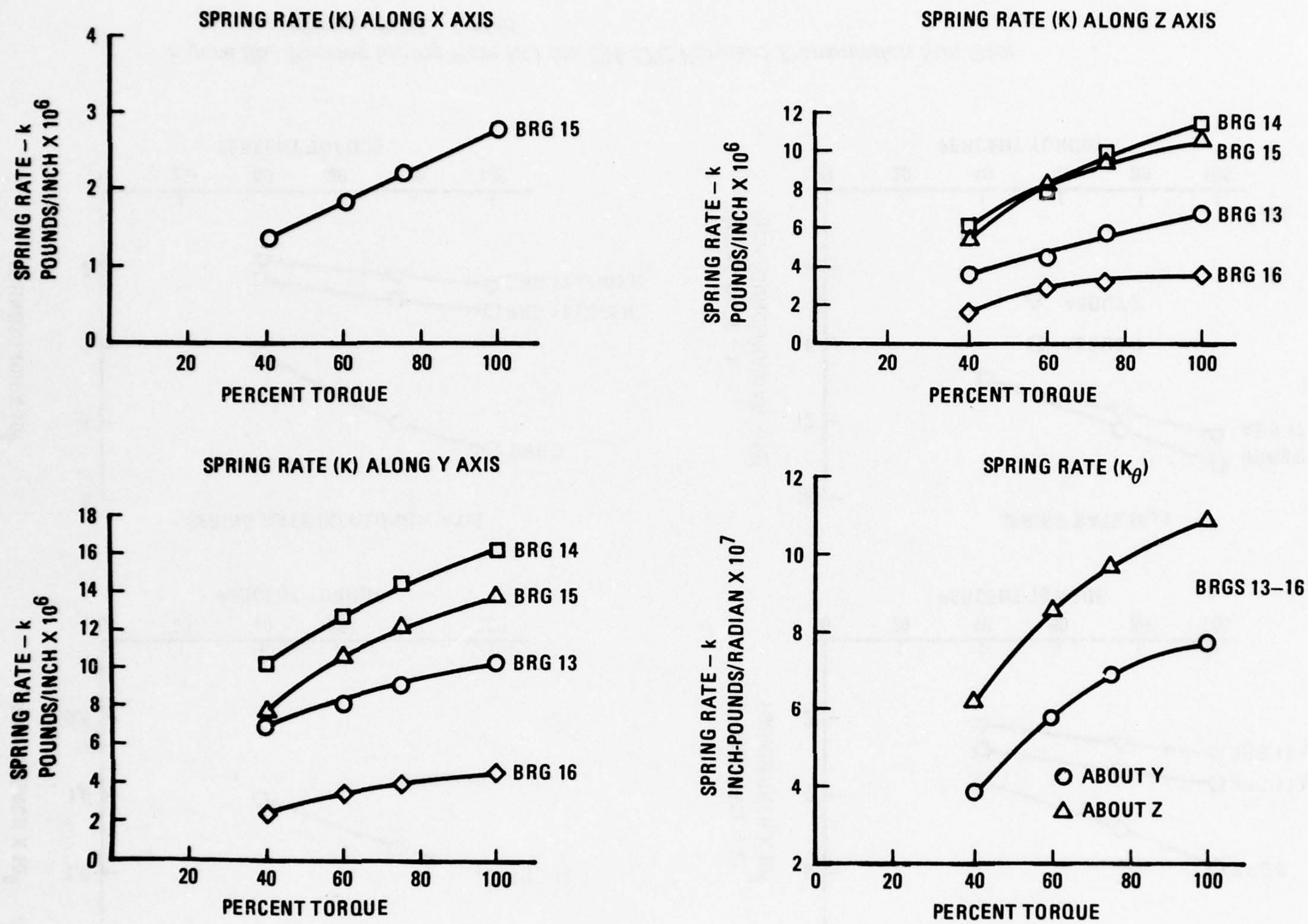

Figure 64. Bearing Spring Rate (K) for CH-47C Forward Transmission Input Pinion (Pinion RPM: 7,460)

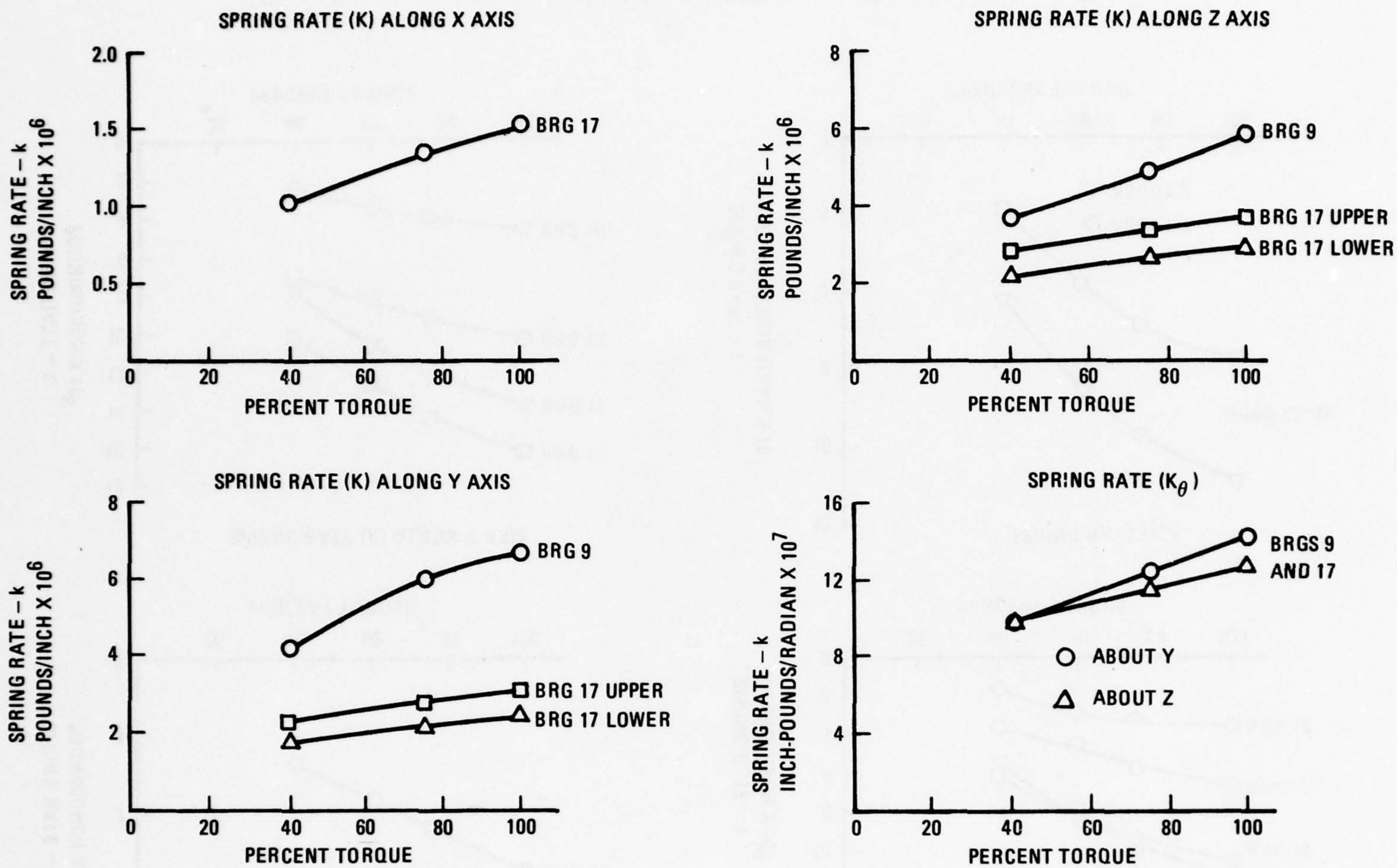

Figure 65. Bearing Spring Rate (K) for CH-47C Forward Transmission Sun Gear (Pinion RPM: 7,460)

no consequence in static and maneuver loadings. However, the nonlinearity of the bearings, which is a function of rotor torque, does affect the natural frequencies of the internal components. These natural modes, when excited by the mesh frequencies, would change the dynamic loading on the case. But even in this dynamic situation, it would be erroneous to overemphasize the nonlinear stiffnesses since the bearings act only in compression, not in tension, which is significantly more nonlinear.

Three maneuver conditions were selected for sample static stress analyses of the CH-47C forward transmission case. The sign convention for these hub loads is shown in Figure 69 and the loads are:

- Symmetric dive and pullout, noseup pitching (Figure 70)
- Yawing (Figure 71)
- Recovery from rolling pullout (counterclockwise) (Figure 69)

Three-per-rev dynamic loads and stresses on the case were determined. Since the natural frequencies of the case start at about 600 Hz, there is no magnification of the 12 Hz exciting frequency (3/rev). The coupled bending/torsion natural frequencies of the internal components start at 560 Hz; so once again, there is no magnification of the loads. Figure 55 shows that the sine and cosine components as output by the rotor loads computer program (Figure 54) had to be applied to the hub in separate runs. A bearing computer program used these separate load conditions to calculate nonlinear bearing loads. In Figure 73, the bearing dynamic loads on the case are illustrated except for the pinion ball bearing in the X-direction (64 lb) and the gear duplex ball bearing load in the Z-direction (24 lb). However, these loads were applied to the NASTRAN model. The sine and cosine bearing loads were combined into single polar loads for the NASTRAN dynamic stress analysis. At a rotor shaft speed of 243 rpm, the dynamic stresses due to mesh excitations were calculated.

(1)	Lower Planetary First Harmonic	1565 Hz (LP1)
(2)	Lower Planetary Second Harmonic	3131 Hz (LP2)
(3)	Spiral Bevel Fundamental	3605 Hz (SB1)
(4)	Lower Planetary Third Harmonic	4697 Hz (LP3)

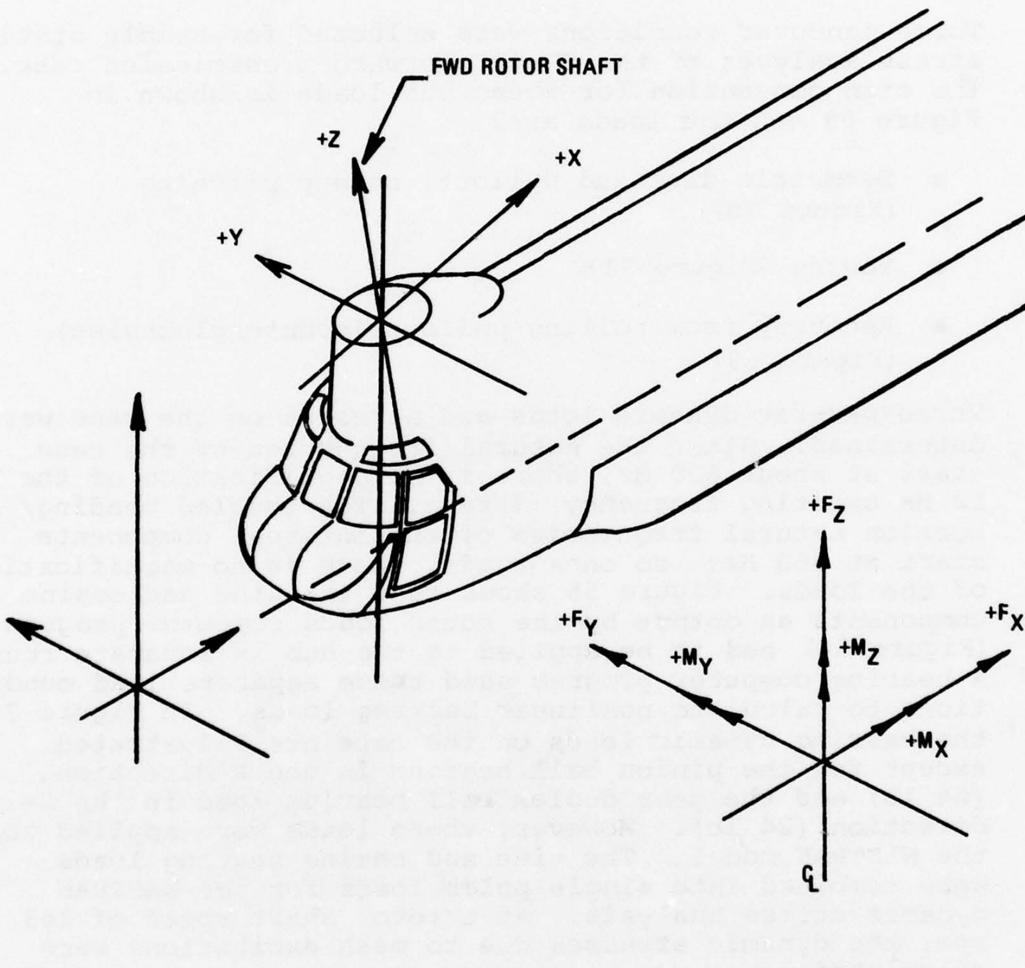

Figure 66. Sign Convention for Hub Loads

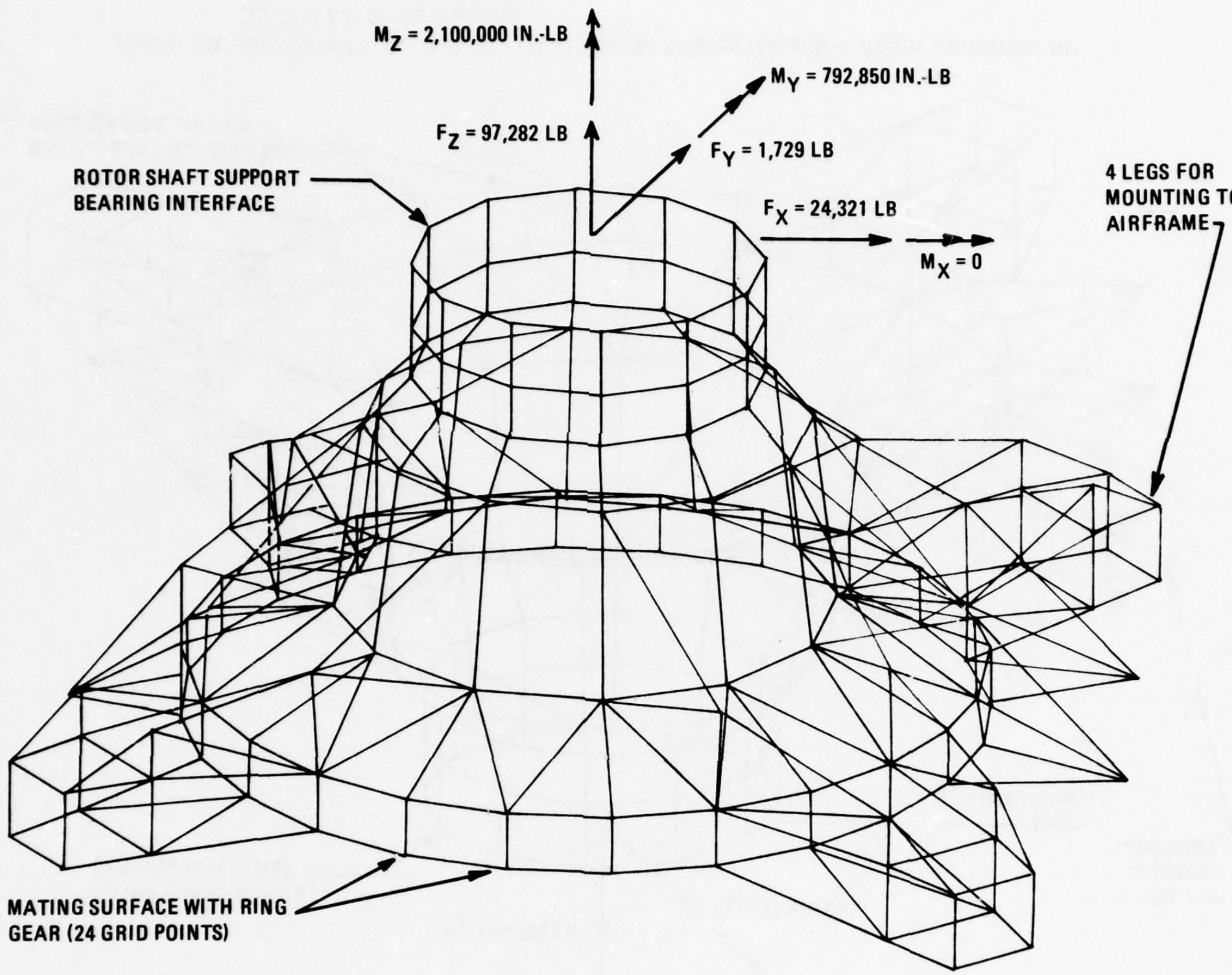

Figure 67. Ultimate Forward Rotor Head Loads; Symmetric Dive and Pullout, Noseup Pitching (Case 4 – Flight Condition 2B, 33,000 Lb Gross Weight)

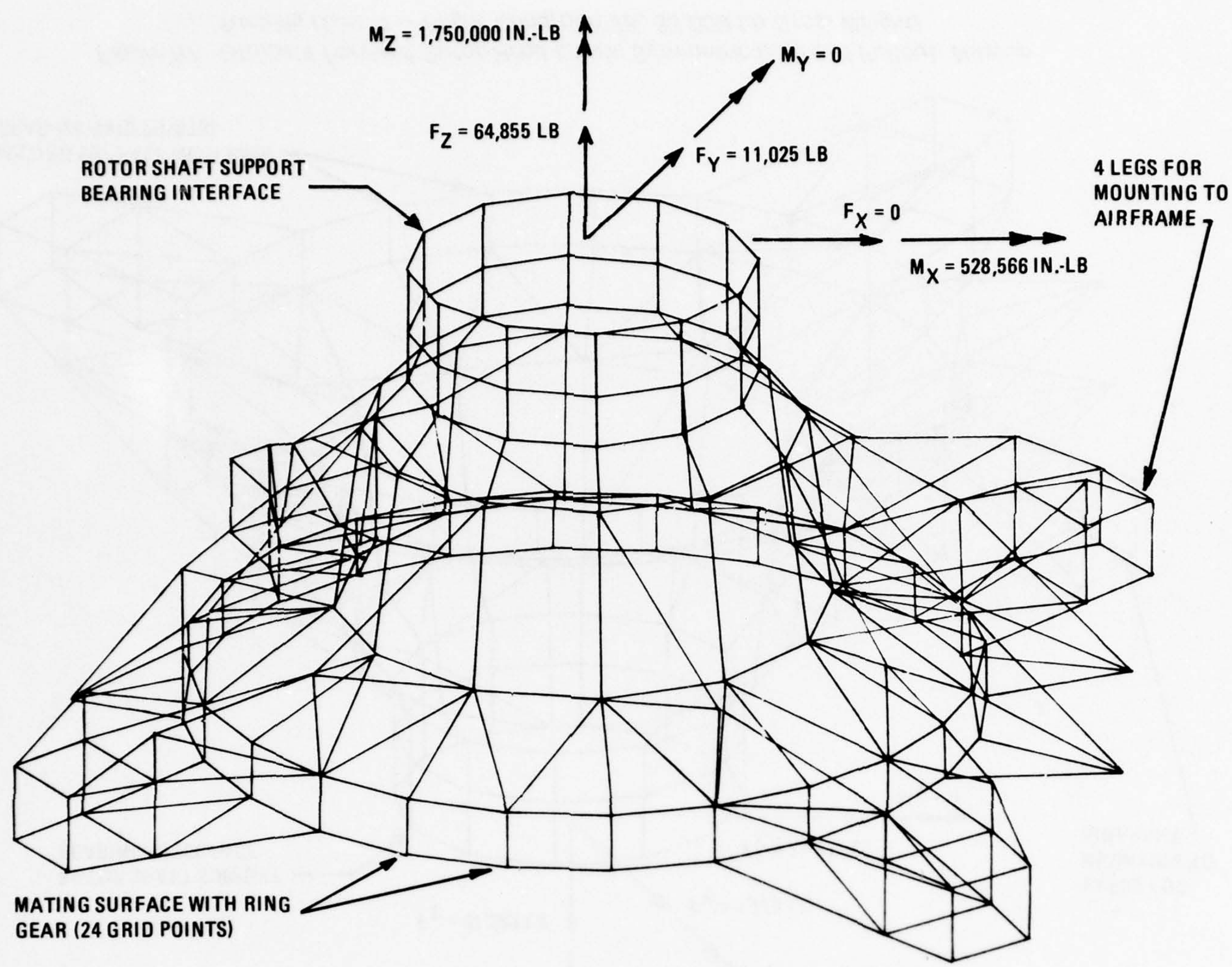

Figure 68. Ultimate Forward Rotor Head Loads; Yawing (Case 5 – Flight Condition 6B, 33,000 LB Gross Weight)

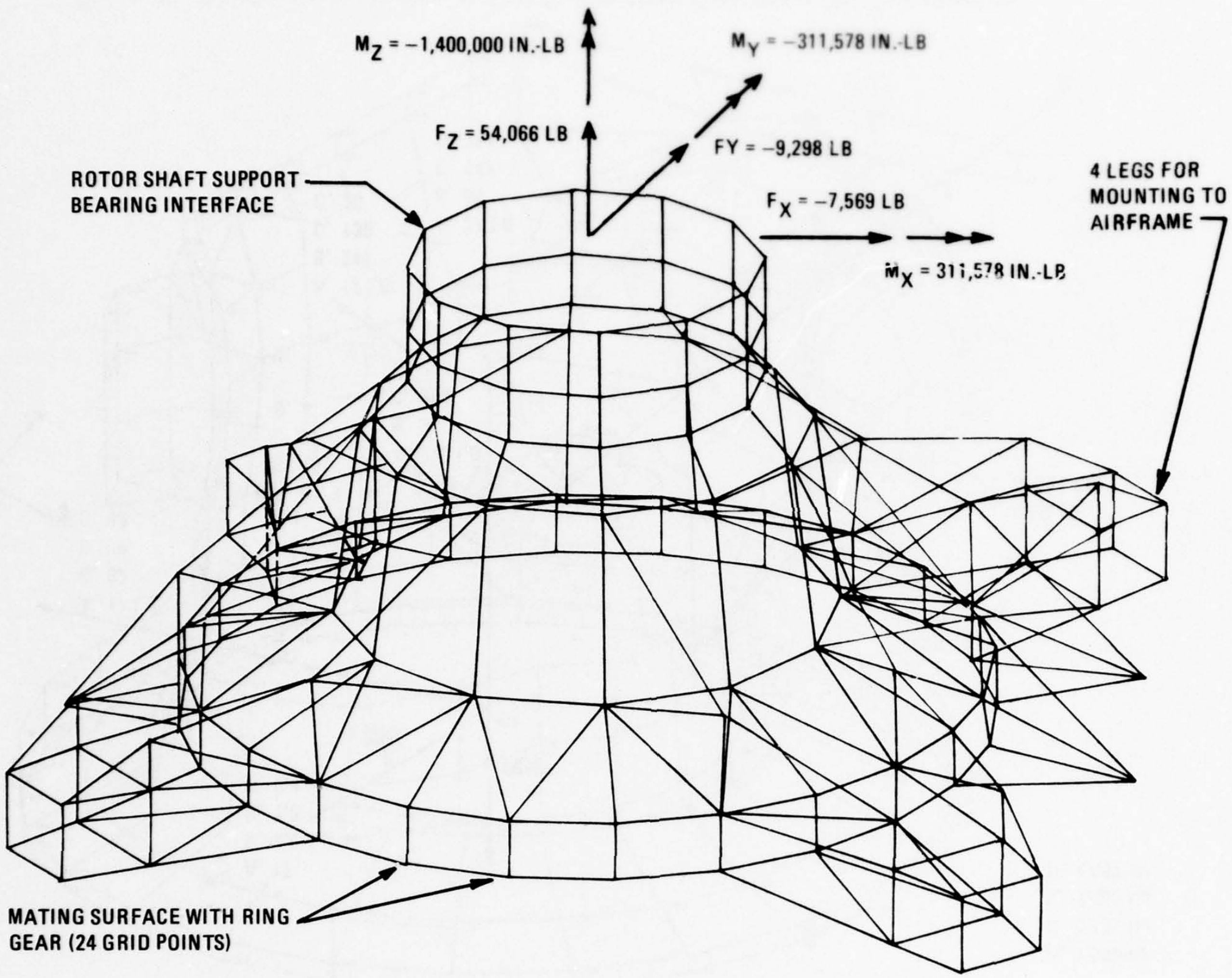

Figure 69. Ultimate Forward Rotor Head Loads; Recovery from Rolling Pullout, Counterclockwise (Case 6 – Flight Condition 5, 33,000 Lb Gross Weight)

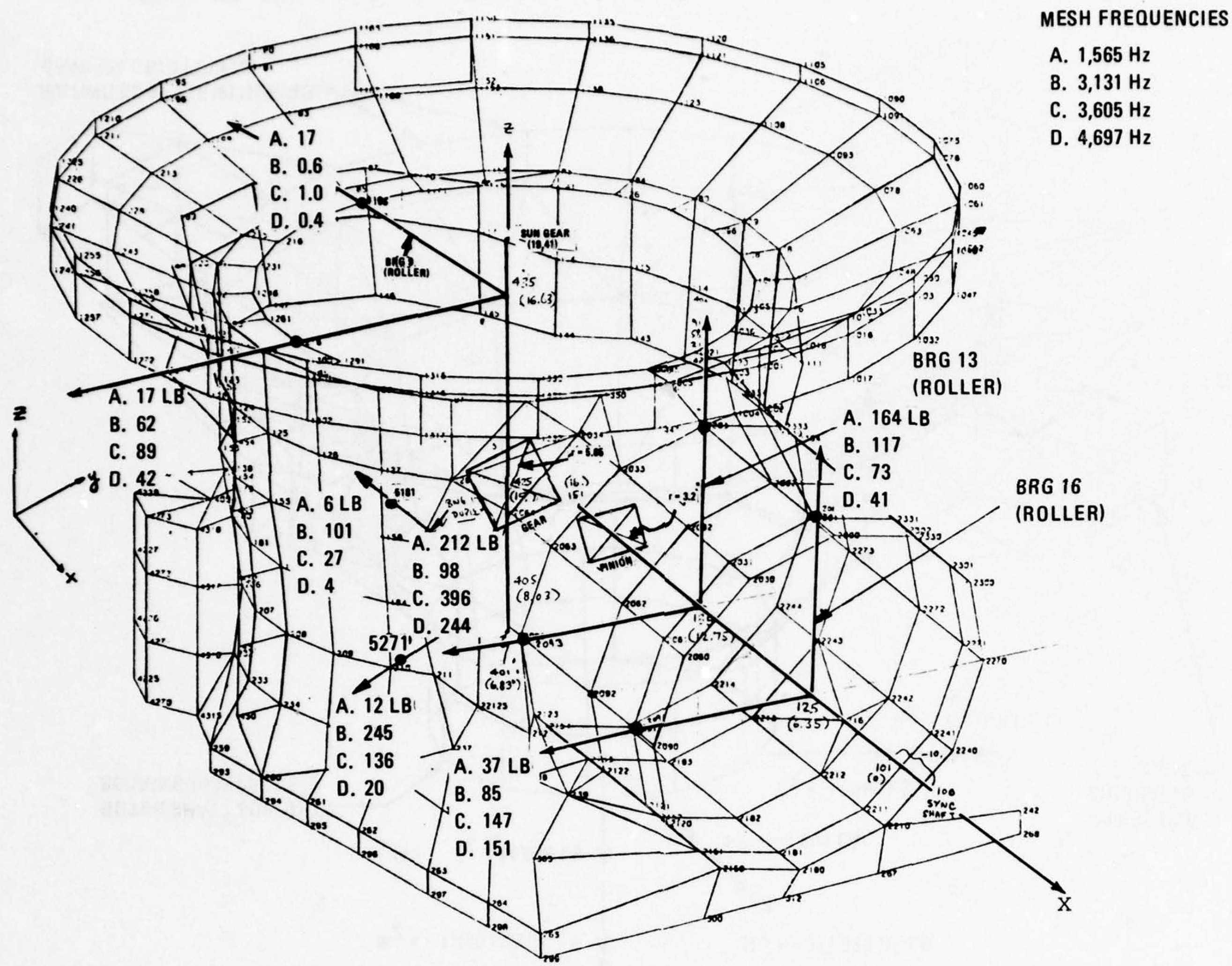

Figure 70. *Bearing Loads Applied to Case Due to Mesh Excitations (lb) Calculated by Beam Model Dynamic Analysis of Internal Components*

The vibratory loads (exclusive of phasing) are shown on Figure 70 for the above four mesh excitations. Other mesh excitations and sidebands exist, but microphone data indicates the predominance of the above. The maximum dynamic stresses indicated by NASTRAN's prodigious output are approximately:

(1) 600 psi for the LP1 Excitation

(2) 500 psi for the LP2 Excitation

(3) 200 psi for the SB1 Excitation

(4) 250 psi for the LP3 Excitation

This is based on an assumed equivalent viscous damping of 3% (6% structural). The values of these loads are contingent on the natural frequencies of the internal components which also include the nonlinear bearing stiffnesses and the gear tooth mesh stiffness (spiral bevel pinion/gear).

Bearing loads for 1g (high-speed level flight) and three maneuver conditions were calculated from hub loads. The hub loads for these conditions are given in Figures 60, 67, 68 and 69. All bearing loads calculated using these hub loads as well as the bearing number convention are given in Appendix E.

Maximum stresses for the static analyses of the case are summarized here:

1. 1g, Steady Flight, $\pm$ 3000 PSI

2. Ultimate Maneuver, $\pm$ 15,000 to 25,000 PSI

3. Yawing Maneuver, $\pm$ 20,000 PSI

4. Recovery from Rolling Pullout, $\pm$ 5,000 PSI

These are "eyeball" numbers and are isolated areas on the case. However, assuming an allowable of $\pm$26,000 psi for AZ91 magnesium, there exists the possibility of high stresses on the case for certain maneuvers.

Deflections for the critical shaft support bearing/housing interface locations were evaluated. Figure 71 is a schematic of the bevel pinion and sun/bevel gear shaft showing the predicted deflections and slopes due to an imposed ultimate load condition for a magnesium and steel housing, respectively. The steel housing was evaluated in order to establish a basis for comparison. The displacements allowed by the magnesium housing are four to five times that of the steel housing. Table 12 summarizes the critical deflection information.

It is evident from Figure 72, which plots deflection versus torque for various housing materials, that the magnitude of the housing displacements can be reduced substantially by the use of stiffer materials. Actual deflection test data is shown for the magnesium housing. A steel housing is apparently very desirable from the stiffness aspect, although obviously unacceptable for aircraft application because of its weight. However, the metal matrix material provides good stiffness characteristics at only a small weight penalty. Furthermore, the slight weight increase can be traded-off against the much improved properties of the composite material and selective stiffening can be utilized, with the net result of a substantially stiffer housing with no weight penalty.

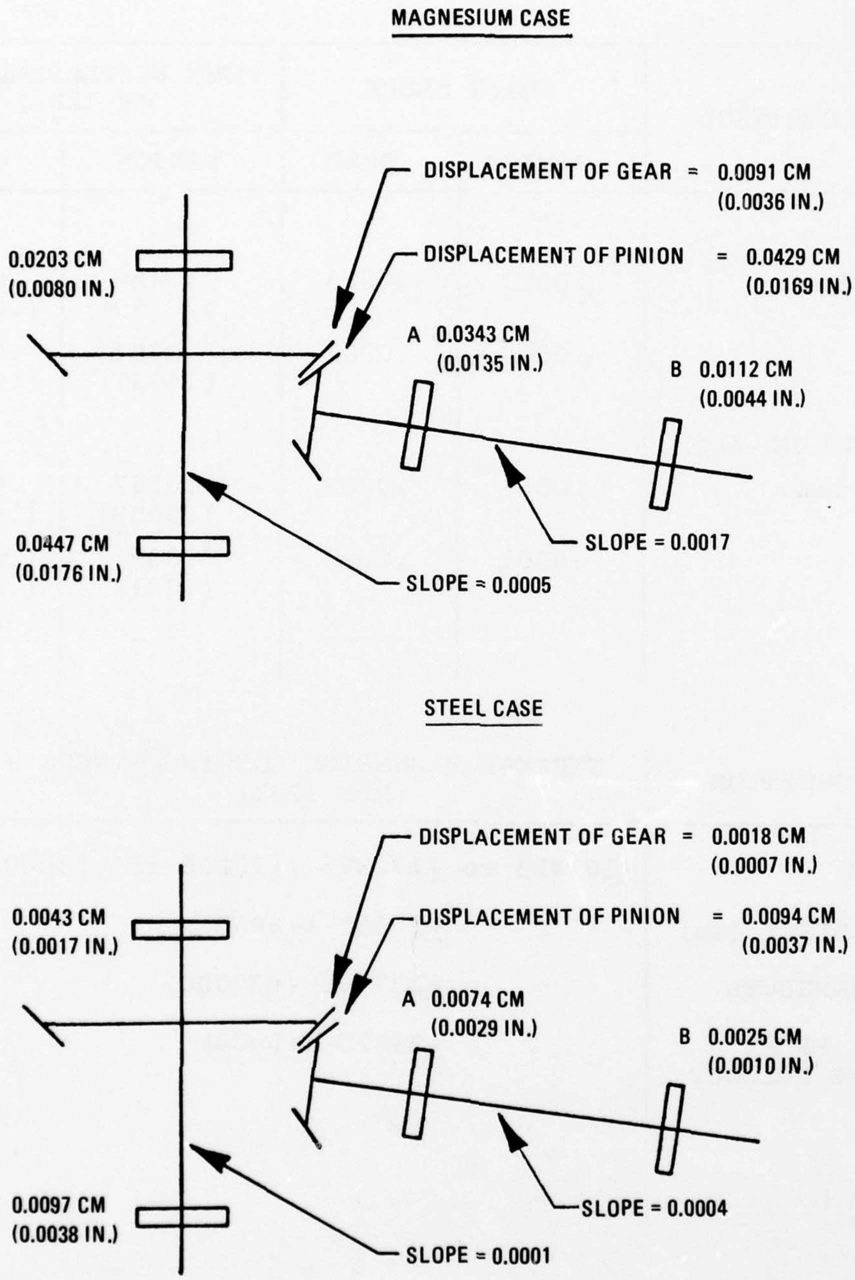

Figure 71. Displacement of Internal Components Due to Ultimate Load Condition

TABLE 12. DEFLECTION AND STRESS SUMMARY

LOAD CONDITION	SHAFT SLOPE		MESH DISPLACEMENT - cm (in.)	
	PINION	GEAR	PINION	GEAR
ULTIMATE				
Magnesium	.0017	.0005	.0429 (.0169)	.0091 (.0036)
Steel	.0004	.0001	.0094 (.0037)	.0018 (.0007)
STEADY FLIGHT (lg)				
Magnesium	.0006	.0002	.0147 (.0058)	.0030 (.0012)
Steel	.0001	.0000	.0033 (.0013)	.0005 (.0002)

LOAD CONDITION	TYPICAL MAGNESIUM HOUSING STRESS - kPa (PSI)
ULTIMATE	±103425 to ±172375 (±15000 to ±25000)
STEADY FLIGHT (lg)	±20685 (±3000)
YAWING MANEUVER	±137900 (±20000)
RECOVERY FROM ROLLING PULLOUT	±34475 (±5000)

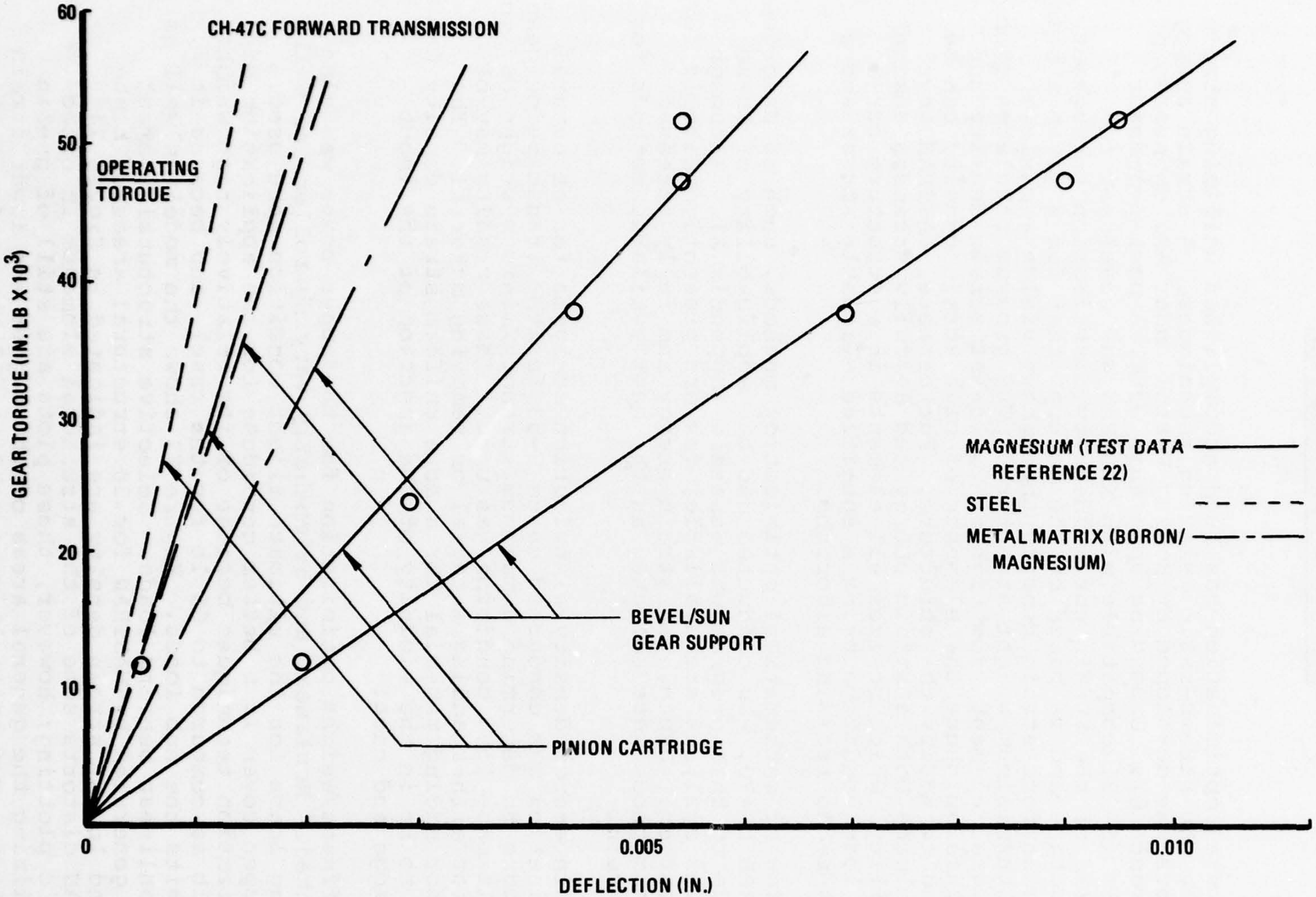

Figure 72. Housing Deflection for Various Materials

22. Patton, H., MODEL YHC-1B FORWARD TRANSMISSION DEFLECTION TEST, Gleason Works Test Report 1842, 1962.

STRUCTURAL OPTIMIZATION

Structural optimization has been accomplished utilizing strain density and stress-ratio resizing techniques. A strain energy analysis was developed by Boeing Vertol under ARO sponsorship (Reference 6). Expanding upon this work, a post-processor program (S-83) compatible with NASTRAN was developed for analysis of the strain energy density distribution throughout a structure and is based on the concept that for a given static load a uniform strain density throughout yields a maximum strength/minimum weight structure. The program tabulates each structural element from highest to lowest strain density and with this guidance the elements of high strain density can be altered to modify the structure. Furthermore, NASTRAN Level 16 includes both a strain energy and a "fully stressed design" capability, which resizes all elements in a structure for a given load condition using a specified allowable stress and a stress-ratio resizing algorithm.

A review of mathematical optimization methods, such as described in AGARD LS-70, was conducted and the applicability of these methods to this program was assessed (Appendix A). Although numerous analyses are available, few are presently suitable for application. Hence, the strain energy and fully stressed design methods were selected as the best available methods for use herein.

A strain energy density distribution analysis for structural optimization was conducted using S-83 for the transmission case structure to determine a maximum strength/minimum weight design. The ultimate load condition was used. These results may be used for either adding material or removing material. The area for adding material for a more uniform strain density was found to be in the vicinity of the junction of the input cartridge and case.

A stiffness/weight optimization for the upper cover was also conducted. Nonlinear and azimuthally varying roller and ball bearing loads for the ultimate flight condition were used. The upper cover is a better candidate for the application of optimization techniques because of its relatively high weight (145 lb as compared to 55 lb for the case), and because it transmits the hub loads. Figure 73 shows the model as well as the nonlinear bearing loads. Selective structural element plots generated by NASTRAN for 30 structural areas of highest and lowest strain density are indicated in Figure 74. NASTRAN distorts some of the structural elements in orthographic plotting; however, these plots are still of use in visualizing the general areas of the higher and lower strain densities. Two criteria were used as indicators for stiffness

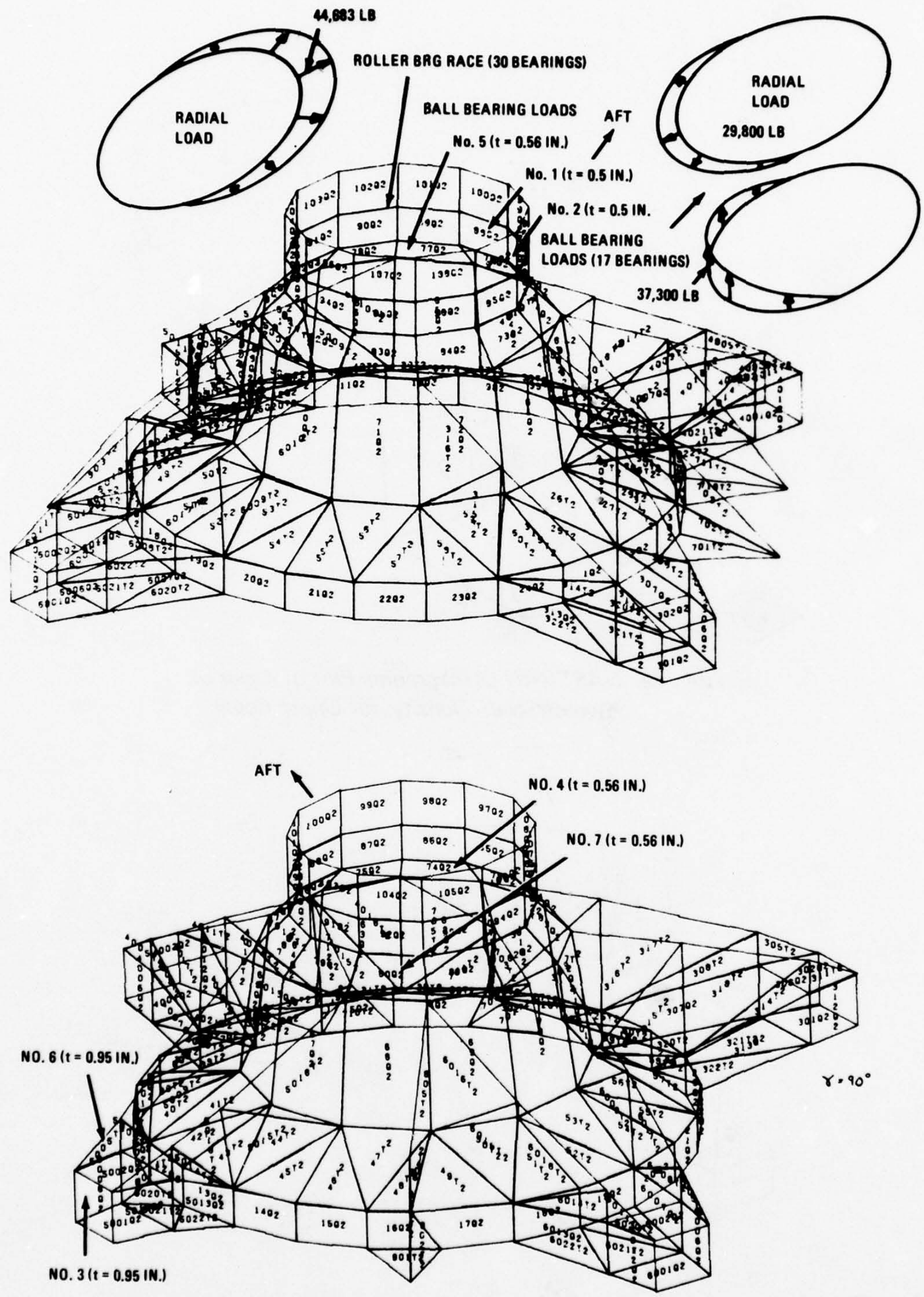

Figure 73. CH-47C Forward Transmission Bearing Load Distribution. Structural Elements With Highest Strain Density Indicated.

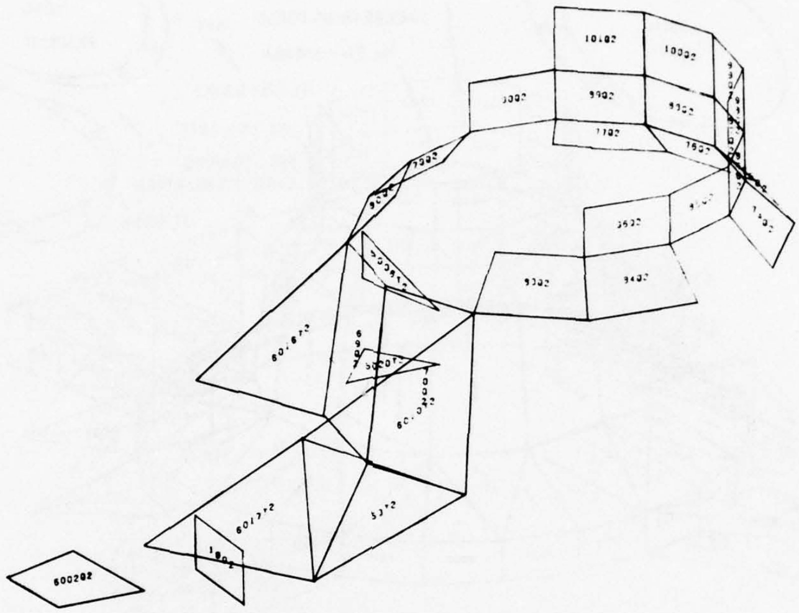

Figure 74a. NASTRAN Orthographic Plot of Areas of Highest Strain Density for Upper Cover

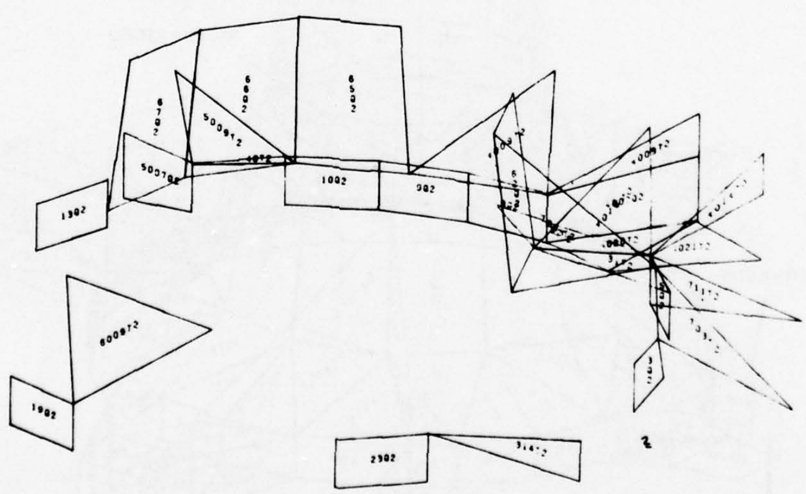

Figure 74b. NASTRAN Orthographic Plot of Areas of Lowest Strain Density for Upper Cover

improvement: 1) stress reduction and 2) bearing outer race misalignment. There are different types of misalignment, such as out of roundness of the outer race, outer race warped azimuthally, the line of centers not geometrically centered for pairs of gears, or outer race tilted. The latter criterion was chosen because of its ease of calculation from the NASTRAN output.

The optimality principle of maximum stiffness for a minimal weight states that for two similar structures under the same loading with the same weight, the structure with the more uniform strain density is stiffer. It follows that when all the strain densities are equal the structure is the stiffest possible. For the typical case of multiple loadings, the optimality principle must be modified such that the largest strain density in each element for all load conditions is the same throughout the structure. The largest strain density is not necessarily caused by the same loading condition in all the elements (Reference 23). In addition, the analytical process is iterative. There may also be side constraints such as displacements, member sizes and stress limitations. Finally, the final optimized design may not be readily producible, or it may be too expensive to manufacture.

This implies that some compromise is needed for all these conditions. For simplicity it is assumed that one iteration with the addition of material in the areas of highest strain density using S-83 with NASTRAN is the best practical start. The sample S-83 output for the upper cover at the ultimate flight condition is given as Appendix F (Table F-1), which includes the principal stresses as well as the element numbers and strain densities. This output is used to illustrate both the addition and the removal of material for stiffness optimization on a weight basis. For 2014-T6 aluminum, the ultimate stress in tension and compression is 65,000 psi; the yield stress in tension is 55,000 psi; and the yield stress in compression is 58,000 psi. From Table F-1 all the stresses are within these limits. The principal stresses are proportional to the strain density, or more precisely the "square" of the principal stresses in the matrix sense ($\sigma^T \sigma$) is proportional to the strain density. Hence the strain density method is somewhat similar to the fully stressed design method (FSD).

The results of adding material are summarized in Table F-2. The weight penalty was 15.7 lb. The thickness of the 30 most highly strained elements was approximately doubled. Most stresses were reduced and the misalignment was reduced in general. For example, the maximum stress went from 39,781 psi to 33,500 psi and the fore-to-aft roller bearing

23. Venkayya, Knot, and Reddy, ENERGY DISTRIBUTION IN AN OPTIMUM STRUCTURAL DESIGN, AFFDL-TR-68-156.

misalignment went from .0031 in./in. to .0027 in./in. For stiffness both added and removed (approximately half removed from the least strained elements), the weight penalty was 2.64 lb. The maximum stress was 34,367 psi, and the fore-to-aft misalignment was .0027 in./in. as before. This is shown in Table F-3. For weight off only (Table F-4), the cover was 13 lb lighter, the maximum stress went up to 40,293 psi, and the fore-to-aft misalignment was .0033 in./in. It appears that adding stiffness is the best choice.

A fully stressed design analysis of the CH-47C forward transmission upper cover was conducted using NASTRAN Level 16. Two iterations were done and a value of .001 was selected for ε , where:

$$\left[\frac{\sigma - \sigma_\ell}{\sigma}\right] = \quad \varepsilon\sigma \text{ is a}$$

σ is a calculated stress, and σ_ℓ is a defined stress limit (tension, compression and shear). Another input parameter, γ , was selected as unity, where:

$$P_{NEW} = \frac{P_{OLD}}{\alpha}\left[\alpha + (1 - \alpha)\gamma\right], \; P_{NEW} \text{ is the new}$$

property, P_{OLD} is the old property and

$$\alpha = \text{MAX}\left(\frac{\sigma}{\sigma_\ell}\right), \text{ for all structural elements.}$$

γ is an iteration factor which limits the property change in a single iteration, and if less than unity, improves the stability of the iterative process.

The maximum change in any property is limited by K_{MAX} and K_{MIN}, where

$$K_{MIN} < \frac{P_{NEW}}{P_i} < K_{MAX},$$

and P_i is the initial value of the property. If K_{MAX} and K_{MIN} are unspecified no limits are imposed. K_{MAX} and K_{MIN} were not specified for the test run here; hence, some unrealistic thicknesses for the upper cover resulted. Nevertheless, it is felt that this new feature in NASTRAN is useful for weight reduction. In the test case for example, the results were:

Original Weight = 145 lb

Iteration no. 1 = 26.5 Lb

Iteration no. 2 = 34.8 Lb

A sample of the output thicknesses for each iteration is given in Figure 75. Since no restrictions were imposed on the

```
441-   MAT1      1        10.5E6    4.0E6              .0002615          &ABCD2
442-   &ABCD2    55000.   57000.    33515.                  STRESS ALLOWABLES
443-   PARAM     GRDPNT   0
444-   POPT      2        1.0E-3    1.        1        YES      PUNCH CONTROL
445-   PQUAD2    1        1         1.25      α
446-   PQUAD2    2        1         1.25           PRINT CONTROL
447-   PQUAD2    3        1    ε    1.25
448-   PQUAD2    4        1         1.25
449-   PQUAD2    5        1         1.25
450-   PQUAD2    6        1         1.25

          NUMBER OF        THICKNESSES
          ITERATIONS                                          INITIAL DESIGN
```

ORIGINAL				ITERATION NO. 1					ITERATION NO. 2				
PQUAD2	7	1	1.25	PQUAD2	7	1	.125318	0.0	PQUAD2	7	1	.151523	0.0
PQUAD2	8	1	1.25	PQUAD2	8	1	.069864	0.0	PQUAD2	8	1	.072639	0.0
PQUAD2	9	1	1.25	PQUAD2	9	1	.059708	0.0	PQUAD2	9	1	.039976	0.0
PQUAD2	10	1	1.25	PQUAD2	10	1	.038912	0.0	PQUAD2	10	1	.018969	0.0
PQUAD2	11	1	1.25	PQUAD2	11	1	.068342	0.0	PQUAD2	11	1	.043547	0.0
PQUAD2	12	1	1.25	PQUAD2	12	1	.143803	0.0	PQUAD2	12	1	.144472	0.0
PQUAD2	13	1	1.25	PQUAD2	13	1	.110862	0.0	PQUAD2	13	1	.080590	0.0
PQUAD2	14	1	1.25	PQUAD2	14	1	.167358	0.0	PQUAD2	14	1	.073987	0.0
PQUAD2	15	1	1.25	PQUAD2	15	1	.126114	0.0	PQUAD2	15	1	.061041	0.0
PQUAD2	16	1	1.25	PQUAD2	16	1	.171339	0.0	PQUAD2	16	1	.040001	0.0
PQUAD2	17	1	1.25	PQUAD2	17	1	.178447	0.0	PQUAD2	17	1	.141895	0.0
PQUAD2	18	1	1.25	PQUAD2	18	1	.351987	0.0	PQUAD2	18	1	.391872	0.0
PQUAD2	19	1	1.25	PQUAD2	19	1	.283126	0.0	PQUAD2	19	1	.224955	0.0
PQUAD2	20	1	1.25	PQUAD2	20	1	.284259	0.0	PQUAD2	20	1	.431983	0.0
PQUAD2	21	1	1.25	PQUAD2	21	1	.239569	0.0	PQUAD2	21	1	.317248	0.0
PQUAD2	22	1	1.25	PQUAD2	22	1	.089622	0.0	PQUAD2	22	1	.275282	0.0
PQUAD2	23	1	1.25	PQUAD2	23	1	.122267	0.0	PQUAD2	23	1	.299664	0.0
PQUAD2	24	1	1.25	PQUAD2	24	1	.169758	0.0	PQUAD2	24	1	.130918	0.0
PQUAD2	61	1	1.02	PQUAD2	61	1	.088225	0.0	PQUAD2	61	1	.060463	0.0

Figure 75. Sample Output for Fully Stressed Design of CH-47C Forward Transmission Upper Cover

ORIGINAL				ITERATION NO. 1					ITERATION NO. 2				
PQUAD2	62	1	1.02	PQUAD2	62	1	.025195	0.0	PQUAD2	62	1	.034645	0.0
PQUAD2	63	1	1.02	PQUAD2	63	1	.100920	0.0	PQUAD2	63	1	.042184	0.0
PQUAD2	64	1	1.02	PQUAD2	64	1	.090322	0.0	PQUAD2	64	1	.062802	0.0
PQUAD2	65	1	1.02	PQUAD2	65	1	.063726	0.0	PQUAD2	65	1	.045690	0.0
PQUAD2	66	1	1.02	PQUAD2	66	1	.084753	0.0	PQUAD2	66	1	.067677	0.0
PQUAD2	67	1	1.02	PQUAD2	67	1	.203630	0.0	PQUAD2	67	1	.109700	0.0
PQUAD2	68	1	1.02	PQUAD2	68	1	.222398	0.0	PQUAD2	68	1	.165720	0.0
PQUAD2	69	1	1.02	PQUAD2	69	1	.319549	0.0	PQUAD2	69	1	.209197	0.0
PQUAD2	70	1	1.02	PQUAD2	70	1	.390298	0.0	PQUAD2	70	1	.467042	0.0
PQUAD2	71	1	1.02	PQUAD2	71	1	.257154	0.0	PQUAD2	71	1	.298760	0.0
PQUAD2	72	1	1.02	PQUAD2	72	1	.210487	0.0	PQUAD2	72	1	.176455	0.0
PQUAD2	73	1	.56	PQUAD2	73	1	.142862	0.0	PQUAD2	73	1	.358966	0.0
PQUAD2	74	1	.56	PQUAD2	74	1	.234671	0.0	PQUAD2	74	1	.361405	0.0
PQUAD2	75	1	.56	PQUAD2	75	1	.257862	0.0	PQUAD2	75	1	.359776	0.0
PQUAD2	76	1	.56	PQUAD2	76	1	.266794	0.0	PQUAD2	76	1	.384103	0.0
PQUAD2	77	1	.56	PQUAD2	77	1	.245416	0.0	PQUAD2	77	1	.501677	0.0
PQUAD2	78	1	.56	PQUAD2	78	1	.138411	0.0	PQUAD2	78	1	.113875	0.0
PQUAD2	79	1	.56	PQUAD2	79	1	.188467	0.0	PQUAD2	79	1	.288095	0.0
PQUAD2	80	1	.56	PQUAD2	80	1	.223536	0.0	PQUAD2	80	1	.346056	0.0
PQUAD2	81	1	.56	PQUAD2	81	1	.111093	0.0	PQUAD2	81	1	.159173	0.0
PQUAD2	82	1	.56	PQUAD2	82	1	.119135	0.0	PQUAD2	82	1	.369609	0.0
PQUAD2	83	1	.56	PQUAD2	83	1	.292901	0.0	PQUAD2	83	1	1.33444	0.0
PQUAD2	84	1	.56	PQUAD2	84	1	.233878	0.0	PQUAD2	84	1	.623464	0.0
PQUAD2	85	1	.50	PQUAD2	85	1	.294675	0.0	PQUAD2	85	1	.685123	0.0
PQUAD2	86	1	.50	PQUAD2	86	1	.418627	0.0	PQUAD2	86	1	.657226	0.0
PQUAD2	87	1	.50	PQUAD2	87	1	.300328	0.0	PQUAD2	87	1	.480216	0.0
PQUAD2	88	1	.50	PQUAD2	88	1	.299678	0.0	PQUAD2	88	1	.529018	0.0
PQUAD2	89	1	.50	PQUAD2	89	1	.432353	0.0	PQUAD2	89	1	.732762	0.0
PQUAD2	90	1	.50	PQUAD2	90	1	.261049	0.0	PQUAD2	90	1	.358331	0.0
PQUAD2	91	1	.50	PQUAD2	91	1	.168527	0.0	PQUAD2	91	1	.309155	0.0
PQUAD2	92	1	.50	PQUAD2	92	1	.063381	0.0	PQUAD2	92	1	.048786	0.0

Figure 75. Continued.

deflections in the analysis, some deflections became unrealistically large (e.g., .6 in.).

The new strain energy capability of NASTRAN Level 16 has been applied to the CH-47C forward transmission upper cover. The output results are given in Table F-5. The strain energy output is calculated for Rigid Format 1 (Static Analysis) only by placing "ESE (Print, Punch) = ALL" in the case control of the NASTRAN deck. This not only prints out the strain energy for each element, but also punches it on cards. This deck may then be used in a post-processor to sort the strain energies, to list the percentage of total strain energy, and to calculate the accumulated percentage. The limitation that strain energies can be calculated only in Rigid Format 1 can be circumvented so that they may also be calculated in Rigid Format 3 (normal mode analysis) by utilizing a post-processor to reformat punched "ASET" displacements for a given mode shape from Rigid Format 3 into "SPC" input for a Rigid Format 1 run.

APPLICATIONS

COMPOSITE MATERIALS

Current cast light alloy (magnesium) transmission housing technology does not provide an optimum support structure for power train dynamic components under operating loads. These structures, limited by current materials and processing techniques which do not permit structural design optimization, exhibit excessive deflections and displacements under load. The metal industry, especially the light metals industry, has been seeking alloys with higher strength-to-weight and modulus-to-weight values. New alloys and new processing methods have achieved small improvements, but the gains are no longer proportionate to the effort required to attain them. Since all of the widely used structural metals reach a limit of specific strength at about 1 million inches and a limit of specific modulus at about 100 million inches, research is being devoted to ways of getting around these specific strength and specific modulus barriers. High-modulus fiber-reinforced composite materials offer promise in providing the solution. These materials provide the needed capability for selectively stiffening the housing structure for reduced deflection and for detuning to reduce vibration/noise levels.

Studies conducted by Boeing have indicated the overall desirability and payoff to be gained from using these high specific strength, specific modulus materials for helicopter transmission housings. For example, increasing the housing wall stiffness reduces the resulting static and dynamic displacements for a specified load condition. This is evident from

$$F = Kx$$

where F = applied static or dynamic load

K = stiffness

x = displacement

Plots of displacement versus load for various materials (Figure 72) indicate that the magnitude of housing displacements can be reduced substantially by using the stiffer metal matrix materials. Steel is also shown in the figure as a point of reference.

A number of composite systems have evolved, such as boron/epoxy, graphite/epoxy, boron/aluminum, graphite/aluminum, FP/aluminum (FP is a trade name of Dupont's polycrystalline Al_2O_3 fiber) and FP/magnesium. Each of these has its own peculiar advantages and limitations. Several metal matrix candidate systems exhibit specific strength in the range of 2 to 3 million inches and specific moduli of 400 to 500 million inches. Metal matrix composites offer unique combinations of improved performance and reliability, in comparison to organic composite systems, due to improved shear strength, compressive strength, resistance to environmental degradation, and improved design flexibility. Also, the metal matrix composites offer better high-temperature capability for elevated temperature applications such as helicopter transmission housings. With improved design concepts, more sophisticated use of materials can be made, and greater weight savings realized by selectively strengthening critical areas of the casting. Reinforcing these highly-loaded areas by imbedding high strength filaments would produce a more efficient design and a more serviceable part. Weight limitations and the potential of significantly reduced maintenance dictates that the use of advanced metal matrix composites for many critical structural applications be examined carefully.

The work reported herein indicates the use of finite element methods utilizing NASTRAN in conjunction with other programs for the analysis of composite materials to define optimum material configurations and orientations. Micromechanics, lamina theory, and the total constitutive relation for a laminated plate provide the basis for analysis and design of composite structures. The theory of composites also includes:

- Thermal stress calculation
- Equivalent coefficients of thermal expansion
- The determination of the strains and stresses in each layer of the laminate
- Transverse shear stress analysis, interlaminar shear stress
- Laminate interaction diagram depictions based on the maximum strain theory of failure
- Optimization of layups

These analyses are available in the form of operational computer programs. Two of these programs, which may be used as pre- and post-processors to NASTRAN, are summarized below.

The "Point Stress Laminate Analysis" (S71) computer program (Reference 24) defines material properties of anisotropic composite materials by computing equivalent orthotropic material properties suitable for use in a NASTRAN analysis. This may also be used after the NASTRAN analysis as a post-processor to obtain interlaminar and laminar stresses. Figure 76 illustrates the lamina or layer coordinate system (1-2) that is transformed to the laminate (X-Y) axis system.

---

24. Reed, D. L., POINT STRESS LAMINATE ANALYSIS, Document FZM-5494, AFML, Advanced Composite Division, WPAFB, Ohio, April 1970.

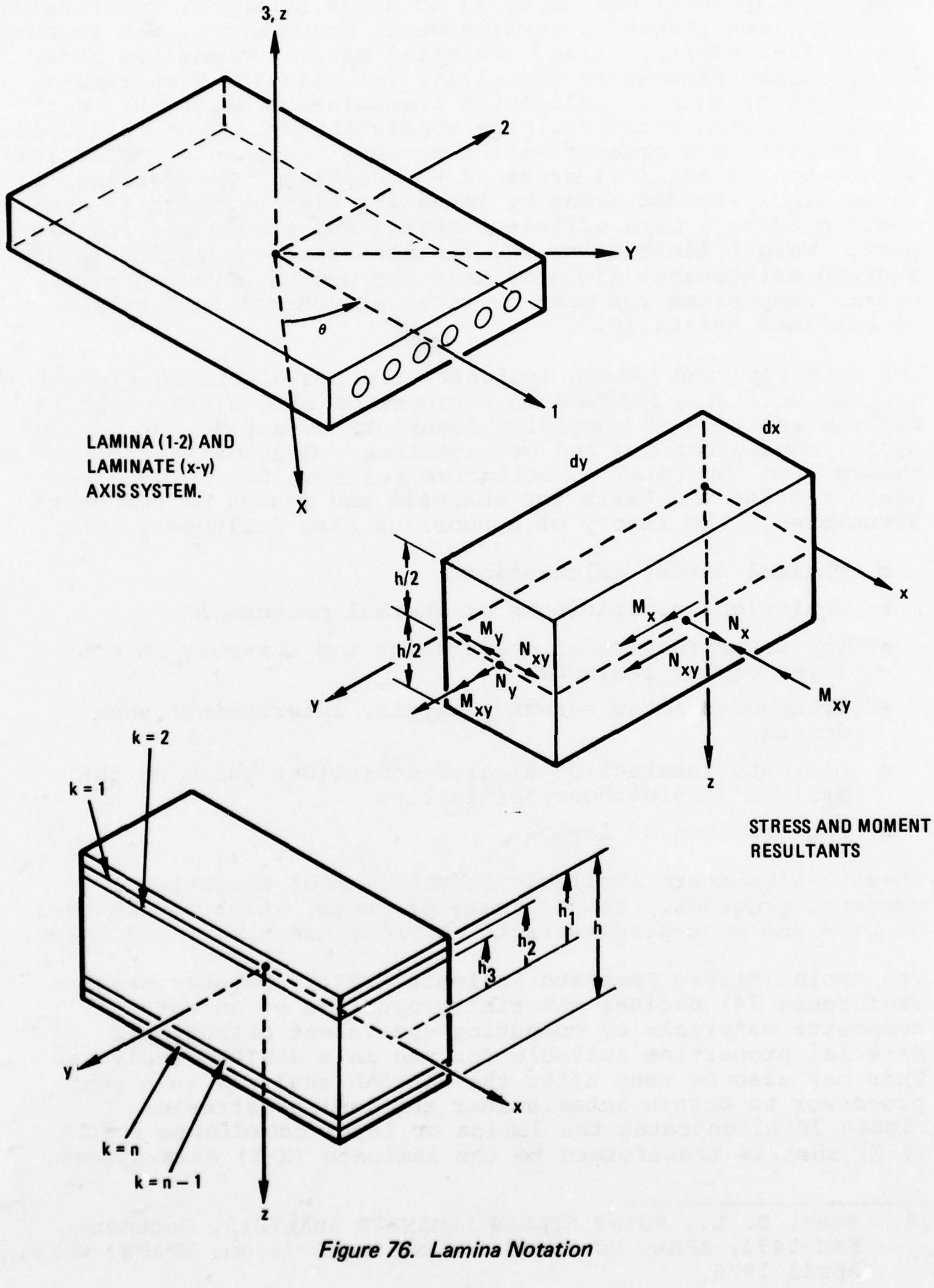

Figure 76. Lamina Notation

The resultant stresses and moments of the laminate are also shown. These represent a system that is statistically equivalent to the stress system that is acting on the laminate. The program will accommodate up to 400 layers, and a point stress analysis can be performed and thermal loads and point stresses may be calculated.

A second computer program for the analysis and optimization of laminated composites is "COOP" (Reference 25). Optimization is achieved by minimizing an objective function, which consists of terms involving laminate weight, cost, stiffness and strength. A materials property table is included in the program with an option to input any material and its properties. Margins of safety are calculated using four different failure criteria. Buckling loads for inplane end load and shear can also be calculated. The program prints out the inplane and bending matrices for the selected lamina. The program takes the elastic moduli E11, E22, G12, α_1, α_2 and the Poisson's ratios, μ_{12}, μ_{21}, of the individual layers within the laminate and computes the elastic moduli E_x, E_y, G_{xy}, α_x, α_y, μ_{xy} and μ_{yx} for the final laminate. The 1-2 axes refer to the layer coordinate system and the x-y axes to the laminate system. The x-y axes correspond to the x-y loading directions. The program uses the classic laminated plate theory (References 26 and 27) in the calculation of the elastic constants, stresses and strains.

An analysis of the CH-47C forward transmission housing using a finite element NASTRAN model to determine the optimum locations and orientations of composite materials for selective stiffening of the lower housing structure was conducted. Static loads representative of operating conditions were applied to the model. Based on a combination of a strain energy and fully stressed design analyses the goal is to achieve maximum stiffness. The NASTRAN preprocesser, Point Stress Laminate Analysis, was used to study the optimum fiber configuration and to define the anisotropic material properties. The determination of the areas for stiffening is contingent on the load condition. Equivalent orthotropic material properties for a quasi-isotropic graphite composite material ($0^\circ/\pm45^\circ/90^\circ$ lamina) were obtained using computer program S-71. A sample output for this run is attached as Appendix G. The selective addition of this quasi-isotropic composite material to the transmission case stiffening was

---

25. Dobyns, A., COMPUTER PROGRAM FOR ANALYSIS AND OPTIMIZATION COMPOSITES, Users Document, October 1976.

26. Tsai, S. W., Adams, D. F., and Doner, D. R., ANALYSIS OF COMPOSITE STRUCTURES, NASA Report CR-620, November 1966.

27. Ashton, J. E., Halpin, J. C., Petit, P. H., PRIMER ON COMPOSITE MATERIALS: ANALYSIS, Technomic Publishing Company, 1969.

based on the strain density distribution. The finite element model was augmented to incorporate the orthotropic material properties and a static analysis was conducted. Using the ultimate load condition, Table 13 summarizes the comparison that was made.

TABLE 13. STRESS COMPARISON - ORIGINAL AND COMPOSITE AUGMENTED HOUSING

ELEMENT NUMBER	Mq ORIGINAL STRESSES ($E = 6.5 \times 10^6$ PSI)		WITH QUASI-ORTHOTROPIC COMPOSITE IN AREAS OF HIGHEST STRAIN DENSITY ($E = 10.5 \times 10^6$) - HIGH-DENSITY GRAPHITE	
	max	min	max	min
2272	448	-957	460	-781
2242	728	-1219	812	-1084
2273	-330	-871	-303	-630
149	-3.6	-720	-34	-735
1065	-78	-963	-36	-943
2062	13702	-10206	6489	-3670
2092	12921	-9229	6552	-2667
2097	2283	-4533	1984	-2562
112	997	-1115	1266	-896
2100	-3630	-30426	-989	-14833
2063	25040	-7062	11530	-1181

The original stresses have generally been cut to about half their original values. Another observation is that the addition of material must be done very selectively in patches, rather than over broad areas, in order to achieve maximum benefit from the strain energy method.

The use of composite materials for transmission housings will allow stiffer yet lighter structures. Further, vulnerability is reduced due to the better ballistic tolerance of composite materials and survivability is improved. It is possible to extend the operation of a marginally lubricated bearing if thermal gradients from inner to outer races can be reduced, thus preventing loss of internal clearance. The low thermal conductivity of the composite housing will impede heat flow from the outer race and tend to equalize the outer-inner race temperatures. If material properties can also be adjusted to approximate the coefficient for expansion of the bearing race, an ideal condition for maintaining bearing clearance exists.

VULNERABILITY/SURVIVABILITY OF A HELICOPTER TRANSMISSION

The minimum vulnerability/survivability standard for a contemporary transmission requires continued safe operation for at least 30 minutes after damage from any single hit by a 7.62mm projectile at a range of 100 meters. More specifically, they are designed to operate at the power required for flight at the speed for maximum range at sea level standard conditions and primary mission gross weight for not less than 30 minutes after depletion of the main lube system lubricant.

The work conducted herein will prove valuable in designing transmissions to meet both the current goals and future, more stringent goals. The vulnerability/survivability benefits to be derived are concentrated in two areas - the housing and the internal gear/bearing system. The analytical methods provided by NASTRAN provide more accurate load path definition and hence allow the designer to build-in improved load path redundancy. Also, the housing can be designed for the efficient use of composite materials with properties that eliminate the brittle fracture characteristics displayed by magnesium when subjected to hydraulic shock loads. Through NASTRAN, a stiffer case can be designed which will improve the load capacity of the gears and bearings by decreasing misalignment and, therefore, theoretically allow the use of smaller components. This would reduce vulnerability by reducing the vulnerable area of the transmission. This size reduction is not likely to materialize in practice for sometime since the effect of misalignment on load capacity is not yet defined with sufficient confidence to permit trade-offs between size and misalignment. The immediate practical benefits will thus be confined to somewhat higher capacity at the sizes determined by current design methods, which will contribute to better survivability.

Further significant advances in survivability result from an improved understanding using the NASTRAN analyses of the thermal conditions existing during normal and emergency loss-of-lubricant conditions. In addition the gears must be designed with sufficient clearance to allow thermal expansion at the gear tips and roots. It is possible to extend the operation of a marginally lubricated bearing if thermal gradients from inner to outer races can be reduced, thus preventing loss of internal clearance. The low thermal conductivity of a composite housing, for example, impedes heat flow from the outer race and tends to equalize the outer-inner race temperatures. By using a NASTRAN model to approximate the coefficient of expansion of the bearing race, an ideal condition for maintaining bearing clearance exists.

Survivability/vulnerability in transmission systems is concerned with the loss of lubrication, radar cross section, and fail-safety. The latter two areas are discussed further in subsequent sections. It has been shown that the heat rejection rate of fins can be calculated by the NASTRAN thermal analyzer for an elimination or a reduction of external oil lines for cooling. Elimination of the oil lines and placement of the cooler in proximity to the case would reduce the vulnerable area of the CH-47 from 11.4 to 6.5 square feet. Using a system that could by-pass the cooler in an emergency would further reduce the vulnerable area to 4.1 square feet. If the sump is armored the vulnerable area becomes 2.3 square feet, and a nonlubrication capability would reduce this to 0.6 square feet. Since experience has shown that no ballistic damage has caused drive system severances, the potential exists for a highly survivable helicopter with the elimination of the vulnerability of the lubrication system. The NASTRAN thermal analyzer is a valuable analytical tool for such a design problem. problem.

It is clear from Table 14, which relates the CH-47 vulnerable area to combat kills, that the drive/lube system is the most vulnerable area. Analysis indicates that the larger the area, the greater the potential for a "kill". Complete loss of oil from a transmission due to a .30- or .50-caliber hit in the cooling system will occur in approximately 20 to 30 seconds. Because of the high heat rejection rate and the large loads carried by the transmission, complete loss of oil is considered to be an A-kill, while total cooling loss with no oil loss is considered to be a B-kill. Of particular concern is the ability of a helicopter to continue its flight for a limited period after loss of transmission lubricant. Boeing Vertol has accumulated considerable experience with non-lubricated operation of components. Much of this has been under actual conditions of oil starvation, while other experience was obtained with tests under simulated oil system failures. These tests indicate that the bearings are the first items to show distress and that tapered roller bearings and ball thrust bearings in particular are susceptible to damage at high speeds and high loads. Spiral bevel gears appear to be the next most vulnerable item, although their damage may be partially ascribed to adjacent bearing failure. The establishment of an emergency nonlubricated capability of 30 minutes or more will reduce the K-, A-, and B-kill helicopter transmission categories to almost zero and thereby save personnel and aircraft.

TABLE 14. A-KILL VULNERABLE AREA TABULATION

Subsystem	CH-47 VULNERABLE AREA, Ft^2	RELATIVE CAUSAL KILL DISTRIBUTION (%)	
		Analysis	Combat Data
Crew	0.37	1.28	1.67
Power Plant	5.85	20.30	21.70
Flight Controls	8.47	29.35	16.60
Drive/Lube	11.40	39.54	40.00
Fuel	2.75	9.53	16.70
Rotor	—	—	1.67
Electrical	—	—	1.67
TOTAL	28.84	100.0	100.0

RADAR CROSS-SECTION

The computer-generated plotting capability afforded by NASTRAN is useful for assessing the cross-sectional area projected by a structure when observed from any viewpoint. Typical radar cross-sectional areas, assuming a transparent fuselage, are plotted in Figure 77 for the CH-47C forward transmission at various angles. Any other orientation may also be evaluated simply by specifying the angular orientation about three axes. Utilizing the plotting scale factor, the cross-sectional areas presented can be calculated from the plots.

The reinforcement and modification to the wall thickness considered herein have no effect on the radar cross-section of the housing since the basic size and geometry are unchanged. However, the modeling capability would be valuable for determining the best housing geometry for minimum overall cross-section during the design or major redesign of a transmission housing.

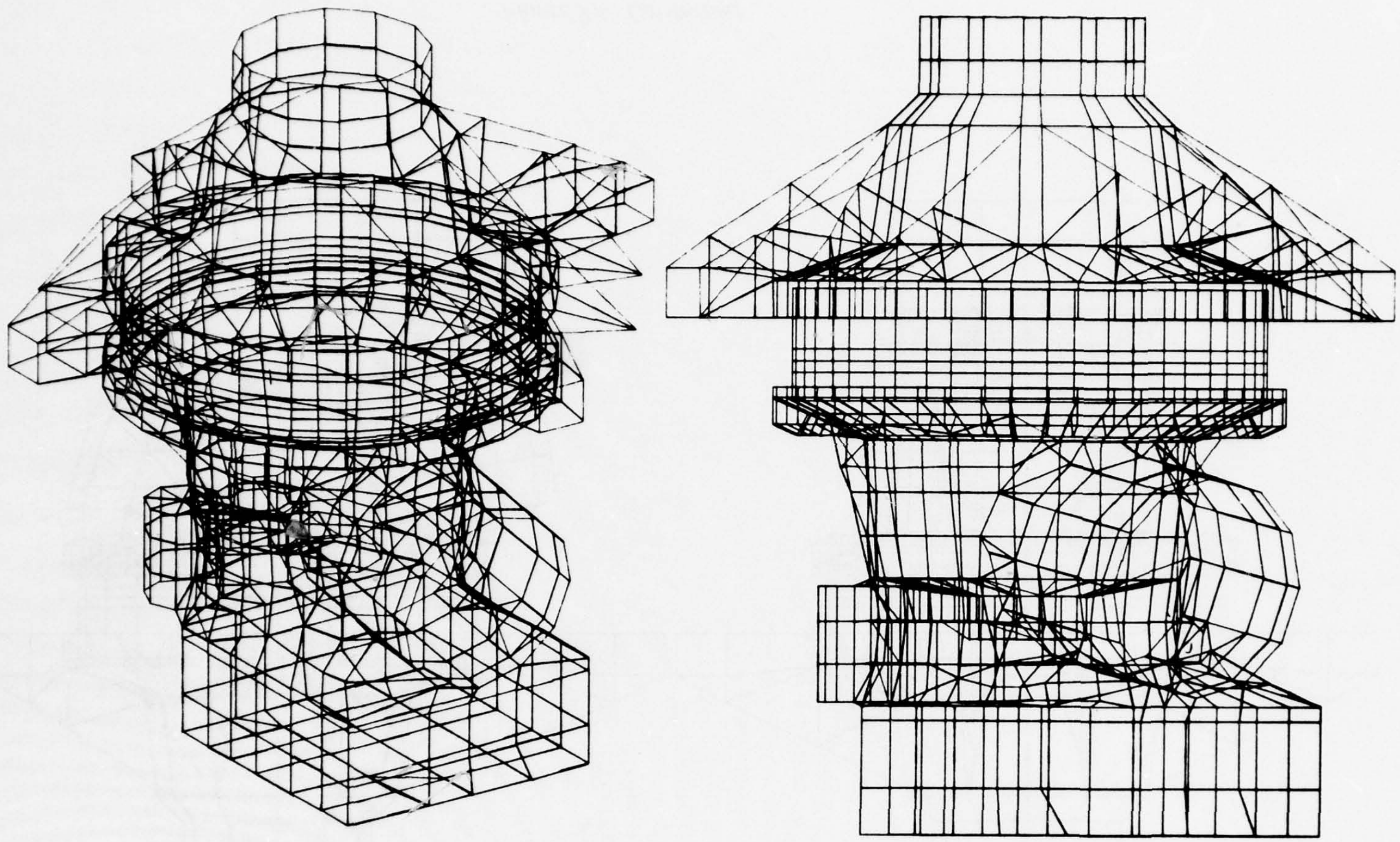

Figure 77. Typical Plots of CH-47C Forward Transmission for Evaluating Radar Cross-Sectional Area

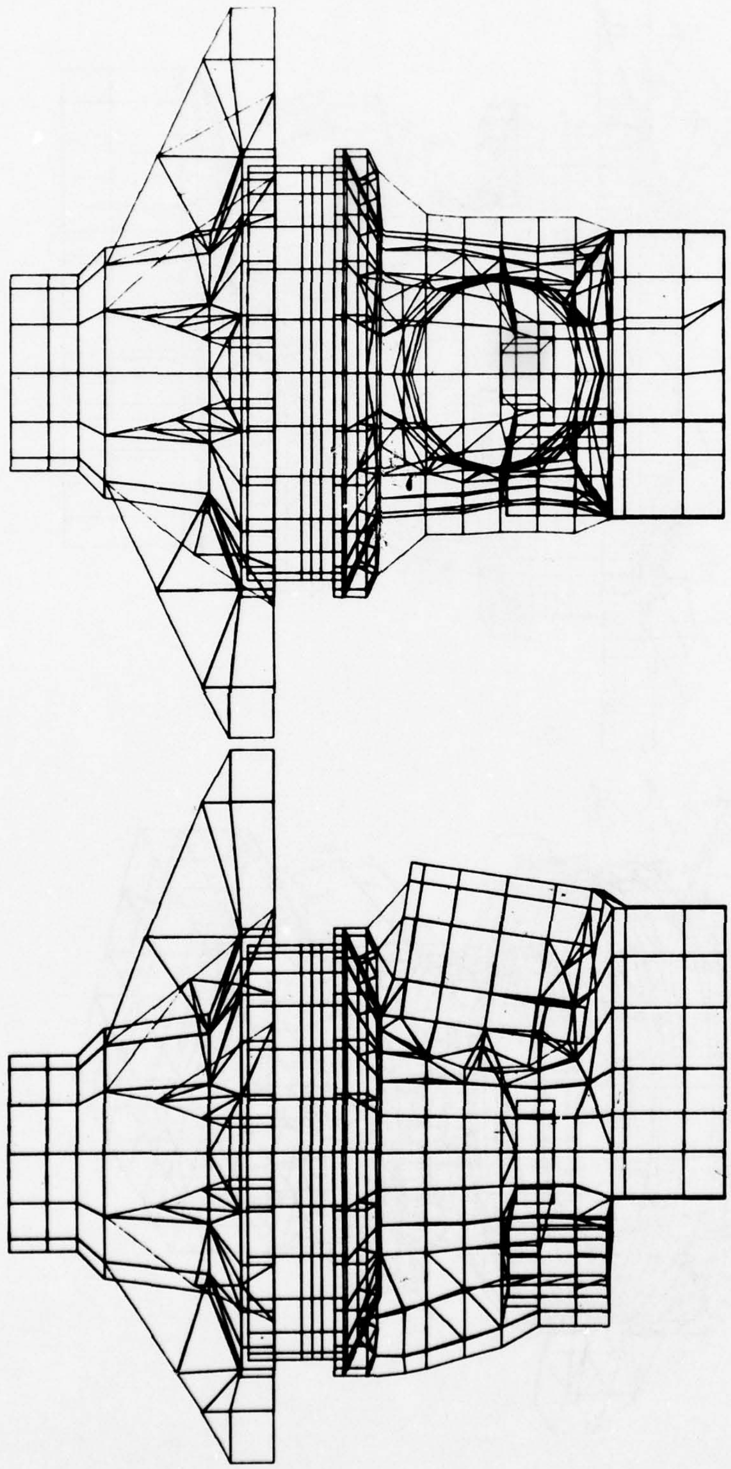

Figure 77. Continued

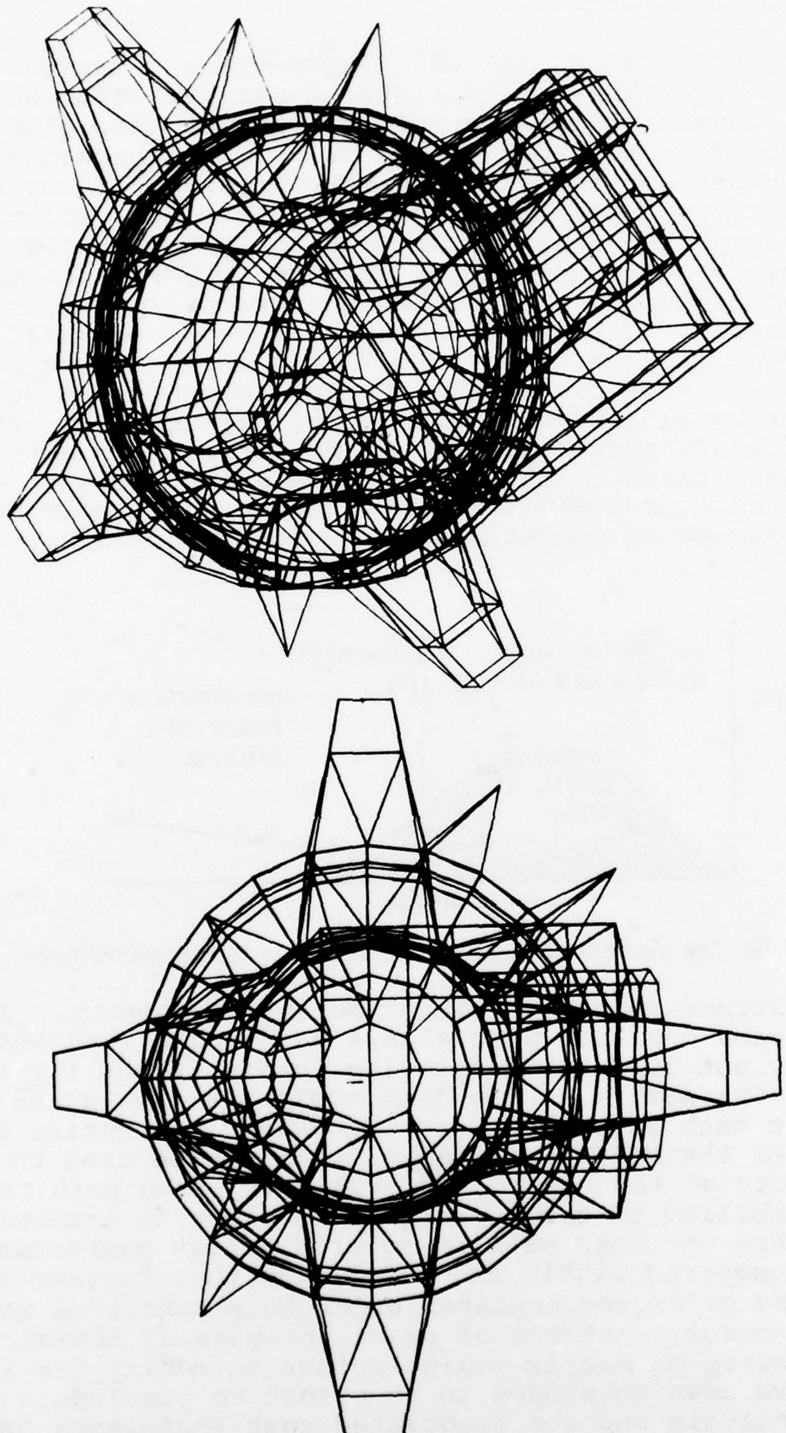

Figure 77. Continued

FAIL-SAFE/SAFE-LIFE DESIGN

Many helicopter fatigue critical components are designed for safe life, whereby they are assigned a service life in operational hours and removed from service at this elapsed time to preclude catastrophic failure. This approach is effective in preventing failure due to statistical variations in the flight spectrum, loads and strength. However, most helicopter component failures are caused by the unknown, the unpredictable, or the unexpected (Figure 78), such as material defects, manufacturing and maintenance errors, pilot errors or battle damage. Current philosophy is to design helicopters to be tolerant of such defects so that the risks from unanticipated causes may be minimized. Defect tolerance, a design concept whereby an incipient or partial failure will not result in catastrophic failure, can be achieved by either providing an alternate load path with a short but sufficient life (fail-safe) or permitting the planned and timely detection of fatigue damage or operational deterioration (safe crack growth).

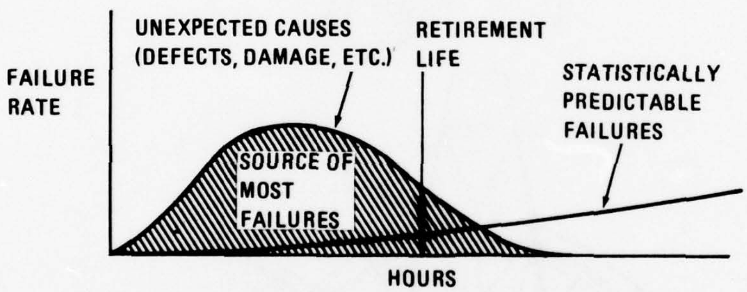

Figure 78. The Unexpected Causes Most Helicopter Component Failures

A fail-safe structure can be either active or passive. The passive system uses one load path always carrying a load and one path normally not loaded but becoming loaded if the first path fails. The active system uses two paths always sharing the load, but each is capable of taking over the entire load. The results of the NASTRAN model analysis can be used to study the fail-safety of the housing by evaluating load path redundancy, that is the ability of the housing to continue to transmit all loads even when one load path is severed. Load paths can be artificially severed within the model, and the stresses in the remaining load paths recalculated under this condition using the modified model. Methods of exact analysis of modified structures, based on matrix manipulations to modify the initial analysis, have been developed in an effort to preclude a complete reanalysis and the associated cost (Reference 28).

28. Melosh, R. J., Johnson, J. R., and Luik, R., STRUCTURAL SURVIVABILITY ANALYSIS, Philco Ford and AFFDL, Paper Based on Contract AF33(615)-5039.

This approach is an extensive subject in itself, however, and has been bypassed herein. Checking of stresses and deflections determines if adequate gear contact and bearing alignment is maintained. Comparison of stresses with allowables indicate the degree of fail-safety.

The alternative approach, safe crack growth, is based on fracture mechanics. It may utilize a periodic inspection or an integral detection system with an obvious failure indicator. In both approaches, parts are sized so that the rate of fatigue crack growth from a defect would be slow enough to assure inspection and detection before any component failure. Defect tolerance is achieved through a sub-threshold crack growth concept for an assumed defect size. This defect may be an inclusion inherent in the material, or it may be introduced during manufacture or in-service. Using this concept, the component is sized to a stress level sufficiently low to assure that the defect will not propagate during the life of the component. No inspections other than those specified for normal aircraft maintenance are required.

The fracture mechanics analysis uses the mean of scatter crack growth data, a crack simulation model, and the maximum load in the mission profile. Crack growth rate characteristics of metals are measured by testing standard compact specimens. Typical test results are shown in Figure 79, where data is presented as crack growth rate versus the stress intensity factor range (ΔK) where:

$$\Delta K = \Delta\sigma \sqrt{\pi a} \quad f(a)$$

and

$\Delta\sigma$ = range of applied fatigue stress, (σ max - σ min)

a = crack size parameter

f (a) = function of crack size and specimen or component geometry

A significant characteristic of the data is that there is a point, designated the ΔK threshold, below which fatigue crack growth is extremely slow or negligible. Generally, the threshold stress intensity factor range will differ with material. For a given material, the threshold stress intensity is primarily influenced by stress ratio and temperature.
Data indicates that environment and loading frequency do not significantly influence the threshold stress intensity range versus stress ratio curve. This "mean-of-scatter" curve is representative of medium strength steels and titaniums. The ultimate tensile strengths of the materials tested to define the curve are in the approximate range of 85 ksi to 180 ksi. Substitution of the threshold stress intensity factor range in the equation for ΔK allows determination of the maximum crack size which will not propagate at a given stress level.

This maximum crack size will vary depending on the crack model (i.e., on f (a)) selected for analysis. Parametric charts may be generated for selected crack models which will define the size of nonpropagating cracks at various stress range conditions. It is useful to convert $\Delta\sigma$ to steady and alternating stresses, and this type of presentation for the surface flaw defect is shown in Figure 80.

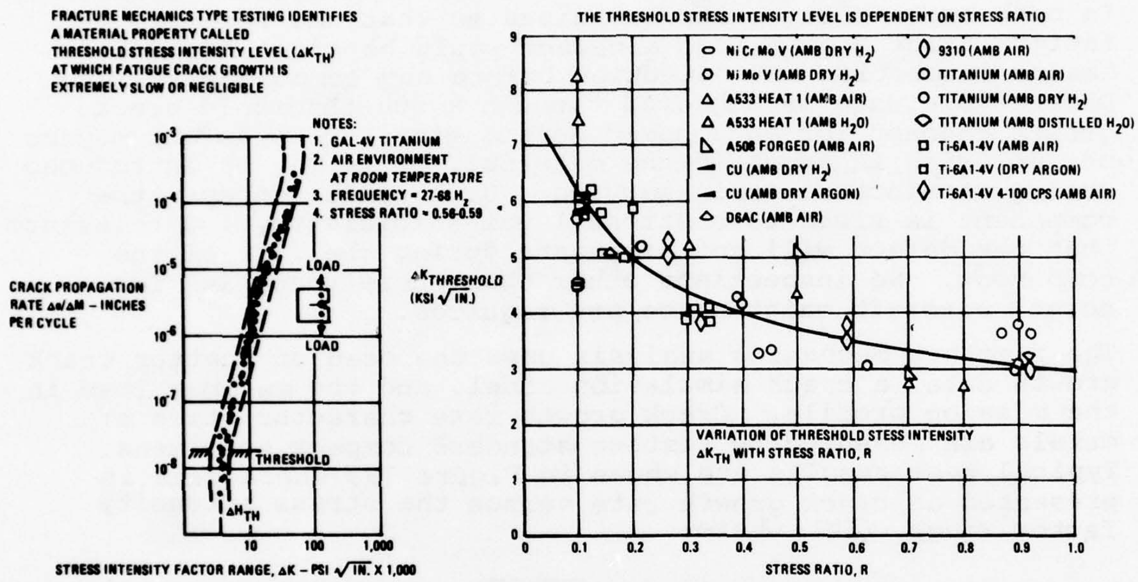

Figure 79. Crack Growth Data for the Application of Fracture Mechanics to Defect Tolerant Design

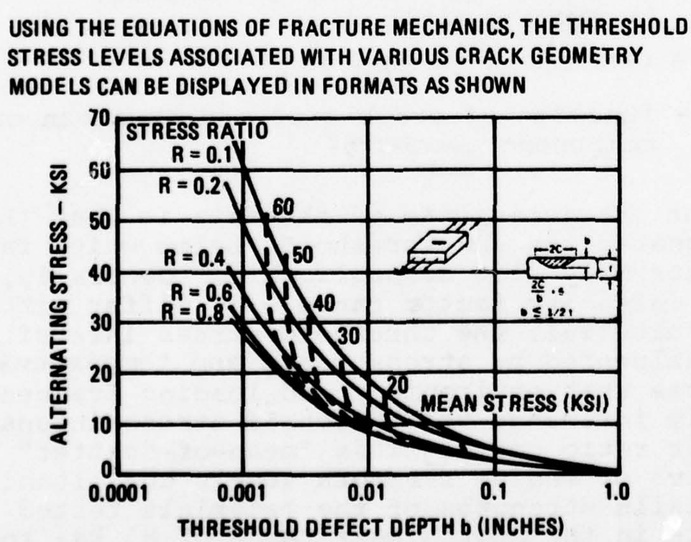

Figure 80. Analytical Model for Application of Fracture Mechanics to Defect Tolerant Design

Realizing that additional safety normally compromises performance, studies were made to assess this penalty. One example of this weight penalty due to the safe crack growth approach is presented for a pitch housing. The 30 hour post-indication crack period requires an 11% heavier section than would a safe life version of the same part as shown in Figure 81.

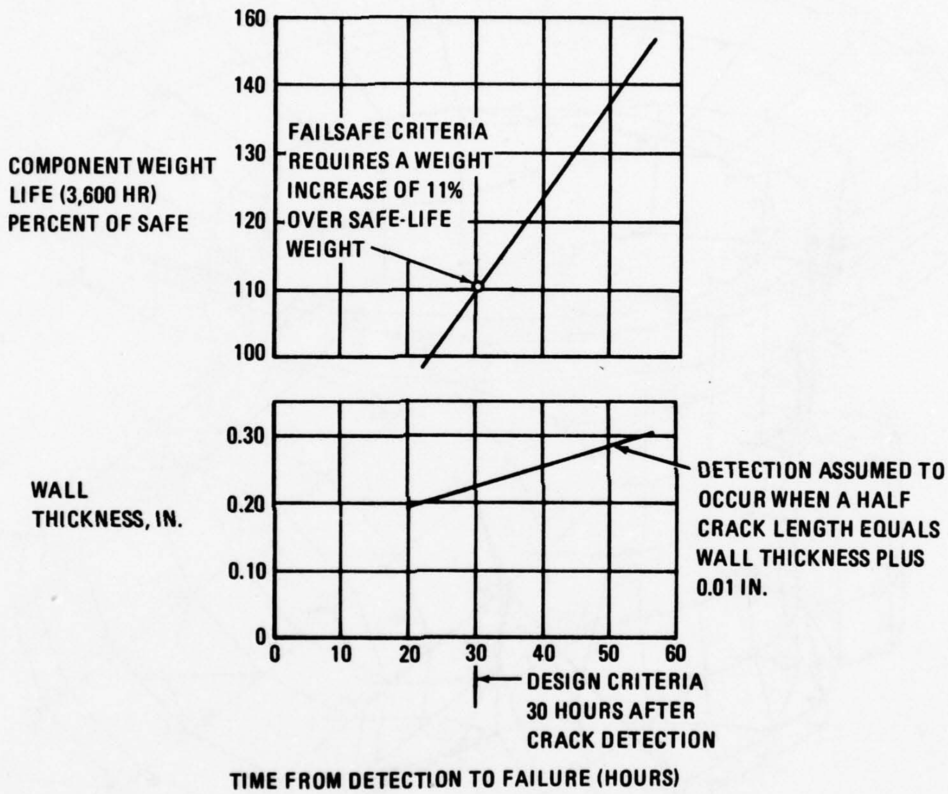

Figure 81. Weight Study for Safe Crack Growth – HLH Pitch Arm

With the above background, it is apparent that application of the NASTRAN finite element model to the stress/fatigue analysis of transmission housings should lead to better understanding of crack propagation and the safe crack growth characteristics of a structure. Previous experience with stress determination at a crack head using finite elements has indicated a need for an extrapolation post processer computer program, since the stress results for quadrilateral or triangular structural elements are assumed to exist at their C.G. Using this extrapolation scheme has led to good correlation with analytical results for circular, elliptical and V-notch cracks. The ability to include temperature in the analysis is also useful. A simulated .1 inch longitudinal crack was introduced into the NASTRAN model at a highly stressed area under an ultimate loading. The crack could have resulted from manufacturing imperfection, fatigue, or missile impact. In general, local stresses increased reflecting load redistribution by the crack, and the crack surfaces separated radially by .032 inch. A summary comparison of stresses before and after introduction of the crack is given in Figure 82.

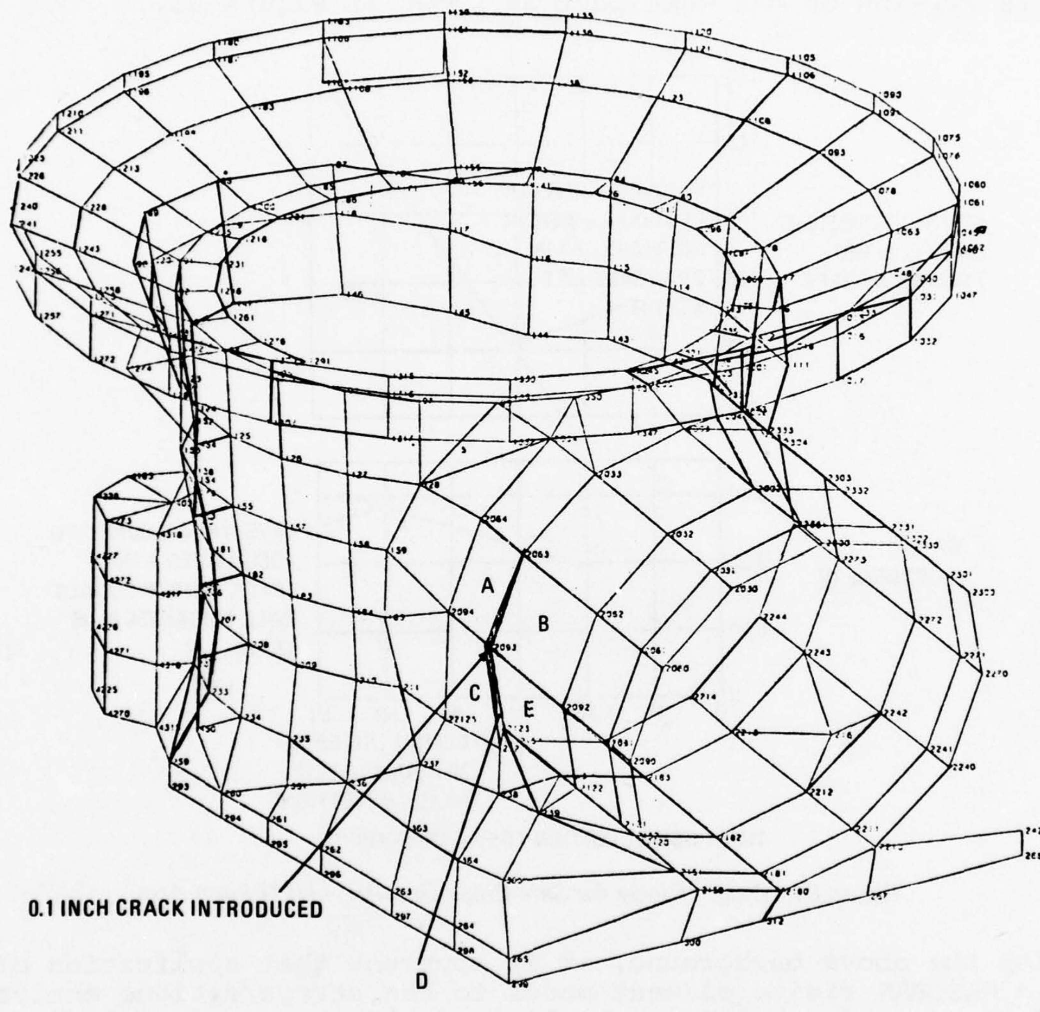

ELEMENT	THICKNESS (INCHES)	MAX σ (PSI)	MIN σ (PSI)	MAX σ (PSI)	MIN σ (PSI)
A	0.72	21600	− 8200	25040	− 25571
B	0.31	17705	− 32076	13702	14000
C	0.10	4288	− 4288	− 3253	− 4533
D	0.45	− 6333	− 43606	− 5677	− 25574
E	0.31	15811	− 11911	12921	− 12118
		CRACK		NO CRACK	

Figure 82. Crack Study

Previous fail-safe/safe-life considerations were primarily applied to the fuselage, hub, and rotor blades (References 29 and 30). The criteria should be more specifically defined with respect to transmissions for improved future designs. As applied to helicopter transmissions, safe-life criteria (fatigue failure, crack propagation) should be primarily applied to the cover and retention mountings. Experience has determined that the retention and mounting hardware have a relatively high incidence of fatigue failure for the CH-47C forward transmission (Reference 31). However, with the advent of new composite materials, safe-life criteria should be extended to the transmission case. Since the cover transmits the steady and vibratory hub loads to the aircraft airframe through the retention lugs, a NASTRAN analysis of the cover/ retention lugs yields useful safe-life information. In addition, since the drive system is one of the heaviest components of a helicopter, a post-processor program such as S-83 to calculate the strain density distribution for weight optimization is useful for weight reduction. The strain density/stress analysis of NASTRAN would also indicate the load paths for fail-safe considerations and would improve crack-growth characteristics by tending to equalize the stress distribution.

---

29. Feldt, G. V., and Russell, S. W., FAIL-SAFE/SAFE-LIFE INTERFACE CRITERIA, Technology Incorporated, USAAMRDL TR 75-12, Eustis Directorate, U.S. Army Air Mobility Research and Development Laboratory, Fort Eustis, Virginia, April 1975, AD A009519.

30. Needham, J. F., FAIL-SAFE/SAFE-LIFE INTERFACE CRITERIA, Hughes Helicopters, USAAMRDL TR 74-101, Eustis Directorate, U.S. Army Air Mobility Research and Development Laboratory, Fort Eustis, Virginia, January 1975, AD006131.

31. USAAMRDL TR 75-56B.

CRASHWORTHINESS

Two indices which have been utilized to assess the overall crashworthiness of an aircraft are the levels of acceleration experienced by the occupants and the preservation of the integrity of the occupied cabin areas during a specified crash condition. The former index reflects such characteristics as fuselage design and occupant restraint systems and is not within the scope of the work reported herein. However, the latter index is directly affected by the design of a helicopter drive system. The attachment of large masses such as engines, transmissions, and rotors to the upper fuselage aggravates the collapse of the structure and often results in loss of occupiable volume and crushing injuries or entrapment of occupants.

Helicopter transmissions, due to their location typically being above or adjacent to the crew or passenger cabin areas, pose a direct hazard to occupants during a crash situation and must be designed with inherent retention strength in excess of the ultimate crash load requirements. Several design criteria relative to restraining the transmission from entering occupied areas must be satisfied to insure crashworthiness: retention of the transmission in the airframe, sufficient strength of the airframe support structure to preclude total collapse, and integrity of the transmission structure including retention of the internal components in the housing. The first two criteria necessarily address topics such as strength of attachment points, strength of mounting bolts and dissipation of kinetic energy by the helicopter structure by elastic and plastic energy absorption. The strength of the fuselage structure can be accurately assessed using a NASTRAN model with loads representative of those occurring at the transmission mounting legs placed at the airframe attachment points. The third criterion, structural integrity of the housing itself, is the focus of the work discussed herein. The NASTRAN model of the transmission housing was used. Hub loads and inertia loads were applied to the transmission, these loads were converted to bearing reactions on the housing model, and a NASTRAN static stress analysis was performed. The strength of the transmission supporting legs and the structural integrity of the housing when loads representative of crash conditions are applied were evaluated.

The contractor's current experience with crashworthiness testing has indicated that loads between 40 and 100g should be considered. Assuming a specified initial flight condition for a given helicopter, the velocity at impact can be calculated. Then, after establishing the duration of the crash load impulse based on recent extensive crashworthiness testing, the acceleration and hence the force at impact may be determined.

Utilizing these loads in the NASTRAN inertia relief analysis, the housing displacements and stresses due to crash loads may be calculated. A comparison of stresses with allowables provides an evaluation of the crashworthiness of the housing and its support structure. The strain energy distribution after impact is a source of information for structural improvement for crashworthiness.

A crashworthiness study was conducted for a CH-47C forward pylon using the inertia relief feature of NASTRAN (Rigid Format 2). The weight of the fuselage section was 5882 lb and extended rearward to Station 160. The forward transmission was attached at 4 points (cover legs) and weighed 1081 lb. Above this was a 683-lb hub assembly with three blades attached (1000 lbs). The angle of impact was 10°, and the impact time was $\Delta T = .25$ sec. The initial altitude was 55 feet, giving a deceleration of 7.4 g's. These numbers reflect a recent crash test at Boeing Vertol conducted under Contract DAAJ02-76-C-0015. The inertia relief capability of NASTRAN is linear elastic, whereas a true crashworthy analysis is elastoplastic. However, NASTRAN gives a first-cut solution. The model was completely free and "SUPORT" cards were used to avoid stiffness matrix singularity. Six nonredundant degrees of freedom were constrained. "CONM2" cards were used for the mass distribution. The original model is shown in Figure 83; the model after impact is shown in Figure 84, indicating the nose plowing into the ground but with no resultant transmission housing impacting into the crew area. Figure 85 shows this earth gouging pictorially. Figure 86 illustrates the need for a crashworthiness study of the transmission housing due to its location above the occupied area. The analytical results obtained in this first-cut solution agreed with the test results under Contract DAAJ02-76-C-0015 (Crashworthiness Study) in that the housing remained intact with only the nose collapsing. NASTRAN (Rigid Format 2) was difficult to interpret because the inertia loads of the concentrated masses of the forward pylon were not printed out. In addition, "SPC" cards could have been used instead of "SUPORT" cards since the inertia-impact loads are self-equilibrating. A second interpretation of crashworthiness would be the integrity of the transmissions internal components after impact.

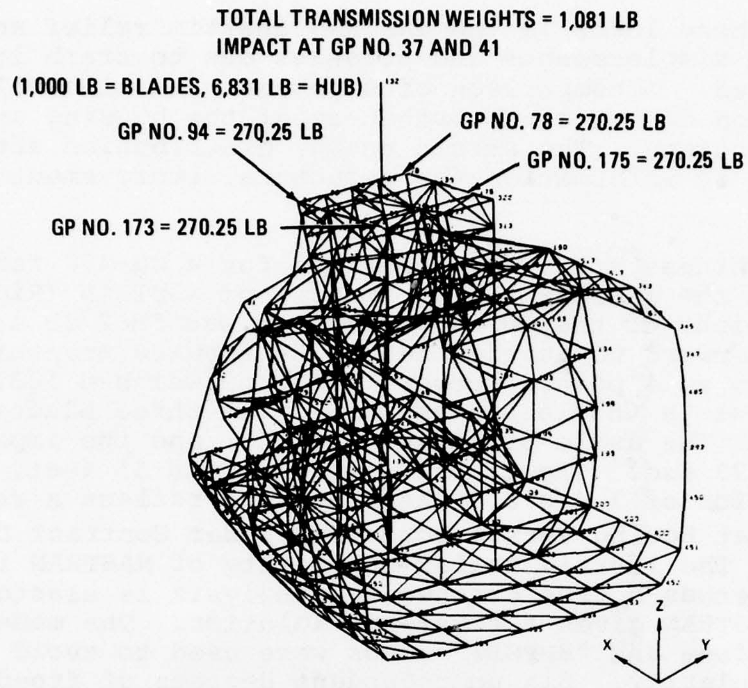

Figure 83. NASTRAN Finite Element Model of CH-47C Forward Pylon Model for Crashworthiness Evaluation of Transmission System

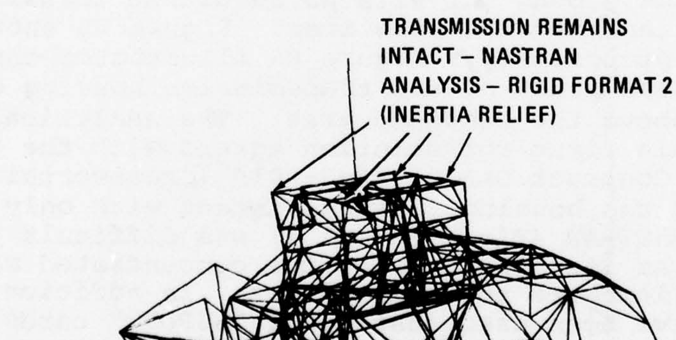

Figure 84. Crashworthiness of CH-47C Forward Transmission as Indicated by NASTRAN "Deformed" Plot

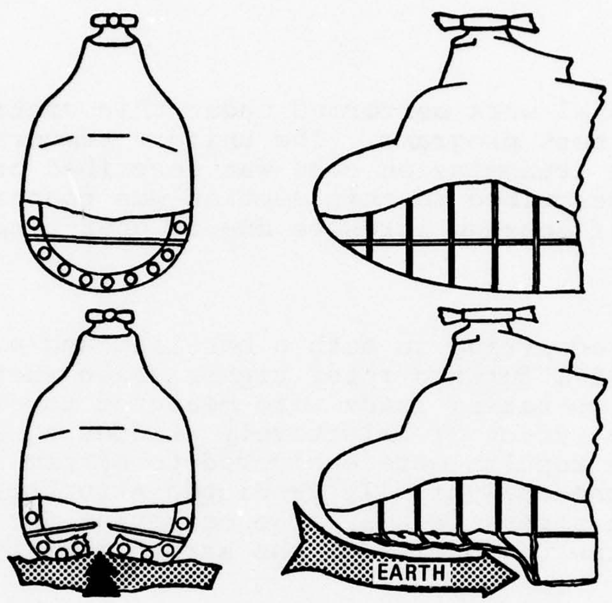

Figure 85. Earth Gouging (Plowing) of Fuselage Under Longitudinal Impact

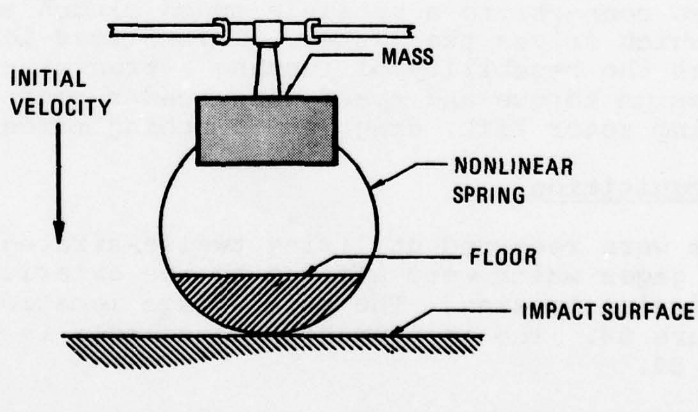

Figure 86. Schematic Diagram of Idealized Aircraft With Transmission Concentrated in Upper Fuselage

EXPERIMENTAL PROGRAM

INTRODUCTION

The experimental work performed under this contract involved two separate test programs. The uniform temperature testing of a baseline transmission case was described previously. The testing described in this section was concerned with the measurement of housing stresses due to operating loads.

OBJECTIVE

The stresses occurring in both a baseline and a modified version of a CH-47C forward rotor transmission when subjected to steady-state operating loads were measured to experimentally determine the effect of selectively stiffening a transmission housing. The results were evaluated to determine the effectiveness of the analytically predicted structural changes for reducing peak stress levels. The criterion for this stiffening process was the uniformity of the strain density distribution.

Test Stand

The transmission was statically and dynamically tested in the Boeing Vertol closed-loop test stand (Figure 87). This stand employs four components to close the torque loop. First, a set of helical gears increases the output or rotor shaft speed to the input or synchronization shaft speed. A torque device connects this gear shaft to a bevel gearbox. The bevel gearbox closes the loop to the input shaft of the transmission and also connects to a variable speed clutch and an electric motor which drives the system. This closed-loop test stand provides the capability of running a transmission over its full design torque and speed range under controlled conditions, including rotor lift, drag, and pitching moments.

Data Acquisition

Strains were recorded utilizing twelve strategically located strain gages which were affixed to the exterior surface of the transmission housing. The strain gage locations are presented in Figure 88. The instrumentation console is shown in Figure 89.

Test Configuration

The transmission used in this program was a CH-47C forward rotor transmission, except as structurally modified per the strain density analysis described below. The baseline transmission was installed in the closed-loop test stand and

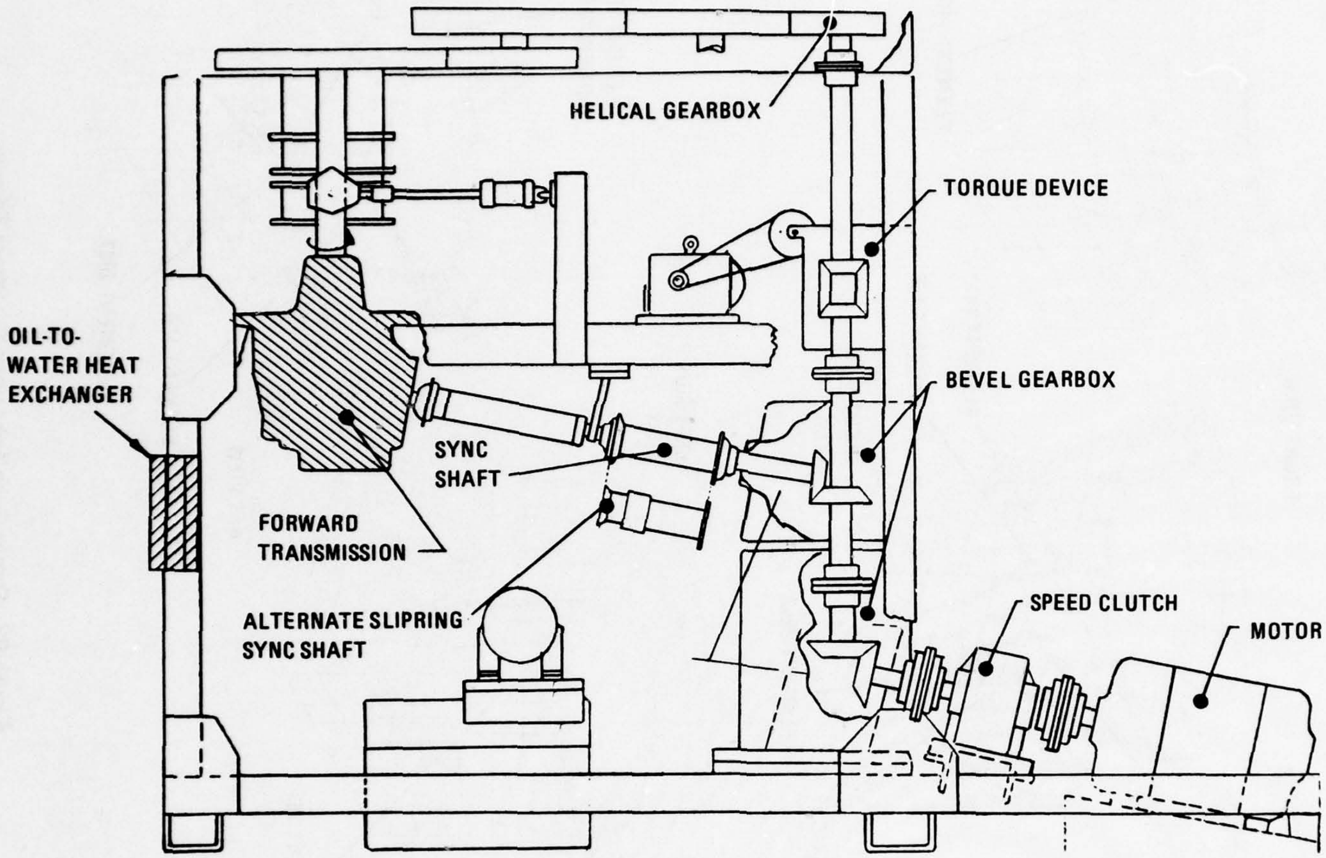

Figure 87. Schematic Diagram of Closed-Loop Test Stand

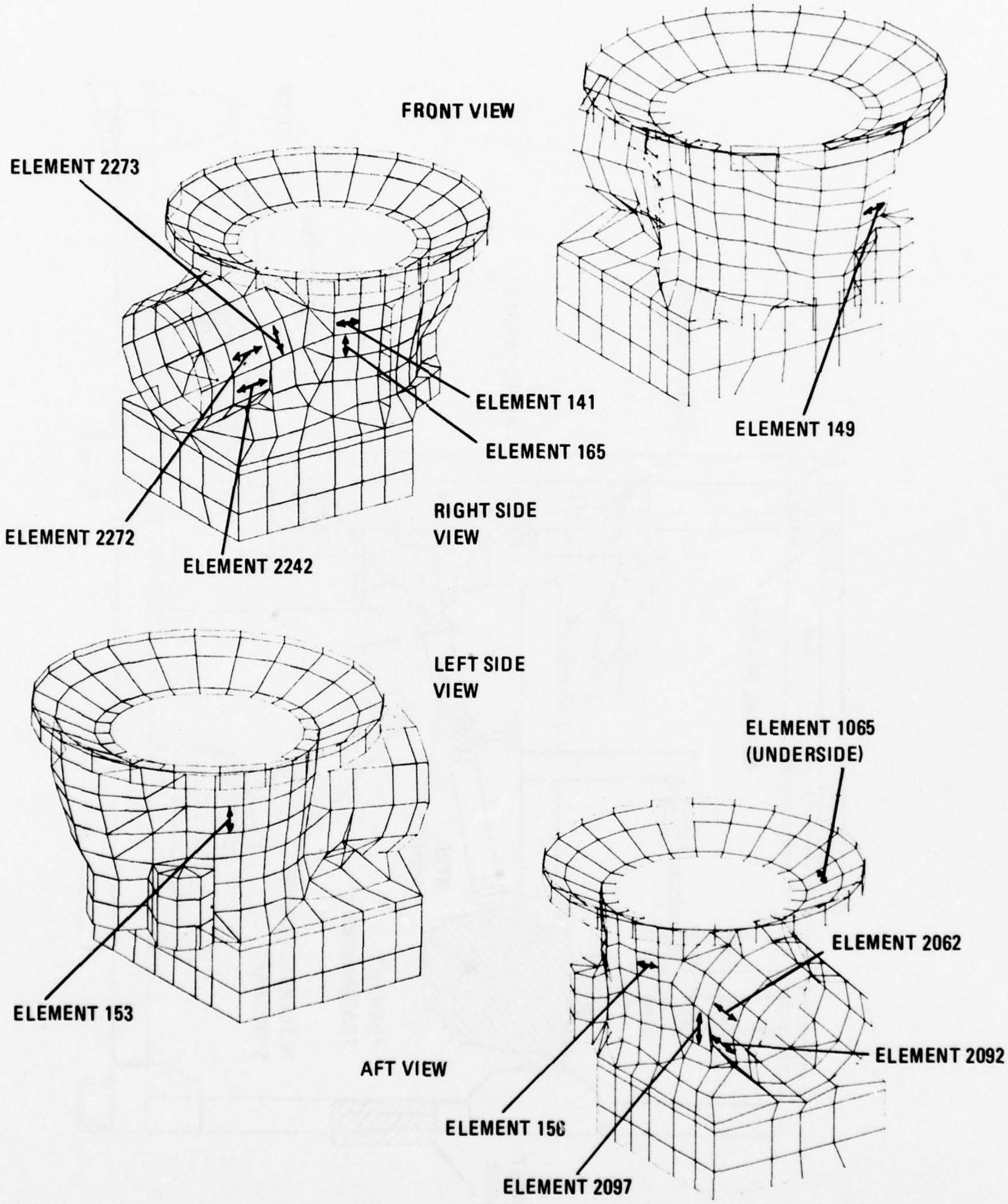

Figure 88. Strain Gage Locations for Stress Testing

Figure 89. Test Stand Instrumentation Console

load representative of steady-state flight loads (lift, drag, pitching and torque) were applied. Strain gage data was recorded for both static (nonoperating) and dynamic conditions with the transmission operating at a synch shaft speed of 7460 rpm. This procedure was then repeated except that the transmission case was selectively stiffened by the addition of contour doubler plates to allow for a more uniform strain density.

Areas for improving the existing housing were determined analytically by the finite element and strain energy methods developed. The optimization of a housing structure should consider both the addition and the removal of material. Nevertheless, no material was removed from the housing for the purpose of the testing presented herein, since at the time of the design process there was no logical criteria for selecting the areas for weight reduction in an existing transmission. A fully stressed design (FSD) capability now exists in NASTRAN Level 16. An FSD analysis, conducted for the housing subsequent to the testing, indicated several areas for reducing wall thickness and hence weight but no additional hardware was built. The casting process dictates the minimum practical thickness allowed. Also, a structure is generally designed using limit loads and requiring that there is no permanent deformation. These two criteria set a limit on the minimum weight. The latter stress analysis would determine a strain density distribution, which, when made uniform would yield a stiffer cover/case.

The criterion for a maximum stiffness structure for a given weight is the uniformity of the strain density distribution (Reference 32). In practice, this strain density distribution, which is a tabular computer listing of the structural element's strain density from highest to lowest, indicates the most efficient areas to add material in order to obtain a more uniform distribution for greater strength. The areas of highest and lowest strain density were determined using the S-83 computer program. The areas in highest strain were determined for all the flight conditions calculated (1g high-speed level flight, ultimate, yawing, recovery from rolling pullout), and the areas of the housing which were modified are shown in Figure 90. Furthermore, the analysis confirmed that both the undesirable structural and vibration/noise characteristics were closely associated with similar areas of high strain energy. Hence, the structural changes recommended herein are compatible with those recommended for vibration/noise reduction studies in Reference 9. The modified transmission housing hardware is shown in Figure 91.

---

32. Howells, R. W., Sciarra, J. J., and Ng, G. S., THERMAL AND STRUCTURAL ANALYSIS OF HELICOPTER TRANSMISSION HOUSINGS USING NASTRAN, NASA TMX-3428, October 1976.

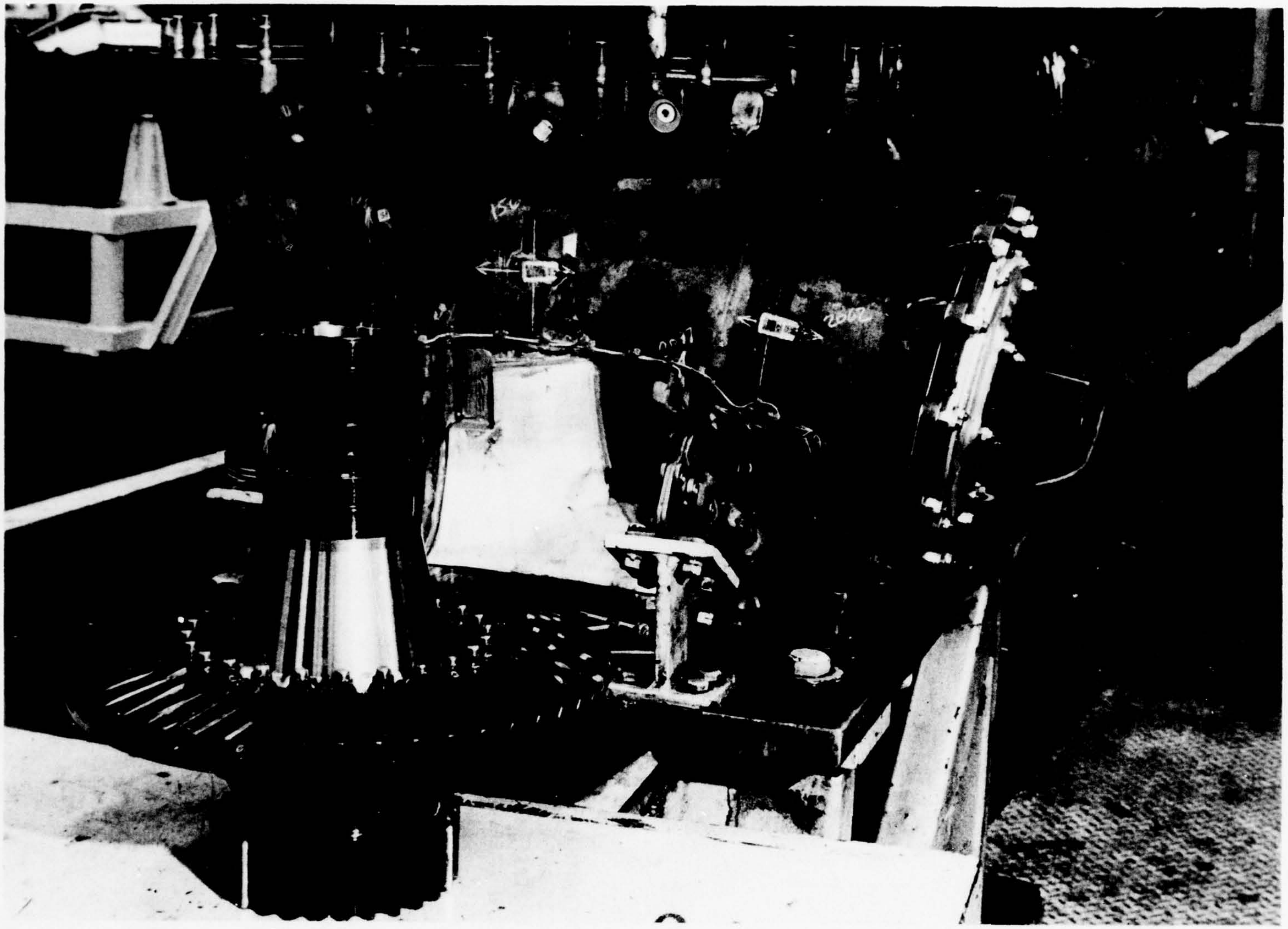

Figure 90. Test Housing Stiffened by Attachment of Doubler Plates

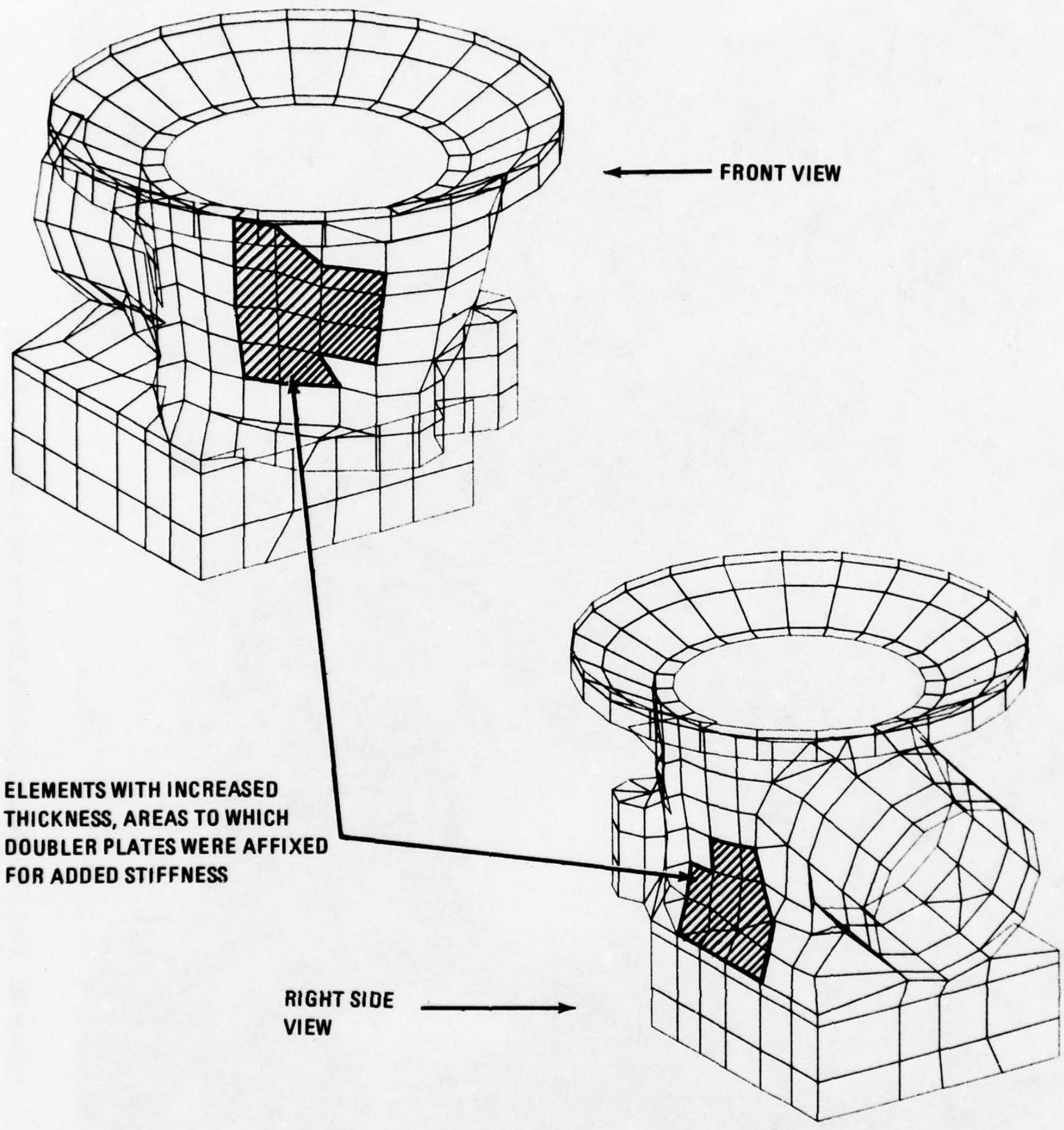

Figure 91. CH-47 Forward Transmission Case With Modifications (Cross Hatched Areas) to Wall Thickness for Selective Stiffening

Test Results and Correlation

The static loading condition simulated rotor shaft loads at 150 knots high-speed level flight (1g) with 25,000 lb lift, 260 lb drag, 84,000 in.-lb pitch (positive noseup) and -720,000 in-lb of rotor shaft torque. The measured stress values for the baseline housing at this static load condition are summarized in Table 15 and compared with the values predicted by the NASTRAN model. Except for element number 156 and the two questionable strain gages noted, the predicted and measured values correlate quite well. The sense of the stress, tension or compression, is indicated correctly and the magnitudes are within a reasonable experimental scatter. The values predicted by NASTRAN for the ultimate load condition are also shown in this table.

A comparison of the magnitudes of the measured static stresses for the baseline housing and the stiffened housing modified according to the strain energy method is shown in Table 16. Of the ten gages that functioned during the test, six showed substantial reduction, three showed essentially no change, and only one increased. The net result was a significant overall decrease in the stress levels. Since the strain energy method utilizes the matrix equivalent of the square of the strains (e.g., analogous to 1/2 $K_X{}^2$ for a simple elastic system), it is appropriate to examine the stress magnitudes.

The baseline and stiffened housings were also tested dynamically at an input pinion speed of 7460 rpm and with the same 1g load condition applied. The dynamic strains/stresses for all ten strain gages were reduced by the addition of the stiffener plates, which were located by strain density principles. Readings were made by taking peak-to-peak readings from an oscilloscope. The stress magnitudes for the baseline and modified housings, which are compared in Table 17, indicate an overall reduction of stress levels.

In addition to the normal experimental error due to equipment tolerances and data recording, the placement of the strain gages was quite critical. The finite element model predicts average stresses at the centroid of each element. Since these stresses can vary substantially across the element, the strain gages were placed as close to the center of each element as possible. Furthermore, the magnitudes of the strains measured were quite small and hence relatively sensitive to small inaccuracies.

TABLE 15. STATIC STRESS SUMMARY - MEASURED AND PREDICTED VALUES FOR BASELINE HOUSING

LOCATION (ELEMENT NO.)	BASELINE HOUSING STRESS (PSI)		
	NASTRAN PREDICTED (1g)	MEASURED (1g)	NASTRAN PREDICTED (ULTIMATE)
141	-157	-214	-449
149	-228	79 Gage Erratic	-667
153	-455	-150	-1297
156	-124	780	-317
165	807	598	2319
1065	127	Gage Lost	371
2062	2095	624	6123
2092	1892	-78 Gage Questionable	5442
2097	1485	1404	4265
2242	146	150	544
2272	41	195	675
2273	568	598	1641

TABLE 16. STATIC STRESS SUMMARY (MEASURED VALUES) FOR BASELINE AND STIFFENED HOUSING

LOCATION (ELEMENT NO.)	1g MEASURED STRESS MAGNITUDE (PSI)		CHANGE
	BASELINE HOUSING	STIFFENED HOUSING	
141	214	215	1
149	79	Gage Lost	
153	150	72	-78
156	780	156	-624
165	598	514	-84
1065	Gage Lost	Gage Lost	
2062	624	150	-474
2092	78	78	0
2097	1404	1125	-279
2242	150	215	65
2272	195	195	0
2273	598	514	-84

Average Change of Stress Magnitude = -156

TABLE 17. DYNAMIC STRESS SUMMARY

LOCATION (ELEMENT NO.)	MEASURED STRESS MAGNITUDE (PSI)		CHANGE
	BASELINE HOUSING	STIFFENED HOUSING	
141	260	208	-52
153	293	260	-33
156	325	260	-65
165	195	130	-65
2062	260	234	-26
2092	260	234	-26
2097	325	260	-65
2242	260	208	-52
2272	325	182	-143
2273	260	156	-104

Average Change of Stress Magnitude = -63

CONCLUSIONS

1. Based on the Thermal/Static/Dynamic Analyses conducted, it is apparent that NASTRAN can be used as an effective tool for transmission analysis and design. In fact, there presently exists no other comprehensive analytical tool. The heat transfer/thermal stress capability of NASTRAN is applicable to lubrication/cooling analysis. The stress/dynamic capability is applicable to analyzing existing configurations and in optimizing new configurations.

2. It is possible to construct an accurate finite element model of a transmission utilizing engineering drawings as evidenced by the plotting and weight generator capabilities of NASTRAN. Essentially the same model can be used to evaluate static, dynamic, and thermal load conditions.

3. The ability of NASTRAN to accurately predict thermal distortions of a transmission housing has been verified by correlation with test data.

4. When analyzing the housing structure, the effect of the internal components (i.e. gears, bearings, shafts) must be considered. It may be necessary to model these components either in detail or in a simplified manner. Furthermore, in some instances such as the thermal growth analysis it may be possible to ignore the internal components.

5. By evaluating the displacements of the housing model (grid points) at the bearing/housing interfaces, the shaft slopes and displacements at the gear mesh can be determined. Although the magnitude of these displacements can exceed .010, further evaluation is needed to establish the precise effect on life and performance.

6. There are numerous theoretical techniques for structural optimization, but practical methods suitable for application to the design process are minimal. The strain energy method and the Fully Stressed Design (FSD) method appear to be the only methods available which are readily useable by a designer.

7. The NASTRAN model predicts stresses which correlate with the experimentally measured stress values.

8. The structural modifications determined from the strain energy method were effective in reducing the overall stress levels. This was confirmed from measured data and analysis.

9. NASTRAN, used in conjunction with other pre- and post-processor programs, has shown that composite materials can be effectively employed, at least in theory, to stiffen transmission housings. Also, the thermal characteristics of a composite housing, which have been the topic of concern for sometime, can be defined.

10. Numerous aspects of the vulnerability/survivability problem can be investigated using finite element modeling. This has been demonstrated for such topics as radar cross-section, loss-of-lubricant emergency operation, fail-safety, crack growth, and crash worthiness.

RECOMMENDATIONS

Based on the results of this effort, it is recommended that:

1. Further study be conducted to establish the precise effect of displacement and misalignment of gears on the life and performance of a helicopter transmission.

2. A further and quite extensive program be conducted to review existing optimization methods, to select the best or develop a new method, and to formulate a practical computer-aided design procedure.

3. Research be concentrated to perfect the manufacturing technology necessary to utilize composite materials, particularly metal matrix materials, for the selective stiffening of helicopter transmission housings.

4. Analyses for the prediction of heat generation at gear meshes and rolling element bearings be refined and extended.

5. Designers be encouraged to apply the finite element methods indicated herein to future helicopter transmissions.

REFERENCES

1. American Gear Manufacturers Association Standard 210.02.

2. George, C., GEAR NOISE SOURCES AND CONTROLS, Detroit Diesel Allison, Division of General Motors Corporation.

3. Lenski, J. W., HLH SWASHPLATE FAILURE ANALYSES, Boeing Vertol Inter-Office Memorandum 8-7462-1-40, dated 10 July 1974.

4. Leibensperger, R. L., WHEN SELECTING A BEARING LOOK BEYOND CATALOG RATINGS, Machine Design, April 1975, Pages 142-147.

5. Everstine, G., BANDIT - A COMPUTER PROGRAM TO RENUMBER NASTRAN GRID POINTS FOR REDUCED BANDWIDTH, Naval Ship Research and Development Center Technical Note AML-6-70, February 1970.

6. Sciarra, J., USE OF THE FINITE ELEMENT DAMPED FORCED RESPONSE STRAIN ENERGY DISTRIBUTION FOR VIBRATION REDUCTION, U.S. Army Research Office - Durham, Final Report Contract DAH-C04-71-C-0048, July 1974.

7. Hartman, R. M., and Badgley, R., MODEL 301 HLH/ATC TRANSMISSION NOISE REDUCTION PROGRAM, Boeing Vertol Company, USAAMRDL TR 74-58, Eustis Directorate, U. S. Army Air Mobility R&D Laboratory, Fort Eustis, Virginia, May 1974, AD 784132.

8. Hartman, R. M., A DYNAMICS APPROACH TO HELICOPTER TRANSMISSION NOISE REDUCTION AND IMPROVED RELIABILITY, Paper Presented at the 29th Annual National Forum of the American Helicopter Society, Washington, D.C., May 1973, Preprint No. 772.

9. Sciarra, J. J., Howells, R. W., and Lemanski, A. J., HELICOPTER TRANSMISSION VIBRATION AND NOISE REDUCTION PROGRAM, USAAMRDL Contract DAAJ02-74-C-0040, Interim Report, October 1975.

10. Howells, R. W., and Sciarra, J. J., FINITE ELEMENT ANALYSIS USING NASTRAN APPLIED TO TRANSMISSION VIBRATION/NOISE REDUCTION, NASA TMX-3278, September 1975.

11. Battles, Roy A., DYNAMIC TESTING OF A COMPOSITE MATERIAL HELICOPTER TRANSMISSION HOUSING, Bell Helicopter Company, USAAMRDL TR 75-47, Eustis Directorate, U.S. Army Air Mobility R&D Laboratory, Fort Eustis, Virginia, September 1975, AD A015521.

12. Tocci, R. C., Lemanski, A. J., and Ayoub, N. J., TRANSMISSION THERMAL MAPPING, Boeing Vertol Company, USAAMRDL TR 73-24, Eustis Directorate, U.S. Army Air Mobility Research and Development Laboratory, Fort Eustis, Virginia, May 1973, AD 767875.

13. NASTRAN User's Manual Level 15, June 1972.

14. Buckingham, E., ANALYTICAL MECHANICS OF GEARS.

15. Harris, T., ROLLING BEARING ANALYSES.

16. Rumbarger, J., and Filetti, E., HIGH TEMPERATURE HELICOPTER MECHANICAL TRANSMISSION TECHNOLOGY, Franklin Institute Research Laboratories, Philadelphia, Pa., FIRL Final Report F-C3229, December 1971.

17. Buckingham and Ryffel, DESIGN OF WORM AND SPIRAL GEARS.

18. Faires, V., DESIGN OF MACHINE ELEMENTS, The MacMillan Company, New York, 4th Edition, 1965.

19. Eckert and Drake, HEAT AND MASS TRANSFER, McGraw-Hill, 1959.

20. NASTRAN User's Manual Level 15.5, 1976.

21. Thornton, E., and Wieting, A., COMPARISON OF NASTRAN AND MITAS THERMAL ANALYSIS OF A CONVECTIVELY COOLED STRUCTURE, 1975 Fourth NASTRAN User's Experiences.

22. Patton, H., MODEL YHC-1B FORWARD TRANSMISSION DEFLECTION TEST, Gleason Works Test Report #1842, 1962.

23. Venkayya, Knot, and Reddy, ENERGY DISTRIBUTION IN AN OPTIMUM STRUCTURAL DESIGN, AFFDL-TR-68-156.

24. Reed, D. L., POINT STRESS LAMINATE ANALYSIS, Document FZM-5494, AFML, Advanced Composite Division, WPAFB, Ohio, April 1970.

25. Dobyns, A., COMPUTER PROGRAM FOR ANALYSIS AND OPTIMIZATION COMPOSITES, Users Document, October 1976.

26. Tsai, S. W., Adams, D. F., and Doner, D. R., ANALYSIS OF COMPOSITE STRUCTURES, NASA Report CR-620, November 1966.

27. Ashton, J. E., Halpin, J. C., Petit, P. H., PRIMER ON COMPOSITE MATERIALS: ANALYSIS, Technomic Publishing Company, 1969.

28. Melosh, R. J., Johnson, J. R., and Luik, R., STRUCTURAL SURVIVABILITY ANALYSIS, Philco Ford and AFFDL, Paper Based on Contract AF33(615)-5039.

29. Feldt, G.V., and Russell, S. W., FAILSAFE/SAFE-LIFE INTERFACE CRITERIA, Technology Incorporated, USAAMRDL TR 75-12, Eustis Directorate, U.S. Army Air Mobility R&D Laboratory, Fort Eustis, Virginia, April 1975, AD A009519.

30. Needham, J.F., FAILSAFE/SAFE-LIFE INTERFACE CRITERIA, Hughes Helicopters, USAAMRDL TR 74-101, Eustis Directorate, U.S. Army Air Mobility R&D Laboratory, Fort Eustis, Virginia, April 1975, AD A009519.

31. Mack, J.C., and Rumberger, W., ADVANDED HELICOPTER STRUCTURAL DESIGN INVESTIGATION - Volume II - Design Application Study for Free Planet Transmissions, Boeing Vertol Co., USAAMRDL-TR-75-56B, Eustis Directorate, U.S. Army Air Mobility Research and Development Laboratory, Fort Eustis, Virginia, March 1976, AD A024478.

32. Howells, R. W., Sciarra, J. J., and Ng, G. S., THERMAL AND STRUCTURAL ANALYSIS OF HELICOPTER TRANSMISSION HOUSING USING NASTRAN, NASA TMX-3428, October 1976.

33. AGARD Lecture Series No. 70 on Structural Optimization, AGARD-LS-70, October 1974.

34. Dwyer, W., Rosenbaum, J., Shulman, M. and Pardo, H., FULLY-STRESSED DESIGN OF AIRFRAME REDUNDANT STRUCTURES, AFFDL-TR 68-150, October 1968.

35. Dwyer, J. W., Emerton, R. K. and Ojalvo, I. V., AN AUTOMATED PROCEDURE FOR THE OPTIMIZATION OF PRACTICAL AEROSPACE STRUCTURES (Volume I - Theoretical Development and User's Information), AFFDL-TR 70-118, March 1971, Air Force Flight Dynamics Lab, Wright-Patterson AFB, Ohio.

36. Schmit, L. A., STRUCTURAL DESIGN BY SYSTEMATIC SYNTHESIS, Proceedings of the Second Conference on Electronic Computation, ASCE, Volume 89, August 1963.

37. Sciarra, J. J., USE OF THE FINITE ELEMENT DAMPED FORCED RESPONSE STRAIN ENERGY DISTRIBUTION FOR VIBRATION REDUCTION, presented at ARO-D Military Theme Review, The Helicopter and V/STOL Aircraft Research Conference, U.S. Army Research Office, NASA-Ames Research Center, Moffett Field, California, AD-751809, September 1972.

38. Venkayya, V. B., Khot, N. S., and Reddy, V. S., OPTIMIZATION OF STRUCTURES BASED ON THE STUDY OF STRAIN ENERGY DISTRIBUTION, AFFDL-TR 68-150, 1968, Pages 111-153.

BIBLIOGRAPHY

1. Gellatly, R. A., and Laszlo, B., OPTIMAL STRUCTURAL DESIGN, AFFDL-TR 70-165, April 1971.

2. Prager, W., and Marcal, P. V., OPTIMALITY CRITERIA IN STRUCTURAL DESIGN, AFFDL-TR 70-166, May 1971.

3. Sciarra, J. J., APPLICATION OF A COMBINED DIRECT STIFFNESS AND MOBILITY METHOD TO VIBRATION ABSORBER STUDIES, ASME/MDD Vibrations Conference, Paper 67-VlBR-65, March 1967.

4. Sciarra, J. J., HELICOPTER FUSELAGE VIBRATION PREDICTION BY STIFFNESS/MOBILITY METHODS, 37th Shock and Vibration Symposium, Orlando, Florida, October 1967.

5. Sciarra, J. J., DYNAMIC UNIFIED STRUCTURAL ANALYSIS METHOD USING STIFFNESS MATRICES, AIAA/ASME 7th Structures and Materials Conference, April 1966.

6. Turner, M. J., DESIGN OF MINIMUM MASS STRUCTURES WITH SPECIFIED NATURAL FREQUENCIES, AIAA Journal, Volume 5, Number 3, March 1967, Pages 406-412.

7. Venkayya, V. B., Khot, N. S., Tischler, V. A., and Taylor, R. F., DESIGN OF OPTIMUM STRUCTURES FOR DYNAMIC LOADS, Third Conference on Matrix Methods in Structural Mechanics, Wright Patterson Air Force Base, Ohio, October 1971.

8. Rubin, C. P., DYNAMIC OPTIMIZATION OF COMPLEX STRUCTURES, AIAA Dynamics and Aeroelasticity Specialists Conference, New Orleans, La., April 1969.

9. Zarghamee, M. S., OPTIMUM FREQUENCY OF STRUCTURES, AIAA Journal, Volume 6, Number 4, April 1968, Pages 749,750.

10. Fox, R. L. and Kapoor, M.P., STRUCTURAL OPTIMIZATION IN THE DYNAMICS RESPONSE REGIME: A COMPUTATIONAL APPROACH, AIAA Dynamics and Aeroelasticity Specialists Conference, New Orleans, La., April 1969.

11. McCart, B. R., Haug, E. J. and Streeter, T. D., OPTIMAL DESIGN OF STRUCTURES WITH CONSTRAINTS ON NATURAL FREQUENCY, AIAA, Volume 8, Number 6, June 1970.

APPENDIX A

REVIEW OF OPTIMIZATION TECHNIQUES

The goal of the helicopter designer has always been a structure that meets all operational requirements and also is of minimum weight. Loads are first determined for the critical conditions (e.g., maneuver, gust, landing, etc.) and the structure is sized for strength based upon these loads. Modification of this original "first cut" structure will generally be required, and thus an iterative procedure is involved. A key step in this procedure is the optimization of the major structural components for strength, based upon the loads applied during a given cycle.

The classical approach to structural optimization has been engineering judgement. Since the development of finite element techniques has made possible the analysis of complex structures, the enormous number of structural elements and side constraints make the number of possibilities for structural changes large. The design trend now evolving is for automated sizing methods which will optimize the complex structures for some specified constraint criteria (e.g., weight, stiffness, displacements, and natural frequency). Typically the general layout, structural component construction, and materials are assumed to be already selected; the optimum member sizes are to be determined. Other factors such as weight penalty, location, and ease of manufacture must also be considered.

There are many schemes which have been put forth for both static and dynamic optimization. These encompass both direct and indirect (optimality criteria) methods. AGARD LS-70 (Reference 33) reviews several of these methods, including

1. Linear programming
2. Nonlinear programming (direct search)
3. Geometric programming
4. Sieve-search
5. Inscribed hyperspheres
6. Fully stressed design
7. Energy methods

---

33. AGARD Lecture Series No. 70 on Structural Optimization, AGARD-LS-70, October 1974.

In addition, several other publications covering structural optimization (see the List of References) were reviewed with the objective of assessing the applicability of these methods and the feasibility of integrating them into the analytical technique for this program. Generally, the theoretical development of these optimization techniques is much further advanced than their practical application to the design of large, complex structures. Sample applications of these methods are typically limited to simple structures such as trusses since the methods become unwieldy for structures representative of those found in practice. As a consequence of the abundance of analytical techniques and lack of a solid practical design method, the need for a separate and quite extensive program is indicated which would have the objectives of reviewing existing optimization methods, selecting the best or developing a new method, and formulating a practical computer-aided design procedure based on the method selected.

The purpose herein is not to develop new methods of structural optimization but rather to select a method from those currently available and apply it. No conclusive evidence is available to show that one method of optimization is clearly superior. However, it is currently believed that while mathematical programming methods are suitable for detailed component optimization they are not practical for the overall optimization of large, complex structures, where optimality methods can be applied more efficiently. Two of the many existing optimality methods, strain energy density (SED) and fully stressed design (FSD), appear to be at least as good as the others and have been applied in practice to the design of some relatively large structures. These two methods have been selected for consideration in this program.

Fully Stressed Design (FSD)

NOTE: Selected portions of this discussion have been taken from NASTRAN documentation.

The Fully Stressed Design (FSD) technique, using the stress-ratio algorithm to drive the design toward a fully stressed state, is probably the most popular resizing method for strength optimization (Reference 34). NASTRAN Level 16 includes a method of design optimization for linear static analysis (Rigid Format 1) based on this relatively simple fully stressed design strategy. The traditional FSD iterative procedure is based upon the intuitive belief that a given structural configuration, subject to stress constraints only, is of minimum weight when the stresses in all the elements are at prescribed limits under at least one design loading

---

34. Dwyer, W., Rosenbaum, J., Shulman, M. and Pardo, H., FULLY-STRESSED DESIGN OF AIRFRAME REDUNDANT STRUCTURES, AFFDL-TR 68-150, October 1968.

condition (Reference 35). According to this concept, the cross-sectional properties of each structural element are resized independently at each design iteration to produce a limit stress (zero margin of safety) somewhere within the element -- assuming that in each iterative cycle the internal load distribution is unaffected by the changes in its cross-sectional properties. This assumption is strictly true only for statically determinate structures. This was demonstrated by Schmit (Reference 36) who found some optimum designs which were also fully stressed. Most practical structures, including a transmission housing/ring/cover/internal components assembly, are redundant.

For indeterminate structures of low redundancy, the above assumption is not badly in error, and a few repetitions of the algorithm will produce a stress distribution throughout the structure which has very nearly a zero margin of safety in every element (i.e., a "fully stressed design"). The procedure will converge more slowly (if at all) in structures of high redundancy, and modifications of the basic strategy may be required to achieve convergence. Furthermore, there is no assurance that the fully stressed design of a highly redundant structure will be an optimum design in any meaningful sense. It is relatively easy to construct examples in which the procedure converges to a "pessimum" design. Consider, for example, the simple case of two parallel rods that are rigidly connected together at their ends and which differ only in their allowable stresses. Since in this case the stresses in the two rods are equal regardless of their areas, the algorithm will increase the area of the weaker rod at the expense of the stronger, and in the limit only the weaker rod will remain.

Practical modifications such as minimum element size requirements are introduced into the basic iterative resizing procedure. Additional complexities associated with members carrying combined bending and membrane loads and biaxial stress states require special attention. When there are no minimum element size requirements to be satisfied, the nonuniqueness of fully stressed designs is most evident since there are at least as many FSD's as there are combinations of statically determinate member formations capable of supporting the specified loads. This raises some doubt as to the convergence of

---

35. Dwyer, J. W., Emerton, R. K. and Ojalvo, I. V., AN AUTOMATED PROCEDURE FOR THE OPTIMIZATION OF PRACTICAL AEROSPACE STRUCTURES (Volume I - Theoretical Development and User's Information), AFFDL-TR 70-118, March 1971, Air Force Flight Dynamics Lab, Wright-Patterson AFB, Ohio.

36. Schmit, L. A., STRUCTURAL DESIGN BY SYSTEMATIC SYNTHESIS, Proceedings of the Second Conference on Electronic Computation, ASCE, Volume 89, August 1963.

related synthesis methods. Although attempts have been made to develop general convergence criteria, no definitive statements concerning the failure of convergence to a single design by FSD based iterative methods can be made.

From the above discussion it is seen that a fully stressed design algorithm cannot be used uncritically. Nevertheless, FSD is very attractive because of its basic simplicity and it will produce excellent designs in many practical cases. FSD based procedures have delivered practical and efficient aircraft structural designs. Furthermore, in many instances where theoretical optimums were computed, it was found that they were also fully stressed. The relative simplicity of the application of FSD techniques also accounts for their further development and use.

In a sample case for a three-spar, five-bay, swept box beam shown in Reference 34, convergence is rapid for two types of FSD design: an average stress method and a nodal stress method. Results for both types of analysis were similar. The weights of the two structures change very little after the initial resizing, as indicated in the following table.

	NODAL STRESS (lb)	AVERAGE STRESS (lb)
Start	179.5	179.5
1 Cycle	119.9	118.9
3 Cycles	119.5	118.5
20 Cycles	119.2	119

Three load conditions were used. For an allowable stress, it was required that the Henky-Von Mises effective stress

$$\sigma_e = (\sigma_X^2 - \sigma_X \sigma_X + \sigma_Y^2 + 3\tau_{XY})^{1/2}$$

be less than 60,000 psi. The structure and loadings are shown in Figures A-1 and A-2.

For each of the two fully stressed designs the skin thicknesses were initially set at a uniform 0.16 in. Twenty redesign cycles were run in each case, and the resulting cover gages are plotted in Figure A-3.

A fully stressed design may not always be the lightest possible structure satisfying the strength and minimum gage constraints. Work is being done in this area using true optimization procedures (i.e., those which focus directly upon the weight of the structure and attempt to minimize it subject to the aforementioned constraints). Currently, the more promising approaches include the penalty function and the gradient search techniques. To date, however, those fully stressed

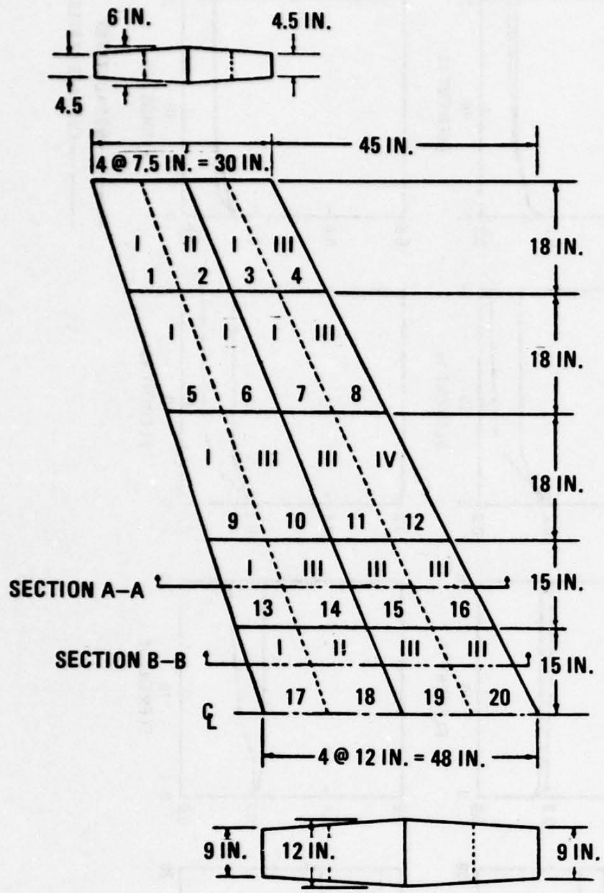

Figure A–1. Example Structure Geometry

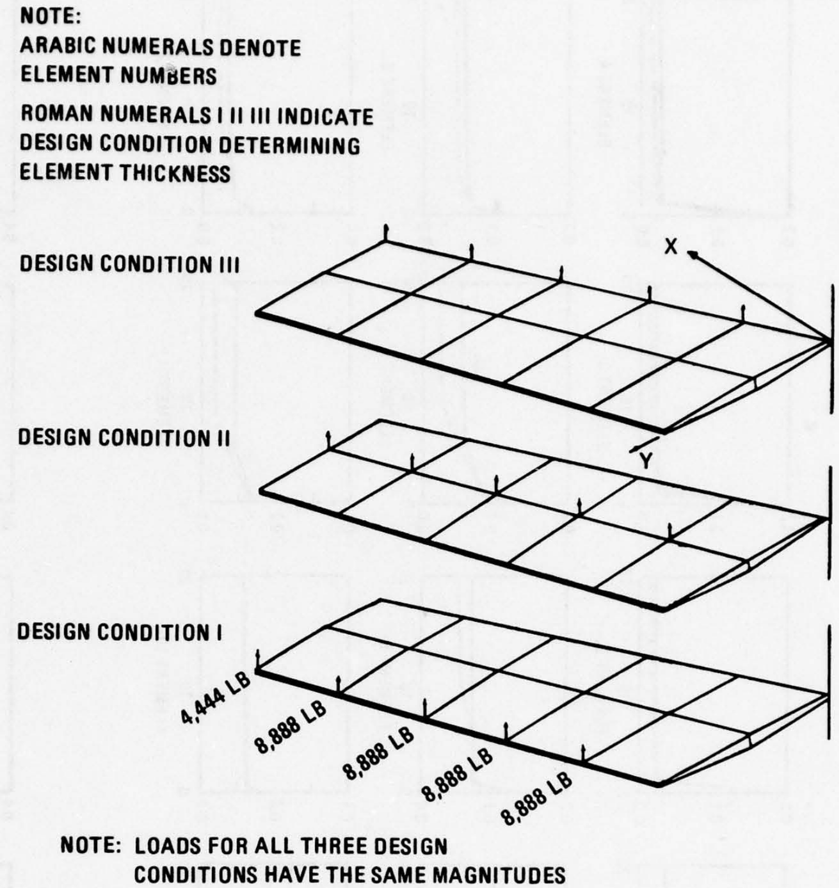

Figure A–2. Example Structure Applied Loads

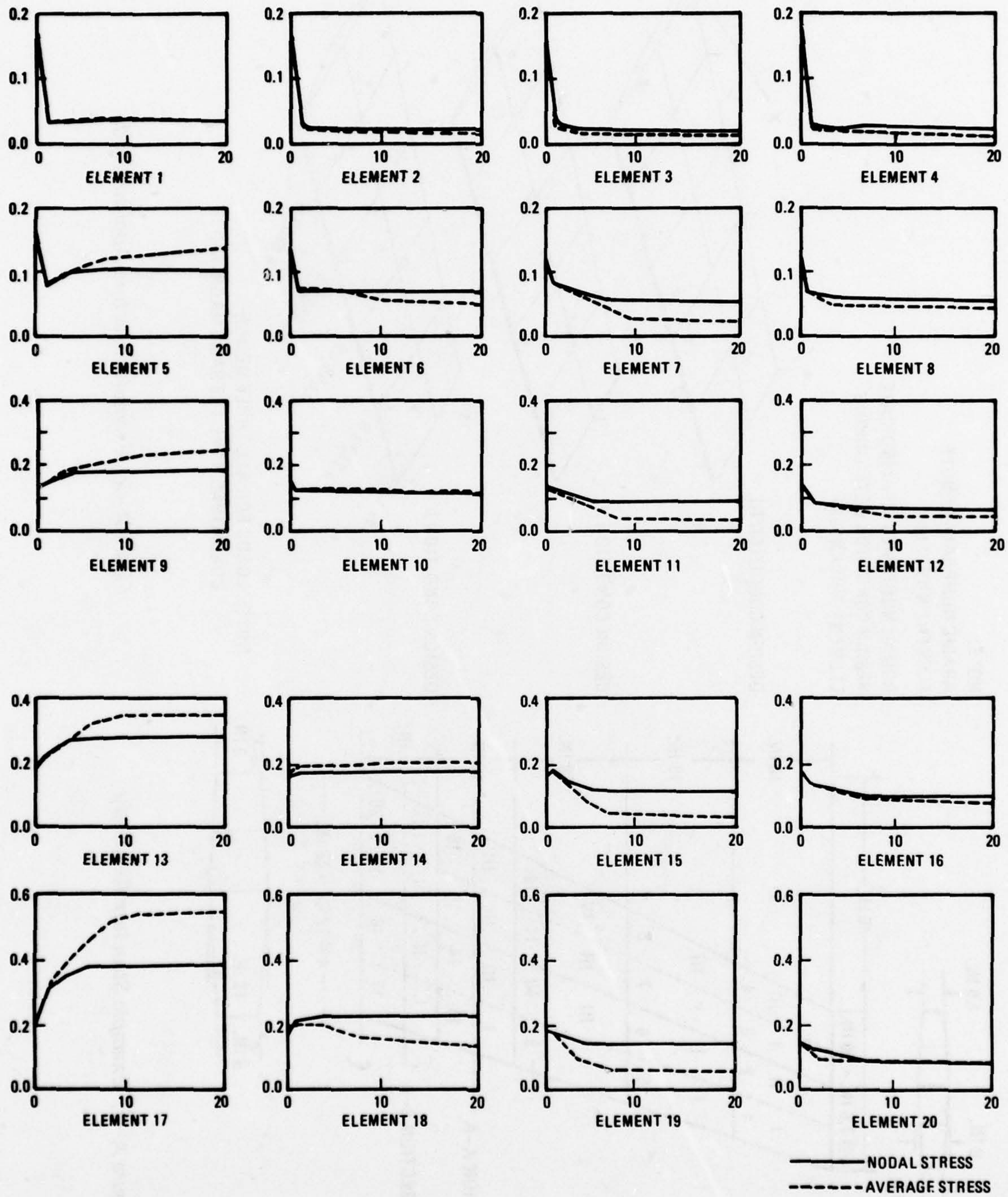

Figure A–3. Element Thickness (Inches) as a Function of the Number of Cycles designs which have been shown to be nonoptimum have fallen into a very restricted class, and even for this group they have been fairly close to optimum. In view of the much greater computer time required for the penalty function and the gradient search techniques, the FSD approach is considered to be an acceptable practical compromise for the present.

The physical quantities involved in the NASTRAN FSD design algorithm are properties, stresses and stress limits. The properties may include thicknesses, cross-sectional areas or moments of inertia. Most NASTRAN elements have several independent properties. They also have several types of stresses and several places where stresses can be evaluated. The stress limits include those for tension, compression, and shear. As an example, the design iteration algorithm of the simple case of an element with one property is presented:

Let

$$\alpha = \mathrm{Max}\left|\frac{\sigma}{\sigma_l}\right| , \qquad (1)$$

where σ = stress, σ_l = stress limit, and where the search for a maximum value is extended over all user-identified stress components and locations and also over all designated loading cases. The new property for the element is evaluated from the old property by the formula

$$A_{new} = A_{old}\left[\frac{\alpha}{\alpha + (1-\alpha)\gamma}\right] , \qquad (2)$$

where γ is a parameter selected by the user. For γ = 1 (the default value), Equation 2 becomes

$$A_{new} = \alpha\, A_{old} \qquad (3)$$

If the product σA were invariant, Equation 3 would give

$$\sigma_{new} = \frac{A_{old}}{A_{new}}\sigma_{old} = \frac{1}{\alpha}\sigma_{old} \qquad (4)$$

so that the value of σ_{new} would just be equal to the limit stress in this special case.

For $\gamma = 0$, it is seen that $A_{new} = A_{old}$, and for values intermediate between zero and one the property is changed by less than a factor of α. Thus γ is a parameter which moderates the property changes at each iteration and may be used to improve the convergence of the algorithm.

For NASTRAN elements with more than one cross-sectional property, all of the properties are changed according to a fixed rule. For example, in the case of the BAR, the moments of inertia are changed in direct proportion to the change in the area. This is equivalent to the assumption that each BAR has a thin-walled cross-section whose thickness is being changed uniformly. The procedures for elements with more than one cross-sectional property cannot be used for the detailed design of individual elements. The incorporation of more elaborate procedures in NASTRAN has been foregone due to the inherent limitations of the fully stressed design algorithm. Indeed, it is not clear that any fully automated general purpose design procedure can successfully cope with the simultaneous requirements of overall and detailed design.

Strain Energy Density

Strain energy techniques have been applied mainly to the dynamic optimization of structures by shifting eigenvalues (natural frequencies) away from exciting frequencies. The objective for an aircraft in particular is a maximum eigenvalue shift for a minimum weight change. The mode shape is used to find the strain energy content of the components of the structure. It can be shown analytically that a complex structure can most efficiently be designed dynamically by ensuring that the modal density differential is uniform throughout the structure. The density differential of a structural element is the difference between the strain density and the kinetic energy per unit volume (kinetic density). In most cases, the strain density may be used as an approximation of the density differential since the kinetic density is relatively small. This objective may also be stated alternatively as: (1) Find the least weight structure with the largest, lowest natural frequency, or (2) Find the least weight structure for a specified natural frequency.

A method for optimizing a structure for a given dynamic loading has been described by Sciarra (Reference 37). This method has been applied to a medium size helicopter (Boeing Vertol Model 347) in high-speed level flight. The results are shown in Figure A-4. The excitations of the fuselage are the n per rev hub loads which are approximately 10% of the gross weight. It is seen that the heights of the sticks that are representative of the vibratory response levels are reduced after proper optimization. Figure A-5 shows that the second natural frequency (73.4) has been moved away from the exciting frequency (79.5). These results are for the forward pylon only. This type of experience is directly applicable to the design of an optimum transmission housing.

37. Sciarra, J. J., USE OF THE FINITE ELEMENT DAMPED FORCE RESPONSE STRAIN ENERGY DISTRIBUTION FOR VIBRATION REDUCTION, presented at ARO-D Military Theme Review, The Helicopter and V/STOL Aircraft Research Conference, U.S. Army Research Office, NASA-Ames Research Center, Moffett Field, California, AD-751809, September 1972.

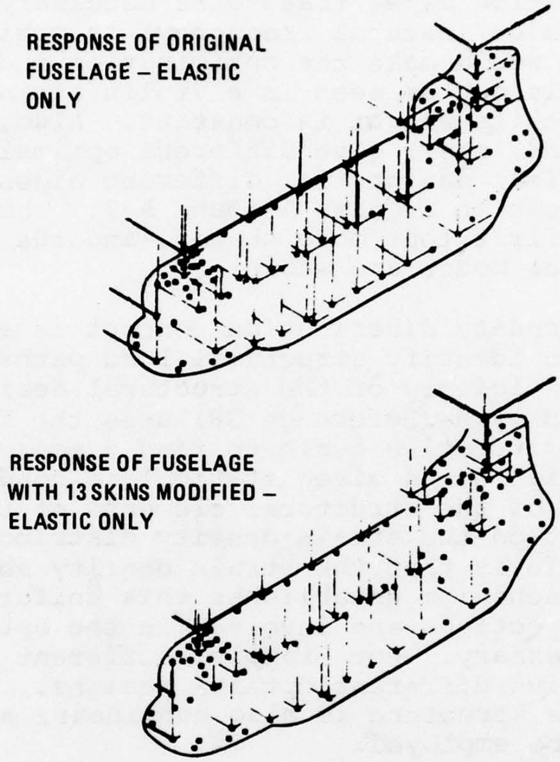

Figure A–4. Vibration Reduction Through Structural Modification, Energy Method. Elastic Modes Only

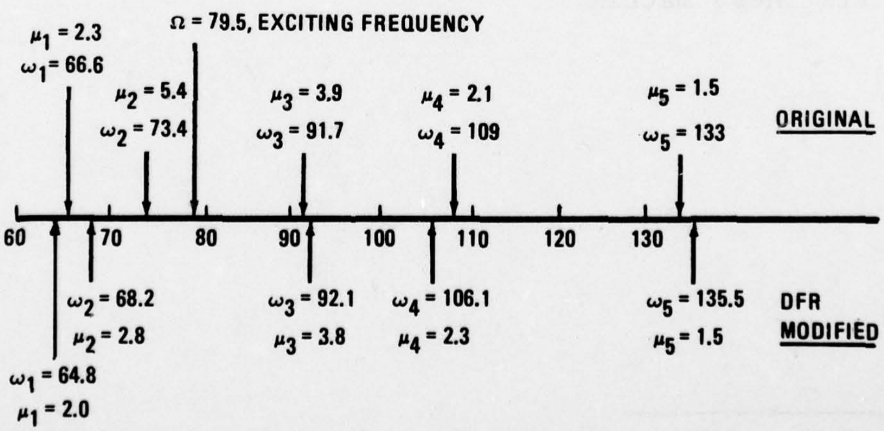

Figure A–5. Forward Pylon Spectrum – Original and DFR Modified

The dependency of the static strain energy distribution on the loading condition makes trade-offs necessary. However, if the first eigenvalue (natural frequency) is maximized for a minimum weight, this would make the optimization independent of the loading. This can be seen in a violin string as its tension is increased yet its weight is constant. Also, different eigenvalues (first, second, etc.) give different optimal designs. As an example, optimal designs for different eigenvalues of the portal frame are shown in Figures A-6 and A-7. The finite element models, the first four mode shapes, and the optimal designs for the first four modes are shown.

The strain density distribution concept is also utilized statically to identify structural load paths and to evaluate the stress efficiency of the structural design (stiffness/weight). Venkayya (Reference 38) uses the finite element method in an iterative cycle to find a minimum weight, maximum strength design for a given static load condition of a structure. The resizing of the structural elements of the complex model is contingent on the strain density distribution. The optimality principle is that the strain density should be uniform. A resizing mechanism establishes this uniformity. Since competing objectives are involved in the optimization, trade-offs are necessary. For example, different static load conditions give different optimal designs. The optimization analysis of a structure is also nonlinear, and an iterative loop should be employed.

The beauty of the strain energy method is that strain energy is easily obtained using finite elements. If the displacements and rotations of a structural element's nodes are obtained and called $\{X\}$, a column matrix, then $1/2\ \{X\}^T\ [K]\ \{X\}$ is the strain energy of the particular structural element where $\{K\}$ is the stiffness matrix.

---

38. Venkayya, V. B., Khot, N.S., and Reddy, V. S., OPTIMIZATION OF STRUCTURES BASED ON THE STUDY OF STRAIN ENERGY DISTRIBUTION, AFFDL-TR 68-]50, 1968, Pages 111-153.

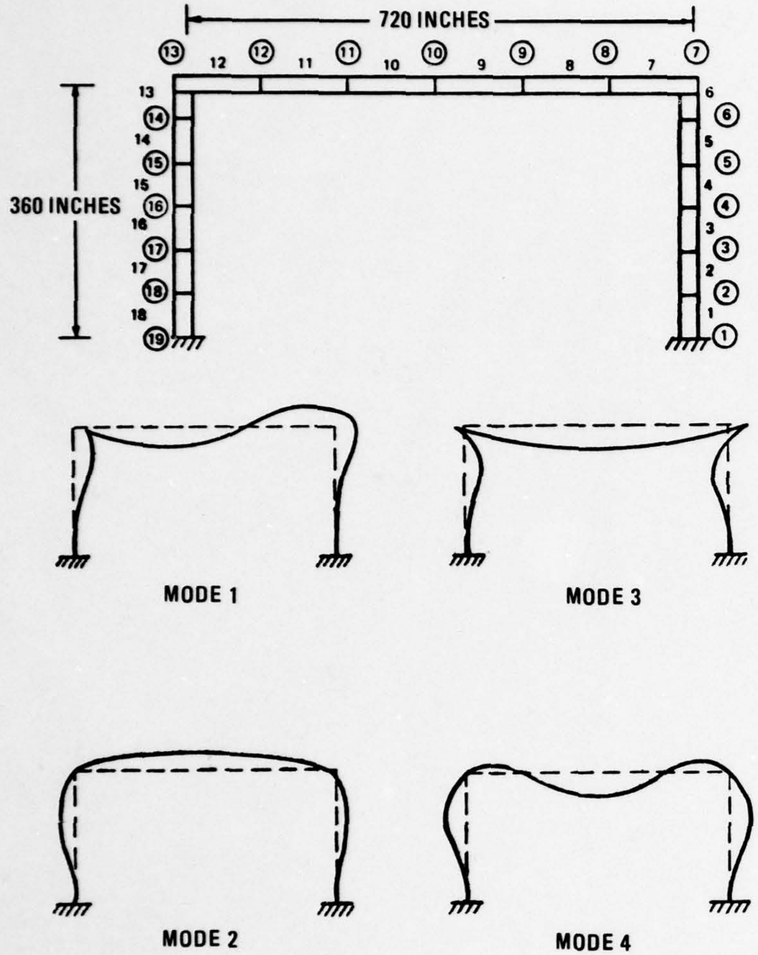

Figure A–6. Portal Frame Model and Modes

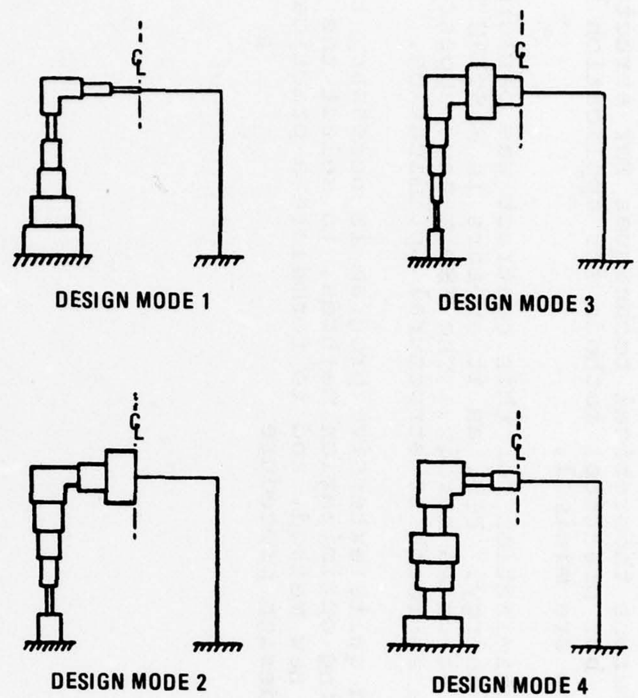

Figure A–7. Optimal Design for Portal Frame

CONCLUSIONS REGARDING STRUCTURAL OPTIMIZATION

1. There are numerous theoretical techniques for structural optimization, but practical methods for application to the design process are minimal.

2. Structural optimization for this contract was performed using strain energy. FSD, as it appears in NASTRAN Level 16 was also evaluated herein. The FSD method appears to be a feasible approach to structural optimization.

3. A further and quite extensive program is necessary to review existing optimization methods, to select the best or develop a new method, and to formulate a practical computer-aided design procedure.

APPENDIX B

SAMPLE CALCULATIONS FOR HEAT GENERATION

Sample calculations for CH-47 input pinion spiral bevel angular contact ball bearing no. 15 (Reference 15).

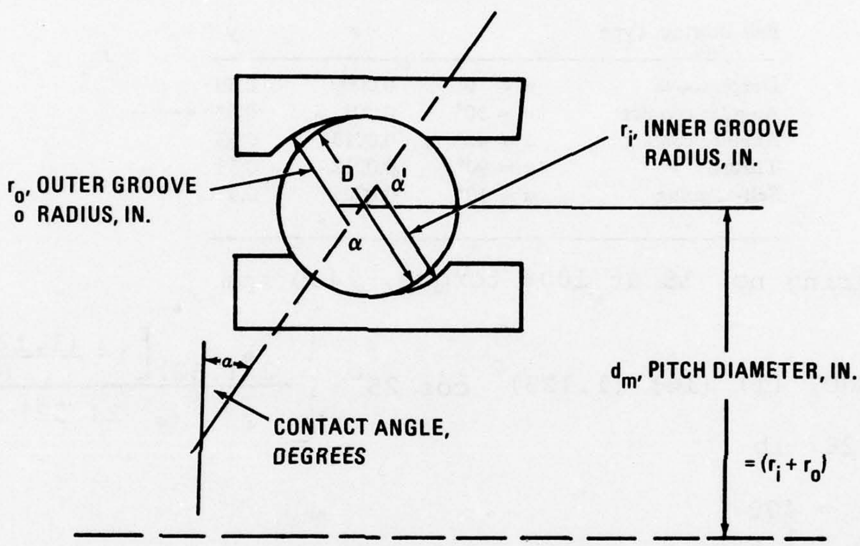

$$C_S = 400\ i\ Z\ D^2 \cos\alpha \left[\frac{2\ f_i\ (1-\gamma)}{2\ f_i - 1}\right]^{1/2}$$

C_S = Basic Static Capacity, lb

i = Number of Rows,

Z = Number of Rolling Elements Per Row

$f_i = \dfrac{r_i}{D}$, Inner Race Curvature (From S04)

$\gamma = \dfrac{D \cos\alpha}{d_m}$

$M_\ell = f_i\ F_\beta\ d_m$, Bearing Friction Torque (From Palmgren) in.-lb

$f_i = Z \left[\dfrac{F_s}{C_s}\right]^Y$

F_S = Static Equivalent Load, Lb (From S04)

z, y from Table B-1

$F_\beta = F_\alpha$ = Applied Axial Load, Lbs (From S04)

TABLE B-1. VALUES OF z AND y

Ball Bearing Type		z	y
Deep groove	$\alpha = 0°$	0.0009	0.55
Angular contact	$\alpha = 30°$	0.001	0.33 ←
Angular contact	$\alpha = 40°$	0.0013	0.33
Thrust	$\alpha = 90°$	0.0012	0.33
Self-aligning	$\alpha = 10°$	0.0003	0.4

For Bearing no. 15 at 100% torque, 7460 rpm

$$C_s = (400)\ (1)\ (14)\ (1.125)^2 \cos 25^o \left\{ \frac{2\ (.52) \left[1 - \frac{(1.125)(.91)}{6.1}\right]}{2(.52)\ -1} \right\}^{1/}$$

$= 30287$ lb

where i = 400
Z = 1
D = 1.125
$\alpha = 25^o$
f = 52
$d_m = 6.1$

$$f_i = .001 \left[\frac{6111}{30287}\right]^{.33} = .00059$$

M = (.00059) (6050) (6.1) = 21.8 in.-lb

= Mechanical Friction Torque

M_V = Viscous Friction Torque (in.-lb)

$= (1.42)\ (10^{-5})\ f_o\ (V_o\ N)^{2/3}\ d_m^{\ 3}$

V_o = Centistokes (e.g. 3 cs at 200°F, MIL-L-7808)

N = RPM (e.g., 7460)

f_o = Factor (Table B-2)

$M_V = (1.42)\ (10^{-5})\ (2)\ (3 * 7460)^{2/3}\ d_m^{\ 3} = 5.1$ in.-lb

$M_{TOTAL} = M_\ell + M_V = 21.8 + 5.1 = 26.9$ in.-lb

$$HP = \frac{(26.9)\ (7460)}{63025} = 3.18\ HP$$

Heat Generated by Bearing no. 3 = (42.42) hp = 134.9 Btu/min

TABLE B-2. VALUES OF f_o

Bearing Type	Mist Lubrication	Oil Bath Lubrication* Grease Lubrication	Vertical Mounting Flooded Oil Lubrication Jet Lubrication
Deep-groove ball bearings (single row), Self-aligning ball bearings (double row), Ball thrust bearings	0.7···1†	1.5···2	3···4
Filling-slot ball bearings (single row), Angular-contact ball bearings (single row)	1	2	4
Angular-contact ball bearings (double row)	2	4	8
Single-row, tapered roller bearings Spherical roller thrust bearings	1.5···2	3···4	6···8
Cylindrical roller bearings (single row)	1···1.5	2···3	4···6
Spherical roller bearings (double row) Tapered roller bearings (double row)	2···3	4···6	8···12

* Oil level reaches center of lowest rolling element in a horizontal mounting.

† Lower values pertain to light series; higher values pertain to heavier dimension series.

Sample calculation for CH-47 input pinion roller bearing heat generation (Reference 15).

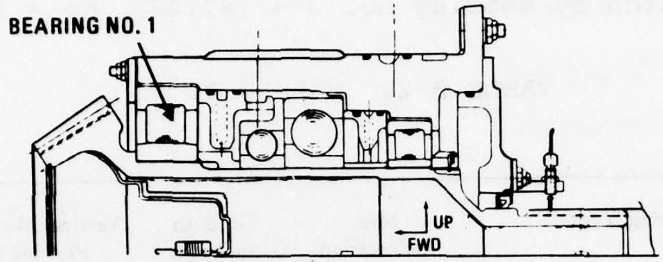

SPIRAL BEVEL INPUT PINION GEAR

Assume for roller bearing no. 1 the Palmgren relation

M_ℓ (Bearing Friction Torque) = f_1 (bearing factor)*
F_β (bearing shaft force)* d_m (pitch diameter)

or M_ℓ = (.0003) (15485 lb) (6.5 in.) = 30.4 in.-lb The f_1 chosen is for cylindrical roller bearings.

Now assume for lubricated roller bearing viscous friction torque (M_V) the Palmgren relation:

$M_V = 1.42 \times 10^{-5}\, f_o\, (v_o N)^{2/3}\, d_m^3$ where

f_o is a factor depending on the type of bearing and the method of lubrication (e.g., 2.5 for single-row cylindrical roller bearings),

v_o = centistokes (e.g., 3 cs @ 200°F, MIL-T-7808)

N = rpm (e.g., 7067)

or $M_V = (1.42)\,(10^{-5})\,(2.5)\,(3 \times 7067)^{2/3}\,(6.5)^3$

M_V = 7.47 in.-lb

$M_{TOTAL} = M_\ell + M_V$ = 37.87 in.-lb

$HP = \dfrac{(37.87)(7067)}{63025} = 4.2$ $\left[HP = \dfrac{2\pi N\, M_{TOTAL}}{(33000)(12)} \right]$

Heat Generated = (42.42)* HP = 178 Btu/min

(1 HP = 42.42 Btu/min)

APPENDIX C
SAMPLE OUTPUT FOR INDUCED MISALIGNMENT PROGRAM

GEAR/BEARING MISALIGNMENT PROGRAM

* * * NASTRAN POSTPROCESSOR * * *

R HOWELLS - POWER TRAIN TECHNOLOGY - APRIL 1976

CH-47C FWD XMSN INPUT PINION SHAFT - 185 DEG F DISPLACEMENTS

INPUT DATA SHAFT END A (NEAREST TO MESH)

GRID POINT LOCATIONS

2003	5.25000	0.00000	8.63400	2183	5.25000	180.00000	8.63400
2033	5.25000	30.00000	8.63400	2213	5.25000	210.00000	8.63400
2063	5.25000	60.00000	8.63400	2243	5.25000	240.00000	8.63400
2093	5.25000	90.00000	8.63400	2273	5.25000	270.00000	8.63400
2123	5.25000	120.00000	8.63400	2303	5.25000	300.00000	8.63400
2153	5.25000	150.00000	8.63400	2333	5.25000	330.00000	8.63400

GRID POINT DISPLACEMENTS

2003	0.113391E-01	-0.618340E-02	0.579231E-021838	0.992758E-03	0.227474E-03	0.167519E-01
2033	0.110801E-01	-0.600609E-02	0.153296E-0.2213	0.111082E-01	0.268117E-02	0.179840E-01
2063	0.998941E-02	-0.552632E-02	0.152158E-012243	0.130264E-01	0.198647E-02	0.190957E-01
2093	0.806837E-02	-0.415390E-02	0.156672E-012273	0.146945E-01	0.224429E-03	0.193844E-01
2123	0.645397E-02	-0.203897E-02	0.161314E-012303	0.156825E-01	-0.233294E-02	0.182980E-01
2153	0.663771E-02	0.124864E-03	0.162203E-012333	0.142121E-01	-0.485268E-02	0.170870E-01

INPUT DATA SHAFT END B (FARTHEST FROM MESH)

GRID POINT LOCATIONS

2000	5.25000	0.00000	14.93400	2180	5.25000	180.00000	14.93400
2030	5.25000	30.00000	14.93400	2210	5.25000	210.00000	14.93400
2060	5.25000	60.00000	14.93400	2240	5.25000	240.00000	14.93400
2090	5.25000	90.00000	14.93400	2270	5.25000	270.00000	14.93400
2120	5.25000	120.00000	14.93400	2300	5.25000	300.00000	14.93400
2150	5.25000	150.00000	14.93400	2330	5.25000	330.00000	14.93400

GRID POINT DISPLACEMENTS

2000	0.164125E-01	-0.538079E-02	0.285838E-012180	0.106174E-01	-0.392253E-04	0.296103E-01
2030	0.122303E-01	-0.672642E-02	0.298825E-012210	0.119787E-01	-0.135791E-03	0.300765E-01
2060	0.868517E-02	-0.594121E-02	0.304151E-012240	0.119395E-01	0.190447E-03	0.317044E-01
2090	0.836684E-02	-0.432274E-02	0.303579E-012270	0.108191E-01	0.105983E-02	0.319164E-01
2120	0.977630E-02	-0.205687E-02	0.298701E-012300	0.115511E-01	0.885209E-05	0.310136E-01
2150	0.104025E-01	-0.517965E-03	0.289240E-012330	0.146958E-01	-0.189538E-02	0.296469E-01

COORDINATES OF SHIFTED CENTER RELATIVE TO ORIGINAL CENTER

SHAFT END A

XMAV = 0.002620 YMAV = -0.003580 ZMAV = 8.650072 DEL ZMAV = 0.016072
TOTAL MOVEMENT OF CENTER= 0.016673

SHAFT END B

XMAV = 0.001922 YMAV = -0.001906 ZMAV = 14.964150 DEL ZMAV = 0.030159
TOTAL MOVEMENT OF CENTER= 0.030280

INDUCED MISALIGNMENT OF SHAFT CENTERLINE

DISPLACEMENT INPLANE (INCHES)= 0.0018
SLOPE (INCHES/INCH)= 0.0003
ANGULAR MISALIGNMENT OF CENTERLINE(DEGREES)= 0.0165

INDUCED DISPLACEMENT OF CENTERLINE AT GEAR PITCH DIAMETER(INCHES)= 0.0051
DISTANCE FROM END B TO PITCH DIAMETER (INCHES)= 8.5300

GEAR/BEARING MISALIGNMENT PROGRAM

* * * NASTRAN POSTPROCESSOR * * *

R HOWELLS - POWER TRAIN TECHNOLOGY - APRIL 1976

CH-47 FWD XMSN BEVEL/SUN SHAFT - 185 DEG F DISPLACEMENTS

INPUT DATA SHAFT END A (NEAREST TO MESH)

GRID POINT LOCATIONS

5000	2.76000	0.00000	-11.82000	5180	2.76000	180.00000	-11.82000
5045	2.76000	45.00000	-11.82000	5225	2.76000	225.00000	-11.82000
5090	2.76000	90.00000	-11.82000	5270	2.76000	270.00000	-11.82000
5135	2.76000	135.00000	-11.82000	5315	2.76000	315.00000	-11.82000

GRID POINT DISPLACEMENTS

5000	0.881108E-02	0.538151E-02	-0.683615E-025180	0.206404E-02	-0.727532E-02	-0.712806E-02
5045	0.118179E-01	0.106174E-02	-0.744948E-025225	-0.216408E-02	-0.302717E-02	-0.634546E-02
5090	0.110788E-01	-0.424765E-02	-0.759006E-025270	-0.163536E-02	0.276363E-02	-0.628018E-02
5135	0.718600E-02	-0.764268E-02	-0.730030E-025315	0.339357E-02	0.621650E-02	-0.649203E-02

INPUT DATA SHAFT END B (FARTHEREST FROM MESH)

GRID POINT LOCATIONS

1006	6.65000	0.00000	-2.50000	1186	6.65000	180.00000	-2.50000
1021	6.65000	15.00000	-2.50000	1201	6.65000	195.00000	-2.50000
1036	6.65000	30.00000	-2.50000	1216	6.65000	210.00000	-2.50000
1051	6.65000	45.00000	-2.50000	1231	6.65000	225.00000	-2.50000
1066	6.65000	60.00000	-2.50000	1246	6.65000	240.00000	-2.50000
1081	6.65000	75.00000	-2.50000	1261	6.65000	255.00000	-2.50000
1096	6.65000	90.00000	-2.50000	1276	6.65000	270.00000	-2.50000
1111	6.65000	105.00000	-2.50000	1291	6.65000	285.00000	-2.50000
1126	6.65000	120.00000	-2.50000	1306	6.65000	300.00000	-2.50000
1141	6.65000	135.00000	-2.50000	1321	6.65000	315.00000	-2.50000
1156	6.65000	150.00000	-2.50000	1336	6.65000	330.00000	-2.50000
1171	6.65000	165.00000	-2.50000	1351	6.65000	345.00000	-2.50000

GRID POINT DISPLACEMENTS

1006	0.121318E-01	0.725121E-02	0.845410E-021186	0.798424E-02	-0.114257E-01	0.494371E-02
1021	0.143274E-01	0.660257E-02	0.764045E-021201	0.559498E-02	-0.105817E-01	0.607704E-02
1036	0.165635E-01	0.523497E-02	0.680431E-021216	0.335056E-02	-0.910392E-02	0.767339E-02
1051	0.184163E-01	0.324386E-02	0.597465E-021231	0.168826E-02	-0.707772E-02	0.900514E-02
1066	0.196033E-01	0.766614E-03	0.527885E-021246	0.857107E-03	-0.476823E-02	0.961411E-02
1081	0.199327E-01	-0.192911E-02	0.497104E-021261	0.632963E-03	-0.240560E-02	0.994351E-02
1096	0.194779E-01	-0.456673E-02	0.488035E-021276	0.941892E-03	-0.807089E-04	0.101606E-01
1111	0.184315E-01	-0.697892E-02	0.486161E-021291	0.186135E-02	0.206281E-02	0.102035E-01
1126	0.167749E-01	-0.901279E-02	0.493198E-021306	0.318318E-02	0.390694E-02	0.102208E-01
1141	0.146862E-01	-0.104744E-01	0.499127E-021321	0.485608E-02	0.542861E-02	0.102245E-01
1156	0.125542E-01	-0.113389E-01	0.459605E-021336	0.691309E-02	0.655730E-02	0.100023E-01
1171	0.103333E-01	-0.116645E-01	0.446441E-021351	0.934163E-02	0.716400E-02	0.946140E-02

COORDINATES OF SHIFTED CENTER RELATIVE TO ORIGINAL CENTER

SHAFT END A

XMAV = 0.003445 YMAV = 0.006352 ZMAV = -11.826910 DEL ZMAV = -0.006920

TOTAL MOVEMENT OF CENTER= 0.010005

SHAFT END B

XMAV = 0.002047 YMAV = 0.009335 ZMAV = -2.492688 DEL ZMAV = 0.007312

TOTAL MOVEMENT OF CENTER= 0.012033

INDUCED MISALIGNMENT OF SHAFT CENTERLINE

DISPLACEMENT INPLANE (INCHES)= 0.0033

SLOPE (INCHES/INCH)= 0.0004

ANGULAR MISALIGNMENT OF CENTERLINE (DEGREES)= 0.0202

INDUCED DISPLACEMENT OF CENTERLINE AT GEAR PITCH DIAMETER (INCHES0= 0,0080

DISTANCE FROM END B TO PITCH DIAMETER (INCHES) = 5.8800

APPENDIX D

FIN STUDY

```
*JOB            SCIARRA,KP=29,PAGES=35,LINES=60,RUN=CHECK,LIST=SUBS
      V=5
      XL2=12.5  INITIALIZATION  V=FT/SEC, XL2 (DISTANCE FROM CENTERLINE TO END OF FIN)=INCHES, T(FIN
      T=.5                                                                      THICKNESS)=INCHES
      DO 6 K=1,2  # OF THICKNESSES
      DO 5 J=1,4  # OF FIN LENGTHS
      DO 4 I=,21  # OF VELOCITIES
      WRITE(6,1)V,XL2,T
    1 FORMAT('  V=',F10.1,'  XL2=',F10.3, '  T='  F10.3)
      IER=0
      BE=V*2./.000181
      XNU=.43+.0239*(RE)**.805
      H=.01565*XNU/2.
      BE=2.*H/)100.*T/12.)
      A=SQRT (BE)<------------ FOR 1 FT, OTHERWISE  A=SQRT (CYLINDER RADIUS*BE)
      B=(XL2/12.)*A
      I1=1
      I0=0
      CALL BESI(B,I1,C,IER)
      WRITE(6,2)B,I1,C,IER
    2 FORMAT(3X,E15.5,15,E15.5 15)
      CALL BESI(A,I1,D,IER)
      WRITE(6,2)A,I1,D.IER
      CALL BESI(A,I0,E,IER)
      WRITE(6,2)A,I0,E,IER
      CALL BESK(A,I1,F,IER)
      WRITE(6'2)A,I1,F,IER
      CALL BESK(8,I1,G,IER)
      WRITE(6,2)B,I1,G,IER
      CALL BESK(A,I0,H,IER)
      WRITE(6'2)A,I0,H,IER
      Q1=5236.*T*A
      ANS=C*F-G*D
      BOI =C*H+G*F
      Q1=Q1*ANS/BOT
      XNUM=204748./Q1
      HT=XNUM*T/12.
      WRITE(6,3)   Q1,ANS,BOT,XNUM,HT
    3 FORMAT('   BTU/HR=',F15.2,2X,'TOP=',E15.5,2X,'BOT=',E15.5,2X,2E15. 15)
    4 V=V+ 5<------ INCREMENT
```

AD-A052 759 BOEING VERTOL CO PHILADELPHIA PA F/G 1/3
FINITE ELEMENT ANALYSIS FOR COMPLEX STRUCTURES (HELICOPTER TRAN--ETC(U)
JAN 78 R W HOWELLS, J J SCIARRA DAAJ02-75-C-0053
UNCLASSIFIED D210-11232-1 USAAMRDL-TR-77-32 NL

3 OF 3
AD A052759

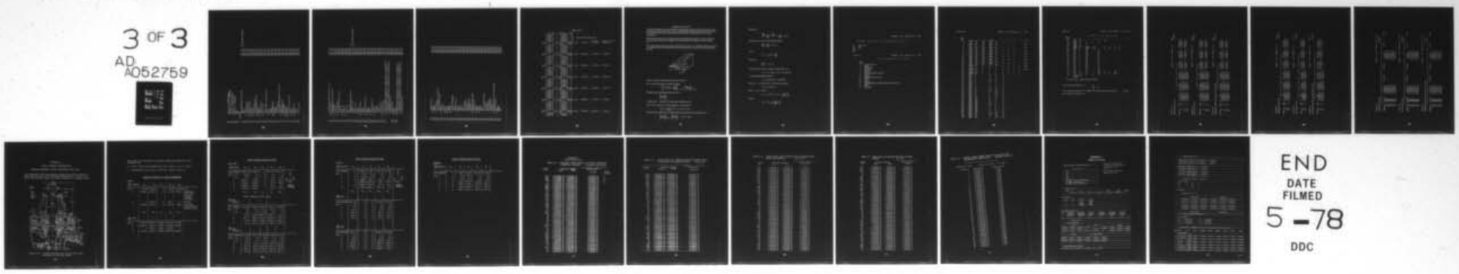

END
DATE FILMED
5-78
DDC

```
      V=5. ———— REINITIALIZE
    5 XL2=XL2+.50 ———— INCREMENT
      V=5. ———— }
      XL2=12.5 —— } REINITIALIZE
    6 T=T+.50 ———— INCREMENT
      STOP
      END
*EXECUTE
      SUBROUTINE BESI(X,N, BI,IER)                         BESI 350   I0 } BESSEL FUNCTIONS
      IER=0                                                BESI 390   I1 }
      BI=1.0                                               BESI 400
      IF(N)150,15,10                                       BES  410
   10 IF(X)160,20,20                                       BESI 420
   15 IF(X)160,17,20                                       BESI 430
   17 RETURN                                               BESI 440
   20 TOL=1.E-6                                            BESI 480
      IF(X-12.)40,40,30                                    BESI 520
   30 IF(X-FLOAT(N))40,40,110                              BESI 530
   40 XX=X/2.                                              BESI 570
   50 TERM=1.0                                             BESI 580
      IF(N) 70,70,55                                       BESI 590
   55 DO 60 1=1,N                                          BESI 600
      FI=I                                                 BESI 610
      IF(ABS(TERM)-1.E-68)56,60,60                         BESI 620
   56 IER=3                                                BESI 630
      BI=0.0                                               BESI 640
      RETURN                                               BESI 650
   60 TERM=TERM*XX/FI                                      BESI 660
   70 BI=TERM                                              BESI 670
      XX=XX*XX                                             BESI 680
      DO 90 K=1,1000                                       BESI 730
      IF(ABS (TERM)-ABS(BI*TOL))100,100,80                 BESI 740
   80 FK=K*(N+K)                                           BESI 750
      TERM=TERM*(XX/FK)                                    BESI 760
   90 BI=BI*TERM                                           BESI 770
  100 RETURN                                               BESI 810
  110 FN=4*N*N                                             BESI 850
      IF(X-170.0)115,111,111                               BESI 860
  111 IER=4                                                BESI 870
      RETURN                                               BESI 880
  115 XX=1./(8.*X)                                         BESI 890
      TERM=1.                                              BESI 900
      BI=1.                                                BESI 910
      DO 130 K=1,30                                        BESI 920
```

```
      IF(ABS(TERM)-ABS(TOL*BI))140,140,120                              BESI 930
  120 FK=(2*K-1)**2                                                     BESI 940
      TERM=TERM*XX*(FK-FN)/FLOAT(K)                                     BESI 950
  130 BI=BI+TERM                                                        BESI 960
      GO TO 40                                                          BESI1000
  140 PI=3.141592653                                                    BESI1010
      BI=BI*EXP(X)/SQRT(2.*PI*X)                                        BESI1020
      GO TO 100                                                         BESI1030
  150 IER=1                                                             BESI1140
      GO TO 100                                                         BESI1050
  160 IER=2                                                             BESI1060
      GO TO 100                                                         BESI1070
      END                                                               BESI1080
      SUBROUTINE RESK(X,N,BK,IER)                                       BESK 410
      DIMENSION T(12)                                                   BESK 420
      BK=.0                                                             BESK 430
      IF(N)10,11,11                                                     BESK 440
   10 IFR=1                                                             BESK 450
      RETURN                                                            BESK 460
   11 IF(X)12,12,20                                                     BESK 470
   12 IER=2                                                             BESK 480
      RETURN                                                            BESK 490
   20 IF(X-170.0)22,22,21                                               BESK 500
   21 IER=3                                                             BESK 510
      RETURN                                                            BESK 520
   22 IER=0                                                             BESK 530
      IF(X-1.)36,36,25                                                  BESK 540
   25 A=EXP(-X)                                                         BESK 550
      B=1./X                                                            BESK 560
      C=SQRT(B)                                                         BESK 570
      T(1)=B                                                            BESK 580
      DO 26 L=2,12                                                      BESK 590
   26 T(L)=T(L-1)*8                                                     BESK 600
      IF(N-1)27,29,27                                                   BESK 610
   27 G0=A*(1.25331414-.15666418*T(1)+.088111278*T(2)-.091390954*T(3)   BESK 650
     2+.13445962*T(4)-.22998503*T(5)+.37924097*T(6)-.52472773*T(7)      BESK 660
     3+.55753684*T(8)-.42626329*T(9)+.21845181*T(10)-.066809767*T(11)   BESK 670
     4+.009189383*T(12))*C                                              BESK 680
      IF(N)20,28,29                                                     BESK 690
   28 BK=G0                                                             BESK 700
      RETURN                                                            BESK 710
   29 G1+A*(1.2533141+.46999270*T(1)-.14685830*T(2)+.12804266*T(3)      BESK 750
     2-.17364316*T(4)+.28476181*T(5)-.45943421*T(6)+.62833807*T(7)      BESK 760
     3-.66322954*T(8)+.50502386*T(9)-.25813038*T(10)+.078800012*T(11)   BESK 770
     4-.010824177*T(12))*C                                              BESK 780
```

$\left.\begin{matrix}K_0\\K_1\end{matrix}\right\}$ BESSEL FUNCTIONS

```
      IF(N-1)20,30,31                                             BESK 790
   30 BK=G1                                                       BESK 800
      RETURN                                                      BESK 810
   31 DO 35 J=2,N                                                 BESK 850
      GJ=2,*(FLOAT(J)-1.)*G1/X+G0                                 BESK 860
      IF(GJ-1.0E70)33,33,32                                       BESK 870
   32 IER=4                                                       BESK 880
      GO TO 34                                                    BESK 890
   33 G0=G1                                                       BESK 900
   35 G1=GJ                                                       BESK 910
   34 BK=GJ                                                       BESK 920
      RETURN                                                      BESK 930
   36 B=X/2.                                                      BESK 940
      A=.57721566+ALOG(B)                                         BESK 950
      C=B*B                                                       BESK 960
      IF(N-1)37,43,37                                             BESK 970
   37 G0=-A                                                       BESK1010
      X2J=1.                                                      BESK1020
      FACT=1.                                                     BESK1030
      HJ=.0                                                       BESK1040
      DO 40 J=1,6                                                 BESK1050
      RJ=1./FLOAT(J)                                              BESK1060
      X2J=X2J*C                                                   BESK1070
      FACT=FACT*RJ*RJ                                             BESK1080
      HJ=HJ=RJ                                                    BESK1090
   40 G0=G0=+X2J*FACT*(HF-A)                                      BESK1100
      IF(N)43,42,43                                               BESK1110
   42 BK=G0                                                       BESK1120
      RETURN                                                      BESK1130
   43 X2J=B                                                       BESK1170
      FACT=1.                                                     BESK1180
      HJ=1.                                                       BESK1190
      G1=1./X+X2J*(.5+A-HJ)                                       BESK1200
      DO 50 J=2,8                                                 BESK1210
      X2J=X2J*C                                                   BESK1220
      RJ=1./FLOAT(J)                                              BESK1230
      FACT=FACT*RJ*RJ                                             BESK1240
      HJ=HJ+RJ                                                    BESK1250
   50 G1=G1+X2J*FACT*(.5+(A-HJ)*FLOAT(J)                          BESK1260
      IF(N-1)31,52,31                                             BESK1270
   52 BK=G1                                                       BESK1280
      RETURN                                                      BESK1290
      END                                                         BESK1300
```

SAMPLE OUTPUT

```
V=       5.0  XL2=      12.500  T=       0.500
     0.80107E 00     1     0.43353E 00     0
     0.76902E 00     1     0.41365E 00     0
     0.76902E 00     0     0.11534E 01     0      BESSEL FUNCTION INPUT/OUTPUT
     0.76902E 00     1     0.91479E 00     0
     0.80107E 00     1     0.86003E 00     0
     0.76902E 00     0     0.59285E 00     0                          # OF FINS        HEIGHT OF FINS (FT)
BTU/HR=             65.83  TOP=     0.40840E-01  BOT=      0.12490E 01       0.31102E 04      0.12959E 03
V=      10.0  XL2=      12.500  T=       0.500
     0.10582E 01     1     0.60672E 00     0
     0.10159E 01     1     0.57636E 00     0
     0.10159E 01     0     0.12751E 01     0
     0.10159E 01     1     0.58592E 00     0
     0.10582E 01     1     0.54592E 00     0
     0.10159E 01     0     0.41158E 00     0
BTU/HR=            114.85  TOP=     0.40844E-01  BOT=      0.94584E 00       0.17827E 04      0.74280E 02
V=      15.0  XL2=      12.500  T=       0.500
     0.12455E 01     1     0.75161E 00     0
     0.11957E 01     1     0.71127E 00     0
     0.11957E 01     0     0.13907E 01     0
     0.11957E 01     1     0.43751E 00     0
     0.12455E 01     1     0.40489E 00     0
     0.11957E 01     0     0.32037E 00     0
BTU/HR=            159.08  TOP=     0.40849E-01  BOT=      0.80387E 00       0.12871E 04      0.53630E 02
V=      20.0  XL2=      12.500  T=       0.500
     0.13983E 01     1     0.88452E 00     0
     0.13424E 01     1     0.83415E 00     0
     0.13424E 01     0     0.15038E 01     0
     0.13424E 01     1     0.34951E 00     0
     0.13983E 01     1     0.32164E 00     0
     0.13424E 01     0     0.26296E 00     0
BTU/HR=            200.44  TOP=     0.40853E-01  BOT=      0.71629E 00       0.10205E 04      0.42563E 02
V=      25.0  XL2=      12.500  T=       0.500
     0.15296E 01     1     0.10114E 01     0
     0.14684E 01     1     0.95068E 00     0
     0.14684E 01     0     0.16162E 01     0
     0.14684E 01     1     0.29033E 00     0
     0.15296E 01     1     0.26588E 00     0
     0.14684E 01     0     0.22277E 00     0
BTU/HR=            239.79  TOP=     0.40857E-01  BOT=      0.65501E 00       0.85386E 03      0.35577E 02
V=      30.0  XL2=      12.500  T=       0.500
     0.16460E 01     1     0.11350E 01     0
     0.15801E 01     1     0.10637E 01     0
     0.15801E 01     0     0.17286E 01     0
     0.15801E 01     1     0.24747E 00     0
     0.16460E 01     1     0.22564E 00     0
     0.15801E 01     0     0.19280E 00     0
BTU/HR=            277.62  TOP=     0.40862E-01  BOT=      0.60888E 00       0.73752E 03      0.30730E 02
V=      35.0  XL2=      12.500  T=       0.500
     0.17513E 01     1     0.12571E 01     0
     0.16812E 01     1     0.11747E 01     0
     0.16812E 01     0     0.18417E 01     0
     0.16812E 01     1     0.21487E 00     0
     0.17513E 01     1     0.19514E 00     0
     0.16812E 01     0     0.16948E 00     0
BTU/HR=            314.21  TOP=     0.40866E-01  BOT=      0.57244E 00       0.65162E 03      0.27151E 02
V=      40.00 XL2=      12.500  T=       0.500
     0.18479E 01     1     0.13786E 01     0
     0.17740E 01     1     0.12848E 01     0
```

THEORETICAL SOLUTION

A metal fin of triangular cross section is attached to a plane surface to help carry off heat from the latter. Assuming dimensions and coordinates as shown in the accompanying figure, find the steady-state temperature distribution along the fin if the root (i.e., wall) temperature is u_w and if the fin radiates freely into air of constant temperature u_a.

We shall base our analysis upon a unit length of the fin, and shall assume that the fin is so thin that temperature variations parallel to the base can be neglected. We also assume that θ is so small that $\cos\theta$ may be replaced by 1.

Now consider the heat balance in the element of the fin between x and $x + \Delta x$. This element gains heat by internal flow through its right face and loses heat by internal flow through its left face and by radiation through its upper and lower

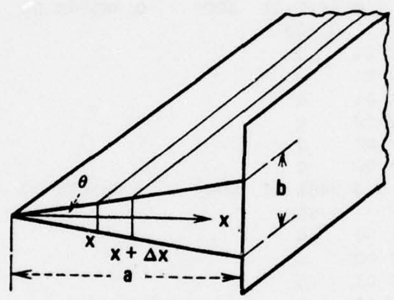

FIG. 8.7.

surfaces. Through the right face the gain of heat per unit time is

Area X thermal conductivity X temperature gradient

$$= \left[\left(1 \times \frac{bx}{a}\right)(k)\left(\frac{du}{dx}\right)\right]_{x+\Delta x} = \left[\frac{bkx}{a}\frac{du}{dx}\right]_{x+\Delta x}$$

Through the left face the element loses heat at the rate

$$\left[\frac{bkx}{a}\frac{du}{dx}\right]_{x}$$

Through the surfa . exposed to the air the element loses heat at the rate

Area X outer conductivity X (surface temperature − air temperature)

$$= \left(2 \times 1 \frac{\Delta x}{\cos\theta}\right)(h)(u - u_a) = 2h(u - u_a)\Delta x$$

Under steady-state conditions the rate of gain of heat must equal the rate of loss, and thus we have

$$\left[\frac{bkx}{a}\frac{du}{dx}\right]_{x+\Delta x} = \left[\frac{bkx}{a}\frac{du}{dx}\right]_{x} + 2h(u - u_a)\Delta x$$

Writing this as

$$\frac{x\dfrac{du}{dx}\Big|_{x+\Delta x} - x\dfrac{du}{dx}\Big|_{x}}{\Delta x} - \frac{2ah}{bk}(u - u_a) = 0$$

and letting $\Delta x \to 0$, we obtain the differential equation

$$\frac{d(xu')}{dx} - \frac{2ah}{bk}(u - u_a) = 0$$

If we set

$$U = u - u_a \quad \text{and} \quad \alpha^2 = \frac{2ah}{bk}$$

this becomes

$$\frac{d(xU')}{dx} \quad \alpha^2 U = 0$$

The general solution of this, according to the theory of Sec. 8.3, is

$$U = u - u_a = c_1 J_0(2\alpha i \sqrt{x}) + c_2 Y_0(2\alpha i \sqrt{x})$$

or, using the modified Bessel functions,

$$u - u_a = c_3 I_0(2\alpha \sqrt{x}) + c_4 K_0(2\alpha \sqrt{x})$$

Since $K_0(2\alpha \quad x)$ is infinite when $x = 0$, c_4 must be zero, leaving

$$u - u_a = c_3 I_0(2\alpha \sqrt{x})$$

When $x = a$, $u = u_w$, and thus

$$u_w - u_a = c_3 I_0(2\alpha \quad a) \quad \text{or} \quad c_3 = \frac{u_w - u_a}{I_0(2\alpha \quad a)}$$

Therefore

$$u = u_a + (u_w - u_a)\frac{I_0(2\alpha \quad x)}{I_0(2\alpha \quad a)}$$

JANUARY 21, 1976   NASTRAN 2/1/73   PAGE 1

N A S T R A N   E X E C U T I V E   C O N T R O L   D E C K   E C H O

```
ID      HEAT, FLOW
APP     HEAT
SOL     1.0
TIME    5
CEND
```

COOLING FIN   JANUARY 21, 1976   NASTRAN 2/1/73   PAGE 2

C A S E   C O N T R O L   D E C K   E C H O

```
CARD
COUNT
  1     TITLE#COOLING FIN
  2     OUTPUT
  3     THERMAL#ALL
  4     ELFORCE#ALL
  5     SPCF#ALL
  6     SUBCASE 1
  7     LABEL#TEMPERATURE SPECIFIED
  8     SPC#100
  9     SUBCASE 2
 10     LABEL#HEAT INPUT AT ROOT
 11     LOAD#10
 12     SPC#7
 13     SUBCASE 3
 14     LABEL#TEMPERATURE SPECIFIED AND HEAT INPUT AT ROOT
 15     LOAD#10
 16     SPC#100
 17     BEGIN BULK
```

CARD COUNT	. 1 ..	2 ..	3 ..	4 ..	5 ..	6 ..	7 ..	8 ..	9 ..	10
1-	CHBDY	101	200	AREA4	1	5	7	2		&CH1
2-	&CH1	101	105	107	102					
3-	CHBDY	102	200	AREA4	2	7	9	3		&CH2
4-	&CH2	102	107	109	103					
5-	CHBDY	103	200	AREA4	1	4	6	2		&CH3
6-	&CH3	101	104	106	102					
7-	CHBDY	104	200	AREA4	2	6	8	3		&CH4
8-	&CH4	102	106	108	103					
9-	CHBDY	105	200	AREA4	5	11	13	7		&CH8
10-	&CH8	105	111	113	107					
11-	CHBDY	106	200	AREA4	7	13	15	9		&CH7
12-	&CH7	107	113	115	109					
13-	CHBDY	107	200	AREA4	4	10	12	6		&CH5
14-	&CH5	104	110	112	106					
15-	CHBDY	108	200	AREA4	6	12	14	8		&CH6
16-	&CH6	106	112	114	108					
17-	CHEXA2	201	1	10	12	13	11	4	6	&E201
18-	&E201	7	5							
19-	CHEXA2	202	1	12	14	15	13	6	8	&E202
20-	&E202	9	7							
21-	CWEDGE	301	1	1	5	4	2	7	6	
22-	CWEDGE	302	1	3	8	9	2	6	7	
23-	GRID	1		0.0	2.	.2				
24-	GRID	2		1.	2.	.2				
25-	GRID	3		2.	2.	.2				
26-	GRID	4		0.0	1.	.1				
27-	GRID	5		0.0	1.	.3				
28-	GRID	6		1.	1.	.1				
29-	GRID	7		1.	1.	.3				
30-	GRID	8		2.	1.	.1				
31-	GRID	9		2.	1.	.3				
32-	GRID	10		0.0	0.0	.0				
33-	GRID	11		0.0	0.0	.4				
34-	GRID	12		1.	0.0	.0				
35-	GRID	13		1.	0.0	.4				
36-	GRID	14		2.	0.0	.0				
37-	GRID	15		2.	0.0	.4				
38-	GRID	101		0.0	2.	.2				
39-	GRID	102		1.	2.	.2				
40-	GRID	103		2.	2.	.2				
41-	GRID	104		0.0	1.	.1				
42-	GRID	105		0.0	1.	.3				
43-	GRID	106		1.	1.	.1				
44-	GRID	107		1.	1.	.3				
45-	GRID	108		2.	1.	.1				
46-	GRID	109		2.	1.	.3				
47-	GRID	110		0.0	0.0	.0				
48-	GRID	111		0.0	0.0	.4				
49-	GRID	112		1.	0.0	0.0				
50-	GRID	113		1.	0.0	.4				

```
                                   S O R T E D   B U L K   D A T A   E C H O
     CARD
     COUNT      .  1  ..  2  ..  3  ..  4  ..  5  ..  6  ..  7  ..  8  ..  9  ..  10  .
       51-      GRID    114             2.      0.0     0.0
       52-      GRID    115             2.      0.0     .4
       53-      MAT4    1       7.6
       54-      MAT4    2       2.
       55-      PHBDY   200     2
       56-      QHBDY   10      AREA4   1.0&3           10      12      13      11
       57-      QHBDY   10      AREA4   1.0&3           12      14      15      13
       58-      SPC     7       101             70.
       59-      SPC     7       102             70.
       60-      SPC     7       103             70.
       61-      SPC     7       104             70.
       62-      SPC     7       105             70.
       63-      SPC     7       106             70.
       64-      SPC     7       107             70.
       65-      SPC     7       108             70.
       66-      SPC     7       109             70.
       67-      SPC     7       110             70.
       68-      SPC     7       111             70.
       69-      SPC     7       112             70.
       70-      SPC     7       113             70.
       71-      SPC     7       114             70.
       72-      SPC     7       115             70.
       73-      SPC     70      10      1       400.    11      1       400.
       74-      SPC     70      12      1       400.    13      1       400.
       75-      SPC     70      14      1       400.    15      1       400.
       76-      SPCADD  100     7       70
                ENDDATA

     **NO ERROR FOUND - EXECUTE NASTRAN PROGRAM**


***USER INFORMATION MESSAGE 3023,         B #    8
                                          C #    0
                                          R #    7

***USER INFORMATION MESSAGE 3027, SYMMETRIC REAL DECOMPOSITION TIME ESTIMATE IS       0 SECONDS.

***USER INFORMATION MESSAGE 3035
```

COOLING FIN JANUARY 21, 1976 NASTRAN 2/1/73 PAGE 5

TEMPERATURE SPECIFIED SUBCASE 1

T E M P E R A T U R E   V E C T O R

POINT ID.	TYPE	ID VALUE	ID&1 VALUE	ID&2 VALUE	ID&3 VALUE	ID&4 VALUE	ID&5 VALUE
1	S	8.183005E 01	6.367873E 01	8.183005E 01	1.628307E 02	1.621151E 02	1.643016E 02
7	S	1.643016E 02	1.621151E 02	1.628307E 02	4.000000E 02	4.000000E 02	4.000000E 02
13	S	4.000000E 02	4.000000E 02	4.000000E 02			
101	S	7.000000E 01	7.000000E 01	7.000000E 01	7.000000E 01	7.000000E 01	7.000000E 01
107	S	7.000000E 01	7.000000E 01	7.000000E 01	7.000000E 01	7.000000E 01	7.000000E 01
113	S	7.000000E 01	7.000000E 01	7.000000E 01			

COOLING FIN JANUARY 21, 1976 NASTRAN 2/1/73 PAGE 6

HEAT INPUT AT ROOT SUBCASE 2

T E M P E R A T U R E   V E C T O R

POINT ID.	TYPE	ID VALUE	ID&1 VALUE	ID&2 VALUE	ID&3 VALUE	ID&4 VALUE	ID&5 VALUE
1	S	7.446457E 01	6.761646E 01	7.446457E 01	1.053896E 02	1.051158E 02	1.063039E 02
7	S	1.063039E 02	1.051158E 02	1.053896E 02	1.960730E 02	1.960978E 02	1.967352E 02
13	S	1.967352E 02	1.960978E 02	1.960730E 02			
101	S	7.000000E 01	7.000000E 01	7.000000E 01	7.000000E 01	7.000000E 01	7.000000E 01
107	S	7.000000E 01	7.000000E 01	7.000000E 01	7.000000E 01	7.000000E 01	7.000000E 01
113	S	7.000000E 01	7.000000E 01	7.000000E 01			

COOLING FIN JANUARY 21, 1976 NASTRAN 2/1/73 PAGE 7

TEMPERATURE SPECIFIED AND HEAT INPUT AT ROOT SUBCASE 3

T E M P E R A T U R E   V E C T O R

POINT ID.	TYPE	ID VALUE	ID&1 VALUE	ID&2 VALUE	ID&3 VALUE	ID&4 VALUE	ID&5 VALUE
1	S	8.183005E 01	6.367873E 01	8.183005E 01	1.628307E 02	1.621151E 02	1.643016E 02
7	S	1.643016E 02	1.621151E 02	1.628307E 02	4.000000E 02	4.000000E 02	4.000000E 02
13	S	4.000000E 02	4.000000E 02	4.000000E 02			
101	S	7.000000E 01	7.000000E 01	7.000000E 01	7.000000E 01	7.000000E 01	7.000000E 01
107	S	7.000000E 01	7.000000E 01	7.000000E 01	7.000000E 01	7.000000E 01	7.000000E 01
113	S	7.000000E 01	7.000000E 01	7.000000E 01			

COOLING FIN JANUARY 21, 1976 NASTRAN 2/1/73 PAGE 8

TEMPERATURE SPECIFIED SUBCASE 1

F O R C E S   O F   S I N G L E - P O I N T   C O N S T R A I N T

POINT ID.	TYPE	ID VALUE	ID&1 VALUE	ID&2 VALUE	ID&3 VALUE	ID&4 VALUE	ID&5 VALUE
10	S	-2.634587E 02	2.629077E 02	5.178735E 02	5.178735E 02	2.629077E 02	2.634587E 02
101	S	-3.617007E 01	-6.017391E 01	-3.617007E 01	-1.181779E 02	-1.178183E 02	-2.372213E 02
107	S	-2.372213E 02	-1.178183E 02	-1.181779E 02	-1.262208E 02	-1.261608E 02	-2.523816E 02
113	S	-2.523816E 02	-1.261608E 02	-1.262208E 02			

COOLING FIN JANUARY 21, 1976 NASTRAN 2/1/73 PAGE 9

HEAT INPUT AT ROOT SUBCASE 2

F O R C E S   O F   S I N G L E - P O I N T   C O N S T R A I N T

POINT ID.	TYPE	ID VALUE	ID&1 VALUE	ID&2 VALUE	ID&3 VALUE	ID&4 VALUE	ID&5 VALUE
101	S	-1.382976E 01	-2.307132E 01	-1.382976E 01	-4.521060E 01	-4.507506E 01	-9.098994E 01
107	S	-9.098994E 01	-4.507506E 01	-4.521060E 01	-4.829364E 01	-4.827695E 01	-9.678828E 01
113	S	-9.678828E 01	-4.827695E 01	-4.829364E 01			

COOLING FIN JANUARY 21, 1976 NASTRAN 2/1/73 PAGE 10

TEMPERATURE SPECIFIED AND HEAT INPUT AT ROOT SUBCASE 3

F O R C E S   O F   S I N G L E - P O I N T   C O N S T R A I N T

POINT ID.	TYPE	ID VALUE	ID&1 VALUE	ID&2 VALUE	ID&3 VALUE	ID&4 VALUE	ID&5 VALUE
10	S	1.634588E 02	1.629078E 02	3.178735E 02	3.178735E 02	1.629079E 02	1.634588E 02
101	S	-3.617007E 01	-6.017891E 01	-3.617007E 01	-1.181779E 02	-1.178183E 02	-2.372213E 02
107	S	-2.372213E 02	-1.178183E 02	-1.181779E 02	-1.262208E 02	-1.261608E 02	-2.523816E 02
113	S	-2.523816E 02	-1.261608E 02	-1.262208E 02			

COOLING FIN JANUARY 21, 1976 NASTRAN 2/1/73 PAGE 13

TEMPERATURE SPECIFIED SUBCASE 1

F I N I T E   E L E M E N T   T E M P E R A T U R E   G R A D I E N T S   A N D   H E A T   F L O W S

ELEMENT-ID	EL-TYPE	X-GRADIENT	Y-GRADIENT	Z-GRADIENT	X-FLOW	Y-FLOW	Z-FLOW
101	HBDY	4.798138E 01			-9.644125E 01		
102	HBDY	4.816029E 01			-9.680086E 01		
103	HBDY	4.816029E 01			-9.680086E 01		
104	HBDY	4.798138E 01			-9.644125E 01		
105	HBDY	2.116040E 02			-4.253181E 02		
106	HBDY	2.117830E 02			-4.256780E 02		
107	HBDY	2.117830E 02			-4.256780E 02		
108	HBDY	2.116040E 02			-4.253181E 02		

COOLING FIN JANUARY 21, 1976 NASTRAN 2/1/73 PAGE 16

HEAT INPUT AT ROOT SUBCASE 2

F I N I T E   E L E M E N T   T E M P E R A T U R E   G R A D I E N T S   A N D   H E A T   F L O W S

ELEMENT-ID	EL-TYPE	X-GRADIENT	Y-GRADIENT	Z-GRADIENT	X-FLOW	Y-FLOW	Z-FLOW
101	HBDY	1.837518E 01			-3.693361E 01		
102	HBDY	1.844365E 01			-3.707123E 01		
103	HBDY	1.844365E 01			-3.707123E 01		
104	HBDY	1.837518E 01			-3.693361E 01		
105	HBDY	8.106319E 01			-1.629348E 02		
106	HBDY	8.112543E 01			-1.630599E 02		
107	HBDY	8.112543E 01			-1.630599E 02		
108	HBDY	8.106319E 01			-1.629348E 02		

COOLING FIN JANUARY 21, 1976 NASTRAN 2/1/73 PAGE 19

TEMPERATURE SPECIFIED AND HEAT INPUT AT ROOT SUBCASE 3

F I N I T E   E L E M E N T   T E M P E R A T U R E   G R A D I E N T S   A N D   H E A T   F L O W S

ELEMENT-ID	EL-TYPE	X-GRADIENT	Y-GRADIENT	Z-GRADIENT	X-FLOW	Y-FLOW	Z-FLOW
101	HBDY	4.798138E 01			-9.644125E 01		
102	HBDY	4.816029E 01			-9.680086E 01		
103	HBDY	4.816029E 01			-9.680086E 01		
104	HBDY	4.798138E 01			-9.644125E 01		
105	HBDY	2.116040E 02			-4.253181E 02		
106	HBDY	2.117830E 02			-4.256780E 02		
107	HBDY	2.117830E 02			-4.256780E 02		
108	HBDY	2.116040E 02			-4.253181E 02		

APPENDIX E

CH-47C FORWARD TRANSMISSION

BEARING NUMBERING SYSTEM CONVENTION AND LOADS

This appendix gives the bearing numbering system convention and loads for the CH-47C forward transmission. Figure E-1 shows the forward rotor hub loads converted to bearing loads.

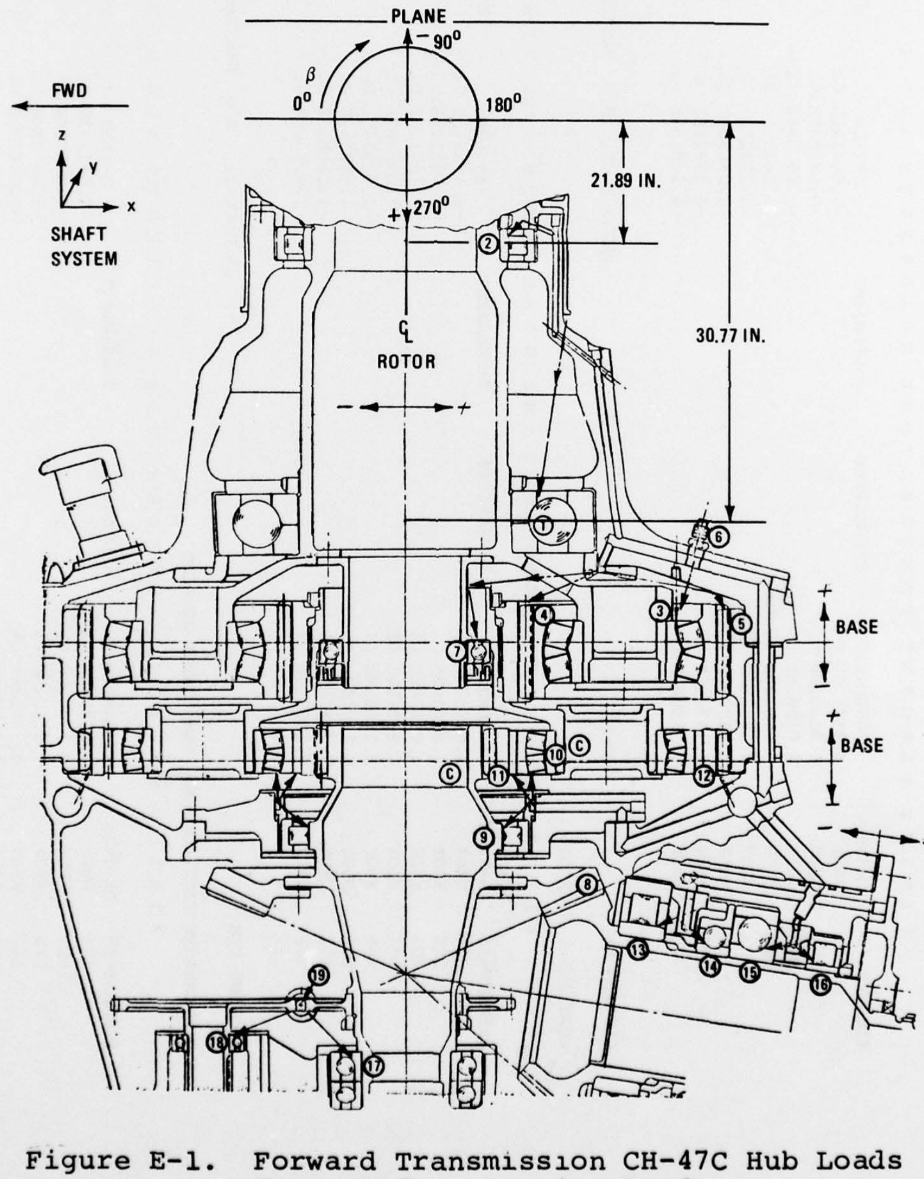

Figure E-1. Forward Transmission CH-47C Hub Loads Converted to Bearing Loads.

Hub loads are converted to bearing loads and applied to the transmission.

1. Cover, Ring and Transmission Case, Cases 3, 4, 5, and 6.

2. Transmission Case Only, 3 Per Rev (Cases 1 and 2).

LOADS ON COVER S-70 SIGN CONVENTION

COVER

2 ROLLER	F_X	F_Y	F_Z	M_X	M_Y	
Case 3	7479.	1918.5	0.	-11.5	45.584	1-g
4	130420.	4746.7	0.	-35.3	1158.3	Symmetric Dive and Pullout, Noseup Pitching
5	0.	-11511.	0.	102.	0.	Yawing
6	-45960.	-50717.	0.	446.7	-408.7	Recovery From Rolling Pullout (cc)

1 BALL	$-F_Z$	$-F_Y$	F_X	M_Z	$-M_Y$
Case 3	-7222.7	-1621.5	25038.	-5851.5	25766.
4	-106100.	-3018.8	97282.	-11006.	381890.
5	0.	22536.	64855.	87003.	0.
6	38390.	41421.	54066.	146850.	-136000.

SHAFT SYSTEM LOADS ON CASE

SUN GEAR

9 ROLLER	F_X	F_Y	F_Z	M_X	M_Y
100% TORQUE	-5802.4	+7082.9	0.	-27.757	-30.377
Case 1 3C	-59.8	73.	0.	-.3	-.3
2 3S	-9.9	12.	0.	-.05	-.05
3	-4471.3	5458.	0.	21.4	-23.4
4	-13055.	15936.	0.	62.4	-68.3
5	-10880.	13280.	0.	52.0	-57.
6	-8703.6	10624.		41.6	-45.6
	$-F_Z$	F_Y	F_X	M_Z	$-M_Y$

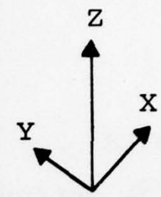

SHAFT SYSTEM

After changing S-04 signs.

17 BALL (Upper)					
100% TORQUE	+52.220	+2349.7	2364.0	2457.3	-124.05
Case 1 3C	.54	24.2	24.3	25.3	-1.3
2 3S	.09	4.0	4.02	4.2	-.2
3	40.2	1810.7	1821.7	1893.6	-95.6
4	117.5	5286.8	5319.	5528.9	-279.1
5	97.9	4405.7	4432.	4607.4	-232.6
6	78.3	3524.5	3546.	3686.	-186.1

17 BALL (Lower)					
100% TORQUE	-12.942	68.971	63.020	-67.641	-15.741
Case 1 3C	-.13	.71	.65	-.7	-.16
2 3S	-.02	.11	.11	-.11	-.03
3	-10.	53.1	48.6	-52.1	-12.13
4	-29.1	155.2	141.8	-152.2	-35.42
5	-24.2	129.3	118.2	-126.8	-29.51
6	-19.4	103.4	94.5	-101.5	-23.6

SHAFT SYSTEM LOADS ON CASE

PINION

13 ROLLER	F_X	F_Y	F_Z	M_Z	M_Y
100% TORQUE	0.	-12826.	1187.	336.07	51.847
Case 1	0.	-132.	12.2	3.5	.53
2	0.	-21.8	2.02	.6	.09
3	0.	-9884.	914.7	259.	40.
4	0.	-28860.	2670.8	756.	116.6
5	0.	-24050.	2225.6	630.	97.2
6	0.	-19240.	1780.5	504.1	77.8

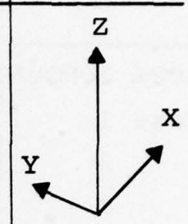

SHAFT SYSTEM

14 BALL	$-F_X$	$-F_Y$	$-F_Z$	$+M_Z$	$-M_Y$
100% TORQUE	-61.523	0.	0.	36.355	10.315
Case 1	-.63	0.	0.	.37	.11
2	-.10	0.	0.	.06	.018
3	-47.4	0.	0.	28.	8.0
4	-138.4	0.	0.	81.8	23.2
5	-115.4	0.	0.	68.2	19.3
6	-92.3	0.	0.	54.5	15.5

15 BALL					
100% TORQUE	6111.5	0.	0.	1260.0	359.48
Case 1	63.	0.	0.	13.	3.7
2	10.4	0.	0.	2.1	.61
3	4709.	0.	0.	970.9	277.
4	13750.	0.	0.	2835.	808.8
5	11460.	0.	0.	2362.	674.
6	9167.	0.	0.	1890.	539.

SHAFT SYSTEM LOADS ON CASE

PINION

16 ROLLER	F_X	F_Y	F_Z	M_Z	M_Y
100% TORQUE	0.	3325.	-2558.	122.50	70.313
Case 1	0.	34.2	-26.3	1.3	.724
2	0.	5.6	-4.3	.2	.12
3	0.	2562.	-1971.	94.4	54.2
4	0.	7481.	-5756.	275.6	158.2
5	0.	6234.	-4796.	229.7	131.8
6	0.	4987.	-3837.	183.8	105.4

APPENDIX F
UPPER COVER S-83

TABLE F-1. ORIGINAL UPPER COVER S-83 OUTPUT INCLUDING PRINCIPLE STRESSES **Original 145.16 Lb**

ELEMENT ID	PRINCIPAL STRESSES MAJOR	PRINCIPAL STRESSES MINOR	S T R A I N D E N S I T Y STRAIN DENSITY CTRIA2'S	ORDER NUMBER
6010	0.1929363E 05	-.6726012E 04	0.237423E 02	14
6017	0.1991434E 05	-.3359676E 04	0.214135E 02	16
6016	0.1974698E 05	-.3229855E 04	0.209637E 02	17
5020	0.1775009E 05	-.2069270E 04	0.163002E 02	20
51	0.1103957E 05	-.1075971E 05	0.148515E 02	22
53	0.1371005E 05	-.5616359E 04	0.127445E 02	27
5018	0.1645783E 05	0.6583102E 04	0.117373E 02	
5016	0.1188723E 05	-.5525008E 04	0.101371E 02	
6018	0.1482290E 05	0.5492383E 04	0.947626E 01	
5022	0.2591676E 04	-.1297479E 05	0.933707E 01	
52	-.9186133E 03	-.1425274E 05	0.932388E 01	
5021	0.8909863E 04	-.7739383E 04	0.868484E 01	
321	0.1038435E 05	-.5922156E 04	0.863536E 01	
4010	0.2555133E 04	-.1244055E 05	0.862681E 01	
5005	0.1034370E 05	-.5340793E 04	0.809730E 01	
50	0.9009824E 04	-.6059434E 04	0.723882E 01	
4017	-.1541250E 03	-.1153795E 05	0.628745E 01	
5017	0.1185657E 05	0.2784605E 04	0.608082E 01	
26	0.1144671E 05	0.5631797E 03	0.606263E 01	
6005	-.4057367E 04	-.1160000E 05	0.579078E 01	
305	-.5539152E 04	-.1119256E 05	0.558130E 01	
4016	0.7862539E 03	-.1045707E 05	0.548130E 01	
320	0.1087479E 05	0.5804180E 03	0.545967E 01	
322	0.3665918E 04	-.8474012E 04	0.498397E 01	
41	0.1062032E 05	0.1699746E 04	0.497133E 01	
6011	-.6968164E 03	-.1007954E 05	0.465205E 01	
5011	0.7153555E 04	-.4701324E 04	0.449025E 01	
56	0.9766148E 04	0.1094711E 04	0.428067E 01	
59	0.8983719E 04	0.6346328E 03	0.369269E 01	
25	0.7079301E 04	-.3410879E 04	0.365915E 01	
58	0.8966762E 04	0.1116159E 04	0.359016E 01	
310	0.8473172E 04	-.3258750E 03	0.350603E 01	
42	0.5892863E 04	-.4609344E 04	0.347373E 01	
38	0.6592012E 04	-.3457495E 04	0.331684E 01	
5010	0.6704359E 04	-.3218500E 04	0.327587E 01	
4018	-.1540317E 04	-.8464039E 04	0.313639E 01	
317	0.7650547E 04	0.1121319E 04	0.259174E 01	
44	0.7226766E 04	0.3475788E 04	0.231467E 01	
29	0.6261605E 04	-.1516281E 04	0.225908E 01	
318	0.6715145E 04	0.4630820E 04	0.224296E 01	
4011	0.6030656E 04	-.1833245E 04	0.222092E 01	
316	0.6703004E 04	0.4199781E 04	0.214162E 01	
6015	0.6835988E 04	0.2123509E 04	0.200797E 01	
805	0.1724153E 04	-.5739316E 04	0.200462E 01	
803	0.6597988E 04	0.3736415E 04	0.200410E 01	
311	-.3485824E 04	-.6646590E 04	0.199274E 01	
4005	0.6748668E 04	0.2173870E 04	0.195719E 01	
315	0.5862691E 04	0.4862328E 04	0.191414E 01	
49	0.5692406E 04	-.1081181E 04	0.178186E 01	
47	0.6223191E 04	0.6351509E 03	0.174577E 01	
5014	0.6263949E 04	0.1902500E 04	0.168611E 01	
43	0.4938375E 04	-.2046125E 04	0.166140E 01	
54	0.4147191E 04	-.2748627E 04	0.151803E 01	
27	0.8352412E 03	-.5296668E 04	0.150082E 01	

TABLE F-2. UPPER COVER S-83 RESULTS WITH STIFFNESS ADDED TO EQUALIZE THE STRAIN DENSITY 160.83 Lb

			S T R A I N D E N S I T Y
ELEMENT ID	PRINCIPAL STRESSES MAJOR	MINOR	STRAIN DENSITY CTRIA2
6010	0.1236197E 05	-.4846574E 04	0.101787E 02
6018	0.1522380E 05	0.3706184E 04	0.100112E 02
5018	0.1460096E 05	0.5791551E 04	0.923232E 01
5016	0.1093799E 05	-.5441570E 04	0.887858E 01
5020	0.1143777E 05	-.3987061E 04	0.834387E 01
6016	0.1186350E 05	-.2392672E 04	0.781945E 01
6017	0.1247090E 05	-.4167930E 03	0.756884E 01
4010	0.3317330E 04	-.1055119E 05	0.686707E 01
5022	0.3035895E 04	-.1053075E 05	0.667117E 01
4017	-.2714063E 03	-.1148384E 05	0.619068E 01
321	0.8583773E 04	-.4761949E 04	0.580497E 01
51	0.7533613E 04	-.5350711E 04	0.526568E 01
5005	0.7266691E 04	-.4879516E 04	0.470360E 01
4016	0.4418789E 03	-.9495762E 04	0.442796E 01
305	-.4996363E 04	-.9563023E 04	0.412154E 01
5021	0.4699344E 04	-.6427461E 04	0.391781E 01
5011	0.6768352E 04	-.4239629E 04	0.389141E 01
26	0.9200598E 04	0.8069414E 03	0.384104E 01
5017	0.9166375E 04	0.8018125E 03	0.381294E 01
53	0.8689625E 04	-.5321230E 03	0.374679E 01
320	0.8998328E 04	0.5498516E 03	0.372285E 01
322	0.3199529E 04	-.7002102E 04	0.348898E 01
310	0.8056563E 04	-.7003340E 03	0.328215E 01
5010	0.7339551E 04	-.2023957E 04	0.320237E 01
38	0.6782473E 04	-.2882902E 04	0.316827E 01
56	0.8229500E 04	0.4386072E 03	0.312672E 01
52	0.1983789E 04	-.7241656E 04	0.311217E 01
44	0.8375789E 04	0.3939224E 04	0.309762E 01
41	0.8155855E 04	0.1956995E 04	0.287487E 01
6011	-.8183811E 03	-.7971906E 04	0.286398E 01
6005	-.3227536E 04	-.7754586E 04	0.261466E 01
58	0.7470883E 04	0.8660132E 03	0.250097E 01
4018	-.1591511E 04	-.7467082E 04	0.242203E 01
29	0.6612586E 04	-.1179699E 04	0.238064E 01
59	0.7051238E 04	0.6109241E 03	0.225718E 01
25	0.5352754E 04	-.2916354E 04	0.223398E 01
317	0.6891234E 04	0.7669395E 03	0.213710E 01
4011	0.5647551E 04	-.1422088E 04	0.185413E 01
4005	0.6370203E 04	0.3452069E 04	0.184534E 01
311	-.2397708E 04	-.6536789E 04	0.184204E 01
42	0.3758810E 04	-.3818315E 04	0.179421E 01
6020	0.5424484E 04	-.1626640E 04	0.178980E 01
316	0.6152207E 04	0.3435745E 04	0.173538E 01
49	0.5014969E 04	-.2129531E 04	0.173140E 01
6015	0.5200816E 04	-.1413939E 04	0.160208E 01
318	0.5549996E 04	0.3402393E 04	0.145603E 01
54	0.2609735E 04	-.4096348E 04	0.144154E 01
50	0.3040607E 04	-.3622755E 04	0.139306E 01
46	0.5349816E 04	0.3029934E 03	0.131901E 01
6008	0.1603876E 04	-.4395719E 04	0.125243E 01
805	0.1666614E 04	-.4301430E 04	0.122669E 01
315	0.4873141E 04	0.3455677E 04	0.119829E 01
5014	0.5023883E 04	0.1381842E 04	0.108619E 01
55	0.3498023E 04	-.2263901E 04	0.106242E 01

TABLE F-3. UPPER COVER S-83 RESULTS WITH STIFFNESS BOTH ADDED AND REMOVED 147.80 Lb

S T R A I N D E N S I T Y

ELEMENT ID	PRINCIPAL STRESSES MAJOR	MINOR	STRAIN DENSITY CTRJAZ
6010	0.1236197E 05	-.4846574E 04	0.101787E 02
6018	0.1522380E 05	0.3706184E 04	0.100112E 02
5018	0.1460096E 05	0.5791551E 04	0.923232E 01
5016	0.1093799E 05	-.5441570E 04	0.887858E 01
5020	0.1143777E 05	-.3987061E 04	0.834387E 01
6016	0.1186350E 05	-.2392672E 04	0.781945E 01
6017	0.1247090E 05	-.4167930E 03	0.756884E 01
4010	0.3317330E 04	-.1055119E 05	0.686707E 01
5022	0.3035895E 04	-.1053075E 05	0.667117E 01
4017	-.2714063E 03	-.1148384E 05	0.619068E 01
321	0.8583773E 04	-.4761949E 04	0.580497E 01
51	0.7533613E 04	-.53507115 04	0.526568E 01
5005	0.7266691E 04	-.4879516E 04	0.470360E 01
4016	0.4418789E 03	-.9495762E 04	0.442796E 01
305	-.4996363F 04	-.9563023F 04	0.412154E 01
5021	0.4699344E 04	-.6427461E 04	0.391781E 01
6011	0.6768352E 04	-.4239629E 04	0.389141E 01
26	0.9200598E 04	0.8069414E 03	0.384104E 01
5017	0.9166375E 04	0.8018125E 03	0.381294E 01
53	0.8689625E 04	-.5321230E 03	0.374679E 01
320	0.8998328E 04	0.5498516E 03	0.372285E 01
322	0.3199529E 04	-.7002102E 04	0.348898E 01
310	0.8056563E 04	-.7003340E 03	0.328215E 01
5010	0.7339551E 04	-.2023957E 04	0.320237E 01
38	0.6782473E 04	-.2882902E 04	0.316827E 01
56	0.8229500E 04	0.4386072E 03	0.312672E 01
52	0.1983789E 04	-.7241656E 04	0.311217E 01
44	0.8375789E 04	0.3939224E 04	0.309762E 01
41	0.8155855E 04	0.1956995E 04	0.287487E 01
6011	-.8183811E 03	-.7971906E 04	0.286398E 01
6005	-.3227536E 04	-.7754586E 04	0.261466E 01
58	0.7470883E 04	0.8660132E 03	0.250097E 01
4018	-.1591511E 04	-.7467082E 04	0.242203E 01
29	0.6612586E 04	-.1179699E 04	0.238064E 01
59	0.7051238E 04	0.6109241E 03	0.225718E 01
25	0.5352754E 04	-.2916354E 04	0.223398E 01
317	0.6891234E 04	0.7669395E 03	0.213210E 01
4011	0.5647551E 04	-.1422088E 04	0.185413E 01
4005	0.6370203E 04	0.3452069E 04	0.184534E 01
311	-.2397708E 04	-.6536789E 04	0.184204E 01
42	0.3758810E 04	-.3818315E 04	0.179421E 01
6020	0.5424484E 04	-.1626640E 04	0.178980E 01
316	0.6152207E 04	0.3435745E 04	0.173538E 01
49	0.5014969E 04	-.2129531E 04	0.173140E 01
6015	0.5200816E 04	-.1413939E 04	0.160208E 01
318	0.5549996E 04	0.3402393E 04	0.145603E 01
54	0.2609735E 04	-.4096348E 04	0.144154E 01
50	0.3040607E 04	-.3622755E 04	0.139306E 01
46	0.5349816E 04	0.3029934E 03	0.131901E 01
6008	0.1603876E 04	-.4395719E 04	0.125243E 01
805	0.1666614E 04	-.4301430E 04	0.122669E 01
315	0.4873141E 04	0.3455677E 04	0.119829E 01
5014	0.5023883E 04	0.1381842E 04	0.108619E 01
55	0.3498023E 04	-.2263901E 04	0.106242E 01

TABLE F-4. UPPER COVER S-83 RESULTS WITH ONLY STIFFNESS REMOVED 132.1 Lb

S T R A I N D E N S I T Y

ELEMENT ID	PRINCIPAL STRESSES MAJOR	MINOR	STRAIN DENSITY CTRJAZ
6010	0.1956978E 05	-.7544402E 04	0.253414E 02
6017	0.2018899E 05	-.2928082E 04	0.215769E 02
6016	0.2003551E 05	-.3226973E 04	0.215354E 02
5020	0.1853384E 05	-.2371160E 04	0.179329E 02
53	0.1474734E 05	-.5956566E 04	0.146603E 02
51	0.1116325E 05	-.9763926E 04	0.137179E 02
5018	0.1719305E 05	0.6939863E 04	0.128185E 02
5022	0.3829840E 04	-.1440469E 05	0.122211E 02
5016	0.1252716E 05	-.5260559E 04	0.107519E 02
6018	0.1539315E 05	0.5878719E 04	0.102357E 02
52	0.2666102E 04	-.1335970E 05	0.989767E 01
5021	0.8886637E 04	-.8663668E 04	0.962622E 01
4010	0.3135535E 04	-.1291580E 05	0.961717E 01
321	0.1084443E 05	-.6065684E 04	0.930981E 01
4017	-.2627344E 03	-.1287309E 05	0.779369E 01
5005	0.1037427E 05	-.4913027E 04	0.779138E 01
50	0.8713559E 04	-.5619422E 04	0.657653E 01
305	-.5835727E 04	-.1184445E 05	0.624505E 01
6005	-.4422484E 04	-.1195999E 05	0.616865E 01
26	0.1150239E 05	0.5356055E 03	0.613054E 01
320	0.1148042E 05	0.5374883E 03	0.610630E 01
322	0.4463922E 04	-.8797250E 04	0.580296E 01
4016	0.5957070E 03	-.1070056E 05	0.565999E 01
6011	-.8747656E 03	-.1051063E 05	0.502343E 01
5017	0.1060345E 05	0.1499875E 04	0.498775E 01
44	0.1067296E 05	0.4420555E 04	0.495074E 01
5011	0.7433371E 04	-.4606508E 04	0.466076E 01
5010	0.8824934E 04	-.2439926E 04	0.463287E 01
41	0.1012871E 05	0.1877117E 04	0.448721E 01
56	0.9982266E 04	0.1293656E 04	0.444039E 01
310	0.8977410E 04	-.9949414E 03	0.415077E 01
58	0.9446078E 04	0.1058836E 04	0.400468E 01
38	0.7407105E 04	-.3429916E 04	0.392896E 01
59	0.9202398E 04	0.5126563E 03	0.390469E 01
25	0.6988113E 04	-.3387402E 04	0.357633E 01
4018	-.1930869E 04	-.8794379E 04	0.335506E 01
311	-.3484292E 04	-.8140113E 04	0.288929E 01
4005	0.7777238E 04	0.4787438E 04	0.286354E 01
29	0.7116492E 04	-.1420547E 04	0.280860E 01
4011	0.6875289E 04	-.1656828E 04	0.272067E 01
317	0.7770340E 04	0.1213876E 04	0.266460E 01
42	0.5207668E 04	-.3975205E 04	0.266002E 01
316	0.6974750E 04	0.4563543E 04	0.236093E 01
318	0.6806883E 04	0.4351590E 04	0.222652E 01
6015	0.7143563E 04	0.1989109E 04	0.219553E 01
315	0.6537805E 04	0.4678027E 04	0.216723E 01
805	0.1809063E 04	-.5818906E 04	0.208150E 01
803	0.6553496E 04	0.3729751E 04	0.198012E 01
54	0.4690391E 04	-.3151950E 04	0.196069E 01
49	0.5907676E 04	-.1172797E 04	0.193364E 01
6020	0.5779137E 04	-.1295853E 04	0.189325E 01
5014	0.6533008E 04	0.1865928E 04	0.183538E 01
46	0.5952234E 04	0.5796028E 03	0.160042E 01
314	0.5103063E 04	-.1462528E 04	0.156404E 01

TABLE F-5. SAMPLE STRAIN ENERGY OUTPUT FOR CH-47C FWD TRANSMISSION UPPER COVER NASTRAN LEVEL 16

E L E M E N T S T R A I N E N E R G I E S

ELEMENT-TYPE # QUAD2 * TOTAL FOR ALL TYPES # 7,8207930E 03 *

ELEMENT-ID	STRAIN-ENERGY	PERCENT OF TOTAL
1	2.257979E 01	0.2887
2	8.476082E 00	0.1084
3	6.368781E 00	0.0814
4	6.808832E 00	0.0871
5	4.959671E 00	0.0634
6	2.260995E 00	0.0289
7	3.314654E 00	0.0424
8	3.556217E 00	0.0455
9	5.658769E 00	0.0724
10	4.591954E 00	0.0587
11	3.398863E 00	0.0435
12	1.219447E 01	0.1559
13	9.520355E 00	0.1217
14	9.603554E 00	0.1228
15	0.827014E 01	0.2336
16	1.783812E 01	0.2281
17	2.961180E 01	0.3786
18	3.610527E 01	0.4617
19	3.091107E 01	0.3952
20	1.604617E 01	0.2052
21	1.110542E 01	0.1420
22	1.276445E 01	0.1632
23	1.785712E 01	0.2283
24	1.529993E 01	0.1956
61	4.895911E 01	0.6260
62	4.659048E 00	0.0596
63	2.098515E 01	0.2683
64	3.505397E 01	0.4482
65	1.205874E 01	0.1542
66	4.163676E 01	0.5324
67	4.552327E 01	0.5821
68	1.097861E 02	1.4038
69	1.843174E 02	2.3568
70	2.751477E 02	3.5182
71	1.467004E 02	1.8758
72	5.067717E 01	0.6480
73	1.999974E 01	0.2557
74	5.673958E 01	0.7255
75	3.864603E 01	0.4941
76	3.998790E 01	0.5113
77	7.116743E 01	0.9100
78	2.801283E 01	0.3582
79	5.886792E 01	0.7527
80	5.292776E 01	0.6768
81	2.711314E 01	0.3467
82	3.510774E 01	0.4489
83	9.691559E 01	1.2392
84	6.472322E 01	0.8276
85	9.587067E 01	1.2258
86	1.594803E 02	2.0393

APPENDIX G

SAMPLE S-71 RUN

SAMPLE S-71 RUN TO PROVIDE INPUT TO NASTRAN. HIGH MODULUS GRAPHITE, QUASI-ISOTROPIC. 4/13/76

COST $1.32

INCLUDING THERMAL COEFFICIENT OF EXPANSION GOOD TO 350°F.

SAMPLE PROBLEM QUASI-ISOTROPIC SCIARRA 4/9/76

*** INPUT DATA ***

KEY1 = 0

KEY2 = 1

KEY3 = 0

KEY4 = 1

KEY5 = 0

THE NUMBER OF LAYERS IN THE LAMINATE IS 4

THE NUMBER OF MATERIAL TYPES IS 1

THE NUMBER OF LOADING CONDITIONS IS 1

*** MATERIAL DATA ***

MATYPE	E1	E2	U1	G	ALPHA1	ALPHA2	ALPHA6
1	0.2500000E 08	0.1700000E 07	0.3000000E 00	0.6500000E 06	-3.3000000E-06	0.1949999E-04	0.0

*** LAYER DATA ***

LAYER NO.	MATYPE	ORIENTATION	THICKNESS
1	1	0.0	0.08000
2	1	45.00000	0.08000
3	1	-45.00000	0.08000
4	1	90.00000	0.0800

*** ALLOWABLE STRAIN DATA ***

MATYPE	LIMIT STRAIN 1 = DIRECTION COMPRESSION	LIMIT STRAIN 2 = DIRECTION COMPRESSION	LIMIT STRAIN SHEAR NEGATIVE	LIMIT STRAIN 1 = DIRECTION POSITIVE	LIMIT STRAIN 2 = DIRECTION POSITIVE	LIMIT STRAIN SHEAR POSITIVE
1	0.0	0.0	0.0	0.0	0.0	0.0

*** OUTPUT DATA ***

COMPOSITE PROPERTIES

A MATRIX			B MATRIX			D MATRIX		
0.33688E 07	0.10937E 07	0.25789E-02	-0.22506E 06	0.0	-0.37509E 05	0.34696E 05	0.33842E 04	0.38512E-04
0.10937E 07	0.33688E 07	0.58628E 00	0.0	0.22506E 06	-0.37509E 05	0.33842E 04	0.34696E 05	0.87551E-02
0.25789E-02	0.58628E 00	0.11375E 07	-0.37509E 05	-0.37509E 05	0.0	0.38512E-04	0.87551E-02	0.37579E 04

(A/T) MATRIX			(A/T) INVERSE MATRIX		
0.10527E 08	0.34179E 07	0.80592E-02	0.10618E-06	-0.34474E-07	0.17527E-13
0.34179E 07	0.10527E 08	0.18321E 01	-0.34474E-07	0.10618E-06	-0.54648E-13
0.80592E-02	0.18321E 01	0.35548E 07	0.17527E-13	0.54648E-13	0.28131E-06

AVERAGE LAMINATE ELASTIC CONSTANTS

EX = 0.94177E 07 EY = 0.94178E 07 UX = 0.32467E 00 GXY = 0.35548E 07

*** THERMAL EXPANSION DATA ***

THERMAL EXPANSION COEFFICIENT X FOR COMPOSITE = 0.1278569E-05
THERMAL EXPANSION COEFFICIENT Y FOR COMPOSITE = 0.1278568E-05
THERMAL EXPANSION COEFFICIENT XY FOR COMPOSITE = -0.1340665E-11

COEFFICIENT OF THERMAL FORCE NX = 0.5705626E 01
COEFFICIENT OF THERMAL FORCE NY = 0.5705626E 01
COEFFICIENT OF THERMAL FORCE NXY = -0.7721391E-06
COEFFICIENT OF THERMAL MOMENT MX = 0.2951049E 00
COEFFICIENT OF THERMAL MOMENT MY = -0.2951049E 00
COEFFICIENT OF THERMAL MOMENT MXY = 0.9836811E-01

*** INPUT DATA FOR COMBINED N = M ANALYSIS ***

LOAD CASE NUMBER 1

NX =	100.	MX =	0.
NY =	0.	MY =	0.
NXY =	0.	MXY =	0.

TEMPERATURE = 0.

*** BENDING OUTPUT DATA ***

A-PRIME MATRIX / B-PRIME MATRIX

0.8250340E-06	-0.3479507E 06	0.2444781E-06	0.5421612E-05	0.1992494E-05	0.4761990E-05
-0.3479508E-06	0.8250325E-06	-0.2444779E-06	-0.1992499E-05	-0.5421597E-05	0.4761975E-05
0.2444781E-06	-0.2444779E-06	0.1042089E-05	0.2471374E-05	0.2471366E-05	0.1156956E-11
0.5421612E-05	-0.1992499E-05	0.2471374E-05	0.6576595E-04	0.9181552E-05	0.3422757E-04
0.1992494E-05	-0.5421597E-05	0.2471366E-05	0.9181552E-05	0.6576578E-04	-0.3422753E-04
0.4761990E-05	0.4761975E-05	0.1156956E-11	0.3422757E-04	-0.3422753E-04	0.3611685E-03

C-PRIME MATRIX / D-PRIME MATRIX

*** MID-PLANE STRAINS AND CURVATURES ***

LOAD CASE NUMBER = 1

EO - X = 0.8250339E-04	K - X = 0.5421611E-03
EO - Y = -0.3479507E-04	K - Y = 0.1992494E-03
EO - XY = 0.2444781E-04	K - XY = 0.4761987E-03

*** COMBINED BENDING AND MEMBRANE STRESSES, STRAINS, AND MARGINS OF SAFETY FOR EACH LAYER ***

LAYER	SIG-1	SIG-2	TAU-12	STRAIN-1	STRAIN-2	GAMMA-12	MAR-1	MAR-2	MAR-12
	LOAD CASE NUMBER 1								
	Z = -0.160000	THETA = 0							
1	-0.1409E 03	-0.1162E 03	-0.3363E 02	-0.4242E-05	-0.6667E-04	-0.5174E-04	-0.1000E 01	-0.1000E -1	-0.1000E 01
	Z = -0.080000	THETA = 45.							
2	-0.3171E 03	-0.4731E 01	-0.5841E 02	-0.1263E-04	0.1022E-05	-0.8987E-04	-0.1000E 01	-0.1000E 01	-0.1000E 01
	Z = 0.0	THETA = 45.							
3	0.9135E 03	0.3841E 02	-0.7624E 02	0.3608E-04	0.1163E-04	-0.1173E-03	-0.1000E 01	-0.1000E 01	-0.1000E 01
	Z = 0.0	THETA = -45.							
3	0.3111E 03	0.6768E 02	0.7624E 02	0.1163E-04	0.3608E-04	-0.1173E-03	-0.1000E 01	-0.1000E 01	-0.1000E 01
	Z = 0.080000	THETA = -45.							
4	0.6029E 03	0.1564E 03	0.9408E 02	0.2224E-04	0.8478E-04	0.1447E-03	-0.1000E 01	-0.1000E 01	-0.1000E 01
	Z = 0.160000	THETA = 90.							
5	0.1352E 02	0.2880E 03	-0.6542E 02	-0.2915E-05	0.1692E-03	-0.1006E-03	-0.1000E 01	-0.1000E 01	-0.1000E 01